

**CHROMATIC RESPONSES IN HUMAN VISUAL CORTEX-**  
**Effects of color, velocity and contrast**

**Dissertation**

**zur Erlangung des akademischen Grades**

**doctor rerum naturalium**  
**(Dr. rer. nat.)**

genehmigt durch  
die Fakultät für Naturwissenschaften  
der Otto-von-Guericke-Universität Magdeburg

von Dipl. Psych. Marcus Grüschow  
geb. am 08. 09. 1976 in Magdeburg

Gutachter: Prof. Dr. med. Ariel Schoenfeld  
Prof. Dr. Karl R. Gegenfurtner

Eingereicht am 26.02.2007  
Verteidigt am 04.06.2007

# ***Acknowledgements***

I express my deepest gratitude to my supervisor Dr. Jochem Rieger. His friendship, knowledge and precision have been inspiring. He truly conveys what it means to be a scientist.

I would like to thank the doctoral committee and the two final reviewers. I thank Prof. Thomas Münte, Prof. Christoph Herrmann, PD Ariel Schönfeld, Prof. Hans-Jochen Heinze and Prof. Herman Hinrichs for their support throughout the last years.

I extend my thanks to Prof. Bob Fendrich who has always been supportive by means of hilarious, but even more so, ingenious comments.

A very special thank you belongs to my two colleagues Franziska Schalk and Nick Köchy, with whom the perception group experience has truly been one. Their friendship and encouragement has been invaluable. The dude obeys.

I am also very grateful for the stimulating social environment that seems natural to the Department of Neurology II at the University Clinic Magdeburg. Big props go to Nico Boehler, Laura Hermann, Jacqueline Lemme, Sascha Tyll, Daniel Bergmann, Bjoern Bonath, Toemme Noesselt, Uwe Mattler, Yariv Festman, Oussama Hamid, Hartmut Schütze, Claus Tempelmann, Jörn Kaufmann, Nils Bodammer, Martin Kanowski and Michael Scholz.

My work could not have been completed without the continuous support from individuals outside of the science world. I owe to the members of my Bands Kantona and Enrico and I thank the TRF. Thanx to Lars, Raul, Peter, Alexis and my dear Anna.

Finally, I would like to thank my parents. Their unconditional support has given me the strength to follow my dreams and allows me to go beyond.

# Contents

<b>1</b>	<b>GENERAL INTRODUCTION.....</b>	<b>1</b>
<b>1.1</b>	<b>A short history of color science .....</b>	<b>1</b>
<b>1.2</b>	<b>Neurophysiological basics.....</b>	<b>4</b>
1.2.1	Anatomy and function of the visual system .....	4
1.2.1.1	Three receptor classes .....	5
1.2.1.2	Neurophysiological implementation of color-opponency .....	6
1.2.2	Spatial response properties of visual neurons.....	8
1.2.2.1	Receptive fields of retinal ganglion cells .....	8
1.2.2.2	Receptive fields of primary visual cortex (V1).....	8
1.2.2.3	Retinotopic organization .....	9
1.2.3	Anatomy and function of geniculo-cortical pathways.....	10
1.2.3.1	Anatomy.....	10
1.2.3.2	Functional specialization in the LGN.....	11
1.2.3.3	Functionally specialized pathways in the cortex .....	12
1.2.3.4	Cortical color mechanisms.....	13
1.2.3.5	Cortical color center ?.....	15
1.2.3.6	Chromatic responses in human cortex .....	17
<b>1.3</b>	<b>Experimental objectives.....</b>	<b>17</b>
<b>2</b>	<b>GENERAL METHODS.....</b>	<b>20</b>
<b>2.1</b>	<b>Stimulus control.....</b>	<b>20</b>
2.1.1	Classifying colors .....	20
2.1.1.1	Physiological color spaces.....	20
2.1.1.2	Luminance .....	22
2.1.1.3	Isoluminance.....	24
2.1.1.4	Luminance vs. achromatic stimuli .....	25
2.1.1.5	Color vs. luminance .....	25
2.1.2	Computing cone-contrast colors.....	26
2.1.2.1	Light to cone excitations .....	26
2.1.2.2	Cone excitations to light.....	29
<b>2.2</b>	<b>Magnetic resonance imaging.....</b>	<b>31</b>
2.2.1	Method 1 – phase encoding .....	32
2.2.2	Method 2 – canonical BOLD fitting (GLM).....	34
2.2.3	Method 3 – deconvoluting BOLD-response functions .....	36
2.2.3.1	Block design vs. event related design.....	36
2.2.3.2	Weighted Maximum Likelihood Estimate (WMLE).....	39
<b>3</b>	<b>EXPERIMENT 1- Retinotopic mapping .....</b>	<b>41</b>
<b>3.1</b>	<b>Introduction.....</b>	<b>41</b>
3.1.1	Retinotopic mapping.....	42
3.1.1.1	Eccentricity .....	42
3.1.1.2	Polar angle.....	43
<b>3.2</b>	<b>Methods .....</b>	<b>43</b>
3.2.1	fMRI measurements of retinotopy .....	43
3.2.1.1	MR-protocols: .....	44
3.2.2	MT+ localization .....	45
3.2.2.1	fMRI measurements of MT+ .....	46
3.2.3	Cortical flat maps.....	46
<b>3.3</b>	<b>Results.....</b>	<b>47</b>
3.3.1	Polar angle measurements.....	47
3.3.2	Eccentricity measurements .....	49
3.3.3	MT+ retinotopy and localizer measurements.....	51

<b>3.4</b>	<b>Discussion</b> .....	<b>55</b>
<b>4</b>	<b>EXPERIMENT 2- Speedtuning</b> .....	<b>58</b>
<b>4.1</b>	<b>Introduction</b> .....	<b>58</b>
4.1.1	Luminance - detection vs. discrimination.....	58
4.1.2	Isoluminance - detection vs. discrimination .....	58
4.1.3	Two motion mechanisms.....	59
<b>4.2</b>	<b>Methods</b> .....	<b>60</b>
4.2.1	Subjects.....	60
4.2.2	Visual display .....	61
4.2.3	FMRI protocol.....	61
4.2.4	Stimulus & experimental design .....	61
4.2.5	Analysis.....	63
<b>4.3</b>	<b>Results</b> .....	<b>63</b>
4.3.1	Analysis of variance .....	65
4.3.1.1	Global BOLD-Analysis .....	65
4.3.1.2	Analysis by velocity.....	65
4.3.1.3	Analysis by brain area.....	66
4.3.1.4	Velocity effects by cone-contrast direction.....	67
4.3.2	Cluster analysis .....	68
4.3.2.1	Stimuli for best separating hV4 and MT+ .....	69
<b>4.4</b>	<b>Discussion</b> .....	<b>70</b>
4.4.1	Two motion pathways in human cortex .....	70
4.4.2	Color opponency in visual cortex.....	72
4.4.3	Colortuning .....	73
4.4.4	Speedtuning .....	76
<b>5</b>	<b>EXPERIMENT 3 - Colortuning</b> .....	<b>79</b>
<b>5.1</b>	<b>Introduction</b> .....	<b>79</b>
<b>5.2</b>	<b>Methods</b> .....	<b>82</b>
5.2.1	Subjects.....	82
5.2.2	Stimulus & experimental design .....	82
5.2.3	MR-protocol.....	85
5.2.4	Fitting contrast response curve .....	85
<b>5.3</b>	<b>Results</b> .....	<b>86</b>
5.3.1	Global effects of color, contrast and velocity .....	87
5.3.2	Interactions.....	87
5.3.3	Contrast response curves.....	88
5.3.3.1	Effects of stimulus contrast and velocity in V1 .....	88
5.3.3.2	Effects of stimulus contrast and velocity in hV4 & V3A.....	89
5.3.3.3	Effects of stimulus contrast and velocity in MT+ .....	92
5.3.4	Comparison at equal cone-contrast.....	93
5.3.4.1	Effects of stimulus velocity and color .....	94
5.3.5	Ellipse fits .....	98
5.3.5.1	Effects of stimulus contrast, color and velocity .....	98
<b>5.4</b>	<b>Discussion</b> .....	<b>103</b>
5.4.1	Neurophysiological studies and speed in V1 .....	103
5.4.2	Neurophysiological studies and color in V1 .....	106
5.4.3	Neurophysiological studies and extra-striate cortex .....	109
5.4.3.1	MT+ .....	110
5.4.3.2	V3A & hV4 .....	111
5.4.4	Striate vs. extra-striate cortex.....	112
<b>6</b>	<b>GENERAL DISCUSSION</b> .....	<b>114</b>
<b>7</b>	<b>APPENDIX</b> .....	<b>118</b>
<b>7.1</b>	<b>Experiment 2 – Speedtuning</b> .....	<b>118</b>

<b>7.2</b>	<b>Experiment 3 - Colortuning</b> .....	<b>120</b>
7.2.1	ANOVA tables .....	120
7.2.2	T-test tables.....	121
<b>8</b>	<b>CITATIONS</b> .....	<b>124</b>

## ***Abbreviations***

Alpha	Flip angle
ANOVA	Analysis of variance
BD-path	Blob dominated path
BOLD	Blood oxygenation level dependent
Bk/Wh	Black/White
B/Y	Blue/Yellow
CO	Cytochromoxidase
CGC	Contrast gain control
EPI	Echo planar imaging
FLASH	Fast low angled shot sequence
FoV	Field of view
fMRI	Functional magnetic resonance imaging
FSPGR	Fast spoiled gradient echo sequence
FWHM	Full width half maximum
GLM	General linear model
HBM	Heterochromatic brightness matching
HFM	Heterochromatic flicker photometry
HRF	Hemodynamic response function
hV4	Human visual area 4
ID-path	Interblob dominated path
ISI	Inter stimulus interval
ITS	Inferior temporal sulcus
K-path	Koniocellular path
L-cones	Longwave sensitive retinal receptors
LGN	Laterale geniculate nucleus
M-cones	Middlewave sensitive retinal receptors
MD-path	Magnocellular dominated path
MEG	Magnetoencephalographic Imaging
M-path	Magnocellular path
MP-RAGE	Magnetization prepared rapid gradient echo sequence
MRI	Magnetic resonance imaging
MST	Medial superior temporal region (monkey)
MT	Medial temporal region (monkey)

MT+	Medial temporal complex (human)
PET	Positron emission tomography
P-path	Parvocellular path
rANOVA	Repeated measures analysis of variance
R/G	Red/Green
RF	Radio frequency pulse
RMS	Root mean square
ROI	Region of interest
S-cones	Shortwave sensitive retinal receptors
SET1	Spin echo T1-sequence
SPM	Statistical parametric mapping
TE	Time to echo
TFT	Thin-film transistor (display)
TI	Time for inversion
TR	Repetition time
V1	Primary visual cortex, striate cortex, Brodmans area 17
V2d/v	Visual area 2 dorsal/ventral
V3d/v	Visual area 3 dorsal/ventral
V3A	Visual area 3 accessory (a dorsal region)
V7	Visual area 7 (a dorsal region)
VO-1	Ventral occipital region 1
VO-2	Ventral occipital region 2
WMLE	Weighted maximum likelihood estimate

## ***Summary***

An organisms' ability to perceive color and movement in its natural environment greatly facilitates orientation and thus survival. Our understanding of cortical mechanisms leading to color and motion perception is still at an early stage. It is known, that light sensitive receptors in the eye give rise to several separate and spatially organized, cortical representations of the visual scene in primate cortex. Extensive monkey research has shown that these brain regions have different functional specializations. In humans, however, their functional properties are still not well understood.

In three experiments multiple retinotopically mapped visual areas in humans were investigated with functional magnetic resonance imaging (fMRI) regarding their characteristic responses to stimuli varying in color, contrast and velocity. The measurements presented quantify BOLD-responses to chromatic stimulation along thirteen directions in cone-contrast-space at four cone-contrast levels and at high and low stimulus velocity. They constitute the most complete characterization of the chromatic response properties in human visual cortex to date. On the basis of their response characteristics to these stimulus combinations, retinotopically mapped visual areas will be associated to two psychophysically determined motion perception mechanisms differing in chromatic sensitivity and temporal characteristics. The lateral region MT+ is suggested to account for a fast motion mechanism, responding well to all stimulus velocities and exhibiting some chromatic sensitivity, while dorsal area V3A and ventral area hV4 are mediating the slow pathway by showing a similarly high sensitivity to color and a preference for slowly moving stimuli. Velocity tuning in primary visual cortex was found to be highly contrast dependent as speed preference in V1 reversed from low to high speeds with increasing stimulus contrast. Evidence for cortical color-opponent mechanisms in several regions is provided and stimulus compositions that allow the best functional separation of dorsal and ventral visual areas are suggested.

In order to facilitate our understanding of cortical computation, this work provides insight into how chromatic and motion signals are transformed as visual information is transmitted from primary visual cortex to extra-striate regions. It is shown that color and motion are processed over several levels of the cortical hierarchy while no stimulus property is the exclusive domain of either processing stage.

# 1 GENERAL INTRODUCTION

## 1.1 A short history of color science

*'The rays to speak properly are not coloured'*. With this statement Sir Isaac Newton emphasizes color as a result of human perception and not a distinct property of the light emitted by an object. He arrived at this conclusion after showing that white day light can be decomposed into rays of different wavelengths, creating a spectrum, and that the color of an object is determined by its surface properties and illumination conditions rather than a physical property. His work *Optiks* (Newton, 1704) built the foundation for modern color science.

The theory of trichromacy, first described by George Palmer in 1777 (Palmer, 1777), rediscovered by Sir Thomas Young in 1802 (Young, 1802) and modified by Maxwell (Maxwell, 1855) and Helmholtz (Helmholtz, 1867/1925) constitutes the first scientific theory of color vision and perception. It is based upon color matching experiments carried out by Maxwell. Maxwell's experiments demonstrated that most colors can be matched by superimposing light from three sources with different colors, known as primaries. This process is well known as additive color mixing. The theory simply states that there are three types of color receptors, each sensitive in a different way to various wavelengths of light (Figure 1.1). One receptor is sensitive primarily to blue light, another primarily to green, and a third primarily to red. The appearance of a given mixture of light may then be described as a point in a three-dimensional space. 'Brightness' is defined as the sum of the responses of the three channels, and 'hue' and 'saturation' are calculated in a 'color triangle'. Thus, the fundamental dimensions of the Young-Helmholtz model of color perception are the responses of three color-channels: Blue (B), Green (G) and Red (R). All other colors are described as combinations of these three channels (B, G, R). The Young-Helmholtz formulation implies that perceived color is a point property, which means color appearance is entirely determined by the mixture of different wavelengths of light incident upon a single point on the retina. Unfortunately, contrast phenomena show, that this is not the case. For example, the color percept of a red region against a green background differs from the percept of the same red region shown against a gray background. This demonstrates that the perceived color at a point is affected by more than just the quality of the light at that particular point. A theory of color appearance must thus take the spectral information of the spatial surround into account.

Also, the dependence of hue on brightness must be explained, namely that for instance blue-greens or blue-reds will shift towards blue as brightness increases. In the basic Young-

Helmholtz color space, hue is the vector from the origin to the point in B, G, R space. If brightness is changed, then the ratios between B, G, and R remain the same. Therefore, the prediction is that the hue remains the same. However, as brightness increases, the perceived hue tends towards either blue or yellow, known as the Bezold-Brücke-effect (Bezold 1873, 1874; Ejima, 1984). Taken together, these difficulties casted doubts upon the complete fidelity of Young-Helmholtz color descriptions to human color perception because it is only valid under certain conditions.

Motivated in part by the fact that there are no greenish-red or bluish-yellow colors as well as the existence of color-after effects, Edwald Hering suggested a somewhat different theory of color perception (Hering, 1878/1964). This theory postulates the existence of three sets of paired variables, Yellow/Blue (Y-B), Red/Green (R-G), and Black/White (Wh-Bk). These variables represent the responses of three "Opponent Processes". Thus, the sensation of blue exists only at the expense of the sensation of yellow. Similarly, red and green are opposing forces, as are white and black. The system is similar to the Young-Helmholtz model in that color sensations are described in terms of a three-dimensional space. However, the dimensions of this space are different. Hering's theory was rejected by many investigators because he seemed to postulate the existence of chemical receptors which were affected in opposite ways by different wavelengths of light (Kaufman, 1974). This mechanism was not considered feasible, and there was no evidence for neural mechanisms, which could account for the behavior of Hering's opponent-processes. However, Hering never claimed that the opponent processes were at the receptor level, and later neurophysiological work showed that such processes indeed exist (Hurvich & Jameson, 1957).

A unification of the two theories described above became known as the Dual Process Theory. This theory was foreshadowed by von Kries (Kries von, 1905) and advanced by Müller and Schrödinger in the early 1920s (Müller, 1924). A complete theoretical synthesis and quantification of Hering's theory occurred not earlier than 1957 by Hurvich und Jameson (Hurvich & Jameson, 1957)

Their "opponent-colors" theory is the basis for interpretation and stimulus generation in the physiologically motivated color sciences (Hurvich & Jameson, 1955; Hurvich, 1956; Jameson, 1956 ; Hurvich & Jameson, 1957). In order to account for above mentioned surround effects, the opponent-colors model postulates an induction process whereby the response at a given point is influenced by the responses at neighboring points (color-contrast). If a stimulus produces a "red" response at some point, then it also produces a "green" response in the surrounding points. Similarly, "blue" responses are accompanied by "yellow" responses in the surrounding area. This mechanism would explain the observation that a red region

against a green background appears "redder" than the same region surrounded by a white background. This phenomenon is a direct analogy to the familiar edge effects in black and white scenes or Mach-Bands. The point is that the appropriate choice of dimensions (R-G, Y-B, Wh-Bk) permits to explain both the chromatic and achromatic contrast effects by the same computational principle, working independently in the three dimensions (Sloan & Bajcsy, 1975). Thus, it seems that the Hering theory of opponent processes, as extended and quantified by Hurvich and Jameson, can account for the difficulties that the Young-Helmholtz model faces.

The last major theory of color and color perception which will be reviewed is that of Edwin Land and colleagues (Land & McCann, 1971 ). While experimenting with color separation photographs (black and white pictures taken through red, green, and blue filters), Land discovered that, under certain conditions, only two colors need to be mixed in order to give the impression of a full color picture. Starting from this observation Land proceeded to experiment with different combinations of filters and varying viewing conditions (Land, 1959). As a result of these experiments, Land has proposed the "Retinex" theory of color perception (Land, 1977). The retinex theory proposes three separate "retinexes", each sensitive to a different segment of the visual spectrum. Within each retinex there is a representation of every object in the scene, rank-ordered according to its relative "lightness"<sup>1</sup> within the retinex. The sensations of color are then described as combinations of these rank orderings. According to Land, it is necessary, that the scene exhibits some randomness in order for the effect to hold. When the scene is relatively uniform, the usual laws of color mixture as described by Newton are observed. According to other researchers, the effects Land demonstrates so vividly are nothing more than color contrast effects, combined with the usual color mixture observations (Hurvich & Jameson, 1957). The Land theory is unsatisfactory because of its explicit reliance upon completely global determination of the color perception at each point. Another difficulty is that Land requires a judgment of "lightness" independent of the illumination. With the right assumptions, this judgment can be made (Horn, 1974). However, the necessary mechanisms are remarkably similar to the induction process described by the opponent-colors model. However, the Land system does provide a method for predicting the effect of two color mixtures, and has been used in the design of a color display system (Panigrahi, 1973).

It is known to us today that both processing steps, photon count by means of wavelength sensitive light receptors as well as opponent color computations, take place as

---

<sup>1</sup> The quality or condition of being illuminated. The perceptual impression of luminance is called *lightness* It refers to the brightness, or intensity value, of an object.

early as in retinal circuits. It is worth noting nonetheless, that above mentioned scientists came to their conclusions without the physiological knowledge available today, which highlights their extraordinary feat.

The following section reviews contemporary neurophysiological knowledge about the visual system. An introductory overview on the anatomy and function of the visual system is given and subsequent sections will describe the consecutive stages of visual information processing in more detail with emphasis on chromatic signal transduction. The chapter closes with the specification of experimental objectives studied in this thesis.

## ***1.2 Neurophysiological basics***

### ***1.2.1 Anatomy and function of the visual system***

The sheer number and size of the cortical areas that participate in visual information processing indicates the importance of primate visual perception. Approximately 60% of the entire neocortex take part in perception, interpretation and reaction to visual information. More than 30 distinct and highly interconnected visual areas could be described in the primate cerebral cortex (Felleman & Van Essen, 1991; Van Essen *et al.*, 1992; Merigan, 1993; Van Essen & Gallant, 1994; Salin & Bullier, 1995).

The path of the visual information processing begins with light absorption in the photoreceptors of the retina. Within the retina a large part of visual processing is conducted by means of these light receptors, bipolar, amacrin, horizontal and ganglion cells. The visual information is transmitted via the optic nerve through the optic chiasm and, by means of the optic tract, transferred to the lateral geniculate nucleus (LGN) in the thalamus. The LGN is considered the main relay station for visual information from retina to cortex. Approximately 90% of the retinal ganglion cells project to the LGN, while the remainders connect to the superior colliculi and the pulvinar. Each thalamic hemisphere contains one LGN, which is distinguishable in 6 layers. The two inferior layers consist of relatively large magnocellular neurons, while the four superior layers contain relatively small parvocellular neurons. In between the parvo- and magno-cellular layers reside the koniocellular layers. Because retinal fibers of the nasal retina cross over in the optic chiasm, each LGN receives visual information stemming from the contra-lateral visual field. For instance, the left LGN receives information from the left halves of each retina, which sample the right visual field. Each individual cell layer in the LGN receives signals exclusively from one eye. The fibers of the nasal contralateral retina project to the layers 1, 4 and 6, while the temporal ipsilateral fibers project to layers 2, 3 and 5 of the LGN. The optical radiation forwards the signals from LGN towards

the primary visual cortex (V1), situated in the calcarine sulcus of the occipital lobe of primates. Primary visual cortex is organized in layers and columns of distinct cell types, while specific color-responsive cells were found in blob-structures known as cytochromoxidase rich blobs (CO-blobs). The energy consumption of these cells could be functionally marked using a technique called cytochromoxidase-staining. After specific stimulus classes have been presented, for instance color, this method generates stained neuronal regions, which have been active during the stimulus presentation. Inactive regions will not be stained with cytochromoxidase leading to the interpretation that active regions functionally contribute to the processing of the presented stimulus because their energy consumption is elevated during the respective experimental stimulation.

Commencing in V1, the cortical processing of visual information is believed to be separated into two main paths (Ungerleider & Mishkin, 1982; Goodale & Milner, 1992). Firstly, the parietal path, projecting into parietal regions of cortex and secondly the temporal path projecting towards inferior temporal cortex. The parietal stream is assumed to be mostly associated with spatio-temporal information processing associated with an ‘action’-system (the WHERE-path), while the temporal stream is believed to be mainly associated with recognition of objects, a perceptual system, and thus with color-, pattern- and form-perception (the WHAT-path) (Ungerleider & Mishkin, 1982; Goodale & Milner, 1992).

While the current knowledge of early visual processing, starting from the retina to primary visual cortex, can be regarded as quite substantial, knowledge of higher cortical processing may be best described as insufficient. If and to what sort of stimuli the higher cortical areas are specialized as well as response properties to ‘simple’ stimulus attributes such as color are still a matter of debate. This thesis attempts to characterize the response properties of several visual areas located in human visual cortex in the color, motion and contrast domain. The next sections describe the path of visual information as it is transmitted in consecutive stages in retino-geniculo-cortical pathways in more detail.

### **1.2.1.1 Three receptor classes**

Light-sensitive photoreceptors in the retina constitute the first processing stage of the visual information. Under photopic viewing conditions (at high light intensity levels) receptors, called the cones, are receptive, while scotopic vision (at low light intensity levels), is maintained by the rods. In a normal human retina three classes of cones are found. Each of which contains a slightly different light absorbing pigment. They can be considered the physiological implementation of Helmholtz’ theory of trichromacy. The absorption spectra of

each class of cones are known (Brown & Wald, 1964; Marks *et al.*, 1964) and can be described by three overlapping functions (Figure 1.1).

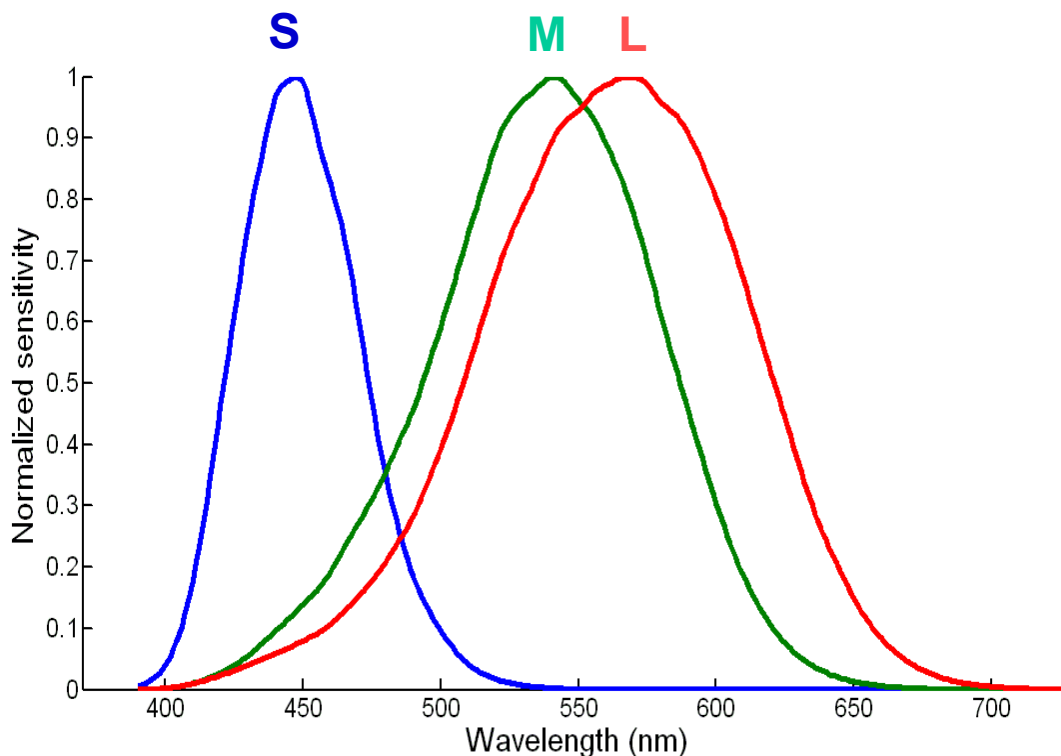


**Figure 1.1: Normalized cone spectral sensitivities**

Lines: blue (short-wavelength sensitive receptor; S-cones), green (middle-wavelength sensitive receptor; M-cones), red (long-wavelength sensitive receptor; L-cones).

The short-wave- or S-cones maximally absorb light at  $\sim 440$  nm, the middle-wave- or M-cones maximally absorb light at  $\sim 530$  nm and the long-wave- or L-cones maximally absorb light at  $\sim 560$  nm (Schnapf *et al.*, 1987). The number and density of each cone class varies across the retinal receptor mosaic (Roorda, 1999). The S-cones amount to 5-10% in the human retina. The ratio of L- and M-cones is highly variable across observers and can range from 0.82 to 9.71 (Brainard *et al.*, 2000). The region of highest acuity in the human retina is called the fovea, in which receptor density is highest. The central  $0.1^\circ$  of the fovea is made up entirely of L- and M-cones. The amount of S-cones at  $1.0^\circ$  increases to 6%.

### 1.2.1.2 Neurophysiological implementation of color-opponency

The following section uses terms such as red, green, blue and yellow light. The perceptual impressions of red, green and blue can however not be regarded equal to excitation of the L-, M- or S-cones (see Figure 5.2). While the excitation of the L-cones yields a reddish percept, excitation of the S-cones results in a dark violet. The notation to describe properties

of receptive fields in the retinal ganglion cells and LGN is conventional but can be misleading.

Russel De Valois and colleagues, pioneered neurophysiological studies of color-opponency by showing that response patterns from color sensitive neurons in the LGN of the macaque are not in concordance with Helmholtz' theory of trichromacy (Helmholtz, 1867/1925), but are in line with the opponent process theory postulated by Hering (Hering, 1964; De Valois *et al.*, 1966). Some cells were found to be excited by red light and inhibited by green light ( $R^+G^-$  cells). Other cells were excited by green light and inhibited by red light ( $G^+R^-$  cells). In addition, cells were found that could be excited by yellow light and inhibited by blue light ( $Y^+B^-$  cells) as well as cells that were excited by blue light and inhibited by yellow light ( $B^+Y^-$  cells). Another population of cells did not show spectral opponent behavior whatsoever. These cells were excited by light containing a mixture of all wavelengths while the absence of light inhibited them ( $Wh^+Bk^-$  cells). The opposite was also found, namely cells, which show inhibition by stimulation with all wavelength light and excitation through absence of all wavelength light ( $Bk^+Wh^-$  cells). Together these cells can be interpreted as neuronal implementation of Herings opponent process theory. However, this kind of opponent processes can already be found in the retinal bipolar- and ganglion cells (de Monasterio, 1982; Lee *et al.*, 1988; Lee, 1990).

The specific response pattern of  $R^+G^-$  cells for instance arises through combination of excitatory input from L-cones with inhibitory input from M-cones. Essentially, output from these cells is governed by the difference between L- and M-cones (L-M). The output from  $G^+R^-$  cells is dominated by excitatory input from M-cones and inhibitory input from L-cones, yielding a similar difference computation (M-L). The output of  $B^+Y^-$  cells is generated through excitatory input from S-cones and the inhibitory sum of L- and M-cones ( $S-(L+M) = S-L-M$ ), while the output from  $Y^+B^-$  cells is produced by the excitatory sum of L- and M-cones opposed by an inhibitory signal from the S-cones ( $(M+L)-S = M+L-S$ ). Output from  $Wh^+Bk^-$  cells originates in the excitatory sum of L-, M- and S-cones (L+M+S), while the output from  $Bk^+Wh^-$  cells is created through inhibitory signals from all cone classes (-L-M-S).

Knowledge of these fundamental neural computations will govern the stimulus generation for all experiments in this thesis. Controlled excitation of retinal photoreceptors and downstream neural pathways, in multiple directions of color-space is essential to achieve the major goal of this work, which is the characterization of chromatic responses in multiple cortical visual areas.

## **1.2.2 Spatial response properties of visual neurons**

### **1.2.2.1 Receptive fields of retinal ganglion cells**

Each retinal ganglion cell receives visual information from upstream-connected photoreceptors, which in turn respond to stimuli in designated positions in the visual field. The location in the visual field in which stimuli affect neuronal activity levels is called the receptive field of that neuron. Retinal ganglion cells have small concentric receptive fields with an antagonistic center-surround organization (Lee, 1996). An ON-center ganglion cell starts firing, when a light source stimulates exactly the center of its receptive field. The firing of the ganglion cell is inhibited, when the antagonistic surround is stimulated exclusively. Similarly, OFF-center ganglion cells exist, for which stimulation of the center causes the highest inhibition, while stimulation of the surround yields an excitation. If, however the entire receptive field is illuminated equally, a relatively weak response can be expected. The antagonistic center-surround organization of retinal ganglion cells causes a high sensitivity for local contrast changes, while equal illumination changes across the entire visual field have little effect on these cells firing rate.

### **1.2.2.2 Receptive fields of primary visual cortex (V1)**

The response properties of neurons in primary visual cortex are more complex than in the retina or the LGN. V1 neurons do not respond very well to point-like stimulation, while responding vigorously to stripes of light. Ground-breaking work on this matter has been presented by David Hubel and Torsten Wiesel using cats and monkeys (Hubel, 1959). They distinguished three cortical types of neurons, depending on their preferred type of stimulation.

*Simple cells* respond to bars of light with a particular orientation. The receptive fields of simple cells are elongated, oriented in a certain direction in space and divided into excitatory and inhibitory zones. A strong response from such a neuron can be expected when a stripe-like stimulus or contrast edge is presented to its receptive field, which is equal in orientation and size to its excitatory zone.

*Complex cells* exhibit no clear distinction between an excitatory and inhibitory zone. They also selectively respond to oriented stripe-like or contrast edge stimuli, but the exact position within the receptive field is irrelevant. As opposed to simple cells, complex cells prefer edges independent of contrast direction. Additionally they respond selectively to stimuli moving over their receptive field in specific directions.

*Hypercomplex cells* respond to stripes and angles of a certain length, which move in the preferred direction across its receptive field. The elongated excitatory and inhibitory zones

of simple and complex cell receptive fields are thought to emerge through combination of several concentrically organized cells (Hubel, 1962).

Neurons with distinct receptive field attributes are organized in columns. Their properties can be differentiated by position of the receptive field (which is fairly equal within one column), ocular-dominance and orientation of the receptive fields. A column representing a certain position in the visual field is called a *hyper column* and contains two ocular dominance columns and numerous orientation columns ( $0^{\circ}$ - $360^{\circ}$ ).

### **1.2.2.3 Retinotopic organization**

Adjacent retinal ganglion cells have adjacent and overlapping receptive fields and project to neighboring neurons of the next stage of visual information processing. Consequently, neighboring locations in the visual field are represented in neighboring neurons in cortex. This organizational principle, by which the spatial arrangement of retinal ganglion cells is preserved, is called *retinotopy*. This spatial organization is maintained in the LGN and cortex until the receptive fields of higher tier areas become progressively larger and spatial information is integrated to abstract categories such as for instance faces and cars (Press *et al.*, 2001; Smith *et al.*, 2001; Huk *et al.*, 2002; Wade *et al.*, 2002; Wandell *et al.*, 2005; Grill-Spector *et al.*, 2006). The retinotopic organization of many visual areas permits measurements of the cortical representation of the visual field efficiently and with high spatial resolution (DeYoe *et al.*, 1994; Engel *et al.*, 1994; Sereno *et al.*, 1995; Engel *et al.*, 1997b). By means of retinotopic mapping, several visual areas can be distinguished solely on their spatial representation of the visual field and independent of any other functional criterion.

However some dispute regarding topographic organization of some higher visual areas pertains in the field (Hadjikhani *et al.*, 1998; Tootell, 2001; Wade *et al.*, 2002; Brewer *et al.*, 2005). Different methods have yielded slightly different results and interpretations. The first series of experiments in this thesis will present several retinotopic measurements, the results of which will serve as a precise cortical location to generate regions of interest (ROIs) representing distinct visual field maps. Subsequent experiments will use these ROIs to investigate the functional properties pertaining to color, motion and contrast dependences within separate visual areas.

### **1.2.3 Anatomy and function of geniculo-cortical pathways**

#### **1.2.3.1 Anatomy**

Several distinct paths project from retina to cortex. The paths can be distinguished on the basis of multiple anatomical criteria. They differ in morphology, density of corresponding cells, connections within the retina and presumably independent projections. To date three major pathways are discriminated and have been extensively investigated in the monkey brain.

The *parvocellular path* (P-path) originates in the midget ganglion cells in the retina (Dacey, 2000). It was named after the parvocellular neurons in LGN layers. These neurons have ON- and OFF-center receptive fields (Dacey, 2003). In the inner fovea these centers consist of only one L- or M-cone. Anatomical studies have shown that S-cones contribute only to OFF-center ganglion cells (Klug, 1993). The midget ganglion cells project into the four parvocellular layers of the LGN and from there mainly to layer 4C $\beta$  (Chatterjee & Callaway, 2003) but also to layers 4A and 6 of primary visual cortex (Lennie, 1988; Fitzpatrick, 1996; Solomon & Lennie, 2005; Conway & Livingstone, 2006).

The *magnocellular path* (M-path) originates in the parasol cells (M-cells) which in turn receive their input from diffuse bipolar cells (Dacey, 2000, 2003). The diffuse bipolar cells obtain additive input from L- and M-cones (Calkins, 1996; Lee, 1996a; Dacey, 2000; Jacoby, 2000; Dacey, 2003; Conway & Livingstone, 2006). The receptive fields of the M-cells have an antagonistic center-surround organization. These neurons project into the two magnocellular layers of the LGN. They exhibit a high sensitivity for luminance contrast (L+M). The magnocellular layers of LGN project mainly to layer 4C $\alpha$  (Chatterjee 2003) but also to layers 4B and 6 in primary visual cortex (Lennie, 1988; Fitzpatrick, 1996; Solomon & Lennie, 2005).

The *koniocellular path* (K-path) originates in the small bistratified retinal ganglion cells (Dacey, 1993; Hendry & Yoshioka, 1994). The receptive fields of these neurons consist of an excitatory S-cone center and an inhibitory surround formed by additive L- and M-cone signals (S-(L+M)). They project into the koniocellular layers of the LGN (Casagrande, 1994; Hendry & Yoshioka, 1994) after which this path was named. These layers reside between the magno- and parvocellular layers in the LGN. In primary visual cortex these cells are known as Blue-ON-cells and can be found in layer 4A (Chatterjee & Callaway, 2003) but also in the CO-rich blobs of the superficial layers (1,2,3) (Chatterjee, 2002; Chatterjee & Callaway, 2003; Sincich & Horton, 2005; Conway & Livingstone, 2006). In layer 4A, Chatterjee (2003) also characterized Blue-OFF-cells which respond most vigorously to pure S-cone stimuli with

negative sign and exhibit weak responses to the sum of L- and M-cones (Chatterjee & Callaway, 2003).

As early as in the primary visual cortex (V1) there are numerous anatomical connections between the magno- and parvocellular streams (Merigan & Maunsell, 1993; Yoshioka *et al.*, 1993; Lund *et al.*, 1995), originating in the LGN, while the interaction with the koniocellular path are currently highly investigated (Sincich & Horton, 2005). Beyond V1, in visual areas V2, V3 and V4, the connectedness between different, anatomically defined compartments, increases substantially (Yoshioka *et al.*, 1992; Levitt *et al.*, 1994). Area V4, for instance, was estimated to receive about an equal proportion of inputs originating from magno- and parvocellular LGN-layers (Ferrera *et al.*, 1994). Even motion sensitive region V5 (MT), which was long believed to solely receive magnocellular input (Maunsell *et al.*, 1990) could be shown, by means of neuroimaging, to receive contributions from other paths as well (Wandell *et al.*, 1999).

### **1.2.3.2 Functional specialization in the LGN**

The anatomically distinct paths are believed to exhibit differential spatial and temporal properties. P-cells for instance are most sensitive at low temporal flicker rates, while M-cells are more sensitive to high flicker frequencies (Marrocco *et al.*, 1982; Hicks *et al.*, 1983; Van Essen, 1990). In humans, the receptive field size of M-cells is up to ten times larger than the receptive fields of P-cells (Van Essen, 1990) and in addition have a much lower retinal distribution density as compared to P-cells (Perry, 1984; Grunert, 1993). K-path-neurons show a low retinal distribution density as well (Dacey & Lee, 1994).

High spatial frequencies seem to be selectively preferred by the P-path. Highest spatial resolution is however known to be inherent to achromatic viewing, associated with the M-path, posing a profound inconsistency with respect to the specific task segregation between M- and P-path. Different receptive field properties as well as the aforementioned anatomical connections within each path, indicate differential specialization regarding transmission of color information. The P-path seems to code color whereas the M-path codes luminance (Spillmann & Werner, 1990). The spatial density and quantity of neurons in the P-path is significantly higher than in any other retinal path. In the fovea for instance, each cone sends signals to two neurons in the P-path (one ON- and one OFF-signal). In fact, the ganglion cell mosaic of the P-path consists of 70% of the 1.25 million retinal ganglion cells (Rodieck, 1998). This suggests the P-path to be responsible for the high spatial achromatic viewing, even though it is thought to mainly transmit color information.

In summary, it can be stated that at least three anatomically distinguishable channels exist (P-, M-, K-path), that carry visual information from retina to cortex. Several lines of evidence suggest that the anatomical segregation as present in the LGN may not be maintained throughout cortex, as visual information from several paths may be merged in order to achieve maximal integration (Nealey *et al.*, 1991; Merigan & Maunsell, 1993; Ferrera *et al.*, 1994; Nassi & Callaway, 2006). The next section reviews relevant findings mainly in the macaque brain.

### **1.2.3.3 Functionally specialized pathways in the cortex**

Comparison of chromatic response patterns in human striate cortex to response profiles in higher tier areas is a major goal of this thesis. The visual information is believed to have reached the extra-striate regions by projections described in the next section.

In cortex, a clear segregation of the three subcortical pathways as found in the LGN cannot be reported, because a blending of the paths is progressively evident as a multitude of interconnections in V1 and higher areas occur (Sincich & Horton, 2005). However, several groups postulate, that the three paths remain highly segregated as they advance into the extra-striate cortical hierarchy (DeYoe & Van Essen, 1985; Livingstone & Hubel, 1987; Roe & Ts'o, 1999). Cytochromeoxidase-staining in the macaque has provided functional landmarks in cortical regions such as CO-rich blobs in V1 and thin, thick and pale stripes in V2, responsivity of which may be investigated regarding the contributions of the known projections from the LGN.

The retino-geniculate M-path is continued as the magnocellularly dominated (MD) path in cortex. This path has been identified as having the least convergence with the other two pathways (DeYoe & Van Essen, 1985) and is mainly, but not exclusively, fed by magnocellular projections. In V2, this path projects into the CO-thick stripes. Livingstone and Hubel report an anatomical and physiological model, which proposes this path to be color blind, highly contrast sensitive and having poor spatial resolution (Livingstone & Hubel, 1988).

The cortical pathway exhibiting highest convergence of all described projection routes is the blob dominated (BD) path (Fitzpatrick *et al.*, 1985). Part of this path are the CO-rich-blobs in V1 which appear to receive input from all three geniculo-striate paths (M-, P-, K-path) (Fitzpatrick *et al.*, 1985; Lachica *et al.*, 1992; Yoshioka *et al.*, 1993; Sincich & Horton, 2005). Experiments in which P-layers of the LGN were selectively deactivated, show nonetheless, that many cells in the blobs could still be activated, presumably by cells that combine M- and P-path information, showing residual magno-cellular responsivity (Nealey *et*

*al.*, 1991). Livingstone and Hubel's model assigns this path high color selectivity, low contrast sensitivity and high spatial resolution (Livingstone & Hubel, 1987).

The third cortical path pertains to the CO-interblob regions in V1 and is called ID-path (interblob dominated). The interblob regions receive substantial input from parvocellular LGN-layers (Lachica *et al.*, 1992; Yoshioka *et al.*, 1993) but also from magnocellular layers (Yoshioka *et al.*, 1993). Selective deactivation of LGN-layers could also show that the interblob neurons in V1 can be excited by parvo- and magnocellular contributions (Nealey *et al.*, 1991). The interblob outputs project to the CO-pale stripes in V2. Beyond V2, this path is believed to supply the ID-path subregions of V4 and the posterior inferotemporal cortex (Felleman *et al.*, 1997a).

The selectivity of neurons comprising each path is characterized by response profiles that seem sensitive to a variety of visual information (DeYoe & Van Essen, 1988; Peterhans & von der Heydt, 1993). The MD-path is highly selective for binocular disparity, motion direction, velocity, orientation and low spatial frequency. The BD-path is highly selective for wavelength information and high spatial frequencies, while the ID-path selectively prefers orientation, disparity, low spatial frequencies and wavelength information (Van Essen & DeYoe, 1995).

#### **1.2.3.4 Cortical color mechanisms**

Color processing and characterization of distinct visual areas with respect to their color sensitivity are actively debated subjects (Gegenfurtner, 1999).

As indicated above, early studies described the existence of color selective cells of the macaque monkey (Hubel & Wiesel, 1968; Dow & Gouras, 1973; Gouras, 1974; Poggio *et al.*, 1975; Thorell *et al.*, 1984). A turning point regarding our understanding of cortical color mechanisms commenced by the work of Livingstone and Hubel in 1984 (Livingstone & Hubel, 1984). They report conglomerates of non-oriented, monocular, color-selective cells in CO-blobs of macaque V1. Within the CO-blobs however, an additional color cell type was identified. Livingstone and Hubel had found the double-opponent cells in V1, which were first found in the goldfish retina (Daw, 1968). These cells respond strongest when their receptive field centers are stimulated with one color and their surround with the opponent color (Daw, 1968; Hubel & Wiesel, 1968; Conway, 2001). Opponent mechanisms, red-green for instance, are hence prevalent in the receptive fields' center as well as in the surround of these cells. Red-green double-opponent cells are thus able to compare the relative amounts of red-green in one part of a scene with the amount of red-green in an adjacent part of the scene. Hence they respond best to local color contrast.

Ts'o and Gilbert observed B/Y or R/G opponent-color mechanisms in the blobs of V1, and specified additional cells with receptive fields having either a B/Y or R/G opponent color mechanism solely in the center, while a broadband inhibitory surround was found (Ts'o & Gilbert, 1988). They called this additional cell class modified Type II-cells (Ts'o & Gilbert, 1988). In addition, they discovered cells that were color selective and orientation sensitive. These cells were most frequently found in between borders of blobs and interblobs. In the same study they could show, that CO-blob color cells are organized in clusters with similar sensitivity to opponent colors. Some CO-blobs are designated to respond to either R/G or B/Y opponent colors.

However, as opposed to LGN neurons, V1 contains cells that are not exclusively sensitive along the two cardinal color mechanisms (S-(L+M), L-M), but also respond vigorously to mixed colors (Lennie *et al.*, 1990; Solomon & Lennie, 2005; Conway & Livingstone, 2006). This mixed color selectivity is also prevalent in macaque V2 (Gegenfurtner *et al.*, 1996) and V3 (Gegenfurtner *et al.*, 1997).

The functional organization and architecture in V2 is different as compared to V1 (Kiper *et al.*, 1997). CO-staining in V2 revealed parallel thin, thick and pale stripes (DeYoe & Van Essen, 1985). It was assumed that color information is primarily processed in the thin stripes, motion information in the thick stripes and form information mostly in the pale stripes. Gegenfurtner and colleagues could show, however, that neurons in macaque V2 are not restricted to one stimulus attribute such as color, form or motion (Gegenfurtner *et al.*, 1996). In addition they report that color sensitive neurons are also not restricted to the thin stripes but occur in other stripe classes which are known for different specializations as well (Gegenfurtner & Hawken, 1996; Gegenfurtner *et al.*, 1996). It became thus convincing that a strict segregation regarding stimulus attributes in parallel processing streams is not prevalent in V2. Combined processing of stimulus attributes (multiplexing) in V2 is more likely.

Similar results could be obtained for area V3 in the macaque (Gegenfurtner *et al.*, 1997). It was found that V3 receives strong inputs, originating from both, the magno- and the parvo-path, and has prominent projections to areas MT and V4, which are believed to be the cortical motion or color center respectively. Area V3 may thus represent an important cortical site for integrating visual signals, originating in anatomically different pathways. Orientation selectivity in V3 was prevalent in 80% of the cells, similar to V2 (Gegenfurtner *et al.*, 1996; Gegenfurtner *et al.*, 1997). However, neurons in V3 seem to prefer lower spatial and higher temporal frequencies than V2 neurons (Gegenfurtner *et al.*, 1997). Contrast thresholds obtained from V3 neurons were extremely low. Approximately 40% of all neurons showed strong selectivity for the direction of a moving stimulus. However, no direction selective cells

were found in layer 4 of V3, which constitutes the input termination site for V1 and V2 projections. This finding indicates, that selectivity for the direction of motion may develop within V3 (Gegenfurtner *et al.*, 1997).

In the macaque monkey the proportion of color selective cells was found to be approximately equal in V2 (50%) and V3 (54%) (Gegenfurtner *et al.*, 1996; Gegenfurtner *et al.*, 1997). In addition it was reported that V3 subpopulations, sensitive to color or motion, are largely overlapping. Cells, responding reliably to directional signals elicited by drifting isoluminant chromatic gratings were also found (Gegenfurtner *et al.*, 1997). In summary, these neurophysiological results indicate, that there is a significant interaction between color and motion processing in macaque area V3.

The motion sensitive area MT, situated at the lateral medio-temporal regions in the macaque is classically believed to receive predominately magnocellular input (Maunsell *et al.*, 1990) and was suggested to completely lack color selectivity (Zeki, 1983c). Using a combination of physiological and psychophysical techniques, subsequent studies were able to show that color information does contribute to the response of MT neurons in monkeys (Dobkins & Albright, 1994; Croner & Albright, 1999; Seidemann *et al.*, 1999; Thiele *et al.*, 1999). Moreover, Gegenfurtner *et al.* (1994) showed that most MT neurons do respond to chromatic modulation, albeit much less vigorously than to luminance variations (Gegenfurtner *et al.*, 1994). Recent imaging reports on human subjects indicate that MT+ as a whole gives responses to chromatically defined stimuli, even though it may contain few, if any, color-opponent cells (Tootell *et al.*, 1995b; Wandell *et al.*, 1999; Liu & Wandell, 2005). The ventral occipital region hV4 is described in detail in the next section.

### **1.2.3.5 Cortical color center ?**

The delineation of a cortical center, specialized for a perceptual property such as color, implies that the perception of this attribute is represented through activity of neurons within this cortical region (Zeki, 1990).

Early indications for the existence of an unequivocal color center originated from single cell investigation of the macaque area V4. It has been argued that V4 is a specialized color center because it contained solely color selective cells (Zeki, 1983b, 1983a, 1983c, 1983d). First estimates proposed 100% color sensitive cells in V4 (Zeki, 1973). Subsequent studies found substantially less color selective cells. Schein *et al.* did not find more than 20% (Schein *et al.*, 1982). Even though the multitude of studies show little congruence, it is highly likely, that V4 contains the same amount of color selective cells as V1, V2 or V3. Schein and Desimone showed that most V4 neurons do not show higher sensitivity with regard to

wavelength-selectivity compared to retinal color-opponent ganglion cells or parvocellular LGN-cells (Schein & Desimone, 1990).

A main argument against a clear-cut color area V4, provide lesion studies. Lesions in V4 of the macaque do not exclusively cause deficits in color perception (Heywood & Cowey, 1987; Schiller, 1993) but include also impairments of other stimulus attributes such as form discrimination (Walsh *et al.*, 1992; Merigan, 1996), object recognition (Schiller, 1995; Merigan & Pham, 1998; Walsh *et al.*, 2000), texture discrimination (Merigan, 2000) and focusing of attention (De Weerd *et al.*, 1999).

In humans, it is long known that bilateral lesions in parts of the fusiform and lingual gyrus on the ventro-medial side of the occipital-temporal cortex (see Figure 3.1.) can cause severe deficits in color perception (Meadows, 1974; Zeki, 1990). For that reason this region on the ventral cortical surface has been assigned the human homologue to macaque V4. Using modern imaging techniques it could be shown that the ventral cortical surface is highly active during color perception (Lueck *et al.*, 1989; Corbetta *et al.*, 1991; Gulyas *et al.*, 1994; Kleinschmidt *et al.*, 1996; McKeefry & Zeki, 1997; Wade *et al.*, 2002; Brewer *et al.*, 2005; Liu & Wandell, 2005). Hadjikhani (1998), using functional magnetic resonance imaging, also found a region in ventral occipital cortex, which was highly activated by colored stimuli (Hadjikhani *et al.*, 1998). They argued that this region is not the homologue to macaque V4 and named it V8 (Hadjikhani *et al.*, 1998). It is however very likely that V8 is not a new separate color area, solely responsible for color perception, as could be shown in a study, investigating the topographic representation of the visual field along the ventral surface (Wade *et al.*, 2002). Wade (2002) found activity elicited through colored stimuli extending from V1 along the ventral surface, showing that V8, if it exists, is not the only region responding strongly to color.

Additional primate studies reported that V4 neurons, similar to neurons in V2, can be selectively excited by certain lengths, widths, orientations and forms of the stimuli used (Desimone & Schein, 1987). V4 seems to feature a multitude of processes besides coding color. An additional indicator against V4 as a clear-cut color center are studies which showed that V4 neurons can selectively respond to direction of motion and can also be modulated by attention processes (Moran & Desimone, 1985; Tolias *et al.*, 2005a).

In summary, it is highly unlikely that a single cortical region exists which responds exclusively to colored stimuli. It is thus more probable, that color perception is the results of simultaneous neural activity in several cortical sites and that color-coding takes place in several visual areas simultaneously.

### **1.2.3.6 Chromatic responses in human cortex**

As indicated above, most of the studies that described the existence of color selective cells have been conducted using single cell recordings in the macaque monkey (Hubel & Wiesel, 1968; Dow & Gouras, 1973; Gouras, 1974; Poggio *et al.*, 1975; Thorell *et al.*, 1984). Compared to the amount of single cell monkey-studies, only few noninvasive human fMRI-studies regarding this field exist (Kleinschmidt *et al.*, 1996; Engel *et al.*, 1997b; McKeefry & Zeki, 1997; Hadjikhani *et al.*, 1998; Zeki & Marini, 1998; Beauchamp *et al.*, 1999; Bartels & Zeki, 2000; Engel & Furmanski, 2001; Wade *et al.*, 2002; Liu & Wandell, 2005). Some PET-studies were also conducted (Lueck *et al.*, 1989; Zeki, 1991). The goal in several of these studies was to measure activity, elicited by colored stimulation, aiming for the cortical color center (Lueck *et al.*, 1989; Zeki *et al.*, 1991; Beauchamp *et al.*, 1999; Bartels & Zeki, 2000). The subtraction methodology was used, which implies the acquisition of functional brain activity, while the subjects view either colored or black/white stimuli in order to subtract the measured achromatic- from the chromatic activity, to be left with cortical regions responding stronger to color than to achromatic stimulation. While this procedure did in fact reveal the ventral cortical surface to show higher activity to chromatic than to achromatic stimuli, conclusions regarding opponent-color mechanisms as described above (see section 1.2.1.2.) cannot be made. If the stimuli are not equated in a way, which takes cone-computations, known to be inherent to retino-geniculo-cortical pathways into account, conclusions beyond a comparison of chromatic versus achromatic responses are not feasible. In addition, how and to what extent distinct visual areas respond to chromatic or achromatic contrast modulation could not be derived because retinotopic mapping was not performed in most of the early studies (Kleinschmidt *et al.*, 1996; McKeefry & Zeki, 1997; Zeki & Marini, 1998; Bartels & Zeki, 2000). A detailed description of chromatic stimulus control is given in section 2.1.2. Studies investigating chromatic responses in human visual cortex using stimuli controlled for cone excitation will motivate the experimental objectives of this thesis and will be introduced in the next section.

## **1.3 Experimental objectives**

The main goal of this thesis is to characterize retinotopically defined human visual areas regarding their differential response patterns to chromatically defined stimuli. A second objective is to assess the dependence of the chromatically induced response patterns to additional stimulus attributes, such as stimulus velocity and contrast. This is of interest because these measurements would allow the assessment as to how the visual information is

transformed on its way from primary visual cortex to extra-striate regions and what particular stimulus attribute combinations may differentially be preferred in distinct visual areas.

In order to study in what way chromatic information, originating in distinct retinogeniculo pathways, is differentially processed in cortex, it is crucial to apply physiological stimulus criteria rather than perceptual (see section 1.2.3.6). It is possible to construct chromatic stimulation that emphasizes activity in neurons of either of these pathways, while modulations of other pathways can be kept constant. To achieve this, one must know the chromatic properties of the first input stage to these pathways, which constitute the spectral sensitivities of three light receptor classes in the retina (see section 1.2.1.1). The experimental color-conditions can thus be controlled in terms of cone excitation. How these cone-signals are processed in post-receptoral mechanisms (see section 1.2.1.2 and 2.1.2.1) should be taken into account, to obtain comparable and conclusive results pertaining to these mechanisms. In order to achieve equitable comparison between the response properties in several visual areas, originating in separate pathways, the presented spectral stimulus energy should be computed equal with regard to the initial encoding stage. Comparison of response patterns generated at equal-cone-contrast allows for conclusions regarding selectivity and chromatic preference across visual areas.

It seems that from previous fMRI studies investigating chromatic responses in human cortex, only a minority used cone-contrast equated stimuli (Kleinschmidt *et al.*, 1996; Engel *et al.*, 1997b; Engel & Furmanski, 2001; Wade *et al.*, 2002; Brewer *et al.*, 2005; Liu & Wandell, 2005). Nonetheless, as this group of studies showed, it is possible to vary the stimulus cone-contrast in stages (parametric design) to assess, in what way retinotopically defined visual areas differ in their response characteristics depending on cone-contrast sensitivity.

An influential fMRI study showed, that if cone-contrast stimulation is applied, it is possible to yield meaningful results regarding chromatic sensitivity in V1 and V2 (Engel *et al.*, 1997b). Engel (1997) presented stimuli at several parameterized cone-contrast levels and several directions in cone-contrast space. The cone-contrast space is a three-dimensional physiologically based color space, in which the three retinal receptor-excitations constitute the axes. For a detailed description of this and other color spaces see section 2.1.1.1. Engel (1997) could show that V1 and V2 respond vigorously to stimuli along the L-M and S-(L+M) axis in cone-contrast space and that temporal flicker frequency may have a differential effect on responses elicited by different combinations of cone excitations.

The chromatic stimuli presented by Engel and colleagues were constructed to sample responses to cone-contrast colors within two planes of cone-contrast space. They presented chromatic stimuli within the constant S-plane as well as in the constant L-M-plane, in which

either S-cones or differentially combined L- and M-cones have no contribution to the observed responses. To derive a roughly complete characterization of chromatic response patterns in human visual cortical areas many more planes in cone-contrast space can be tested. We use the same two planes and extend the chromatic stimulus array to essentially five planes in cone-contrast space. Additional planes constitute the constant M-plane, constant L+M-plane and the constant L-plane, in which, either M-, L+M or L-cones have no contribution to the measured responses respectively.

Another main objective of this thesis is to compare how chromatic response patterns in extra-striate areas differ as compared to striate cortex. For that reason, extra-striate regions hV4, V3A and MT+ are compared to primary visual cortex (V1) with respect to their responses to the above described chromatic stimulus array. Furthermore it is of interest to what extent the response characteristics may change as different stimulus velocities and chromatic contrasts are applied in order to achieve a more complete understanding of cortical color and motion processing in the participating regions.

A prior study has explored some effects of presenting cone-contrast colors at different temporal frequencies (Liu & Wandell, 2005). The authors reported cone-contrast sensitivity curves for three color-directions at two velocities. We are able to extend these findings to measure cone-contrast sensitivity curves for thirteen directions and two velocities and additionally measuring five of these directions at three velocities. We are thus able to report speed tuning curves for five cone-contrast space directions in visual areas V1, hV4, V3A and MT+.

These extensive measurements allow for strong conclusions regarding chromatic color contrast preferences throughout visual cortex and its dependence on speed. We are able to relate chromatic speed tuning properties in several visual areas to psychophysically derived motion channels (Gegenfurtner & Hawken, 1996). Additionally, the results provide clues for previously uncertain cortical sources regarding motion detection thresholds using achromatopsic patients (Cavanagh *et al.*, 1998). Furthermore, mixed color responses will be compared to stimuli emphasizing cardinal color directions in human visual cortex. This is of interest because recent neurophysiological studies reported that, starting in striate cortex, neuronal response preferences may shift away from colors solely stimulating the cardinal directions as found in monkey LGN (Lennie *et al.*, 1990; Solomon & Lennie, 2005; Conway & Livingstone, 2006).

The next section will describe in detail how stimulus control was achieved, how cone-contrast colors have been computed as well as a short description of the three applied fMRI analysis methods.

## 2 GENERAL METHODS

### 2.1 Stimulus control

#### 2.1.1 Classifying colors

Colors are often represented in three-dimensional color spaces. The choice of the basis (axes) differs depending on motivation and assumptions. Some color spaces are related in a way that allows for a relatively simple mapping between them, in cases when they have similar theoretical background. This thesis measures and describes physiological correlates of color, contrast and motion velocity variations. A natural choice for a color space to parameterize stimuli for such measurements is the physiologically motivated 3D-cone-contrast space. This color space incorporates the spectral sensitivity of the three cone classes in the human retina and the contrast normalization implemented in the visual system.

##### 2.1.1.1 Physiological color spaces

A well known physiologically motivated color space is the *DKL-space* (Krauskopf *et al.*, 1982; Derrington *et al.*, 1984). It constitutes a three-dimensional extension to the two-dimensional MacLeod and Boynton chromaticity diagram (MacLeod & Boynton, 1979). DKL-space assumes that two chromatic mechanisms exist in which signals from different cone-classes are combined (L-M, S-(L+M)). Activity regarding these mechanisms is represented along two orthogonal axes forming an isoluminant plane. The third axis is (nearly) orthogonal to the isoluminant plane and represents the luminance mechanism. The excitation of the three mechanisms by the adapting background field constitutes the origin of this color space, while excursions along either axis represent excitation through visual stimuli that selectively stimulate the mechanism represented by that axis. Each axis is considered cardinal because signals varying along these directions are carried along separately adaptable pathways (Krauskopf *et al.*, 1982).

The three axes of the *cone-excitation space* are proportional to the quantal catch of the three receptor classes (L, M, S). To represent a test stimulus around the adapting field the quantal catch value from the adapting field is subtracted from the quantal catch values of the test stimulus for each receptor (axis). It can thus be defined as to how much difference in quantal catch can be expected from the test stimulus for each receptor class determined by the cone excitation difference values. The DKL-space is a linear transformation of the axes of local cone excitation space (Eskew *et al.*, 1999).

The color space used to compute the color stimuli used in this thesis is the *cone-contrast space*. It has been recently applied in neurophysiological and behavioral experiments and thus facilitates comparison of results with this work (Engel *et al.*, 1997b; Wade *et al.*, 2002; Chatterjee & Callaway, 2003; Liu & Wandell, 2005; Solomon & Lennie, 2005; Conway & Livingstone, 2006). It is based on physiological mechanisms and takes the adaptational state of the visual system into account. The latter is achieved by dividing the cone excitation difference between adapting background and test stimulation for each cone class, and scaling it with the adapting value (the cone excitation by the background) for each cone class. Hence the three axes represent proportional changes for each cone class of the adapting light level after Webers-Law. In other words: On the three axis we plot  $\Delta S/S$ ,  $\Delta M/M$  and  $\Delta L/L$  respectively, while  $\Delta S$ ,  $\Delta M$  and  $\Delta L$  represent the change in each cone class elicited by the test stimulation as compared to the background excitation (adapting level). L, M and S represent the excitation of the background for each cone class by which the excitational difference is then divided. The cone-contrast space represents sensitivity scaling effects as they are found in the visual system. Cone-contrast coordinates can be transferred into cone excitation space as long as the adaptational level, the background, is kept constant.

The three cardinal mechanisms (Krauskopf *et al.*, 1982) can be incorporated into cone-contrast space. The L-M-mechanism (R/G) would form a diagonal axis within the iso-S-cone-excitation-plane spanned by L- and M-cones, as long as an excitational increase of the L-cone-system is associated with an excitational decrease of the M-cone-system, again, relative to the background. The two opponent colors that stimulate the L-M mechanisms best are either *red*, weighting the L-cones with 1 and the M-cones with -1, and *green*, weighting the L-cone-system with -1 and the M-cone-system with 1 (Cole *et al.*, 1993; Sankeralli & Mullen, 1996; Newton & Eskew, 2003). Keeping the ratios of the weights equal ensures equal stimulation of both receptor classes, albeit of opposite sign for one color.

Another important consequence of assigning equal weights is, that within one plane of the three-dimensional color space, simple sign changes of axes weights generate stimuli along orthogonal mechanisms. For instance assigning equal weights of equal sign to the respective L- and M-cone axis ( $1*L + 1*M$  or  $-1*L -1*M$ ) generates stimuli along a proposed luminance mechanism which also spans a diagonal within the iso-S-cone-excitation-plane lying orthogonal to the afore described L-M mechanism.

Arranging the cone-contrast color stimulation in this way has the following advantages. Firstly, stimulation of either cardinal mechanism (L-M, L+M or S) does not stimulate either mechanism of the other two, a consequence of orthogonality, which is essential to study mechanism responses throughout cortical regions. Secondly, any additional

linear combination of the 3 cone classes can easily be implemented to study higher stage cortical color mechanisms. A pure, perceptually, achromatic B/W-axis can for instance be introduced, weighting all three cone systems equally (L+M+S; see table), by forming one main diagonal within this three-dimensional-space. Thirdly, activity can be plotted in terms of physical stimulus content and thus excitation of the cone systems and not in terms of detection/discrimination mechanisms the properties of which may change as different stimulus form or temporal frequencies are employed (Wandell, 1995; Wandell, 1999).

Table 1 describes the weights we have used to form the axes in cone-contrast space along which cone-contrast stimuli were computed for the experiments reported in this thesis. The associated color perceptions can be judged in Figure 5.2.

	L	M	S
L	1	0	0
M	0	1	0
S	0	0	1
L+M	1	1	0
L-M	1	-1	0
L+S	1	0	1
-L+S	-1	0	1
M+S	0	1	1
-M+S	0	-1	1
L+M+S	1	1	1
L-M+S	1	-1	1
L-M-S	1	-1	-1
S-(L+M)	-1	-1	1

**Table 1: Weights for multiple vector directions in cone-contrast-space** as they are employed in the presented experiments to study chromatic properties of human visual cortex.

Throughout this thesis terminology like luminance and isoluminance is employed. These terms are frequently used in the literature sometimes even without precise definition. The following sections aim to clarify the origin, definition and methodological background that led to the establishment of these terms.

### 2.1.1.2 Luminance

The definition of luminance has been derived from psychophysical measurements on humans by the Commission Internationale de l'Eclairage (CIE) in 1924 and represents the relative luminous efficiency of a human standard observer under photopic conditions (CIE, 1926). The function describes how sensitive the human visual system is to lights at every wavelength of the visible spectrum. The result is the spectral luminosity function,  $V(\lambda)$ . Knowing this standard luminous efficiency function enables one to calculate visual

effectiveness directly from the spectral distribution of energy in a given light source. Specifically, the luminance value of a light is calculated as the integral over wavelength of the radiance of that light weighted with the spectral luminosity function  $V(\lambda)$ .

Physiological correlates of this sensitivity curve are ambiguous, making the exact choice of a cone weight ratio to isolate an alleged pure luminance channel a somewhat difficult matter. It is believed that at some stage beyond the receptor level, signals from the three classes of cones are combined to yield three transformed signals.  $V(\lambda)$  may represent the spectral sensitivity of one of these postreceptoral mechanisms, while the possibility of all three contributing to  $V(\lambda)$  could not be ruled out to date. Lennie and colleagues speculate that  $V(\lambda)$  may be explained as linear combination of the signals from L- and M-cones, approximately in proportions as they exist in the human retina (Lennie *et al.*, 1993). The ratio of L- and M-cones across observers is highly variable (Hagstrom *et al.*, ; Brainard *et al.*, 2000; Krauskopf, 2000b) rendering such criteria nonspecific. General observations exist, stating that the  $V(\lambda)$ -curve could be approximately derived by summing the separately measured L- and M-cone sensitivity curves, but weighting the L-cone sensitivities with a factor of 2 (Nerger & Cicerone, 1992; Dobkins *et al.*, 2000a), resembling an L:M proportion of 2:1. Krauskopf finds the retinal L/M ratio to be equal to 1 (Krauskopf, 2000b), while other investigators report retinal L/M-ratios to lie between 0.82 and 9.71 (Brainard *et al.*, 2000). A relative invariance of these ratios regarding foveal to peripheral position was reported (Nerger & Cicerone, 1992), while it seems as if the ratios approach equilibrium in more peripheral positions (Krauskopf, 2000b; Wikler *et al.*, 2004).

A requirement for our visual stimulation was to design targets that emphasize expected post-receptoral mechanisms while keeping stimulation of other mechanisms minimal (Derrington *et al.*, 1984). For that reason, the stimulus configuration to excite the luminance mechanism was chosen to assign equal weights to L- and M-cones, and thus follows the orthogonality constraint with respect to the R/G-mechanism, taking the difference of the equally weighted L- and M-cone signals. This choice also provides orthogonality with respect to the B/Y mechanism varying the signs of the equally weighted S-cone signals.

While there is wide agreement that S-cones have negligible contribution to  $V(\lambda)$  (Wyszecki & Stiles, 1982; Lennie *et al.*, 1993), it is worth noting that most techniques derive  $V(\lambda)$  with spatial or temporal frequencies that discriminate against signals from short wave sensitive receptors (Lee *et al.*, 1988; Lennie *et al.*, 1993). In addition the form of the curve may change as different techniques are applied to derive it (Lennie *et al.*, 1993). The method that formed the basis for the CIE 1924 standard is the heterochromatic flicker photometry (HFP), in which an observer adjusts the intensity of two flickering lights until the perceived

flicker is minimized. At the point of minimum flicker the two lights are believed to be equiluminous or isoluminant.

### **2.1.1.3 Isoluminance**

It has been reported that chromatic and luminance motion mechanisms appear to have fundamentally different properties (Ramachandran & Gregory, 1978). As indicated above, the methodological dependence of luminance measures directly applies to isoluminance measurements accordingly. It is thus of interest in what way these two entities relate and how they are typically derived. Ex ante, the definition of isoluminance is tightly coupled to the methodology by which it is derived.

Heterochromatic flicker photometry (HFP) uses fairly high flicker rates (~15 Hz) to equalize luminosity intensities of two colors with different spectral compositions and thus derives at some magnocellularly biased luminance match (Lee *et al.*, 1988; Lennie *et al.*, 1993; Dobkins *et al.*, 2000; Dobkins *et al.*, 2000a), which can be modeled as the sum of L- and M-cone sensitivities (L+M) (but see section 2.1.1.2). There is reason to believe that differential L- and M-cone signals (L-M) might also contribute to luminance matches as temporal frequency is lowered (Cavanagh *et al.*, 1987 ; Webster & Mollon, 1997; Dobkins *et al.*, 2000; Dobkins *et al.*, 2000a). The method of heterochromatic brightness matching (HBM) is thought to rely on signals from both L+M and L-M mechanisms and involves directly assessing and matching the brightness of two stationary colors (Dobkins *et al.*, 2000). The two colors will be perceived as equally luminous, and thus isoluminant, when the signals of L- and M-cone excitation, produced by the spectral composition of one color, equal the L- and M-cone excitation produced by the spectral composition of the other color. As expected from a task which theoretically employs two mechanisms (HBM), the two colors set to be equally bright in HBM are mostly not perceived equiluminant in the HFP-task, theoretically relying only on one mechanisms (Webster & Mollon, 1993; Smith *et al.*, 1994). Webster and Mollon inferred that at low temporal frequencies both perceived lightness and minimum-motion settings appear to depend on channels that do not represent luminance and color independently (Webster & Mollon, 1993).

The arguments above make clear, that concepts, such as luminance or isoluminance are highly dependent on the methodology by which they are derived. The main interest of this work lies in cortical responses to color, for which a physically motivated stimulus control seems more appropriate as a perceptual but physiologically biased one. We thus indicate our colors as chromatic stimuli as opposed to isoluminant, while the luminance stimulation follows conventional nomenclature (but see next section). Stimuli used in this thesis follow

the conventions of the cone-contrast space and its applications (see above), because the spectral cone sensitivities have a solid, task independent, foundation. Using cone-contrast space, the stimuli can be parameterized, which would not be possible using just isoluminance criteria (Schnapf *et al.*, 1987; Stockman & Sharpe, 1998; Stockman *et al.*, 1999; Stockman & Sharpe, 2000).

#### **2.1.1.4 Luminance vs. achromatic stimuli**

Luminance and perceptually achromatic stimuli are often erroneously employed as being synonymous. Perceptually these two stimulation types can be very easily distinguished.

Neuronal projections from the retina to LGN constitute at least three independent mechanisms (Derrington *et al.*, 1984). A first one responds to the difference of L- and M-cones (L-M) and a second responds to the difference between the excitation of the S-cones on the one hand and the sum of L- and M- cones on the other hand (S-(L+M)). These two mechanisms are chromatic mechanisms because stimuli that isolate the R/G mechanism best (L-M) appear red/green and stimuli that excite the B/Y mechanism best (S-(L+M)) appear blue/yellow. In order to isolate the B/Y mechanism best however, stimuli should only vary the modulation of the S-cones to control for luminance contribution. These stimuli appear greenish/purple.

A third axis, perpendicular to the chromatic axis is believed to represent the luminance axis. As indicated above, a luminance mechanism may sum L-and M-cone responses and omit S-cone signals (Judd 1951, Wyszecki & Stiles 1982). Stimuli exciting only the L- and M-cones with the same sign appear purple/yellow and not black and white (achromatic). A stimulus designed to excite all three cone classes equally, however, would appear black and white and can thus be referred to as perceptually achromatic. This axis, unfortunately, is not precisely orthogonal to the S and L-M axis in cone-contrast space. A perceptually achromatic stimulus would thus also activate the presumed luminance mechanism (L+M) and the B/Y mechanism (S). We stress this, because we will show that cortical responses to L+M-compared to L+M+S-stimuli differ substantially especially at high speeds. Unless indicated differently, we refer to L+M+S-modulation as achromatic, L+M-modulation as luminance and opponent (difference in sign) modulation as chromatic ((L-M & -L+M), (S & -S), (S-L-M & -S+L+M)).

#### **2.1.1.5 Color vs. luminance**

Experiment 2 will investigate in what way responses to chromatic stimuli in several visual areas differ as the targets are moved at different velocities. In order to allow for

equitable comparison between responses in visual areas to the various color- and the luminance-stimulation and clearly assess the effects of a given additional stimulus attribute, in the case of experiment 2, pattern velocity, it is crucial to match all stimuli regarding their cone-contrast excitation. It is well established that low-level visual functions depend heavily on the magnitude of the input signal (contrast). Nearly all neurons in the visual system give faster and stronger responses to stimuli of higher contrasts (Albrecht & Hamilton, 1982). This effect can also be observed using fMRI in human V1 (Boynton *et al.*, 1996) and extra-striate areas investigated with incremental chromatic-contrast (Engel *et al.*, 1997b; Wandell *et al.*, 1999; Liu & Wandell, 2005). In order to measure response differences, arising from differential chromatic preferences in the visual areas, independent of the applied (chromatic) contrast, we compute all stimulus colors along cone-contrast space direction in a way, that their contrast modulation matches physically at the initial retinal input stage (Wandell, 1995; Kaiser & Boynton, 1996). It becomes thus possible to measure sensitivity hierarchies for the visual areas, derived solely from chromaticity differences as one compares responses at the same pattern velocity. Additionally, it is possible to report response differences depending on pattern velocity as responses to the same color are compared, moving at different speeds. One can thus be certain that observed response differences did not arise from contrast differences but must be associated to the tested stimulus attributes as for instance various colors or speeds.

The following section describes how cone-contrast of the stimulation is controlled.

## **2.1.2 Computing cone-contrast colors**

### **2.1.2.1 Light to cone excitations**

Light sources in color experiments are typically projectors or monitors, which generate light through three red (R), green (G) and blue (B) phosphors (guns) at each pixel. Each single phosphor class emits light over the entire visual spectrum; radiated energy however is not equal at all wavelengths. For instance, the R-gun emits more energy in the long-wave range of the visual spectrum, where light appears red. The G-gun emits more energy in the middle-wave range of the visual spectrum, where light appears green and the B-gun emits more energy in the short-wave range of the visual spectrum, where light appears blue.

Two sets of data are essentially required in order to compute the intensity levels by which each class of retinal receptors is stimulated by a given light. Firstly, the spectral sensitivity of each cone class and secondly, the energy distribution (spectral density) of the given light over the whole visible spectrum. The spectral sensitivity of each cone class is

provided in the literature (Schnapf *et al.*, 1987), and tables can also be downloaded from the internet ([www.cvision.ucsd.edu](http://www.cvision.ucsd.edu)). The spectral density of the light source can be measured by the means of a photospectroradiometer for a set of wavelengths in the visible part of the spectrum.

As stated above, each cone class is sensitive to light of all wavelengths by a certain amount, but it is most receptive within a certain wavelength range. If one wishes to compute how strongly a cone class, let's say the L-cones ( $l$ ), is excited at *one* particular wavelength ( $\lambda$ ), one must weight the spectral sensitivity of the L-cone class at that particular wavelength ( $l(\lambda)$ ) with the emitted energy from the light source, e.g. R-gun at that wavelength ( $r(\lambda)$ ). In order to compute the excitation of one cone class, e.g. the L-cone system, by the, e.g. R-gun of a CRT over all wavelengths, the spectral density of the R-gun must be weighted by the spectral sensitivity of the L-cone system. The products of the excitation values at every wavelength step give the excitation in the L-cones, elicited solely by the R-gun. This can be expressed as:

$$L_R = \sum_{\lambda} l(\lambda) * r(\lambda).$$

$L_R$  = L-cone excitation values by R-gun,

$l(\lambda)$  = L-cone sensitivity at wavelength  $\lambda$ ,

$r(\lambda)$  = spectral density (energy radiance) of the R-gun at every wavelength of the visual spectrum.

To compute the excitation of the L-cones elicited by all three phosphors, each spectral density function per phosphor has to be weighted with the L-cone system sensitivity function separately and then summed:

$$L = \sum_{\lambda} l(\lambda) * r(\lambda) + \sum_{\lambda} l(\lambda) * g(\lambda) + \sum_{\lambda} l(\lambda) * b(\lambda).$$

$L$  = L-cone excitation,

$l(\lambda)$  = L-cone sensitivity at wavelength  $\lambda$ ,

$r(\lambda), g(\lambda), b(\lambda)$  = spectral density (energy radiance) of the R-, B-, and G-gun at wavelength  $\lambda$ .

The excitations elicited by all three phosphors in all three cone-types can be calculated by the following system of equations:

$$\begin{aligned}
 L &= \sum_{\lambda} l(\lambda) * r(\lambda) + \sum_{\lambda} l(\lambda) * g(\lambda) + \sum_{\lambda} l(\lambda) * b(\lambda), \\
 M &= \sum_{\lambda} m(\lambda) * r(\lambda) + \sum_{\lambda} m(\lambda) * g(\lambda) + \sum_{\lambda} m(\lambda) * b(\lambda), \\
 S &= \sum_{\lambda} s(\lambda) * r(\lambda) + \sum_{\lambda} s(\lambda) * g(\lambda) + \sum_{\lambda} s(\lambda) * b(\lambda).
 \end{aligned}$$

L, M, S = cone excitation values

$l(\lambda), m(\lambda), s(\lambda)$  = cone sensitivity values at wavelength  $\lambda$

$r(\lambda), g(\lambda), b(\lambda)$  = spectral density (energy radiance) of the R-, B-, and G-gun at wavelength  $\lambda$

All of the above is valid, at any one specific radiance intensity of the RGB-guns. The intensity level for each gun can be altered separately. For this reason an additional vector is introduced, representing the intensity levels for every single gun. The above cone excitation computation can be summarized as a 3x3 transformation matrix. This transformation matrix can now be multiplied with the intensity vector of each single gun depending on the adjusted intensity of each gun on the CRT-screen:

$$\begin{bmatrix} L \\ M \\ S \end{bmatrix} = \begin{bmatrix} \sum_{\lambda} l(\lambda) * r(\lambda) & \sum_{\lambda} l(\lambda) * g(\lambda) & \sum_{\lambda} l(\lambda) * b(\lambda) \\ \sum_{\lambda} m(\lambda) * r(\lambda) & \sum_{\lambda} m(\lambda) * g(\lambda) & \sum_{\lambda} m(\lambda) * b(\lambda) \\ \sum_{\lambda} s(\lambda) * r(\lambda) & \sum_{\lambda} s(\lambda) * g(\lambda) & \sum_{\lambda} s(\lambda) * b(\lambda) \end{bmatrix} \begin{bmatrix} R \\ G \\ B \end{bmatrix}$$

R, G, B = Scaling values for Red-, Green- and Blue-gun (between 0 and 1)

Values of the intensity vector typically range between 0 and 1, where 0 means that the gun does not emit any photons, while 1 represents the maximal amount of photon emission possible. In conventional monitors the increase of emission of each single gun is rarely a linear function of the RGB-values used in the intensity vector. This is however assumed when using the above matrix multiplication. It is thus essential to measure the intensity function for each gun at each intensity level (typically 0 to 255) and linearize the intensity curve. This is achieved by creating lookup tables in which for instance a doubling of intensity is actually accompanied with a doubling of photon emission. This point is stressed because it entails physiological reasoning. Throughout this thesis, cone-contrast will be represented as the vector length of the three dimensional vector  $s$ , representing the cone-contrast in the direction of the vector in cone-contrast space.

$s = (\Delta L/L, \Delta M/M, \Delta S/S)$  (Three dimensional color vector).

$|s| = [\Delta(L/L)^2 + \Delta(M/M)^2 + \Delta(S/S)^2]^{1/2}$  (RMS-cone-contrast)

$L, M, S$  = excitation by the background for each cone class,

$\Delta L, \Delta M, \Delta S$  = excitation by the test color in each cone class,

$\Delta L/L, \Delta M/M, \Delta S/S$  = change in each cone class elicited by the test stimulation, as compared to the background excitation (adapting level).

In the experiments presented here, RGB-values had to be computed to produce a certain cone-contrast. This approach will be described in the next section.

### **2.1.2.2 Cone excitations to light**

In order to derive RGB-values which stimulate the visual system at a desired cone-contrast, the above equation must adopt the appropriate values for L, M and S (e.g.:  $[L+L*0.1, M+M*0, S+S*0]$ ). This cone-contrast for instance would stimulate the L-cone system 10% more than the background, while keeping stimulation of the other two cone classes equal. In order to obtain the RGB-values that produce this contrast the inverse of the transformation matrix must be multiplied with the LMS-vector.

The afore mentioned device dependence on spectral and intensity distributions for each gun poses limitations regarding maximal attainable cone-contrasts. Along some cone-contrast space directions, for instance L-M, the highest maximal cone-contrast is lower than any other direction, because the M- and L-cones have highly overlapping sensitivity functions, which means that the probability of catching photons is highly similar. It follows that strongest limitations occur when two cone types need to be stimulated differentially, as necessary for L-M stimuli. Figure 2.1 illustrates two examples:

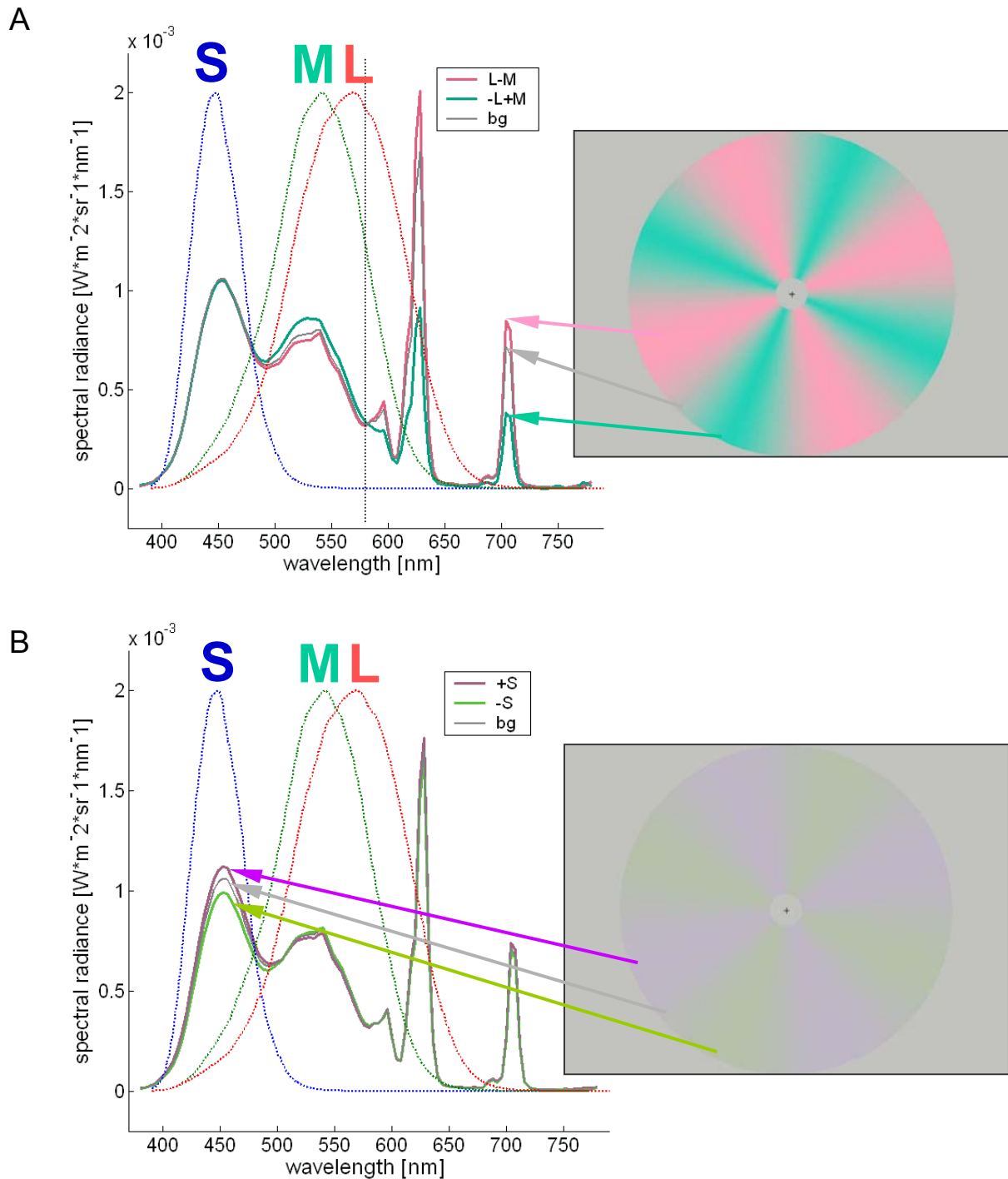


**Figure 2.1: Stimulus control for cone-contrast stimulation**

**A: L-M-cone-contrast stimulus control:** Right panel: 14% L-M RMS-cone-contrast radial sinusoidal grating (annulus) as presented in Experiment 2. Left panel: Spectral energy plot of the stimulus components as measured with a pr650 spectroradiometer. Solid lines (spectra of the components): gray (background), pink (L-M), green (-L+M). Dotted lines (normalized cone sensitivity functions): blue (S-cones), green (M-cones), red (L-cones), vertical black dotted line (lights with wavelengths beyond this point excite the L-cones more than the M-cones). Note: averaging the spectral radiance over wavelength for both test colors would result in the background spectral radiance. A L-M stimulus contains higher spectral radiance in wavelengths exciting the L-cones than the background resulting in a reddish percept. A -L+M stimulus contains more spectral radiance in wavelengths exciting the M-cones than the background resulting in a greenish percept. A higher spectral energy exciting L-cones in the L-M color is counterbalanced with a lower excitation of the M-cones and vice versa, for the -L+M color. The color spectra do not diverge from the background spectra for wavelengths, which would excite the S-cones. This stimulus configuration isolates the L-M (R/G) mechanism.

**B: S-cone-contrast stimulus control:** Right panel: 14% pure S- RMS-cone-contrast radial sinusoidal grating (annulus) as presented in Experiment 2. Left panel: Spectral energy plot of the stimulus components as measured with a pr650 spectroradiometer. Solid lines (spectra of the components): gray (background), blue/purple (+S), greenish/yellow (-S). The dotted lines represent the normalized cone sensitivity functions as in A. Note: averaging the spectral radiance over wavelength for both test colors would result in the background spectral radiance. A +S-color contains higher spectral radiance in wavelengths exciting the S-cones than the background resulting in a bluish/purple percept. A -S-color contains less energy in wavelengths exciting the S-cones than the background resulting in a greenish/yellow percept. The color spectra do not diverge from the background spectra for wavelengths, which would excite the L- or M-cones. This stimulus configuration isolates the S-cones.

## 2.2 Magnetic resonance imaging

Functional magnetic resonance imaging must be considered the fastest growing application for noninvasive neurophysiological methods for in vivo human brain imaging. The technique is based on metabolic processes leading to changes of oxygen content and blood flow in the living brain. These factors are coupled with neural activation, albeit indirectly. High spatial resolution is an advantage this method provides. Experiments in this thesis put emphasis on spatial precision to distinguish responses in different areas within human cortex, making fMRI the method of choice.

Brain activity is associated with depolarization of membrane potentials of neurons in active regions. Neural activity is energy consuming, at the expense of oxygen. Within a few seconds of regional neural activity, compensatory processes lead to local increase of blood flow and blood volume. This process is known as neurovascular coupling. The local increase of oxygenated blood exceeds the metabolically needed oxygen consumption, which leads to a netto increase of oxygenated hemoglobin in the vessels and capillaries of active brain tissue. This local increase of blood oxygenation can be detected by the blood oxygenation level dependent (BOLD) functional magnetic resonance imaging (fMRI) technique, using for instance an echo-planar imaging sequence (EPI), exploiting the different magnetic properties of oxygenated and deoxygenated blood (Thulborn *et al.*, 1982). While oxygenated hemoglobin shows diamagnetic properties (magnetically transparent), deoxygenated blood is paramagnetic (not magnetically transparent). The ratio between dia- and paramagnetic hemoglobin is accountable for the MR-signal, which can be observed in contrast changes in the MR-images, where active cortical regions are typically brighter than inactive regions. This spawned the term: BOLD-contrast or BOLD-signal (Blood Oxygenation Level Dependent) (Ogawa *et al.*, 1990; Turner *et al.*, 1991; Ogawa *et al.*, 1992).

The differences of signal strength between stimulus condition and rest condition depends on the static magnetic field strength of the MR-magnet and is typically less than 4% for scanners up to 3T (Tesla). The low signal to noise ratio may be accommodated by multiple

presentations of the experimental stimulation and additional averaging of the stimulus related images.

Within this thesis, three different fMRI-analysis methods are employed. Common to all three methods is an initial motion correction of the acquired brain volumes removing movement artifacts of the subject's head during the MR-measurements. The artifacts are caused by the subjects' motion, respiration and pulse. The rigid-body-motion-correction algorithm implemented in the SPM99 software was used (SPM99, Wellcome Department for Cognitive Neurology, London, UK). All three methods initially reconstruct the fMRI time series in each voxel independent of neighboring voxels, which entails linear trend removal from the individual voxel time series.

### **2.2.1 Method 1 – phase encoding**

This method was used for retinotopic mapping of the borders of the visual areas and in MT localizer experiments. A prerequisite for this method constitutes a periodic presentation of the visual stimuli. A simple example for only two stimulus conditions will illustrate this method.

Any cortical region that represents the entire visual field retinotopically should by definition contain neurons that respond to visual stimulation in the center of the visual field and spatially separated neurons that respond to visual stimulation outside of the central visual fields. In order to identify these regions a simple periodic visual stimulation may be used that alternates between a center and a surround stimulus at constant frequency. We map these regions routinely by presenting a center stimulus for 12 s followed by a surround stimulus for 12 s, while sampling brain activity every 2 s. This stimulus sequence is presented 20 times per run leaving us with an alternating frequency of 20 cycles per run which lasts for 8 minutes equivalent to 240 acquired scans or brain volumes.

Figure 2.2 illustrates the stimuli, stimulation time course and corresponding BOLD response time courses for small regions of interest in primary visual cortex. Dotted red and blue boxcar functions describe the time course of the center and surround stimulus onsets respectively. They are out of phase by 180°. Firstly, the fMRI time series for each voxel is generated by concatenating the intensity values at every single voxels' coordinates from the scanned brain volumes measured every 2 s. Secondly, the time series for each voxel is computed as a percentage modulation of its mean intensity value. Activity elicited by the stimulation is measured by fitting the phase and amplitude with a sinusoidal function (black dotted line in Figure 2.2) at the stimulus alternation frequency (1/20 cycles/scan = 20 presentations) to the time series, essentially by performing a Fourier analysis. At each voxel

the response phase indicates the preferred stimulus. Figure 2.2 demonstrates how voxels, taken from separate locations in V1, follow either stimulus time course. Note how the BOLD-response time courses differ regarding their phase while the frequency is equal and corresponds to the stimulus alternation frequency. Red arrows indicate different phases following the preferred visual stimulation within the underlying voxels from which these two responses were taken (ROIs).

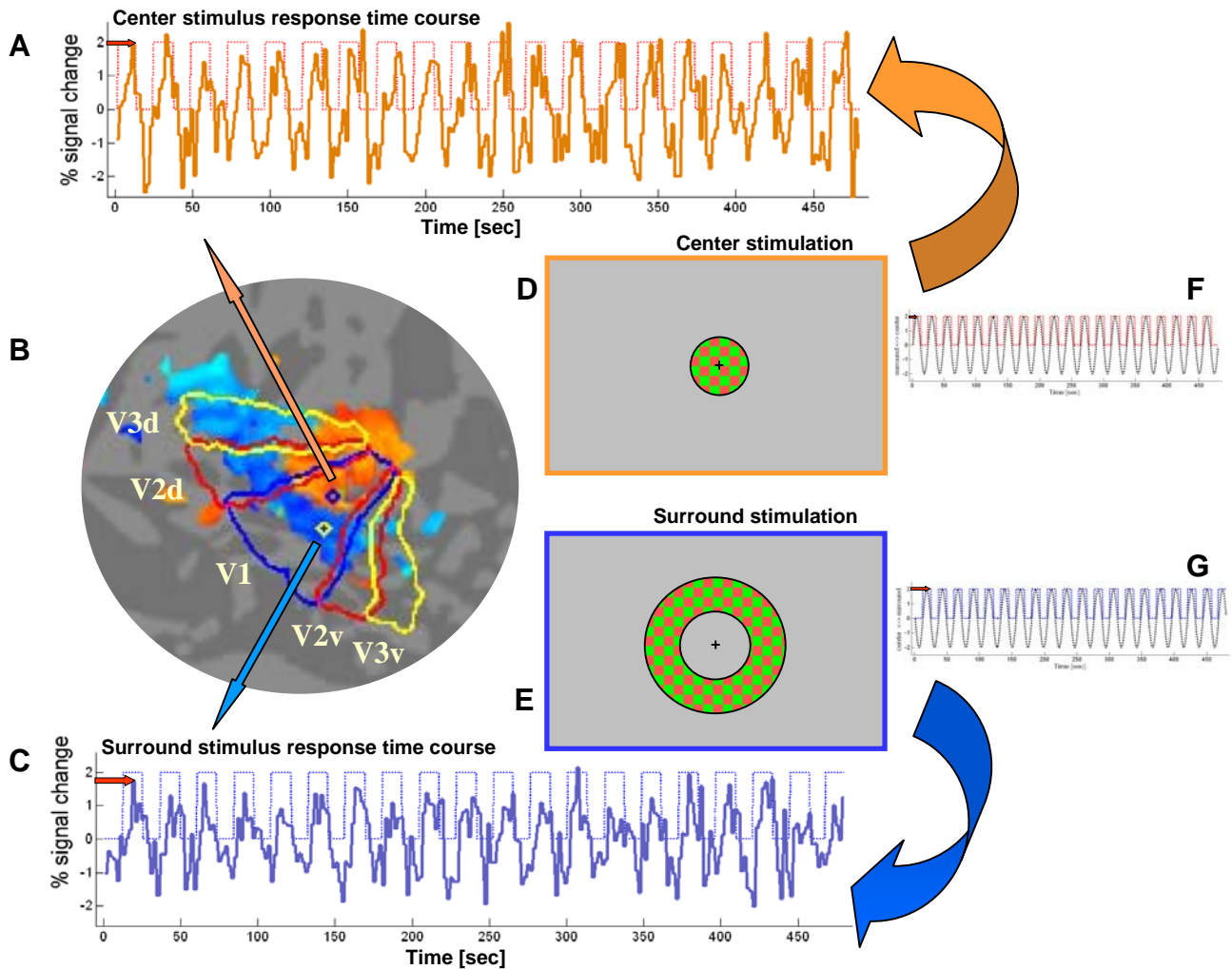


**Figure 2.2: Phase Encoding.** **A** and **C**: The BOLD-activation time courses elicited by a center-surround stimulus in occipital cortex. The solid orange line represents the measured response time course for a region of interest (ROI) indicated as a blue circle in **B**. The dotted red line indicates the stimulus on- and offset for center stimulus presentation as illustrated in panel **D**. **B**: Center (orange) and surround (blue) activation on flat map representation for one hemisphere. Solid lines represent borders of visual areas (V1=blue, V2=red, V3=yellow). **C**: The solid blue line represents the measured response time course for a region of interest (ROI) indicated as yellow circle in **B**. Dotted blue line indicates the stimulus on- and offset for surround stimulus presentation as illustrated in panel **E**. **D**: Center stimulus. **E**: Surround stimulus. **F**: Red dotted line shows stimulus on- and offset for center stimulus presentation. Black dotted line represents the alternation frequency for the center stimulus. **G**: Blue dotted line stimulus on- and offset for surround stimulus presentation. Black dotted line represents the alternation frequency for the surround stimulus. Red arrows in **A** and **F** show the short phase of the alternation frequency for center stimulation. Red arrows in **C** and **G** exemplify the longer phase of the alternation frequency for surround stimulation.

Many more stimulus conditions and orders can be presented as long as the alternation frequency is kept equal and constant. This will be demonstrated in Experiment 1. This procedure implicitly models the BOLD-response as a harmonic function (Bandettini *et al.*, 1993; Press *et al.*, 2001), which differs from Method 2.

### 2.2.2 Method 2 – canonical BOLD fitting (GLM)

The basic principle of method 2 constitutes a comparison of a theoretically predicted time course with the measured BOLD time series at every voxel. The background for the theoretical time course is the characteristic BOLD-signal distribution over time known as the hemodynamic response function (HRF) (Figure 2.3). Specifically the assumption, that with the onset of neural activity elicited by some experimental stimulation (stimulation condition), the HRF raises with temporal delay in an active cortical region and drops with the absence of stimulation as neural activity decreases accordingly (rest condition) (see Figure 2.4 and 2.5).

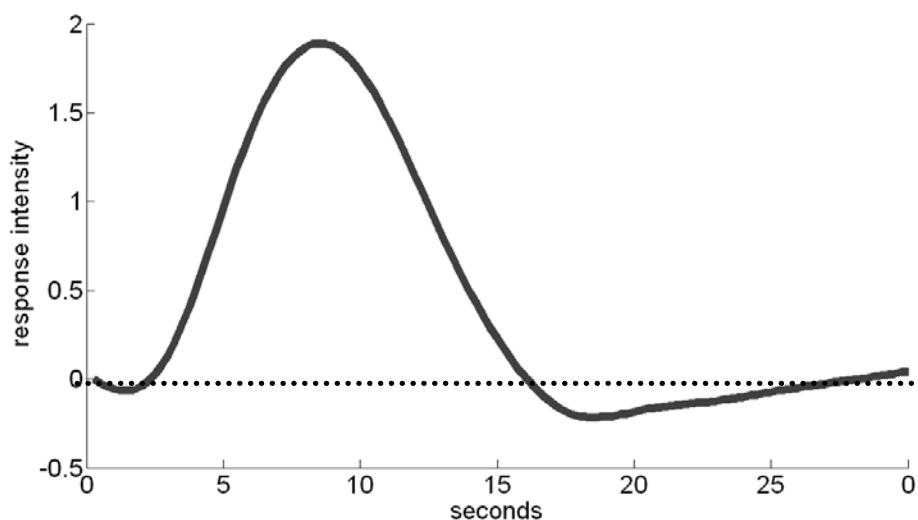


**Figure 2.3: A canonical BOLD-response function as it is used in SPM**

The BOLD-response onset lags behind stimulus onset, hypothetically given at 0 seconds, a well-known feature of the BOLD contrast. The maximum BOLD-response amplitude is reached 4-10 s after stimulus onset while the BOLD relaxation period after stimulus offset can range from 10-20 s.

The comparison of the empirically measured and the theoretically predicted time courses for every voxel can be accomplished by application of multiple regression analysis using matrix notation and the general linear model (GLM). The expected BOLD-response time courses are coded in a design matrix, in which each column represents an experimental condition and each row one image acquisition of the entire fMRI measurement, depicted in Figure 2.4. For each condition, the theoretically predicted response time course (predictor variable) is obtained by convolving the stimulus time course for each condition with the same

assumed canonical HRF-function, as depicted in Figure 2.3. Hence the design matrix should explain the variance of the measured empirical signal time course with minimal residual error. The goal is to minimize the least-square-error by assigning appropriate weights to the predictor variables using multiple regression and the GLM.

In common analysis tools such as SPM99 (<http://www.fil.ion.ucl.ac.uk/spm>) multiple regression is applied at every voxel. Within each voxel, the value of the weight at a predictor variable represents the contribution to the measured time course for that condition. Cortical regions are identified which follow a predicted time course for a given condition and thus may be associated with the cortical processing of that condition. Figure 2.4 illustrates the GLM weighting procedure for one voxel using the center/surround stimulation as an example. Interpretatively, one would conclude that the voxel from which the BOLD response time course in Figure 2.4 was taken responds stronger and follows the expected time course of the first condition substantially better. Hence neural populations within that voxel represent the central visual field. This procedure is applied to every voxel resulting in maps of brain activity representing strength of BOLD-response and fitting values (betas) for any predefined time course and condition.

In order to find cortical regions that prefer one stimulus condition over the other, as in method 1, respective statistical maps can be calculated using the subtraction method. A response map elicited by, for instance condition one, is subtracted from a response map elicited by condition two, resulting in a difference map which contains only voxels, exceeding a predefined significance level. These statistically significant voxels regarding the difference between the two conditions, yielded BOLD-response time courses, which fit the predicted response of condition two significantly better than condition one. Since many voxels are compared simultaneously, the ‘problem of multiple testing’ arises which entails that at constant alpha of 5% ( $\alpha$ = first order error) the probability of observing false positive results increases proportionally to the number of conducted single tests (number of compared voxels). To control for this problem many procedures exist, but the most prevalently used is the Bonferroni correction, which corrects the applied significance level  $\alpha$  by the number  $k$  of conducted independent tests ( $\alpha_{corrected} = \alpha/k$ ). Another approach to decrease the number of independent tests is by restricting the analysis to one or a few pre-defined regions of interest (ROI-analysis) the number of comparisons by ROI-analysis. A priori hypothesis are necessary to define ROIs, amongst which are for instance anatomical landmarks or localizing regions of interest based on their functional properties.

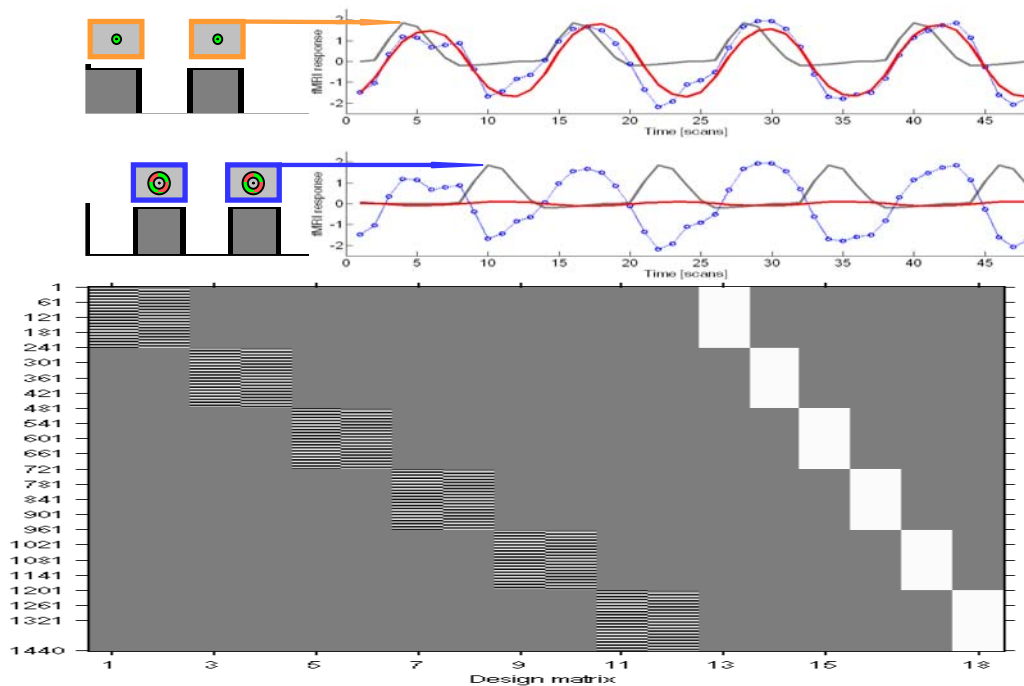


**Figure 2.4: GLM weighting procedure for one voxel using the center/surround stimulation.**

Blue lines plot the measured BOLD response values in that voxel. The dark gray lines represent the predicted time course for the first condition (center stimulation) in the upper panel and second condition (peripheral stimulation) in the lower panel respectively. The red lines indicate the fitted response function generated by SPM99. In the upper panel the fitted response follows the predicted time course for the first condition, while in the lower panel a rather poor fit between the predicted time course of the second condition and the measured values is obvious. The GLM would hence attribute a high weight (beta) to the explanatory variable condition one, while the second explanatory variable, condition two, would be weighted substantially lower and can also become negative. The two different time courses can statistically be compared by means of F-tests or t-tests in which the absolute weight (beta) difference determines the effect size.

### 2.2.3 Method 3 – deconvoluting BOLD-response functions

The following section is divided into two parts. The first part will describe the assumptions underlying a reliable deconvolution of time-series data by contrasting block- and event-related designs. The second part will describe the weighted maximum likelihood estimate analysis (WMLE) employed in Experiment 3 (Hinrichs *et al.*, 2000).

#### 2.2.3.1 Block design vs. event related design

The major challenge facing every complex fMRI design is the overlapping of BOLD responses, which occurs when two stimuli are presented closely in time<sup>2</sup>. The overlap effect is however specifically desired in block stimulation in which, for an elongated period of time,

<sup>2</sup> In the case of fMRI, close means within 30s.

the same condition is presented in order to increase the signal to noise ratio. A linear summation of the BOLD-responses is assumed.

Figure 2.5 illustrates the phenomenon of linear summation considering light flashes as stimulus events which, presented in succession, compose a block presentation. In panel 2.5A, a light is flashed for a short amount of time in the beginning of the scanning session. Panel 2.5B depicts the sluggish BOLD response that can be encountered in regions of visual cortex being responsive to this kind of stimulation. Note, that approximately 4-10 s (2-5 scans,  $TR=2$ ), are needed for the BOLD response to reach a maximum. The response curve in panel 2.5B was modeled by convolving the stimulus time course with the canonical HRF depicted in Figure 2.3. Panel 2.5C shows another light stimulus that was flashed later within the scanning session and the result is a likewise delayed BOLD response. When both flashes are presented fairly close in time to one another, as in panel 2.5E, both BOLD response functions show substantial overlap (2.5F). The resultant BOLD response function is characterized by increased amplitude, which again was modeled as a convolution of the sum of the single stimulation time courses with the canonical BOLD function in Figure 2.3.

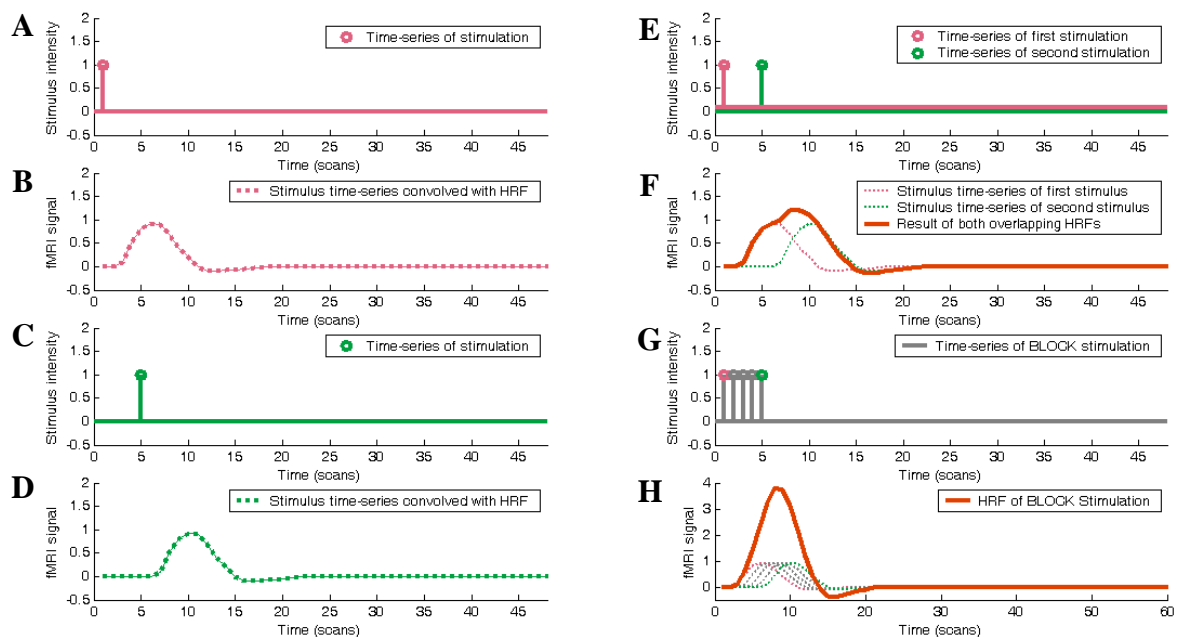


**Figure 2.5: Linear summation assumption of BOLD-responses.**

**A:** A light flash presented at the beginning of the scanning session. **B:** Expected BOLD-response for voxels associated with visual processing from stimulation in A. The response time course represents a convolution of the stimulus presentation time course in A and the canonical BOLD-response function (Figure 2.3). **C:** A light-flash presented 10 seconds after the beginning of the scanning session. **D:** Expected BOLD-response from stimulation in C. The response time course is a convolution of the stimulus presentation time course in C and the canonical BOLD-response function (Figure 2.3). **E:** Two light flashes are presented in closer succession. **F:** Substantial overlap of BOLD-responses generated by stimulus presentation in E. **G:** Successive presentation of light flashes forming a stimulus block. **H:** Substantial overlap generated by stimuli in G. Additive overlap raises the signal to noise ratio considerably. The linearity assumption however is not infinitely valid because BOLD-response amplitudes typically reach a saturation plateau which cannot be exceeded (Boynton *et al.*, 1996).

The desired increasing signal to noise effect of block stimulations becomes clear in panel 2.5G and 2.5H. As light flashes are presented in temporally close succession, the single events form a block of stimulation (2.5G). The overlapping response functions are assumed to add up linearly, increasing the signal to noise ratio substantially (Boynton *et al.*, 1996). Nonetheless, block design stimuli take time, not only because the actual stimulus presentation is rather long, but also because stimulations containing no experimental variable are typically presented (baseline condition). The presentation of a baseline condition after the experimental block-condition allows the large BOLD-response in active regions to relax and provides the experimenter with a neutral condition, with which the experimental conditions can be statistically compared.

If a block design is desired in combination with a multitude of conditions however, it has been shown that a balanced randomization of conditions permits omission of a designated baseline between the experimental stimulus presentations (Engel, 2005). A balanced randomization of the stimulus presentation order is subject to the constraint that each condition is to be preceded by each of the other conditions equally often. This procedure leads to the same prior block history for every condition and was used to generate the stimulus presentation sequence for experiment 2. The underlying assumption is, that equal overlap of BOLD-response functions does not alter response differences between conditions, which may subsequently statistically be analyzed.

In contrast to the traditional block design fMRI experiment, event related fMRI experiments have become increasingly popular, addressing research questions, which cannot be tested using blocked stimulation. Block design disadvantages such as adaptational, sequential and habitational effects, can be minimized by event related fMRI experiments, applying randomization and rapid presentation of various experimental conditions (Buckner *et al.*, 1996; Dale & Buckner, 1997; Josephs *et al.*, 1997; Rosen *et al.*, 1998; Dale, 1999). Stimuli may be presented with ISIs in the range of a few seconds, taking into account that subsequent HRFs will overlap significantly (Boynton *et al.*, 1996). Figure 2.5E to 2.5H showed how overlapping response functions elicited by different types of light flashes sum to generate the measured BOLD-signal, but implicitly assumed that different light flashes elicit the same BOLD-response amplitude, which must not necessarily be the case. Figure 2.6 illustrates how the measured BOLD-signal time course can have numerous underlying BOLD-response functions presumably elicited by different stimulation conditions. However, responses to the same stimulus may be present in several regions of the brain but shape and amplitude may vary due to different vascularization and hemodynamic properties of the

constituting cell conglomerates within the respective regions (Logothetis, 2003). This must be taken into account as rapid event related stimulus sequences are analyzed.

As stated above and exemplified in Figure 2.5, an expected HRF could be modeled by convolution of the known stimulus time course and a theoretically assumed BOLD-response function (Figure 2.3). This process can also be reversed, applying a deconvolution of the measured BOLD-response time course and the known stimulus presentation sequence. First ideas towards deconvolving fMRI-time series have been proposed by Josephs et al. (1997) and refined by Dale and Buckner (1997) and Rosen et al. (1998) (Dale & Buckner, 1997; Josephs *et al.*, 1997; Rosen *et al.*, 1998).

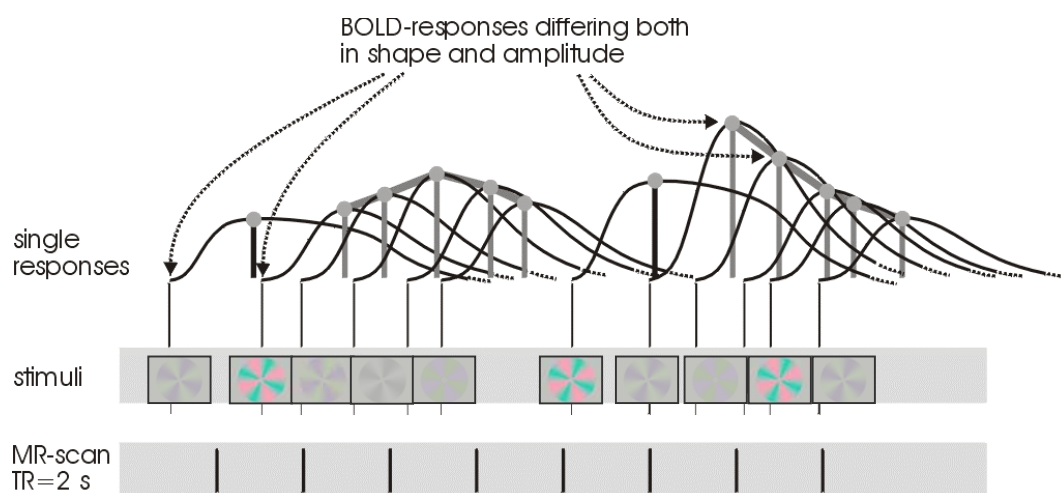


**Figure 2.6: BOLD-response functions may differ in shape and amplitude**

Shape and amplitude of BOLD-response functions may differ depending on stimulus type as well as differing hemodynamic response properties of cortical regions

### 2.2.3.2 Weighted Maximum Likelihood Estimate (WMLE)

Because event-related designs are more susceptible to the shape of the canonical BOLD-response function, a deconvolution method is chosen to analyze the event-related data set of experiment 3. The method of choice was the weighted maximum likelihood estimate (WMLE), which was put forth by Hinrichs et al. (2000), as a refinement of Dale and Buckners approach (Dale & Buckner, 1997; Hinrichs *et al.*, 2000). While method 1 (phase-encoding) correlates a predefined sinusoidal function representing the stimulus alternation and method 2 (canonical BOLD fitting) fits a predefined canonical BOLD-response function at the stimulus presentation time-course, the WMLE approach is a data based procedure with no fixed prior canonical response function. In short, the procedure simultaneously estimates and weights the shape of the most probable hemodynamic response function based on the measured BOLD-response function per voxel, and the presented stimulus event time course. The estimated

weights for each presented condition can then be statistically compared and used to model cortical sensitivity depending on different levels of each applied condition.

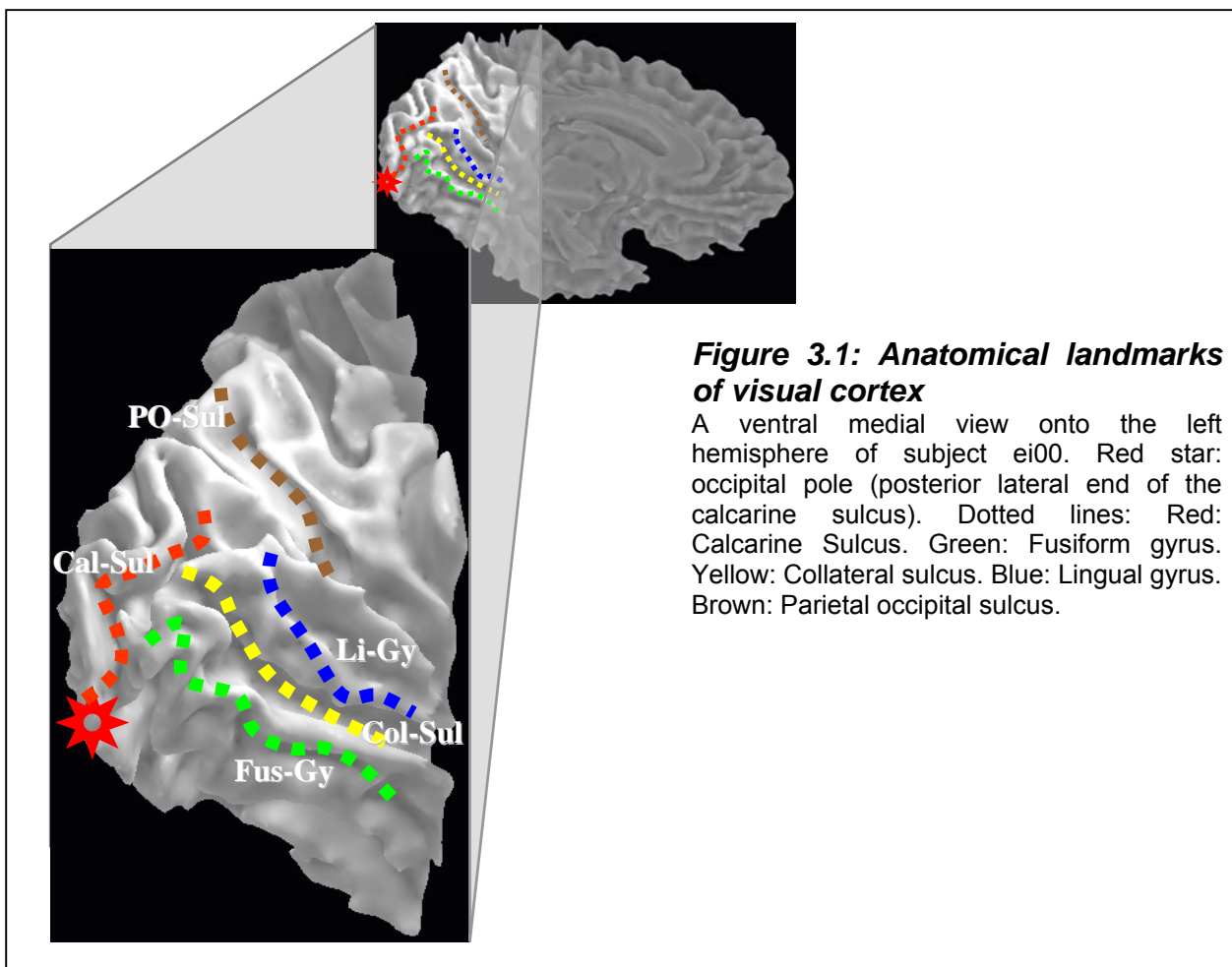
Stimulus presentation in Experiment 3 for instance constituted several color conditions, which were parameterized in four cone-contrast-stages. The analysis of Experiment 3 using WMLE yields the most likely HRF, derived from deconvoluting responses to all color conditions. The resultant HRF function is restricted in its shape and only the amplitude is free to vary as the fixed HRF is weighted for all cone-contrast-stage conditions to maximally reconstruct the measured BOLD-response time course at every voxel. These weights are then averaged across measurements, conducted over several days and can be used to construct contrast response functions. These contrast response functions can teach us, how distinct visual areas in the human brain differ, regarding contrast sensitivity depending on color and speed.

In order to allow for inferences about distinct visual areas, they firstly have to be precisely located, separately for each subject. If suitable, the respective location can be confirmed using a functional localizer. These measurements will be presented in Experiment 1. Experiment 2 will investigate speed dependent differences at equal cone-contrasts across human visual areas and Experiment 3 will extend the speed dependence explorations into the contrast domain.

### 3 EXPERIMENT 1- Retinotopic mapping

#### 3.1 Introduction

Measurements in this thesis regarding motion, color and contrast dependence were preceded by precise localization of the borders of the visual areas V1, V2, V3 V3A, hV4 and MT+. Two MR-scanners with different magnetic field strength were used in experiment 2 and 3 respectively. Retinotopical mapping as well as localization of motion sensitive visual area MT+ were conducted using both scanners, providing an opportunity to confirm spatial organization of cortical visual field maps for subjects that underwent retinotopical measurements in both scanners. This chapter reports precise visual field map representation in human visual cortex and the spatial relation between those regions. The detailed maps will be used in experiments 2 and 3 to define regions of interest for which investigations of motion, color and contrast dependencies on BOLD-responses will be conducted.



### 3.1.1 Retinotopic mapping

The spatial structure of the visual scene falling onto the retina is preserved in LGN and several cortical visual areas (see Section 1.2.2.3). More precisely, adjacent neurons in the LGN and visual cortex respond to adjacent points in the visual field. Hence cortical neurons, spatially organized to represent the visual field, should represent two orthogonal dimensions of the visual field, namely *polar angle* and *eccentricity*. If several spatially distinct cortical responses to the same portion of the visual field are found, they must correspond to separate visual field map representations.

A variety of procedures exist that can be used to derive a general idea of cortical retinotopic organization. It is for instance possible to stimulate solely the vertical or horizontal meridian of the visual field and apply differential imaging techniques. By doing so, responses to vertical meridian stimulation will be subtracted from responses to horizontal meridian stimulation to yield cortical horizontal meridian representation or vice versa to yield vertical meridian representation (Grill-Spector & Malach, 2001; Hasson *et al.*, 2002; Fize *et al.*, 2003). This may yield rather imprecise borders for early visual areas (V1-3), while borders of higher order areas, such as V4, V3A and MT+, elude this procedure. The same is true for eccentricity measurements. Simply comparing two eccentricities, namely central versus peripheral, can evidently only yield a rough approximation of the cortical eccentricity representation (Hadjikhani *et al.*, 1998; Levy *et al.*, 2001; Hasson *et al.*, 2003).

#### 3.1.1.1 Eccentricity

Stimuli measuring the polar angle representation more precisely are preferably several wedges of high contrast reversing checkerboard patterns, rotating around a central marker on which the subject fixates. The wedge stimulation is presented at predefined visual field locations and not only at the horizontal or vertical meridians. The more locations are used and the thinner the wedge, the more precise the measurement, while restrictions are imposed by the spatial resolution of the functional BOLD response measurement (Engel *et al.*, 1997a).

Polar angle measurements within a cortical visual field map can yield a quarter field (either vertical meridian to the horizontal meridian) or hemi-field representation (upper vertical meridian to the lower vertical meridian and vice versa). At the edges of one visual field, the cortical representation of either meridian could mark one end of this map or may reverse into the polar angle map of a neighboring field map. These reversals will be used to locate boundaries between adjacent representations of separate cortical visual field maps (DeYoe *et al.*, 1994; Engel *et al.*, 1994; Sereno *et al.*, 1995; Engel *et al.*, 1997a).

### **3.1.1.2 Polar angle**

The second dimension, cortical visual field maps must represent, is the eccentric extent from fixation within the visual scene. An eccentricity map progresses from a central visual field representation in an orderly fashion towards increasingly more peripheral field representations. Eccentricity measurements are preferably conducted by the means of eccentrically expanding ring stimulation at more than just two positions (Figure 3.2E).

The described temporal/spatial stimulus sequence creates a traveling wave of activity in retinotopic cortex (DeYoe *et al.*, 1994; Engel *et al.*, 1994; Sereno *et al.*, 1995; Engel *et al.*, 1997a; Wandell, 1999; Wandell *et al.*, 1999). Cortical neurons respond as the spatial configuration of the stimulus (wedge or ring) lies within their receptive field. The MR-signal is detected as net response of these neurons in voxels of the measured brain volume at distinct times and corresponding visual field locations. The timing of the peak response indicates the visual field position that most effectively excites the neurons in that voxel. The response phase for each voxel at the fundamental stimulus frequency thus encodes the preferred stimulus angle or eccentricity within the visual field. This methodology is called phase encoding method because the phase of the BOLD response for each voxel measures the most effective stimulus position for that voxel and thus yields cortical representations of the visual field. The phase encoding method has been described in detail in section 2.2.1.

## **3.2 Methods**

### **3.2.1 fMRI measurements of retinotopy**

In order to achieve high precision retinotopic mapping, a stimulation protocol was applied stimulating essentially eight separate positions of the visual field in the angular as well as the eccentricity domain. The phase information at each voxel is subsequently analyzed (Engel *et al.*, 1997b; Dougherty *et al.*, 2003; Brewer *et al.*, 2005; Liu & Wandell, 2005; Wandell *et al.*, 2005). The wedge and ring stimulation used in the reported retinotopic measurements is described in Figure 3.2.

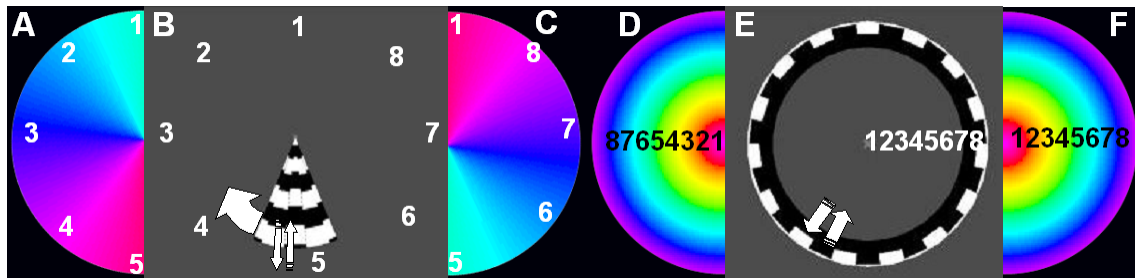


**Figure 3.2: Angular and eccentricity stimuli used in retinotopic mapping**

Cortical polar angle representations are measured using wedge stimuli as in **B**. The 45° wedge is presented at eight different positions in the visual field indicated by ciphers. **A** and **C** represent pseudocolor legends used in subsequent figures and flat maps to indicate the preferred stimulus location of respective cortical locations (voxels) with regard to polar angle. For instance panel **A** indicates stimulus presentation in the left visual field. Cyan represents the upper vertical meridian, blue the left horizontal meridian and magenta the lower vertical meridian. Panel **E** shows the maximal extent of eight rings used to measure cortical eccentricity representation. Ciphers indicate the respective radius of the used rings. **D** and **F** represent pseudocolor legends used in subsequent figures and flat maps to indicate the preferred stimulus location of respective cortical locations with regard to eccentricity. For instance panel **F** indicates ring stimulation in the right visual field. Red and yellow code central stimulus preference while green and blue represent more peripheral targets.

### 3.2.1.1 MR-protocols:

Retinotopic measurements were conducted using the neuro-optimized GE 1.5T Signa Horizon LX (General Electric Medical Systems, Milwaukee, Wisconsin, USA) and a 3T whole-body Magnetom Trio (MRI systems, Siemens Erlangen, Germany).

Two anatomical brain volumes were acquired for each subject and retinotopic measurement. Firstly a 3D high-resolution full head volume, using a fast spoiled gradient echo sequence (FSPGR), supplying excellent white/gray matter contrast in addition to high spatial resolution, was obtained. In the 1.5T system the high-resolution volume subtended 124 sagittal slices with voxel dimensions of 0.98x0.98mm and 1.5mm slice thickness; (TR=24s, TE=MinFull, alpha=30°, FoV=25 cm). The high-resolution scan in the 3T system was acquired using a 3D-magnetization prepared rapid gradient echo sequence (MP-RAGE) and subtended 192 sagittal slices with 1mm isotropic voxels (TR=2.5s, TE=4.77ms, TI=1100ms, alpha=7°, FoV=25.6 cm). These whole head high-resolution scans were measured only once per subject and scanner, and served as an individual anatomical standard space for all subsequent functional measurements.

The second additional anatomical volume with lower resolution but faster acquisition time was obtained using a spin echo T1-weighted sequence (SET1), measuring 20 slices, oriented orthogonal to the calcarine sulcus and identical slice orientation as the functional volumes in the 1.5T system, while in the 3T system a 3D-fast low angled shot sequence (FLASH) was used, yielding 0.7 x 0.7mm voxel dimensions with 3mm slice thickness (TR=1.5s, TE=4.9ms; alpha= 25°; FoV=180x180mm).

Functional measurements in the 1.5T system were obtained using an EPI-gradient recalled sequence, yielding 144 functional brain volumes with 20 slices of 2.2mm slice thickness and 3x3mm voxel dimensions (TR=2s, TE=35ms,  $\alpha=80^\circ$ , FoV=130mm). Functional measurements in the 3T system were obtained using also BOLD sensitive EPI-sequence received in a 5" surface coil (RAPID Biomedical GmbH, Würzburg, Germany) placed at the occipital pole yielding 20 slices with 2.81 x 2.81mm voxel dimensions and 3mm slice thickness (TR=2s; TE=30ms;  $\alpha=80^\circ$ , FoV=180x180mm) covering the occipito-parietal cortex. The initial four scans were discarded.

Polar angle and eccentricity measurements per subject were repeated three times. The respective black and white checkerboard pattern was presented for 24 seconds containing 8 phase steps. This cycle was presented 12 times per run. The stimuli were projected onto a screen in the scanner room using a Sharp XG-SV1E projector with a resolution of 800x600 pixels, mean luminance of 1175 cd/m<sup>2</sup> and Michelson-contrast  $((\max-\min)/(\max+\min))$  of 98%. Subjects viewed the stimuli by means of a mirror system within the scanner while fixating a central marker. The largest eccentricity ring subtended 14° visual angle while each single ring step obtained 1.75° of the visual field. Each of the polar angle wedges measured 45°.

Time series for every voxel underwent the phase encoding method described in detail in section (2.2.1.) which yields amplitude and phase of the periodic BOLD-response for all frequencies. Only voxels whose time series correlated no less than 0.3 with the fundamental stimulus frequency were included into retinotopical analysis of phase reversals and eccentricity measurements. Flat maps in Figures 3.6 to 3.9 depicting polar angle and eccentricity measurements are thresholded at that value. Flat maps representing MT-localizer stimulus activity are presented at 0.5 coherence threshold. The MT-localization procedure is explained in the next section.

### **3.2.2 MT+ localization**

As investigations regarding color and motion dependence on the responses of visual cortex are conducted we chose to include a region known to be highly sensitive to moving stimuli. For that reason we functionally map a cortical region, exhibiting high motion sensitivity. The area is known as MT-complex (MT+), named after presumed homologous motion sensitive regions in the medial temporal (MT) and medial superior temporal (MST) cortex in the macaque monkey. In humans, this region lies on the lateral surface of the occipital lobe, mainly within the dorsal/posterior limb of the inferior temporal sulcus (ITS) (Zeki *et al.*, 1991; Watson *et al.*, 1993; Tootell *et al.*, 1995a; Dumoulin *et al.*, 2000). Relative

to other visual areas, MT+ shows increased sensitivity to low-contrast moving stimuli (Tootell *et al.*, 1995a) and its activity underlies direction-selective neurons (Heeger, 1999; Huk & Heeger, 2000; Huk *et al.*, 2002). Chromatic signals in MT+ have been reported (Seidemann *et al.*, 1999; Thiele *et al.*, 1999; Wandell *et al.*, 1999; Liu & Wandell, 2005) but while the relative proportion compared to achromatic or luminance contribution is controversial there is strong evidence that MT+ plays an important role in motion perception (Salzman *et al.*, 1990; Newsome *et al.*, 1991; Shadlen *et al.*, 1996).

### **3.2.2.1 fMRI measurements of MT+**

Localization of MT+ in human visual cortex in this thesis, was based on responses to stimuli that alternated in time between moving expanding/contracting- and stationary dot fields, the conventional method (Zeki *et al.*, 1991; Watson *et al.*, 1993; Tootell *et al.*, 1995b; Huk *et al.*, 2002) in addition to identification of angular and eccentricity representation within that region. The dot fields subtended 15° visual angle, had approximately 10% Michelson-contrast and were presented on a mean gray background. The dot fields moved towards and away from fixation for 12 seconds alternating their direction every 3 seconds followed by 12 seconds of stationary dot field presentation. Subjects were to fixate a central marker while attending to the dot fields. To keep the attentional load constant, subjects were asked to indicate a sudden change in speed of the dots by means of a button press as stimuli moved while in the stationary condition a sudden contrast change of the dots was to be indicated. This procedure was repeated 20 times per run with a TR of 2s yielding 240 brain volumes per run. Two functional runs were measured per subject. Anatomical scans regarding the two MR-systems were identical to the retinotopic measurements protocol for both MR-systems (see section 3.2.1.1), while the high-resolution anatomical scan was omitted. Voxelwise time series were analyzed using the phase encoding procedures at fundamental stimulus frequency of 1/20 cycles per scan, as described above (section 2.2.1.). Correlation values were thresholded at 0.5 for measurements of both MR-systems and projected onto flattened maps of the segmented gray matter sheet of the occipital cortex. Flat map generation is described in the next section.

### **3.2.3 Cortical flat maps**

In order to visualize average data from multiple slices, a flattened representation (flat map) of the occipital gray matter was produced per subject and hemisphere. On flattened 2D surfaces, the spatial relationship between cortical visual areas can be inspected much more precisely as compared to multiple slices of 3D brain volumes, because medial, ventral and

lateral views are simultaneously visible. The mrVista Toolbox was used ([www.white.stanford.edu/software/](http://www.white.stanford.edu/software/)). The flatmaps were generated passing through essentially four steps, (Teo *et al.*, 1997), identical for measurements in both MR-systems.

Initially, a high-resolution anatomical T1-weighted 3D whole head scan (FSPGR) was segmented manually once for each hemisphere respectively using mrGray (mrVista). The high-resolution anatomical brain volume served as anatomical reference for all subsequent functional measurements. The segmented gray matter sheet was computationally flattened using mrFlatMesh (mrVista). An additional anatomical volume (SET1) was acquired for every functional session and subject with the same slice position as the subsequent functional scans. The anatomical SET1 brain volume was rotated onto the high resolution FSPGR-anatomy, yielding rotation- and translation parameters. The rotation was performed using the software package mrAlign2, which is part of the mrVista toolbox. Since SET1 and functional EPI volumes were acquired using the same slice orientation, identical rotational and translational parameters could be applied to the functional volumes. It is thus possible to transform the coordinates of activated voxels for a given visual stimulation from functional brain volumes into high resolution anatomical coordinates which can then be reliably transferred to flattened cortical maps. By doing so, it is assured, that representation of cortical activity on flat maps originates from gray matter. The final step contains a combination of semiautomatic software (mrFindBorders) and manually inspecting the phase reversals on cortical representations of borders of the visual areas, generated by polar angle stimulation, and simultaneously taking activity patterns, generated by eccentricity stimulation, into account.

Flat maps representing activity elicited by polar angle and eccentricity stimuli as well as MT+ localization in two MR-systems will be compared in the next section for two subjects. Furthermore, two additional subjects will be presented regarding their cortical organization of visual areas, measured in the 3T system.

## **3.3 Results**

### **3.3.1 Polar angle measurements**

V1 represents a homogenous visual contralateral hemifield within the entire calcarine sulcus extending from a lower vertical meridian representation to an upper vertical meridian representation found on the upper and lower lip of the calcarine sulcus respectively as illustrated in Figure 3.3F (Dougherty *et al.*, 2003; Wandell, 2004; Brewer *et al.*, 2005; Tyler *et al.*, 2005). These two V1 meridian representations are shared on the ventral side with V2

ventral (V2v) and on the dorsal side with V2 dorsal (V2d). Each of these V2 maps represents a visual quarterfield, which, taken together, represent an entire hemifield. The quarter field representation for both regions ends at a horizontal meridian representation, which is shared by quarterfield maps of V3 ventral (V3v) and V3 dorsal (V3d) on the ventral and dorsal side respectively. Both maps, V2 and V3 are therefore regarded as discontinuous maps. Logically, the anterior dorsal border of V3d represents a lower vertical meridian, while the anterior ventral border of V3v represents an upper vertical meridian (Dougherty *et al.*, 2003). These spatial relationships were found in all of the hemispheres tested and can be scrutinized in the left columns of flatmap graphs in Figures 3.6 to 3.9 and in Figure 3.3. Every hemisphere investigated displayed a full hemifield representation, sharing an upper vertical meridian with V3v and extending through a horizontal meridian representation towards a lower vertical meridian representation as measured using polar angle stimuli (Figure 3.2). This full hemifield representation extends from the posterior end (upper vertical meridian) towards more anterior portions (lower vertical meridian) of the fusiform gyrus and occupies lateral parts of the collateral sulcus in some hemispheres (compare with Figure 3.1).

The first full ventral hemifield representation beyond V3v was highly regular across subjects and resulted in hV4 mapping. The first full dorsal hemifield representation beyond dorsal V3 draws a somewhat different picture. The anterior border of dorsal V3 constitutes a lower vertical meridian representation. In order to map a full hemifield cortical representation should anteriorly extend through a horizontal meridian followed by a representation of an upper vertical meridian.

Anterior to V3 dorsal we find in fact a clear upper vertical meridian following a horizontal meridian representation. This upper vertical meridian representation appears, however discontinued in most of the hemispheres or is missing a posterior part in some hemispheres. Flat maps of the left and right hemisphere of subject Jm05 in Figure 3.6 illustrate this discontinuity. The upper vertical meridian representation follows a relatively parallel path to the V3 dorsal border starting somewhat near to what can be expected to be the confluent V1-V3 central (foveal) representation. However, following that path towards more peripheral representations (compare to eccentricity scans) this upper vertical meridian representation is interrupted somewhere midway. The gap coincides with at least one foveal representation on the dorsal lateral surface as the eccentricity map is inspected (middle columns). The same pattern is observed for both hemispheres in that subject.

In some hemispheres, at coherence threshold of 0.3, our polar angle measurements revealed no upper vertical meridian representation oriented roughly parallel to the posterior V3 border, but instead another lower vertical meridian was found, essentially representing a

quarter field (see for instance left hemisphere, subject Dn45 in Figure 3.7). Some hemispheres on the other hand exhibit obvious representation of an upper meridian at both posterior and anterior locations (see for instance left polar angle maps for subject Jm05 in Figure 3.6).

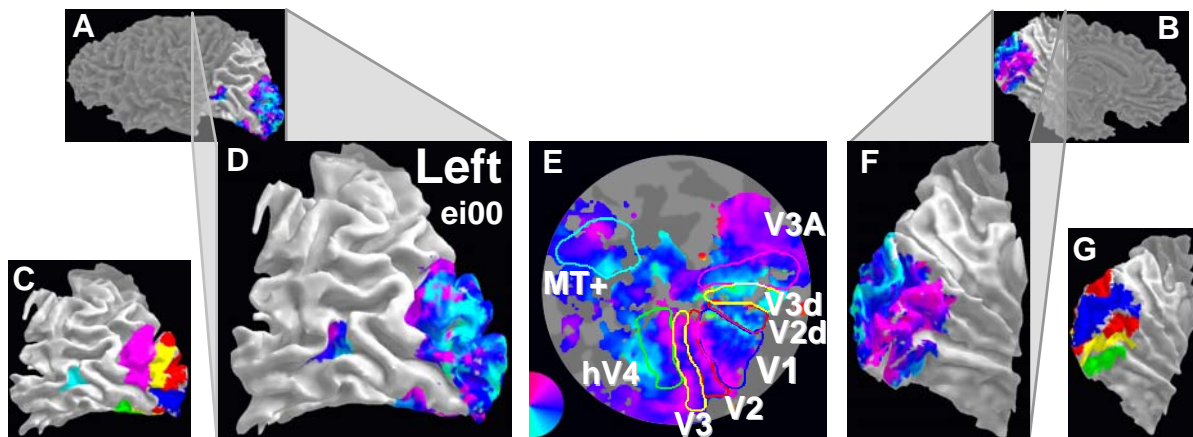


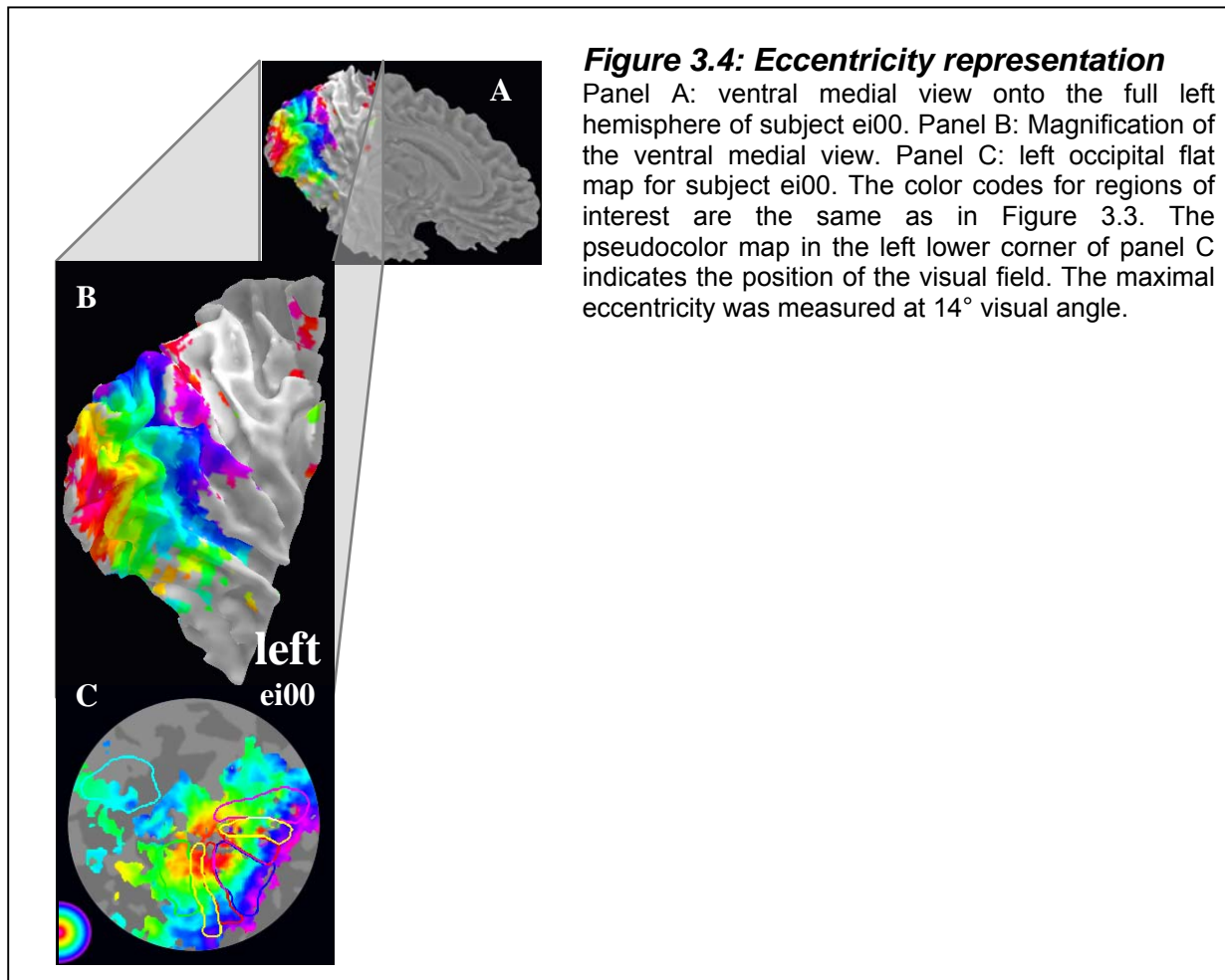
### **Figure 3.3: Polar angle maps identify borders of visual areas**

A and B show a lateral and medial 3D rendering of subject ei00's full left hemisphere respectively. Panel D and F magnify the lateral and medial view of the subject's occipital cortex respectively. Panel A, B, D and F: Polar angle representations are overlaid and restricted to the region of interest coordinates defined in E. Panel E shows clear retinotopic organization of the left occipital cortex of ei00 generated by means of polar angle stimulation in the right visual field (see pseudo-color-map, left lower corner in E). Magenta represents upper vertical meridian, blue represents horizontal meridian and cyan lower vertical meridian. Solid colored lines in panel E mark the borders of the visual areas as identified by phase reversals. Color codes for visual areas remain identical throughout this thesis. V1 ~> blue; V2d/V2v ~> red; V3d/V3v ~> yellow, hV4 ~> green, V3A ~> magenta and MT+ ~> cyan. ROIs are overlaid onto the lateral and medial surface of ei00's occipital cortex respectively in panel C and G. Besides V1 three additional continuous hemifield representations could be precisely mapped in several regions of occipital cortex. A clear hemifield map on the ventral surface, extending from an upper vertical meridian representation at the border to V3v to a lower vertical meridian representation was classified as hV4. On the dorsal surface a clear hemifield map extends from a lower vertical meridian representation at the border to V3d to an upper vertical meridian representation anteriorly and was classified as V3A. In addition, a spatially distinct but quite obvious hemifield representation was identified on the lateral surface. MT+ localization scans (see Figure 3.5) confirmed this region as human motion selective area MT+. These additional maps could be confirmed in several other subjects (see Figures 3.6 to 3.9).

### **3.3.2 Eccentricity measurements**

Eccentricity measurements revealed clear continuous representation for several visual areas (V1, V2, V3, hV4). Starting with a large central (foveal) representation at the posterior end of the calcarine sulcus extending towards increasingly anterior positions along the medial surface representing increasingly more peripheral positions in the visual field. Eccentricity representations form a semicircular pattern on flat maps, which can be fully appreciated along the middle columns of the flat map graphs in Figures 3.6 to 3.9 and in Figure 3.4. Eccentricity representation in hV4 is however clearly distinguishable from V1-V3 with respect to more peripheral stimulus locations in the visual field. While V1 to V3 represent the entire

contralateral visual hemifield, hV4 exhibits a bias for more central targets. This can be observed on all eccentricity flat maps in the middle columns of Figures 3.6 to 3.9 and in Figure 3.4. While V1-V3 represent peripheral targets up to the largest eccentricity measured ( $14^\circ$  visual angle) coded by the blue pseudocolor, the hV4 map does not exceed the green pseudocolor, representing approximately  $10^\circ$  of visual angle.



Recent reports suggest to separate what appears to be a full hemifield beyond V3 dorsal, preferably at a dorsal foveal representation, displaced from the confluent fovea (Smith *et al.*, 2001; Tyler *et al.*, 2005; Wandell *et al.*, 2005). This procedure will assign the smaller, more posterior part of this hemifield representation to V3B, leaving the larger, anterior part to V3A while both still represent a full hemifield. A clear central (foveal) representations on the dorsal surface could not be mapped in all subjects and is for instance completely missing in the left hemisphere of subject Ei00. Others propose one homogenous hemifield map in that region like its putative macaque counterpart (Tootell *et al.*, 1997).

In order to use equal criteria regarding the border of the dorsal visual hemifield map for all subjects, we chose to guide our definition of the anterior border of the dorsal hemifields along the upper vertical meridian representation wherever present to derive a complete hemifields representation within that area. For simplicity we adapted a naming convention set

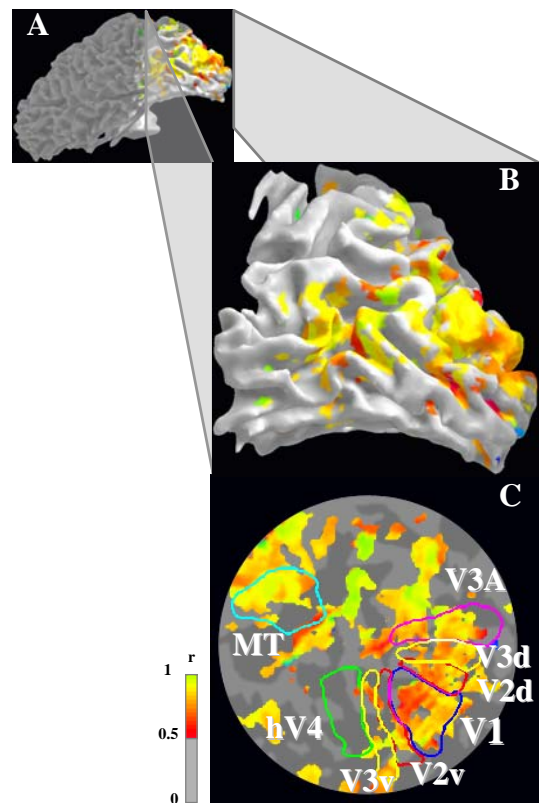
forth by Tootell (Tootell *et al.*, 1997) describing a human dorsal hemifield adjacent to dorsal V3 as V3A, homologous to macaque. Our definition yields a dorsal representation of the entire contralateral hemifield along the borders of dorsal V3 in all subjects. The largest fraction of this region will contain V3A but also V3B, satisfying newer conventions (Brewer *et al.*, 2005; Tyler *et al.*, 2005; Wandell *et al.*, 2005).

### 3.3.3 MT+ retinotopy and localizer measurements

Experimental procedures aiming at motion selective cortex in addition to retinotopic mapping permit to precisely localize MT+. Polar angle measurements on the lateral occipital surface revealed clear retinotopical organization. We confirm a full contralateral hemifield representation mostly in the ascending branch of the posterior portion of the inferior temporal sulcus. Upper and lower vertical meridian representation were robustly measured in every hemisphere exceeding a coherence threshold of 0.3.

#### Figure 3.5: MT+ Localization

Panel A: Lateral view of full left hemisphere of subject ei00. Panel B: Magnification of lateral occipital cortex of subject ei00. Panel C: Flat map of left hemisphere. The location coordinates and color codes for regions of interest are the same as in Figure 3.3. All panels show cortical regions where voxel time series correlated stronger than 0.5 coherence threshold to moving versus static dot field stimulation (see text for details). Note multiple regions are highly activated by motion stimuli. MT+ localization based solely on moving versus static targets is not sufficient. Polar angle and eccentricity information must be taken into account. Experiment 2 will suggest an alternative approach.



Eccentricity measurements revealed a more variable organization of MT+. Applying a high coherence threshold of 0.3 decreased activity representation in some hemispheres, while wedge stimulation gave still robust signals. However compared to the full ventral hemifield representation (hV4), the lateral hemifield representation (MT+) responds to largest eccentric stimuli while hV4 does not. This can be best appreciated in Figure 3.6 and 3.8 for subjects Jm05 and Dn45.

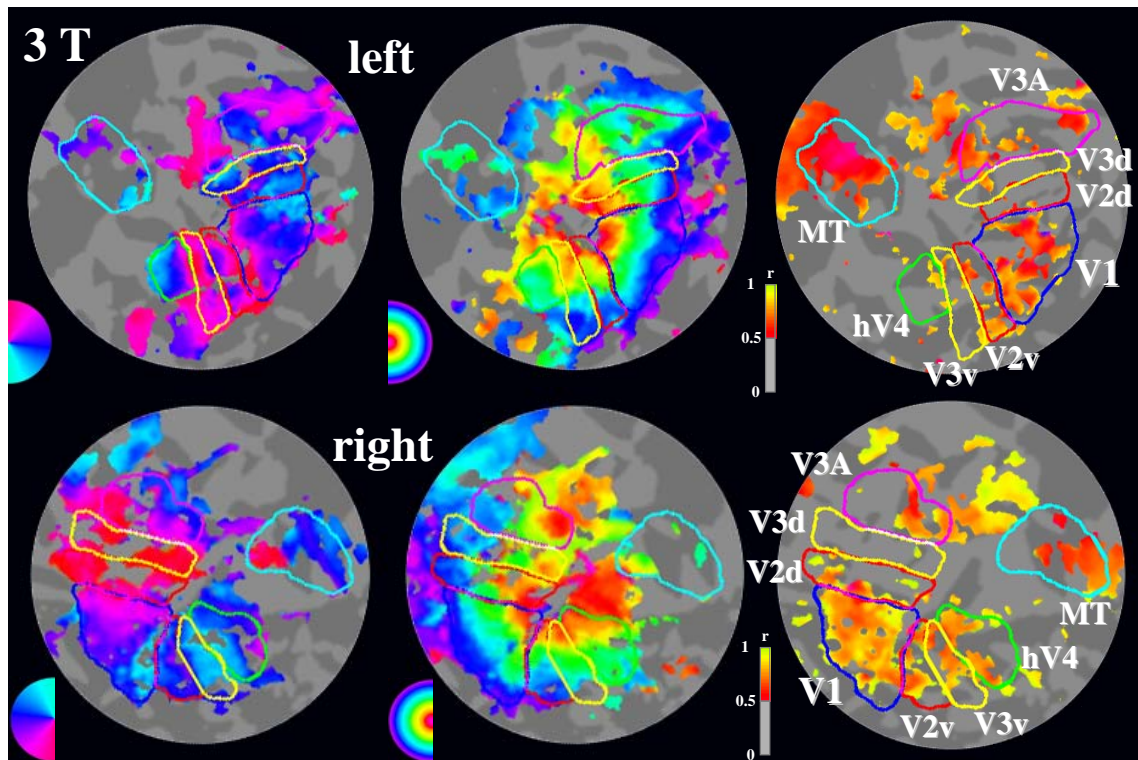


**Figure 3.6: Retinotopic organization and MT+ localization for subject Jm05 (3T)**

Left column: phase reversal maps for rotating wedge stimulation (Coherence Threshold 0.3). Middle column: eccentricity maps for expanding ring stimulation (Coherence threshold 0.3). Right column: MT+ localization measurements expanding/contracting dot fields vs. stationary dotfields (Coherence threshold  $> 0.5$ , see legend). Insets in lower left corner of left and middle column panels indicate stimulus position in the visual field. Colored solid lines mark the borders of visual areas.

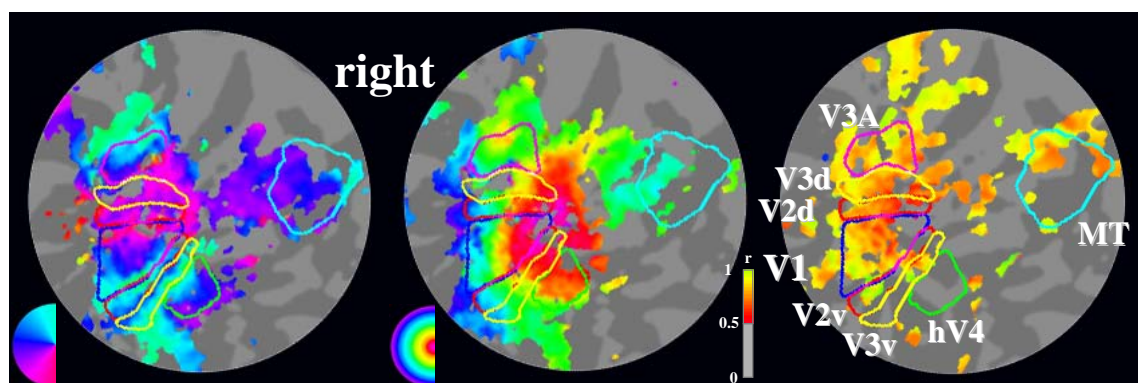


**Figure 3.7: Retinotopic organization and MT+ localization in right hemisphere of subject Ei00 (3T).**

Left hemisphere flat maps can be seen in Figure 3.3, 3.4, and 3.5. Plotting conventions as in Figure 3.6.

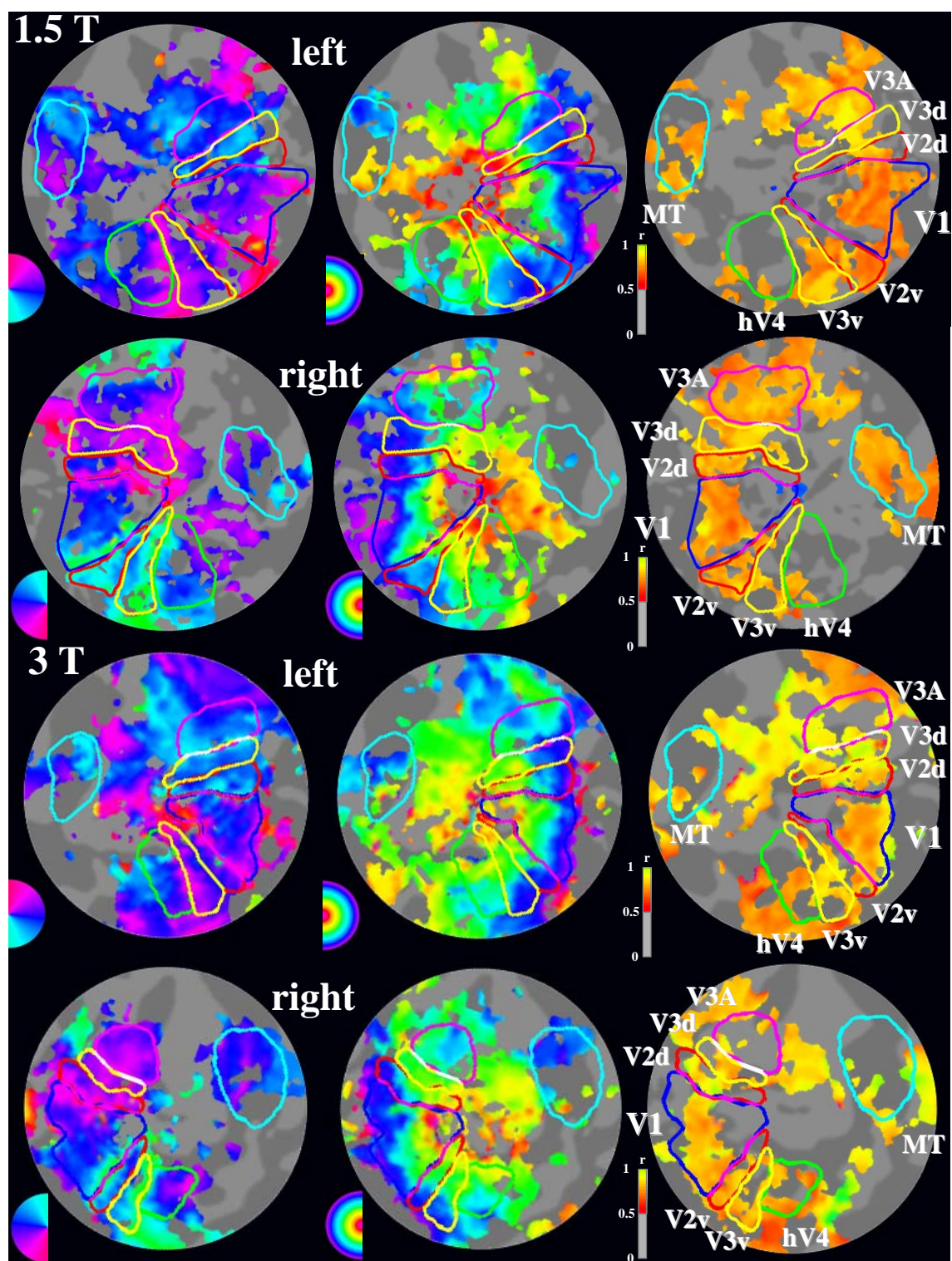


**Figure 3.8: Retinotopic organization and MT+localization for subjects Dn45 in 1.5T and 3T-MR-systems.**

First and third row left hemisphere. Second and fourth row right hemisphere. First and second row 1.5T, third and fourth row 3T-measurements. All other plotting conventions as in Figure 3.6.

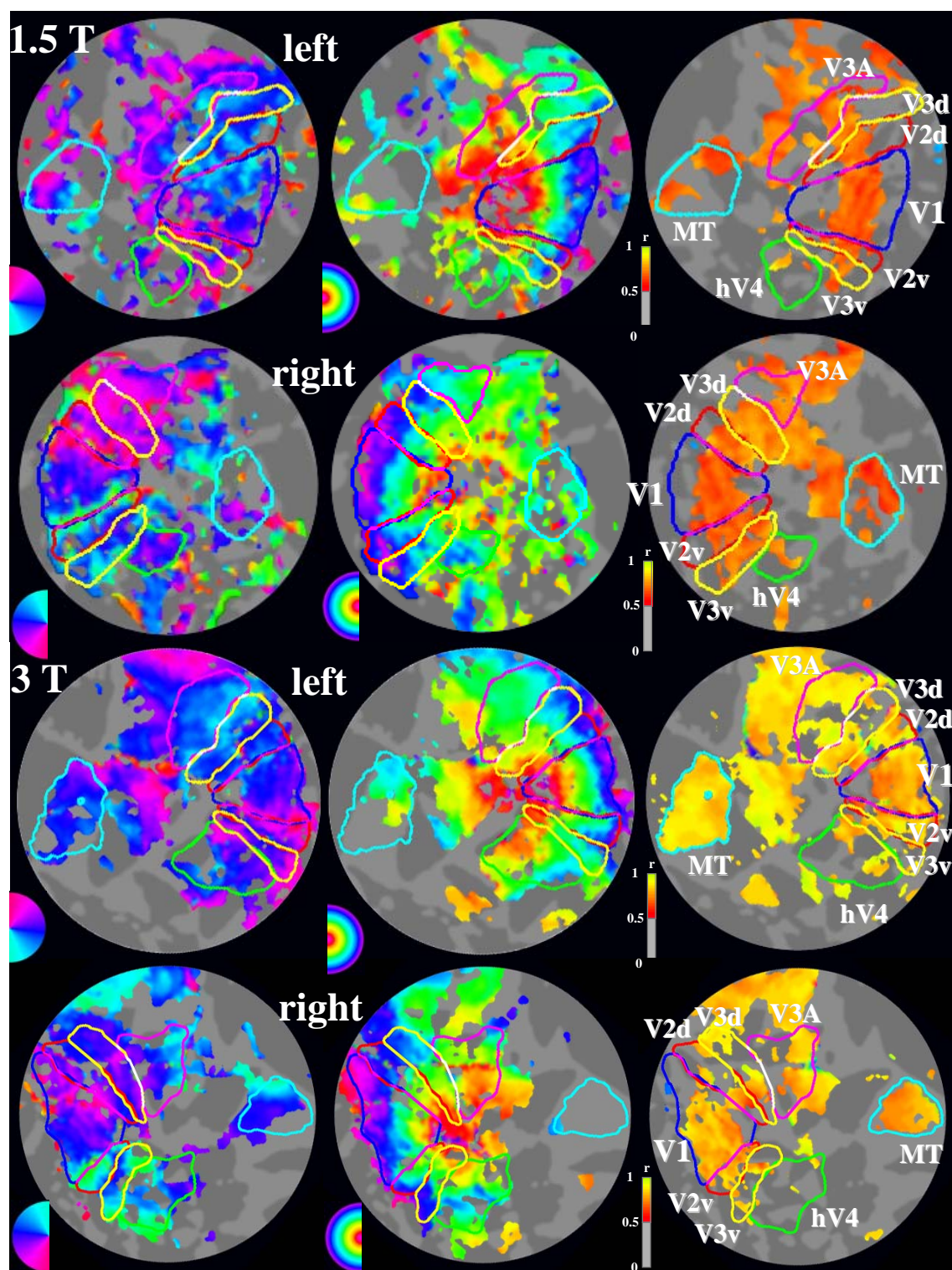


**Figure 3.9: Retinotopic organization and MT+localization for subjects Lk13 in 1.5T and 3T-MR-systems.**

First and third row left hemisphere. Second and fourth row right hemisphere. First and second row 1.5T, third and fourth row 3T-measurements. All other plotting conventions as in Figure 3.6.

The orientation of the foveal/peripheral visual field representation of MT+ with respect to the other visual areas on the unfolded cortical surface appears quite variable between subjects, but data from different magnets for the same subjects reveal the same organization principle. We attribute this observation to variable degrees of folding of the gray matter sheet for each subject, which will result in variable positions on the flat map, as well as probable different hemodynamic delays (Tyler *et al.*, 2005).

### 3.4 Discussion

Human medial occipital representations of the visual field have been under substantial investigation, especially in the field of neuroimaging. Using fMRI, three robust visual hemifield maps, namely V1, V2 and V3 are routinely localized and well established (DeYoe *et al.*, 1994; Engel *et al.*, 1994; Sereno *et al.*, 1995; Engel *et al.*, 1997a; Dougherty *et al.*, 2003; Wandell *et al.*, 2005). In addition to these three maps we report precise localization of the borders of visual areas hV4, V3A and MT+, which as V1, contain continuous representation of the full contralateral visual hemifield.

While the location and spatial extent of primary visual areas (V1-V3) are well documented (Dougherty *et al.*, 2003; Brewer *et al.*, 2005; Wandell *et al.*, 2005) cortical representations of full hemifields beyond primary cortex are subject to intense controversy. Probably most contentiously discussed in the recent literature is the spatial representation of the visual field in the first ventral surface map, V4.

Guided by macaque anatomy, Tootell and Hadjikhani set out to clarify whether human V4 is split into ventral and dorsal components which would entail, each of those regions to represent only a respective quarterfield of the contralateral visual field (Tootell, 2001). It is, however, pointed out by this group, that the dorsal region, which they suspected to represent dorsal V4, lacks many features that would qualify it as the dorsal quadrant of V4 ventral, making a ventral or dorsal quarterfield representations in V4 unlikely (Tootell, 2001; Tyler *et al.*, 2005). A recent report persuasively showed that the first ventral map beyond V3v is indeed a full hemifield representation, bordered anteriorly by a lower vertical meridian representation (Brewer *et al.*, 2005). Our data is in concordance with these proposals as all hemispheres measured in this work show a full hemifield representation with a lower vertical meridian running roughly parallel to the V3 ventral (Wandell *et al.*, 2005).

In addition it is generally agreed that hV4 shares the confluent fovea with V1-V3 while dorsal area V3A/B may have its own foveal representation, displaced to the large foveal confluence (Press *et al.*, 2001; Smith *et al.*, 2001; Brewer *et al.*, 2005; Wandell *et al.*, 2005). The measured eccentricity maps support the foveal hV4 representation to be confluent with

the V1-V3 foveal representation in all hemispheres shown. On the dorsal cortical surface however the majority of hemispheres reveal a foveal representation distinct from the confluent foveal representation (see Figures 3.6 to 3.9 and 3.4) (Tyler *et al.*, 2005). These foveal representations are thought to be shared by two full hemifield representations beyond V3d, namely V3A and V3B (Tyler *et al.*, 2005; Wandell *et al.*, 2005). Since this non-confluent dorsal foveal representation was not observed in all hemispheres these putative separate hemifield representations have been joined to form the, what we named V3A hemifield map, in this work. Future imaging research, focusing on the dorsal surface of human cortex is necessary to clarify the existence and spatial relationship of dorsal foveal representations.

Scrutinizing the eccentricity maps again reveals besides the confluent V1-V3 foveal representation, two additional ventral foveal representations in all hemispheres and two additional dorsal foveal representations in some hemispheres well separated from the confluent fovea (best seen in Figure 3.6: left hemisphere for subject Jm05; Figure 3.7: right hemisphere for subject Ei00 and Figure 3.8: left hemisphere subject Dn45). The posterior but displaced ventral foveal representation has already been associated with ventral occipital area VO-1, being situated anterior to hV4 (Brewer *et al.*, 2005). A similar organization may be found on the dorsal surface, in which the first displaced foveal representation, seen in most of the eccentricity maps in our data, could be associated with the hemifield representation of V3A, while V3B may share the confluent foveal representation of V1-V3 and hV4.

Finally, an additional ventral occipital full hemifield representation (VO-2) an associated foveal representation was found anterior to VO-1 (Brewer *et al.*, 2005). A similar organization on the dorsal surface may correspond to a full hemifield representation known as V7 (not shown in our flat maps), having its own foveal representation (Tootell *et al.*, 1998; Press *et al.*, 2001; Tyler *et al.*, 2005). A similar symmetrical canonical scheme has been suggested by Tyler *et al.* (Tyler *et al.*, 2005).

However, the percentage of eccentric representation varies substantially within and across visual areas. The cortical magnification factor leads to a cortical representation of the fovea of about 8% in V1 while the area of highest acuity obtains only 0.01% of the entire retina (Sharpe & Nordby, 1990). This may partly be explained by the increased density of the retinal photoreceptors in that region as compared to the peripheral density (Wässle *et al.*, 1990), while the central visual field map in primate V1 may be magnified beyond what may be derived from foveal receptor density (Inouye, 1909; Talbot & Marshall, 1941; Daniel & Whitteridge, 1961; Perry & Cowey, 1985; Horton & Hoyt, 1991a; Dougherty *et al.*, 2003).

The motion responsive region MT+ on the lateral occipital surface has been characterized as having coarse retinotopically organized maps, while the subdivision MST of

the MT+ complex may not be retinotopically organized (Huk *et al.*, 2002). Polar angle representations in the inferior temporal sulcus reported here replicate previous finding and securely map MT+ within that region. Every hemisphere showed clear upper and lower vertical meridian representation. The upper vertical meridian representation was located more anteriorly than the lower vertical meridian representation in every hemisphere, confirming a prior report (Huk *et al.*, 2002). Eccentricity organization in area MT+ have been characterized to represent more peripheral targets in the superior part of MT+ while central targets are being represented in the inferior part (Huk *et al.*, 2002). We find the same organization in most hemispheres, even though the left hemisphere of subject Jm05 exhibits reverse eccentricity representation (see Figure 3.6). In general, the local cortical anatomy of the MT+ region is quite variable across individuals (Watson *et al.*, 1993; Tootell *et al.*, 1995b; Dumoulin *et al.*, 2000).

This chapter summarized experimental procedures leading to definition and determination of visual field map representations. We securely identified visual field maps in V1, V2 V3, hV4, V3A and MT+. These regions will serve as an outline to define regions of interest in subsequent experiments of this thesis. The next experiment will investigate speed dependence on the BOLD-response in these visual field maps using equal cone-contrast stimuli.

## **4 EXPERIMENT 2- Speedtuning**

### **4.1 Introduction**

How neural activity relates to the experience of moving colors is controversial, because key behavioral results remain at odds with existing neurophysiological data. Experiment 2 aimed to provide speed-tuning properties for several visual areas that suggest an association with psychophysically derived motion perception mechanisms. In addition the effects of speed at a suprathreshold contrast level for five color directions (L+M, L-M, S-(L+M), L+M+S, S) will be investigated within these areas. Best separating stimuli between area hV4, representing the ventral path, and area MT+, representing the dorsal path, will be provided, to facilitate future research regarding strict segregation of these paths. The results will be discussed in the context of contemporary neurophysiological and imaging studies, addressing color and speed tuning in human- and monkey visual cortex as well as the long lasting controversy regarding the magnitude of color-opponency in human visual cortex.

#### **4.1.1 Luminance - detection vs. discrimination**

For moving luminance gratings, contrast thresholds for detection and discrimination of direction of motion are highly similar at all temporal frequencies and for all eccentricities within 5 deg of the fovea (Levinson & Sekular, 1975; Watson *et al.*, 1980; Lindsey & Teller, 1990; Derrington & Henning, 1993; Metha *et al.*, 1994; Gegenfurtner & Hawken, 1995; Stromeyer *et al.*, 1995). Interpretations of these results yield the idea, that the same neural mechanism is employed for detection and discrimination of luminance motion and that this mechanism is direction-selective (Watson & Robson, 1981).

#### **4.1.2 Isoluminance - detection vs. discrimination**

On the other hand, psychophysical experiments investigating isoluminant motion perception draw a different picture. These reports have shown that, although motion perception is possible at isoluminance (Cavanagh *et al.*, 1984; Lindsey & Teller, 1990; Cavanagh & Anstis, 1991), the perceived speed is slower than for cone-contrast matched luminance stimuli (Cavanagh *et al.*, 1984; Mullen & Boulton, 1992).

For stimuli with low temporal frequencies, presented foveally, the motion detection sensitivity is better than the sensitivity for motion discrimination. This difference increases at more peripheral locations and is more pronounced at higher temporal frequencies (Gegenfurtner *et al.*, 1994; Gegenfurtner & Hawken, 1995, 1996).

### 4.1.3 Two motion mechanisms

The discrepancy between detection and discrimination of isoluminant motion has led to the assumption of two motion processing streams that differ mostly in their temporal characteristics and are essentially sensitive to color (Hawken *et al.*, 1994). Gegenfurtner and Hawken (1996) distinguish a fast channel from a slow channel. The fast channel veridically represents the velocity of moving patterns (also at isoluminance) but might not code the color of such patterns. Conversely, the slow channel is highly sensitive to color and signals the direction of slowly moving patterns while the coding of stimulus velocity is not veridical (Gegenfurtner & Hawken, 1996). The neuronal substrates of these two different functional channels in humans are unknown.

The main question being addressed in the second experiment is consequently, which cortical area(s) can be attributed to these two motion channels derived psychophysically. In the course of action we may additionally ask, if chromatic response differences within and between visual areas, found in previous fMRI studies and described in section 1.2.3.6, change depending on speed (Kleinschmidt *et al.*, 1996; Engel *et al.*, 1997b; Zeki & Marini, 1998; Wandell *et al.*, 1999). A third question will address chromatic response differences as we investigate hierarchically higher tier visual areas?

Gegenfurtner and Hawken suggest area MT as a candidate for the fast channel because it is of paramount importance in the processing of visual motion (Zeki, 1974; Movshon *et al.*, 1985), smooth-pursuit eye movement (Newsome *et al.*, 1985), is highly direction selective (Newsome *et al.*, 1991) and responds to isoluminant stimuli (Saito *et al.*, 1986; Charles & Logothetis, 1989; Dobkins & Albright, 1994; Gegenfurtner *et al.*, 1994; Wandell *et al.*, 1999). MT can however not be held responsible for the slow channel, because contrast sensitivity in MT cells (for chromatic stimuli) is not sufficient for the excellent behavioral sensitivity to slowly moving isoluminant gratings (Gegenfurtner *et al.*, 1994) (see experiment 3).

Further evidence supporting separate speed dependent motion channels comes from a patient suffering from bilateral damage to the lateral temporo-occipital cortex, resulting in cerebral akinetopsia. Motion perception in this patient was only impaired for fast moving stimuli while no deficit could be reported for slowly moving stimuli below 4Hz (Zihl *et al.*, 1983; Hess *et al.*, 1989). Residual responses to motion stimuli in area V3 could be observed in this patient (Shipp *et al.*, 1994).

Gegenfurtner and Hawken (1996) suggest a network comprised of V3 and V4 for the slow channel, since single-cell recordings in macaque V3 revealed joint selectivity for color and motion (Gegenfurtner *et al.*, 1997), while V4 is well known for its color sensitivity (Zeki, 1983b; Kleinschmidt *et al.*, 1996; McKeefry & Zeki, 1997; Zeki & Marini, 1998; Beauchamp

*et al.*, 1999; Wade *et al.*, 2002; Brewer *et al.*, 2005) and is sensitive to the direction of motion (Desimone & Schein, 1987; Tolias *et al.*, 2001a; Tolias *et al.*, 2005b). In addition, a number of studies have shown that chromatically opponent mechanisms most likely underlie both the detection and discrimination of moving chromatic targets (Krauskopf & Farell, 1990; Metha *et al.*, 1994; Gegenfurtner & Hawken, 1995; Stromeyer *et al.*, 1995).

To investigate an association of cortical regions to the differential properties of the proposed fast and slow motion perception channels, two assessment criteria should be tested. The first criterion pertains to temporal frequency sensitivity and will be tested in the present experiment. The second criterion pertains to differential chromatic contrast sensitivity between the two motion channels and will be part of the measurements conducted in experiment 3.

As for the first criterion, temporal frequency sensitivity differences, a visual area corresponding to the highly-contrast-sensitive, color-opponent slow mechanism should prefer chromatic over luminance stimulation at slow speeds (< 4Hz) and responses should decrease as temporal frequencies exceed 4Hz (Gegenfurtner & Hawken, 1996). By contrast, an area belonging to the fast motion pathway should consequently be equally responsive to all stimulus velocities regardless of color direction and responses should not decline at frequencies above 4Hz (Gegenfurtner & Hawken, 1996).

Experiment 2 will present speed tuning properties for retinotopically mapped visual areas V1, hV4, V3A and MT+ elicited by stimuli presented at equal cone-contrast of 14% along five directions of cone-contrast space and three velocities. These response patterns suggest MT+ as neural substrate for the fast channel while hV4- and V3A- response patterns allow association with the slow channel.

## **4.2 Methods**

### **4.2.1 Subjects**

Six human subjects participated in fMRI measurements. Four were naive to the purpose of the study. All subjects had normal or corrected to normal vision and gave their written informed consent prior to the experiment. The ethics committee of the University of Magdeburg approved the experiment.

### **4.2.2 Visual display**

For the fMRI-measurements the stimulus presentation was controlled using Cogent 2000 (available at [www.vislab.ucl.ac.uk](http://www.vislab.ucl.ac.uk)) under Matlab 6.5. (Math Works, Natick, MA) on a pentium 4 Desktop Computer with an integrated WinFastA350 Graphics Card and displayed on a flat-panel TFT-display (NEC, MultiSync LCD 2180UX, Ithaca, Illinois) with a resolution of 1600x1200 pixels and a screen refresh rate of 60 Hz. The TFT display was inside a front-transparent shielded box in the scanner room. Subjects viewed the display through binoculars.

The spectral properties of the displays were characterized with a pr650 Photoresearch (Chatsworth, CA) spectroradiometer. The cone-contrast stimuli were calculated with the 10° Stockman and Sharpe sensitivity functions (Stockman & Sharpe, 1998, 2000).

The temporal stability of the display was assessed for all our stimuli by measuring the photoelectric current elicited in a photodiode. We found no signal attenuation for any contrast direction across the different speeds.

### **4.2.3 FMRI protocol**

Functional magnetic resonance imaging was performed on a 3T whole-body MRI system (Siemens Magnetom Trio, Erlangen, Germany) with a BOLD-sensitive EPI-sequence (TR=1500ms; TE=30ms; alpha=80°) using a 5" surface coil (RAPID Biomedical GmbH, Würzburg) placed at the occipital pole. Twenty slices (matrix size 64 x 64 voxels; spatial resolution: 2.81 x 2.81 x 3mm; no gap) were oriented approximately perpendicular to calcarine sulcus and covered the occipito-parietal cortex. An additional T1-weighted anatomical volume was acquired (3D-FLASH-Sequence: matrix: 256 x 256; FoV: 180 x 180 mm; spatial resolution: 0.7 x 0.7 x 3mm; TE=4.9 ms; TR=15000ms, alpha: 25°) with the same slice positions as the functional images. This anatomical image served to align the functional data with a whole head high-resolution anatomy volume (3D-MP-RAGE-Sequence: matrix: 256 x 256; 192 slices per volume; FoV: 256 x 256mm; spatial resolution: 1 x 1 x 1mm; TR=2500 ms; TE=4.77ms; TI=1100ms; alpha: 7°). This high-resolution scan served as an individual standard space in which the results from the functional scans could be referenced to the location of visual areas obtained by retinotopic mapping as described in section 3.2.1.

### **4.2.4 Stimulus & experimental design**

A rotating radial sinusoidal grating was presented on a mean gray background in an annulus (inner radius ~0.5°, outer radius ~10° visual angle) centered on a fixation marker (Figure 2.1). The grating contrast was modulated along 5 directions in cone-contrast-space

(L+M, L-M, S-(L+M), L+M+S and S, with  $(L= \Delta L/L, M=\Delta M/M, S=\Delta S/S)$  and rotated at 3 different temporal frequencies (1, 4 and 10Hz, cycles per second). The direction of motion changed periodically. Cone-contrast (i.e. the length of the stimulus vectors in cone-contrast-space, RMS) was held constant in all color directions at 14%, the maximum contrast in the (L-M) direction in which our display produced the least cone-contrast out of all five directions. The stimuli were presented in a balanced block design (each condition having the same prior-block-history). The order of conditions was changed between runs. All subjects performed 7 runs of 16 minutes.

To control for attention in the fMRI experiment, subjects performed an attention binding number discrimination task at the fixation marker throughout the runs. The runs started and ended with 30s blocks of the attention task on a mean gray background without additional stimulation. These blocks were used to define the baseline BOLD-level.

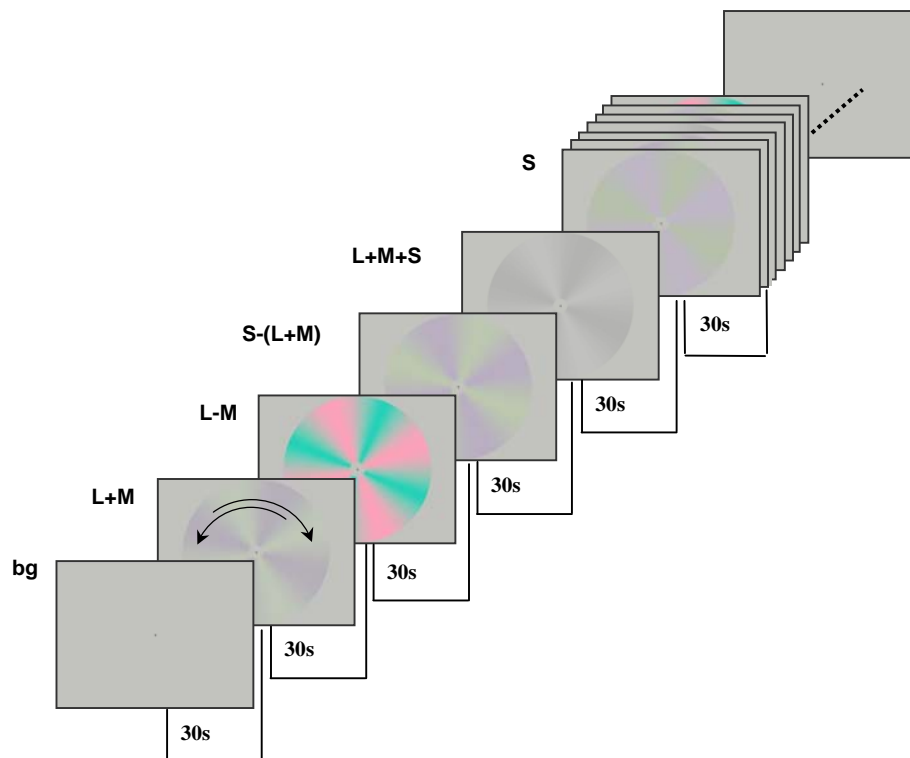


**Figure 4.1: A sample stimulus presentation sequence.**

Each run started and ended with a mean gray background for 30 seconds. A fixation task was present throughout the run. Stimuli consisted of sinusoidal gratings, modulated along 5 directions in cone-contrast-space (L+M, L-M, S-(L+M), L+M+S and S) and rotated at 3 different speeds (1, 4, and 10 Hz, cycles/s). The rotation direction changed periodically. The stimuli were presented in a balanced block design (each condition having the same prior-block-history) and the cone-contrast was kept constant at 14%. Note that physical equality pertaining to cone-excitation leads to substantially different perceptual saliency and saturation of the colors (Mullen *et al.*, 2005).

### 4.2.5 Analysis

Functional MR-Images were realigned and smoothed (6mm kernel, FWHM) using spm99 (Wellcome Department of Cognitive Neurology, University College, London UK). BOLD-signal modulation was determined for all conditions by fitting a box-car-function, reflecting the stimulus time course, convolved with a standard hemodynamic response function to the time-series of each voxel (see General Methods Section 2.2.2.). The result is a weight factor (beta) that reflects the strength of BOLD modulation in each voxel for each condition. Individual t-images were computed for each subject, revealing activation clusters in which the cone-contrast stimuli led to significant activation compared to the baseline condition (no annulus presented).

Areas V1, V2, V3, V3A and V4 were determined using the mrVista-toolbox (Teo *et al.*, 1997) and standard retinotopic mapping methods described in section 3.1.1 (Engel *et al.*, 1994; Sereno *et al.*, 1995; Wade *et al.*, 2002). Area MT+ was functionally identified based on responses to stimuli that alternated between moving and stationary dot patterns described in section 3.2.2 (Zeki *et al.*, 1991; Tootell *et al.*, 1995b; Huk *et al.*, 2002) in addition to retinotopic mapping (see section 3.1.1).

The visual-area-ROIs from the independent localizer scans were overlaid onto the t-image to confirm the localization of the activation within the visual areas under investigation. For the subsequent ROI based analysis the mean of responses at 27 voxel coordinates, forming a cube, centered on the local maximum of the individual t-map-cluster that could be safely assigned to lie within the borders of the visual areas (V1,V3A, V4, MT) was used. These values were individually normalized for each ROI by the standard deviation over all stimuli presented. The measure obtained that way reflects the individual BOLD-gain changes over stimulus conditions and renders the BOLD-signal changes better comparable between cortical sites (Logothetis, 2003). It further reduces effects of absolute inter-individual BOLD-amplitude differences. The former are partially due to local differences in the signal-to-noise ratio of the fMRI setup.

### 4.3 Results

Previous studies found that V1 is most responsive to (L-M)-cone stimulation, less responsive to (L+M)-cone stimulation, and least responsive to pure S-cone stimuli using the cone-contrast metric (Engel *et al.*, 1997b; Liu & Wandell, 2005). We asked if this holds true for extra-striate visual areas using high constant cone-contrast (14%), and extended the stimulus range with additional cone-contrast-space-directions, such as S-(L+M) and L+M+S.

We also asked if known sensitivity differences between chromatic responses within a given visual area change when the stimulus pattern velocity is varied at 1, 4, or 10Hz. Finally we aimed to find response pattern differences as predicted by behaviorally identified motion channels (Gegenfurtner & Hawken, 1996)

Figure 4.2 shows examples for the localization of the V1/V3A/V4 and MT+ ROIs. Figure 4.3 shows the normalized BOLD responses in the four visual areas investigated, averaged over subjects.

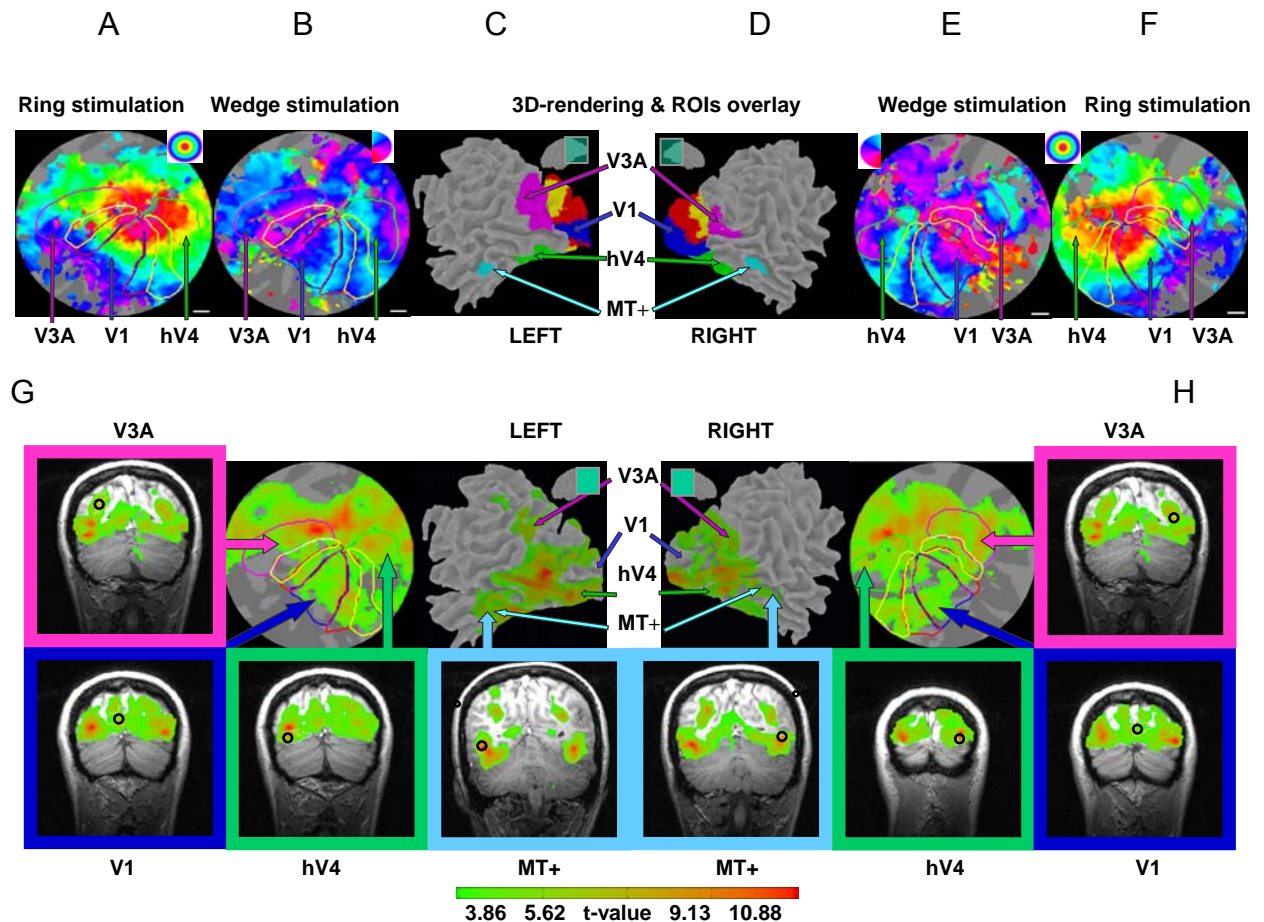


**Figure 4.2: Borders of visual areas and location of region of interest.**

V1 (blue), V2 (red), V3 (yellow), V3A (magenta) and hV4 (green) on cortical flat-maps determined by expanding ring- (A,F) and rotating wedge-stimulation (B,D) for the left (A,B) and right hemisphere (E,F) of one subject. MT+ (cyan) was identified using an independent localizer scan contrasting moving vs. stationary dot-fields (see experiment 1). 3D-renderings of the left (C) and right (D) hemispheres of the same subject with the visual areas overlaid (lateral view).

Panels G and H describe the identification of regions of interest (ROIs) for the left and right hemisphere respectively. SPM99 was used to determine where any of the stimuli elicited a significant activation in the occipital lobe (contrast stimulus vs. gray background). The resulting t-image and the pre-determined borders of visual areas were overlaid onto flat maps to identify activity clusters within the visual areas. The data from a cubic ROI (27 voxels) around this peak voxel were used in the subsequent analysis. The colored boxes show the contrast t-image, overlaid on T1-weighted slices of the same subject. The circles indicate the approximate location of the center-peak-voxel within V1 (blue-box), hV4 (green-box), MT+ (cyan-box) and V3A (magenta-box).

### **4.3.1 Analysis of variance**

#### **4.3.1.1 Global BOLD-Analysis**

The means (over twelve brain hemispheres) of the standard deviation normalized BOLD-responses obtained under all stimulus conditions in the four visual areas under investigation are shown in Figure 4.3. A three-way repeated measures analysis of variance (rANOVA) revealed significant main effects of brain area (four levels: V1, V3A, hV4, MT+ F(3,33)=7.74,  $p < 0.001$ ), of color (five levels: L+M, L-M, S-L-M, L+M+S and pure S, F(4,44)=41.72,  $p < 0.001$ ), and a significant interaction between these two factors (F(12,132)=2.37,  $p < 0.01$ ). Interestingly, there was only a marginal effect of pattern velocity (three levels: 1Hz, 4Hz, 10Hz, F(2,22)=2.73,  $p < 0.088$ ) in this global analysis but the interactions between velocity and both color or brain area were significant (velocity-color: F(8,88),  $p < 0.001$ ; velocity-brain area: F(6,66)=4.0,  $p < 0.005$ ). Finally, a three way interaction (F(24,264)=3.88,  $p < 0.001$ ) indicates that the investigated brain areas are differently activated by the color-velocity combinations used in the experiment. In the following these interactions will be further explored to investigate how color and velocity interact in the different brain areas.

#### **4.3.1.2 Analysis by velocity**

This analysis investigates whether the relative amplitudes of the BOLD-responses elicited by the different colors are similar in the four brain areas over velocity. The analysis can also reveal possible changes in the preference for specific colors in the investigated brain areas over speed. Three two-way ANOVAs were computed with factors color and brain area (all five colors and all four brain areas), one for each velocity. Color has a highly significant effect at all speeds (1Hz: F(4,44)=23.13;  $p < 0.001$ ; 4Hz: F(4,44)=40.3,  $p < 0.001$ ; 10Hz: F(4,44)=11.0,  $p < 0.001$ ) indicating higher BOLD-responses for some colors than for others at all speeds.

Note that the effects on the factor brain area have no clear interpretation when BOLD-responses are analyzed. Conversely, the interaction between brain area and another factor has a clear interpretation and is informative on how different brain areas process different stimuli. However, the interaction between color and brain area reaches significance only at the highest velocity presented (1Hz: F(12,132)=1.5,  $p > 0.1$ ; 4Hz: F(12,132)=1.8,  $p > 0.05$ ; 10Hz: F(12,132)=5.1,  $p < 0.001$ ) indicating that the brain areas respond similarly to stimuli with different chromatic content at the slower velocities (1Hz and 4Hz), but differ at the highest velocity (10 Hz). The qualitatively same results were obtained when only responses to stimuli

that emphasize cardinal mechanism were included in the analysis (L-M, L+M+S, and S). The results indicate that the BOLD-responses elicited by different chromatic stimuli differ between brain areas, but mostly at higher velocities.

#### **4.3.1.3 Analysis by brain area**

Separate two-way ANOVAs for each brain area were computed, aiming to reveal effects of stimulus combinations of speed and color within each visual area. In V1 we find a main effect of color ( $F(4,44)=20.1$ ;  $p<0.001$ ) but no main effect of velocity ( $F(2,22)=0.99$ ;  $p>0.25$ ), and a significant interaction between color and motion was found. A similar pattern is found in area MT. While color has a strong differential effect on the BOLD-activation in this area ( $F(4,44)=27.53$ ;  $p<0.001$ ) no differential response over speeds was found ( $F(2,22)=0.1$ ;  $p>0.5$ ) but, as in V1, a significant interaction ( $F(8,88)=4.6$ ;  $p<0.001$ ).

Areas V4 and V3A provide a somewhat different picture. Similar to V1 and MT both show an effect of color (V4:  $F(4,44)=26.7$ ,  $p<0.001$ ; V3A:  $F(4,44)=16.9$ ,  $p<0.001$ ). In contrast to V1/MT areas hV4 and V3A show an additional effect of velocity (V4: velocity  $F(2,22)=9.2$ ,  $p<0.001$ , interaction:  $F(8,88)=7.96$ ,  $p<0.001$ ; V3A: velocity  $F(2,22)=4.5$ ,  $p<0.05$ ). These results suggest a greater similarity in the processing of V1/MT as compared to V3A/V4. Figure 4.3 suggest that the differential velocity effect is due to the fall-off of the BOLD-responses in areas V3A and hV4 as temporal frequency increases. Conversely, areas V1 and MT+ do not show such an effect. V1 and MT+ revealed a response profile one might expect from brain areas that represent velocity in populations of neurons tuned to a wide range of velocities. However, the significant color-velocity interactions we found in all visual areas indicate that the main effects of velocity might differ between different color-directions. Therefore, we analyzed the effects of velocity for each color separately.

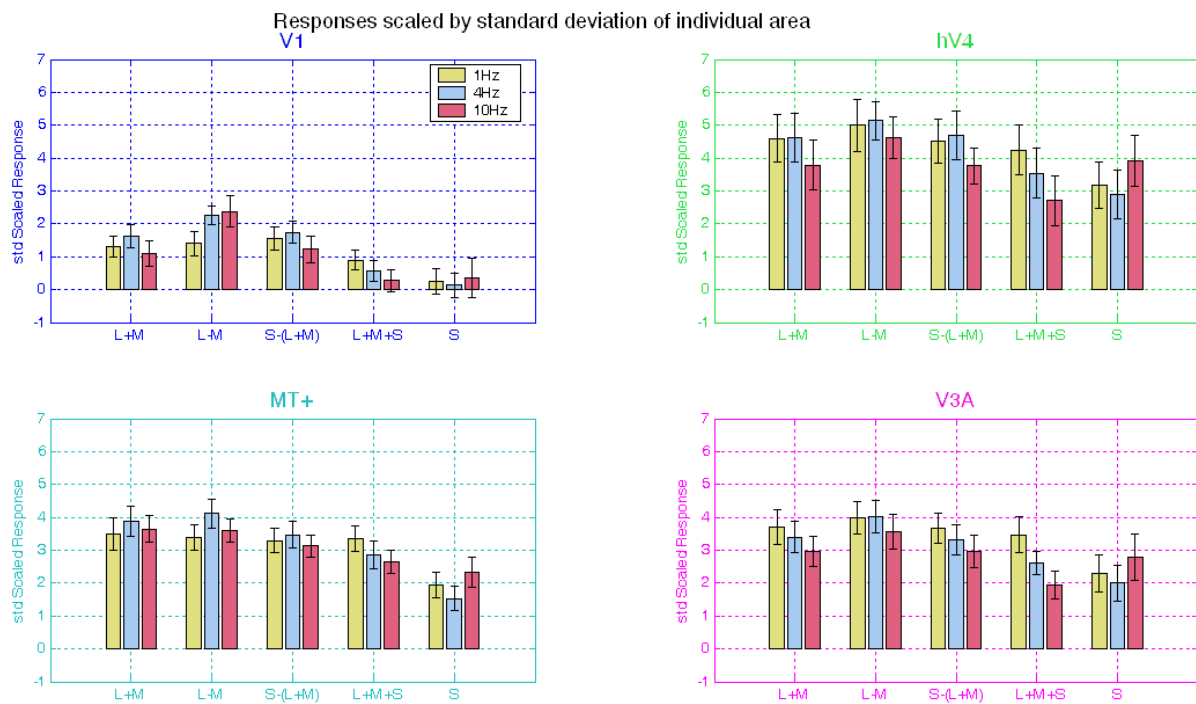


**Figure 4.3: Speed tuning in V1, MT+, hV4 and V3A for five cone-contrast directions and three speeds**

Abscissa: cone-contrast colors; Ordinate: amplitude of standard deviation scaled response; Bars: yellow=1Hz, blue=4Hz, red=10Hz; hV4 and V3A exhibit response decline as temporal frequencies reach 10 Hz for achromatic (L+M+S), luminance (L+M), B/Y (S-(L+M)) and R/G (L-M) stimuli indicative of low-pass properties. MT+ responses show slight increases at 4 Hz responses indicative of band-pass properties. V1 responses increase for L-M as temporal frequency is raised. Low S-cone responses as compared to extra-striate regions.

#### 4.3.1.4 Velocity effects by cone-contrast direction

The effects of the stimuli that emphasize the putative detection mechanism responses (L-M, L+M+S, S) were analyzed separately for each visual area investigated. The critical F-value for the Bonferroni-correction of the 12 comparisons (3 cone-contrast directions in 4 brain areas) is 7.1 and the corresponding p-value is 0.0042. For completeness the uncorrected p- and their corresponding F-values are report.

The BOLD-response to the L-M stimulus changed only in V1 significantly over the three speeds (V1:  $F(2,22)=7.89$ ,  $p<0.003$ ). In V3A, hV4 and MT+ there appears to exist a non-significant tendency that the 4Hz L-M stimulus elicits the highest response (see Figure 4.3; V3A:  $F(2,22)=1.8$ ,  $p>0.1$ ; hV4:  $F(2,22)=1.7$ ,  $p>0.1$ ; MT+:  $F(2,22)=2.56$ ,  $p>0.1$ ). The strongest effect is found in the decrease of the L+M+S response with increasing speed in areas V3A ( $F(2,22)=11.0$ ,  $p<0.001$ ) and V4 ( $F(2,22)=17.24$ ,  $p<0.001$ ). Neither in V1 ( $F(2,22)=4.1$ ,  $p<0.05$ ) nor in MT ( $F(2,22)=4.78$ ,  $p<0.025$ ) was the decrease significant when corrected for multiple comparisons, but the effects were of similar size in these two areas. The apparent increase with increasing velocity of the S response reaches in none of the brain areas

significance. However, the effect sizes observed draw a similar picture as for the L+M+S stimulus. V1 and MT+ show the least effect sizes (V1:  $F(2,22)=0.24$ ; MT+:  $F(2,22)=2.58$ , both  $p>0.05$ ) and both would not reach significance, even without correction for multiple comparisons. In areas V3A and hV4 stronger effect sizes are obtained that would reach significance without the correction (V3A:  $F(2,22)=4.53$ ,  $p<0.025$ ) and hV4 ( $F(2,22)=6.78$ ,  $p<0.005$ ). The most important source for the interactions by velocity found in the global ANOVA appears to be the weaker response to the L+M+S stimulus with increasing speeds in areas V3A and hV4. Since the L+M+S stimulus emphasizes the response in the luminance-mechanism this suggests that the effect is due to the luminance contrast. This could be interpreted as an indicator that V3A and hV4 exhibit the properties expected from the slow mechanisms for motion perception since regions associated with the fast mechanisms should not exhibit substantial BOLD-response decline as the velocity of luminance pattern increase (Gegenfurtner & Hawken, 1996).

### **4.3.2 Cluster analysis**

One tendency suggested by the ANOVAs was that BOLD responses obtained at the various color and velocity combinations are more similar between areas V1 and MT and more alike in areas V3A and hV4. A hierarchical cluster analysis on the responses to the fifteen color-velocity combinations obtained in each hemisphere was performed to investigate the similarity between the response profiles of the four visual areas.

Areas V3A and hV4 cluster more closely than any other group. The correlations between the mean response vectors in the 15 conditions investigated (3 velocities and 5 color directions) are listed in Table 4.1. The Pearson-correlation coefficient measures the angle between two response vectors. This angle can be interpreted as a measure of similarity between the response profiles of two visual areas and neglects differences in BOLD-response strength. As already indicated by the cluster analysis, the highest similarity was found between V3A and hV4 ( $r=0.974$ ). This correlation is higher than between any other pair of visual areas (at least  $p<0.05$  for all comparisons). The angle between the feature vectors of V3A and hV4 is nearly a third of the angle between the other pairs, specifically V3A and MT+.

Correlation				
	V1	V3A	hV4	MT+
V1	1	0.838	0.862134	0.859132
V3A	33.02	1	0.974161	0.826175
hV4	30.44	13.05	1	0.81027
MT+	30.78	34.29	35.88	1
Angle (deg)				

**Table 4.1: Results of cluster analysis and Pearson-correlation coefficient**

Response profiles of hV4 and V3A are highly similar as indicated by the highest correlation coefficient and lowest angle difference of the response vectors of these two regions compared to any other pair.

#### 4.3.2.1 Stimuli for best separating hV4 and MT+

Color and velocity are stimulus attributes that are often used to separate dorsal and ventral stream processing. We performed an exploratory analysis to find the best separating combinations. Therefore we calculated the differential effects (t-values) for all stimulus combinations in areas hV4 and MT+ (see table 4.2 in the appendix). These areas are often regarded as representative for the ventral and dorsal stream, respectively (Livingstone & Hubel, 1988). Our stimulus set comprises 105 unique combinations of color and motion.

The separation of the ventral and dorsal stream could be achieved by at least two approaches: Stimulus combinations that modulate one stream without having a significant effect in the other could be used to modulate one stream selectively. Furthermore, stimulus combinations that produce a strong positive effect in one stream and a reverse effect in the other stream could be used to emphasize one stream and simultaneously suppress the other.

As for the first approach we found that the comparisons (L-M 4Hz) – (L+M+S 10Hz) and (L+M 1Hz) – (S 1Hz) produced highly significant effects in hV4 but no effects in MT+, after Bonferroni-correction for multiple comparisons. In these comparisons the effects in hV4 exceed those in MT+ by more than seven t-values (for a complete list of corrected t-values see appendix table 4.3). Area MT+, but not area V4 exhibits the most reliable effects in the comparisons (L+M 10Hz) – (S 4Hz), (L+M 10Hz) – (S 10Hz), and (L-M 10Hz) - (S 10Hz). In these comparisons the effects in MT+ exceed those in hV4 by more than 6 t-values. It is interesting to note that most stimulus combinations that favour effects in hV4 involve combinations of L+M, L-M or S-L-M equal to or below 4Hz as the minuend and L+M+S  $\geq$  4Hz or S at 1Hz as the subtrahend, i.e. the first lead to higher BOLD-responses in hV4 than the second. These results match the general picture of hV4 as an area that prefers slow

chromatic over fast achromatic stimuli. However, it should be noted that area MT+ shows no preference for the above combinations, in neither direction of the subtraction. This argues strongly against area MT as an area that generally prefers fast achromatic over slow chromatic stimuli. The full set of results is given in table 4.3 in the Appendix.

As for the second approach, we found no stimulus combination that produced a significant positive effect in one area and a concurrent negative effect in the other. All differences between conditions that were significant in both MT+ and hV4 went in the same direction. However, among these stimulus combinations the largest differences between the effects in hV4 and MT were found in the comparison (L+M 10Hz) – (L+M+S 10Hz), with an effect in V4 that was by 4.5 t-values higher than in MT+. The strongest effect in favour of MT was found for the combination (L+M 4Hz) – (S 4Hz). Here the MT effect exceeded the hV4 effect by 4.14 t-values. Such effects were only found with stimulus combinations involving S-stimuli (see table 4.4 in the appendix).

## **4.4 Discussion**

The goal of this experiment was to investigate response differences depending on stimulus color and velocity at one fixed cone-contrast level in several visual areas known to be involved in cortical color and/or motion processing.

On the basis of differential response patterns in several visual areas to various stimulus color and speed combinations, associations regarding psychophysically determined motion perception channels were achieved. It was shown, that BOLD-responses to equal cone-contrast stimuli differ between brain areas, but mostly at higher velocities. Additionally, best stimulus combinations to separate the ventral (hV4) and dorsal (MT+) path were presented.

### **4.4.1 Two motion pathways in human cortex**

Gegenfurtner et al. (1996) proposed two non-color-blind processing streams for motion perception that differ mostly in their temporal characteristics (Gegenfurtner & Hawken, 1996). The authors describe a fast motion pathway, that veridically represents the velocity of moving patterns, and also responds to moving isoluminant stimuli, but might not code the color of such patterns. A putative second slow pathway is suggested to show a high sensitivity to color, signals the direction of slowly moving patterns, but its coding of stimulus velocity is not veridical. The authors attributed visual area MT as a likely candidate for the fast motion pathway and hypothesize area V4 to be involved in the slow motion mechanism (Gegenfurtner & Hawken, 1996).

Visual areas that correspond to the fast motion perception mechanism are expected to respond invariantly to the stimulus velocity and also show responses to chromatically defined moving patterns. On the other hand, cortical regions that correspond to the slow motion perception mechanism are expected to show high sensitivity to chromatically defined moving patterns especially at low speeds, while responses should decline as velocities increase above 4Hz (Gegenfurtner & Hawken, 1996).

In concordance with this view our measurements show a relative invariance of MT+ responses to temporal frequency regardless of color direction while hV4 and even more so area V3A, show a clear response decline at high temporal frequencies.

This effect was most obvious for achromatic moving stimuli, which emphasize a proposed luminance detection mechanism (Derrington & Henning, 1993; Krauskopf, 2000a). Responses in visual area hV4 and V3A to achromatic moving gratings declined substantially, while no such effect was observed for visual areas MT+. In addition all three regions respond well to moving chromatic stimuli, especially area hV4 and V3A, for which BOLD-response profiles to chromatic gratings, suggest a preference for slowly moving R/G-gratings up until 4Hz.

We thus suggest neurophysiological evidence for a color-motion processing network derived psychophysically and set forth by Gegenfurtner et al., in which MT+ responds to all temporal frequencies regardless of color direction and thus accounts for a fast motion mechanism, while V3A and hV4 seem to prefer slowly moving chromatic stimuli as their response declines dramatically as temporal frequencies exceed 4Hz and thus account for the slow mechanism of motion (Gegenfurtner & Hawken, 1996).

Further evidence supporting several cortical motion processing sites comes from a behavior study investigating chromatic detection and direction of motion thresholds in individuals with cerebral achromatopsia using slow stimulus velocities (2Hz) and fairly high chromatic contrasts (Cavanagh *et al.*, 1998). This study found that the subjects, despite their profound loss in the subjective experience of color and their inability to detect the motion of faint colors, showed surprisingly strong responses to high-contrast, moving color stimuli, equal in all respects to the performance of subjects with normal color vision (Cavanagh *et al.*, 1998). The authors could not determine the cortical site, which may be responsible for processing slow moving isoluminant motion stimulation. They were able to dismiss ventral region hV4 as a likely candidate, since it is severely damaged in cerebral achromatopsia (Zeki, 1990). They additionally argued against area MT+ as likely candidate, because chromatic sensitivity of monkey MT+ neurons is not sufficient to explain the excellent chromatic motion sensitivity (Gegenfurtner *et al.*, 1994; Cavanagh *et al.*, 1998).

Data presented here suggest area V3A to be responsible for nearly normal chromatic motion thresholds in subjects suffering from cerebral achromatopsia at slow moving high contrast color patterns. V3A is a likely candidate, because it exhibits a preference for slowly moving chromatic stimuli. In addition it is located on the dorsal side of the human occipital cortex, rendering it highly unlikely to be damaged in cerebral achromatopsia, which follows damage to the ventral occipital cortex. Furthermore it is distinct from lateral occipital region MT+ and represents a complete hemifield (see section 3.3.1 and 3.3.2). Finally there is evidence in our data for color-opponent mechanisms in V3A, which is further discussed in the next section.

#### **4.4.2 Color opponency in visual cortex**

A long lasting controversy regarding color-opponent mechanisms in visual cortex is fueled by neurophysiological findings reporting relatively few color-opponent cells in V1 (Livingstone & Hubel, 1984), while an opposing view is supported by neuroimaging studies, which suggest that such neurons might be relatively numerous (Schluppeck & Engel, 2002). Schluppeck et al. (2002) argue that when cortical responses to L-M stimulation exceed those for luminance, given equal cone-contrast, a color-opponent mechanism must be the underlying source. Applying this criterion to our data set reveals strong color-opponent responses not only in V1, but also in V3A and not surprisingly in hV4. In all of these visual areas L-M responses exceeded luminance responses.

Color opponent mechanism in motion selective cortex (MT+) are controversial because this area is believed to receive mainly magnocellular and thus luminance input, which sum cone signals, as opposed to differentiating them in an opponent fashion (Maunsell *et al.*, 1990). The applied stimulus set in the present experiment contained two color directions that emphasize the magnocellular pathway, namely L+M+S and L+M. If indeed MT+ solely processes luminance information, responses to chromatically defined stimuli such as L-M, emphasizing the color-opponent, parvocellular pathway, should be substantially lower in that region compared to luminance generated signals. Our data do not show response patterns supporting a clear luminance preference in MT+. Instead, we find, BOLD-response patterns, elicited by stimuli emphasizing parvo- and magnocellular mechanism to be roughly equal. This finding does not allow for strong conclusions regarding the presence of color-opponent mechanisms in MT+, applying the criterion set forth by Schluppeck et al. (Schluppeck & Engel, 2002). The results are however in concordance with and consolidate recent findings from neurophysiological reports on monkeys and human imaging studies, showing that MT+

may adhere to signals from both magno- and parvocellular pathways (Seidemann *et al.*, 1999; Wandell *et al.*, 1999; Nassi *et al.*, 2006).

Furthermore, above discussed study by Cavanagh *et al.* (1998) reported that individuals with cerebral achromatopsia perceive moving isoluminant colored stimuli just as well as normal observers, given a fairly high cone-contrast (Cavanagh *et al.*, 1998). Cavanagh *et al.* argue that cortical sites outside of MT+ must mediate chromatic motion signals based on the assumption, that MT+ receives little or no parvocellular input. Another group, however, showed clear ‘color signals in human motion-selective cortex’, albeit pure S-cone-signals, arguing that the MT pathway contains enough information to permit individuals with cerebral achromatopsia to perform motion judgement (Seidemann *et al.*, 1999; Wandell *et al.*, 1999). Our data support both arguments. The strong L-M responses in MT+ suggest that it contains enough parvocellular input to allow individuals with cerebral achromatopsia to perform veridical chromatic motion judgments. Nonetheless, another motion sensitive area, V3A, is also highly responsive to L-M stimulation, rendering it a candidate for chromatic motion processing independent of MT+, as well as exhibiting properties that suggest color-opponent mechanisms in this dorsal region.

### **4.4.3 Colortuning**

Many neurophysiological studies on monkey visual cortex aim to determine the specialization of single cells regarding a specific stimulus attribute, for instance color, by systematically varying certain stimulus parameters, as for instance contrast or temporal frequency (Gegenfurtner *et al.*, 1994; Hawken *et al.*, 1996; Seidemann *et al.*, 1999; Solomon & Lennie, 2005; Conway & Livingstone, 2006). An indication for specialization of a given neuron in these studies is typically a higher firing rate to one stimulus configuration as compared to another. The stimulus configuration yielding the highest firing rate is associated with the cells stimulus preference, while the response profile over many stimulus attribute levels is called the tuning with respect to the investigated stimulus attribute.

Recent human imaging studies have adopted this approach to determine the specific tuning properties of cell conglomerates in specific regions of the human brain or retinotopically mapped visual field representations (Engel *et al.*, 1997b; Liu & Wandell, 2005). An indication for stimulus preference in fMRI-studies is typically the magnitude of the measured BOLD-response. Higher BOLD-responses elicited by a certain stimulus level A compared to lower BOLD-responses elicited by stimulus level B are interpreted as a preference to stimulus level A of the region yielding the response differences. It is thus

possible to determine the tuning of a human visual area with respect to specific stimulus attributes.

To further advance the understanding of human cortical color and motion processing we aimed to measure speed tuning curves using equal cone-contrast colors which will be discussed in the next section. In this section the characterization of the visual areas with respect to the measured BOLD-responses depending on different chromatic stimulation is discussed. By comparing BOLD-responses elicited by stimuli at equal cone-contrast levels of 14% we can draw conclusions regarding the colortuning of the measured visual areas for this specific contrast level. It has to be noted that the drawn conclusions regarding colortuning may only be valid at the used cone-contrast level and one should be cautious in extrapolating the results to other cone-contrast stages because the relative response strengths (the tuning) may change when cone-contrast is varied. Extensive color and speed measurements at different chromatic contrast levels in experiment 3 of this thesis will investigate this possibility.

For the visual areas V1, hV4 and V3A, we observed a response magnitude hierarchy in the order of  $L-M > S-(L+M) > L+M > L+M+S > S$ . This response hierarchy can be interpreted as color-tuning property for these areas at equal 14% cone-contrast. The results for V1 are well in line with a prior imaging study in humans, reporting greater sensitivity in primary visual cortex to L-M stimuli compared to L+M stimulation (Engel *et al.*, 1997b). As an extension to this prior V1 report, our results suggest that the colortuning properties at 14% cone-contrast do not change substantially in extra-striate regions with the exception of MT+, which responds equally to all but S-cone stimulation. BOLD-responses in human MT+ emphasizing solely S-cone contribution is small but present. This observation is in concordance with an fMRI study showing markedly reduced sensitivity of neurons in MT+ to S-cone stimuli compared to luminance (L+M) stimulation (Wandell *et al.*, 1999). Wandell *et al.* (1999) also reported higher responses in V1 to L+M as compared to S-cone stimuli, which is in concordance with the measured response hierarchy described above (Wandell *et al.*, 1999).

The underlying source for human cortical color responses is still an open issue. Neurophysiological monkey studies have suggested some links to provide insight into the neuronal sources of the observed BOLD signals in humans. A recent study was able to convincingly show that signals stemming from the three classes of neurons, organized in three layers of the lateral geniculus (see section 1.2.3.1), are transmitted via distinct thalamo-cortical pathways and terminate into separate projection sites in different layers of primary visual cortex (Chatterjee & Callaway, 2003). The spatial resolution of fMRI is currently not

able to resolve distinct cortical layers. This restriction renders application of neurophysiological findings in monkey cortex to human cortex speculative because it cannot be tested with the same methods. However, after methodological progress has occurred over the past years, many findings from the monkey model have subsequently been confirmed in humans (Dougherty *et al.*, 1999; Seidemann *et al.*, 1999; Wandell *et al.*, 1999), and hence motivate a discussion of the human colortuning properties found in experiment 2, in the realm of properties of single cells in monkey visual cortex.

Our data obtained for primary visual cortex suggests a preference for R/G over B/Y responses, which may either indicate a higher sensitivity of color selective cells to R/G or a higher neuronal density for R/G preferring cell populations. Several groups have found that there are more red-green double-opponent cells than blue-yellow ones, supporting the later argument and suggesting double-opponent cells as a candidate neural source of the chromatic tuning properties in our data (Wiesel & Hubel, 1966; Livingstone & Hubel, 1984; Ts'o & Gilbert, 1988; Conway & Livingstone, 2003). Some groups have confirmed the existence of double-opponent cells in primary visual cortex which are sensitive to color *and* luminance contrast (Thorell *et al.*, 1984; Conway, 2001; Johnson *et al.*, 2001; Conway *et al.*, 2002; Johnson *et al.*, 2004). It is thus also likely that observed responses to R/G and luminance stimuli were generated by the same neural population of cells.

There have been speculations whether distinct cell types may be responsive to more than just one stimulus attribute (Gegenfurtner *et al.*, 1996; Gegenfurtner & Kiper, 2003), and that for instance double opponent color-luminance cells might multiplex color, form (Johnson *et al.*, 2004) and even direction of motion (Conway & Livingstone, 2003). The applied methodology does not allow for strong conclusion regarding multiplexing of several stimulus attributes other than to note that temporal frequency of the moving patterns does have an effect on the measured subpopulation of neurons responding to our stimulus configurations, which will be discussed in the next section and further investigated in experiment 3.

However, neurophysiological studies regarding direct projections from V1-color-sensitive-blobs to the form 'sensitive' area V4 suggest, that color selective cells in V1 might be suitable for tracking moving isoluminant borders (Schein & Desimone, 1990; Ghose & Ts'o, 1997; Pasupathy & Connor, 2001). V1 may thus build the initial encoding stage for signals of moving objects, which might further be integrated in hV4 where the receptive field size is much higher (Zeki, 1978a; Smith *et al.*, 2001) and neurons are also direction selective (Nealey *et al.*, 1991; Tolias *et al.*, 2001b).

#### 4.4.4 Speedtuning

As described in the previous section, the response profile over several stimulus levels for one visual attribute is called the tuning with respect to the investigated stimulus property. When more than two stimulus attribute levels are measured the response pattern can be interpreted as tuning curve for this specific stimulus attribute. Experiment 2 applied three different rotation velocities to every chromatic stimulus patterns. It was thus possible to derive speedtuning curves per color direction and visual area.

The speed tuning curves for a given color-direction are similar across all extra-striate cortical areas measured (hV4, MT+, V3A), while marginal deviations from that scheme are observed in striate cortex (V1). This deviation is especially prevalent for high-frequency L-M modulated targets compared to luminance targets, indicating differences in temporal filter properties between striate and extra-striate cortex.

The first fMRI-study applying retinotopic mapping as well as parametric modulation of cone-contrast presented iso-response curves of BOLD-signal responses in area V1 and V2 to three temporal frequencies of a cone-contrast reversing checkerboard flicker stimulation (Engel *et al.*, 1997b). Their data agree well with a prior study (Kleinschmidt *et al.*, 1996) showing highest responses in striate cortex to L-M-stimulation, which we confirm as well here (see section colortuning).

However, the temporal frequency measure used by Engel *et al.*, cannot be regarded as real motion stimulation since they used contrast reversing checkerboard flicker which has recently been shown to activate substantially less than real motion stimulation in area V1 and MT+ (Liu *et al.*, 2004; Muckli *et al.*, 2005). Our V1 L-M responses reveal higher responses to higher temporal frequencies which differs from data presented by Engel *et al.* (Engel *et al.*, 1997b). The divergence may arise because of stimulation differences in the temporal domain as well as substantially higher equal cone-contrast in our study. The applied stimulation in the present experiment did move (rotate) in the visual field, simulating real motion, which is not the case for stationary flicker stimuli. However, it is long known that some color-opponent neurons in primary visual cortex can follow high temporal frequencies well above heterochromatic fusion frequencies (Gur & Snodderly, 1997). It may thus be possible to find strong responses to color-opponent stimulation at high temporal frequencies in V1. But why do we observe this increase only in V1 for one color direction?

Since the 14% cone-contrast was constant in all color-directions, the L-M stimulation was the most salient. Although every effort was made to keep the attentional load constant and away from the rotating color patterns by means of a demanding number discrimination task at the fixation cross, we cannot completely rule out that automatic attentional

mechanisms attributed to L-M responses at increasing velocities. It has been shown that pop-out stimulus context effects, such as a highly salient, 14% equal cone-contrast pattern, might bias visual processing and this effect seems to have its origin in early visual cortex (Beck & Kastner, 2005; Yantis, 2005). In addition it has been shown that color and luminance stimulation attract independent attention (Morrone *et al.*, 2002). Moreover, there is recent evidence that a change-detection mechanism sensitive to unattended changes in motion direction may exist in the human visual system (Pazo-Alvarez *et al.*, 2004).

A recent study reported the first parametric fMRI-measurements in which cone-contrast and the stimulus velocity were systematically modulated (Liu & Wandell, 2005). Most of the results agree well with the present study such as color-opponency in striate- and extra-striate cortex and its implications (see section 4.4.2 color-opponency) but some of the inferences need to be reconsidered in the realm of this thesis.

Liu and Wandell propose a common functional network between area V3A and MT+ by referring to two studies that found common response profiles to achromatic stimuli (Tootell *et al.*, 1997; Smith *et al.*, 1998). These two studies have only used achromatic stimuli. If L-M stimulation would have been tested as well, they may have found differences between V3A and MT+ at least at higher frequencies. In addition Liu and Wandell state that V3A and MT+ have weak responsivities to L-M and pure S-cone stimuli compared to other visual areas as well as profoundly different properties than a ventral occipital area. Our data, and partially theirs, suggest otherwise. We find equal responsivity in MT+ to L-M and L+M stimuli regardless of temporal frequency as well as higher activity in V3A to L-M than to L+M stimuli which both decrease at frequencies higher than 4Hz in this region. Also, the hV4 L+M-speedtuning curve is quite similar to the V3A L+M-speedtuning.

We speculate that the similarities in the measured response profile between V3A and hV4 might be indicative of extensive cross talk between these areas in a common network that interprets and integrates motion signals, may they be of chromatic or luminance nature. Our data suggests a functional color-motion-network comprised of at least hV4, MT+ and V3A (leaving open additional contribution from future motion areas), which responds well to all chromatic modulations.

The equal cone-contrast level of 14% differs substantially from prior investigations, characterizing chromatic response properties in human cortex (Kleinschmidt *et al.*, 1996; Engel *et al.*, 1997b; Liu & Wandell, 2005) and may partially be responsible for some diverging conclusions (Liu & Wandell, 2005). To test the effects of different chromatic contrast levels, the following experiment will provide extensive fMRI measurements using

visual stimuli that besides differing in chromatic axes and velocity will be modulated in the contrast domain.

## **5 EXPERIMENT 3 - Colortuning**

### **5.1 Introduction**

Experiment 2 investigated BOLD-response profiles in several visual areas to various combinations of stimulus color and velocity at an equal cone-contrast level. The measured response profiles were used to associate visual areas to one of two mechanisms of motion perception, because specific properties and limitations of these mechanisms have been characterized neurophysiologically and psychophysically (Gegenfurtner *et al.*, 1994; Gegenfurtner & Hawken, 1995, 1996). These reports provided predictions with respect to the expected temporal characteristics and chromatic sensitivity of visual areas associated with either of the two motion channels. On the basis of these predictions we generated two criteria. The first criterion pertains to the temporal properties of the two channels and was tested in experiment 2. It states that one mechanism is not sensitive to stimuli moving at high temporal frequencies, rendering it the slow motion channel, while the second is responsive to stimuli moving at a wide range of temporal frequencies, hence called the fast motion channel.

The data obtained in experiment 2 suggested an association of area MT+ to the fast motion channel, because high temporal frequency stimulation did not reduce responses compared to slow or medium temporal frequencies in that region. Contrarily, V3A and hV4 responses to high temporal frequency stimuli declined substantially while responding considerably well to low and medium temporal frequencies. On the basis of the observed response characteristics of these two areas, an association with a perceptual slow motion channel was deduced. The first criterion to assign visual areas to either of two psychophysically derived motion channels, differing in their temporal characteristics, was supplied.

The second criterion to associate visual areas to the proposed motion channels pertains to differential chromatic contrast sensitivities of the two channels and will be part of the investigations in experiment 3. This criterion is directly related to the original motivation to employ a two-channel model as opposed to only one channel for motion perception, because no single region was neurophysiologically identified, that could account for luminance as well as chromatic motion thresholds observed in monkeys and humans (Metha *et al.*, 1994; Gegenfurtner & Hawken, 1995; Stromeyer *et al.*, 1995). For instance, the candidate region MT+, known to be involved in motion perception (Newsome *et al.*, 1985; Newsome *et al.*, 1991) could not be held responsible for the excellent human detection and discrimination sensitivity for slowly moving red-green stimuli, because MT+ neurons in the macaque monkey did not respond sufficiently well to low contrast chromatic patterns (Metha *et al.*,

1994; Gegenfurtner & Hawken, 1995; Stromeyer *et al.*, 1995). To be specific, a trained monkey can detect drifting, chromatic gratings with color contrasts lower by a factor of three, than can be detected by even the most sensitive MT cells (Gegenfurtner *et al.*, 1994). Visual areas responding to low contrast moving chromatic stimuli other than MT+ must therefore exist and play some role in the detection and discrimination of motion defined by color-contrast edges (Thiele *et al.*, 1999). The second criterion to associate visual areas to either of the two motion channels must thus require the candidate regions to exhibit a higher sensitivity to chromatic contrasts than area MT+, in order to account for human detection and discrimination sensitivity specifically to slowly moving red-green stimuli for which behavioral data is established (Metha *et al.*, 1994; Gegenfurtner & Hawken, 1995; Stromeyer *et al.*, 1995).

As data from experiment 2 has shown, visual areas hV4 and V3A seem to prefer slowly moving chromatic stimuli up to 4Hz at equal cone-contrast of 14%. However, chromatic contrast sensitivity cannot be judged from experiment 2, because 14% cone-contrast is well above human detection threshold (Mullen, 1985) and all visual areas responded strongly to these stimuli. To measure cone-contrast sensitivity in a cortical region, several cone-contrast levels have to be measured. The optimal contrast levels should range from contrasts at which the region does not respond to contrasts at which the region responds maximally. Using fMRI in humans, which measures neural population responses, the appropriate cone-contrast levels for sensitivity measures of visual areas cannot directly be inferred from single-cell threshold data. It is thus appropriate to make a choice of contrasts, which contain low contrast values for each cone-contrast directions of interest, in order to uncover response sensitivity differences between candidate areas for the neural correlates of the slow motion channel. Furthermore the cone-contrast stages should also contain sufficiently high contrasts to allow comparisons with Experiment 2. If higher chromatic contrast sensitivity in hV4 and V3A as compared to MT+ is found, the second criterion, stating higher chromatic contrast sensitivity in regions associated with the slow motion perception channel would be fulfilled and the proposed associations of cortical regions to the two motion channels, as suggested in Experiment 2 could be consolidated. Experiment 3 will employ 4 cone-contrast stage values along each color direction under study ranging from 3% to 100% of the maximally possible cone-contrast, which may differ for the respective color directions (see section 2.1.1.1).

The chromatic stimulus conditions used in experiment 2 were chosen to lie along directions in cone-contrast-space emphasizing post receptor mechanisms (see section 2.1.1.1). However, little is known about human cortical response characteristics to chromatic patterns, stimulating along cone-contrast space directions other than the cardinal directions.

An influential study by Engel et al. (1997) reported measurements in human subjects, using contrast reversing checkerboard patterns modulated in two cone-contrast planes, in which the putative chromatically opponent and achromatic mechanisms are located (Engel *et al.*, 1997b). Isoresponse contours were reported for V1 and V2.

In order to derive a more complete picture of human cortical chromatic response properties, measurements along color directions, located in planes of cone-contrast space not investigated yet, are thus of high interest. Furthermore, extra-striate regions are likely to contribute to chromatic motion processing, as shown in experiment 2 and earlier reports (Gegenfurtner & Hawken, 1996; Cavanagh *et al.*, 1998; Thiele *et al.*, 1999; Wandell *et al.*, 1999; Liu & Wandell, 2005). Experiment 3 will present results consistent with measurements made by Engel et al. (1997) but extend the findings to visual areas hV4, V3A and MT+, in addition to a more complete sampling of cone-contrast space. The chromatic stimulus range will be extended to five planes in cone-contrast space including the two planes used by Engel et al. to facilitate comparison with this influential report (Engel *et al.*, 1997b).

As indicated above chromatic stimulation in each of thirteen color directions forming the five planes will be parameterized in four cone-contrast stages to derive cone-contrast response curves. These contrast response curves can be compared across retinotopically-mapped regions of visual cortex to derive color direction specific sensitivity differences. To facilitate comparison with experiment 2, and further investigate the effect of stimulus velocity, all parameterized color conditions will be presented at high and low stimulus velocities.

Only two studies exist so far that combine parametric cone-contrast stimulation control with stimulus modulation in terms of temporal frequency (Engel *et al.*, 1997b; Liu & Wandell, 2005). While the first, Engel et al. (1997), modulated the temporal frequency using stationary contrast reversing cone-contrast checkerboard patterns, the second study, by Liu and Wandell (2005), applied moving patterns, stimulating along only three axes in cone-contrast space (Liu & Wandell, 2005). Liu and Wandell (2005) report cone-contrast response functions for these three color conditions and two velocities in striate and extra-striate visual areas (Liu & Wandell, 2005).

Unfortunately the later study had several shortcomings (Liu & Wandell, 2005). Adaptational or sequential effects were not controlled, because each functional scan contained only one cone-contrast condition and the cone-contrast levels were chosen in a way, which made the comparison between color directions difficult. Furthermore the authors admit that they could not obtain good signals from area V3A and MT+, which constitute cortical regions of great interest in this thesis.

Results reported here aimed to overcome these shortcomings by extensively measuring two experienced observers in a total of 18 fMRI-scanning sessions at 18 different days, while presenting them with all color-contrast conditions in one session, using an event-related stimulus presentation. At nine of these days the stimulus presentation protocol was conducted with stimulus patterns moving at a velocity of 1Hz, while nine remaining measurements presented the same stimulus presentation protocol at a temporal frequency of 10Hz (see Methods, section 5.2). These extensive measurements yield reliable signals in every retinotopically mapped visual area (see Experiment 1) and allowed for strong conclusions regarding chromatic color contrast preferences throughout visual cortex and its dependence on speed. Furthermore, the data provide a quantification of differential visual signal representation, as the chromatic information is being passed on and processed from lower to higher tier visual cortical areas in human subjects.

## **5.2 Methods**

### **5.2.1 Subjects**

Two male, right-handed subjects participated in the experiment. They gave their written informed consent before scanning. The University of Magdeburg ethics committee approved the experimental protocol.

### **5.2.2 Stimulus & experimental design**

Stimuli were rotating rings with radial gratings presented in an annulus with  $8.8^\circ$  visual angle outer radius and  $2^\circ$  visual angle inner radius (Figure 5.1). Two velocities resulting in temporal frequency flicker of 1Hz and 10Hz were used in separate scanning sessions. Direction of rotation was randomly assigned and changed on average every 4s. Each color condition was presented at 4 different contrast levels of the maximally attainable RMS-cone-contrast per color direction (3%, 10%, 30% and 100%). For example in the L+M direction, the maximal RMS-contrast was 96% therefore L+M stimuli were presented at 2.9%, 9.6%, 29% and 96% RMS-cone-contrast (see section 2.1.2). Stimulus colors were generated along thirteen cone-contrast color-directions. Figure 5.2 illustrates the maximally attainable cone-contrast colors for each color direction and the resultant percepts as different cone-contrast values are applied. The background color was set to gray with the mean luminance level of the grating ( $417 \text{ cd/m}^2$ ).

The gratings were presented for 1s, followed by mean gray background without any pattern presentation. The inter-stimulus interval (ISI) varied between 2s and 6s with a mean

ISI of 2.5s (mean gray presentation). The pseudo randomized sequence of ISIs and the stimulus levels were optimized to allow for the efficient deconvolution of the event related BOLD-response (Hinrichs *et al.*, 2000).

Each run took 240s and ended with the presentation of a blank screen for 55s. Each subject was scanned nine times (18 runs) for each of the two velocity condition. Over all runs every stimulus combination of cone-contrast direction and cone-contrast level was presented 396 times. During the entire run subjects performed a demanding form discrimination task at the fixation cross (tall cross vs. wide cross) with the aim to keep attention allocation constant. The stimuli were back-projected onto a screen mounted in the magnet bore at 27cm distance to the eyes and viewed via a mirror. The RGB-value to luminance functions were measured (PR650 spectroradiometer, SpectraScan) for all three colors of the LCD-projector (Sharp, SX21) and linearized with a lookup table (see section 2.1.2).

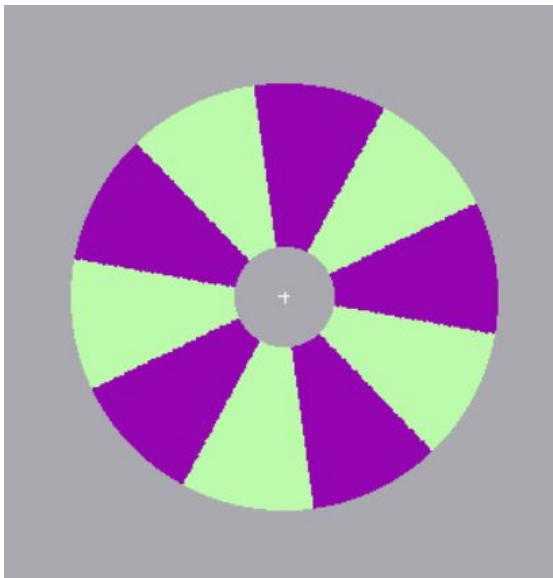


**Figure 5.1. *Representative stimulus pattern*** used in Experiment 3. Adjacent wedges contain colors stimulating along one direction in cone-contrast space. This example represents colors modulated along the L+M-direction (96% RMS-cone-contrast, equivalent to 100% contrast attainable with the equipment used for L+M). Stimuli rotated at 1 or 10Hz in randomly assigned directions. Stimulus generation was accomplished as described in section 2.1.2 and illustrated in Figure 2.1.

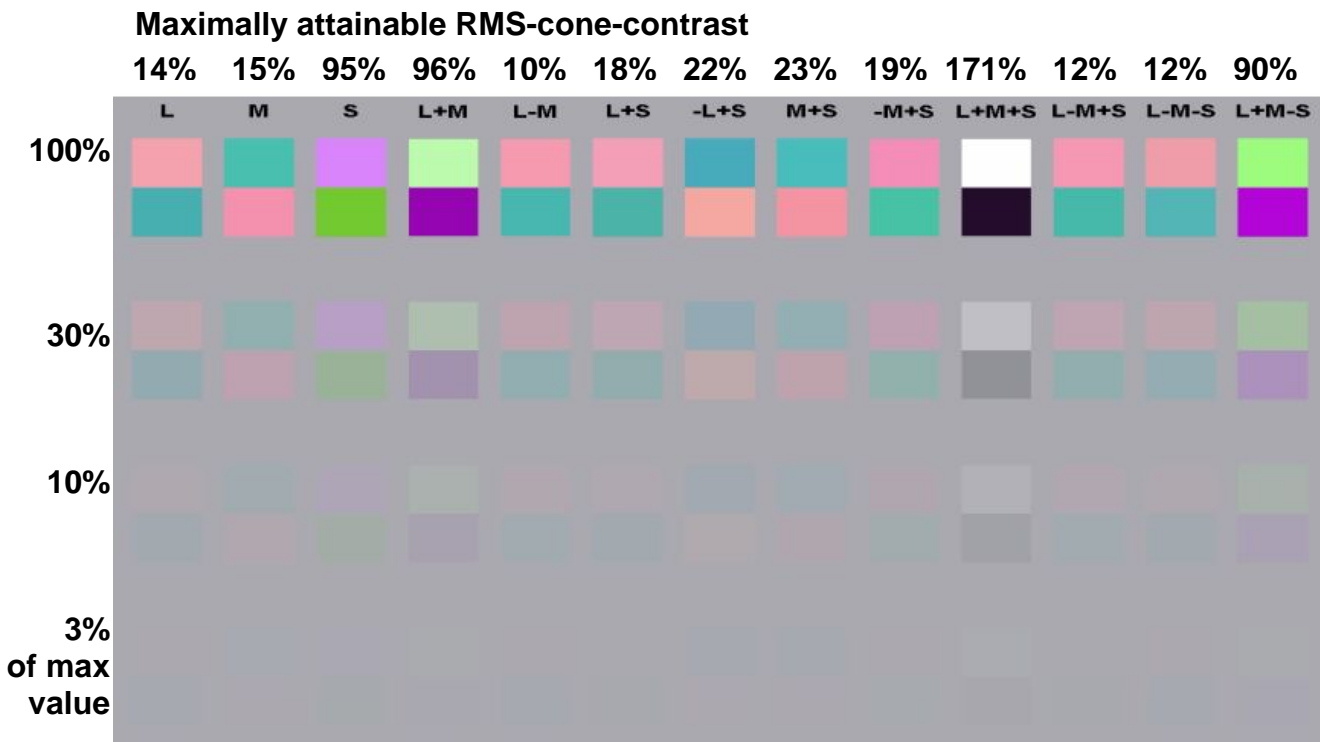


**Figure 5.2.** Horizontal order: *Maximally attainable RMS-cone-contrast for 13 color-directions* used. Vertical order: Contrast stage values and their perceptual appearance. As cone-contrast decreases colors desaturate. Note, the cone-contrast stimuli were generated with respect to the calibration of the projector used in the fMRI experiment. Hence saturation and detectability might be compromised in this figure. For instance, the lowest L-M stimulus contains 0.3% cone-contrast, which is proximally double the detection threshold at 1.5Hz temporal frequency and below detection threshold at 7.5Hz (Liu & Wandell, 2005).

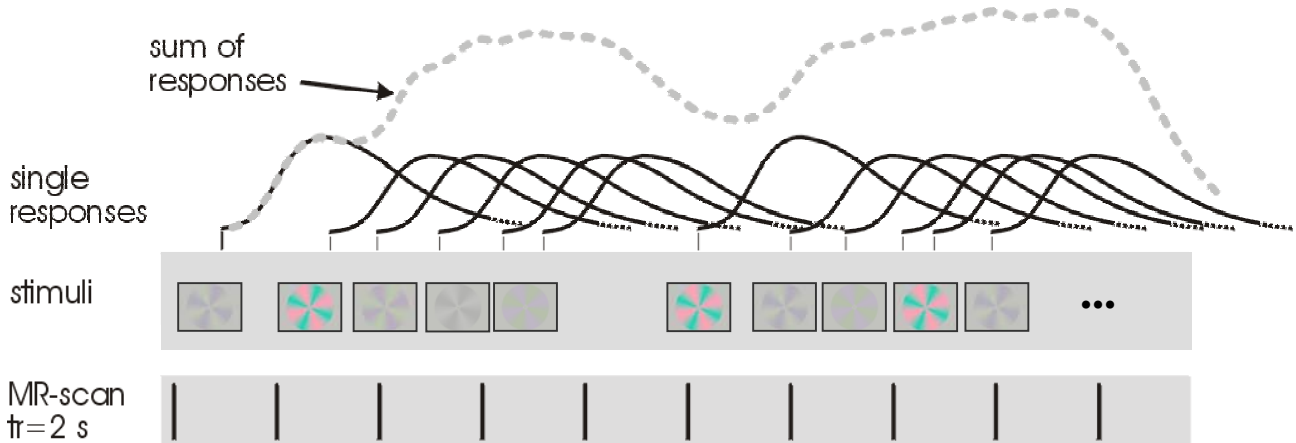


**Figure 5.3. Exemplification of stimulus time course** (presentation of stimulus events), and the resultant hypothetical BOLD-response time course as could be expected from a voxel located in a cortical region associated with visual processing. Each run started with 10s fixation task on the mean gray background only. Stimulus events were presented for 1s. ISIs of mean gray presentation and fixation task varied between 2s and 6s (mean 2.5s). Presentation of all stimulus colors and contrast levels were randomized. Each run ended with 55s blank screen presentation.

Figure 5.3 illustrates the stimulus presentation time course and a hypothetical BOLD-response time course for one voxel, the result of the overlapping BOLD-responses elicited at each stimulus event. Deconvolution was established using the WMLE-procedure introduced by Hinrichs *et al.* and described in section 2.2.3.2 (Hinrichs *et al.*, 2000).

### 5.2.3 MR-protocol

The subjects were scanned in a GE-Signa LX 1.5T neuro-optimized system with a 5” surface coil positioned at the occipital pole. BOLD-contrast images were acquired with a gradient echo planar imaging (EPI) sequence (TR=2s; TE=40ms; flip angle 80deg). 23 slices were oriented approximately perpendicular to the occipital sulcus (no gap). The voxel size was 2.81\*2.81\*3mm (64\*64 pixel in-plane matrix). For the anatomical localization of the functional images T1 weighted images (2D-spin-echo sequence) were scanned with the same slice position and thickness as the BOLD-images at a higher inplane resolution (0.7\*0.7mm, in-plane resolution 256\*256 pixels). For both subjects retinotopic maps were obtained using a standard protocol (Engel *et al.*, 1994; Engel *et al.*, 1997b) and the software package mrVista as described in Experiment 1, section 3.2.1 (Teo *et al.*, 1997; Press *et al.*, 2001).

### 5.2.4 Fitting contrast response curve

In the further analysis only voxels activated by the highest contrast that fell into the borders of the ROIs under study were included. For each measured scanning session and for each color-contrast-speed condition, the WMLE-procedure (Hinrichs *et al.*, 2000) yields one weight for a fixed hemodynamic BOLD-response function which was determined in a data based procedure, described in section 2.2.3.2. The weights determined this way can be interpreted as BOLD-amplitudes with the same but arbitrary scaling over conditions. For each of the thirteen color directions, nine measurement values (weights) were obtained (one for each session on separate days) for each of the 4 cone-contrast stages and two velocity conditions. In order to visualize cone-contrast dependence for each color-speed condition we chose to fit these weights with a sigmoid function for each visual area (Boynton *et al.*, 1996; Logothetis & Wandell, 2004; Liu & Wandell, 2005). The BOLD-contrast response function was modelled as follows:

$$R = M \frac{(c/s)^p}{(c/s)^p + 1} \quad (\text{Eq.: 5.1.}),$$

where  $R$  is the BOLD response amplitude,  $c$  is the presented stimulus contrast,  $M$  is the saturation amplitude (maximal amplitude value),  $s$  is the semi-saturation contrast parameter (mean of all amplitude values) and  $p$  is the slope of the sigmoidal function.

Fitting these parameters per color and velocity combination is based on multiple BOLD-amplitude estimates, which were collapsed over hemispheres for each subject. Every fit is therefore based on 72 data points (i.e.: 4 cone-contrast levels \* 9 days of measurements \* 2 hemispheres). Weights for a given visual area from both hemispheres were included into the fitting procedure giving a total of 18 measurements per color-contrast level and temporal frequency condition. The matlab function *fminsearch* was used (Math Works, Natick, MA) to minimize the sum of squared differences of the sigmoidal function and the obtained BOLD-responses per contrast level. Errorbars for each measured contrast level indicate the standard deviation derived from 18 underlying measurements. Error tubes have been added to the fitted curves, which were derived through linear interpolation between each consecutive upper and lower error range respectively.

### 5.3 Results

The goal of this experiment was to characterize chromatic properties of human visual cortex by using an array of 13 cone-contrast colors, spanning all major axes and thus five planes in cone-contrast space, parameterized in four cone-contrast stages and investigating the effects of two stimulus velocities. Measurements were conducted on 18 days per subject (9 days\*1Hz, 9 days\*10Hz). Since only two subjects were available for these kinds of extensive measurements they were separately analyzed, which in turn allows for a check of the replicability of the results.

Eight three-way rANOVAs for eight different ROIs (V1, V2d, V2v, V3d, V3v, hV4, V3A & MT+) parted by subject were conducted. The factors were speed (2 levels, 1 & 10Hz), color (13 levels) and contrast (4 levels, 100%, 30%, 10% and 3% percent of the maximally attainable cone-contrast in every color direction). The degrees of freedom were Greenhouse-Geisser corrected when appropriate. The Bonferroni-correction for 8 rANOVA-tests yields a p-value of 0.0063 (0.05/8). In addition, posthoc t-tests will examine specific effects of speed when called for by the global analysis and specific hypothesis generated through examination of the contrast response curves of the two speeds for each subjects ROI-color combination. The corrected p-value for multiple comparisons for follow up t-tests within one ROI is equivalent to  $p \sim 0.001$  ( $0.05 / (13 \text{ colors} * 4 \text{ contrasts}) = 0.00096154$ ) and over all ROIs  $p \sim 0.0001$  ( $0.05 / (13 \text{ colors} * 4 \text{ contrasts} * 8 \text{ ROIs}) = 0.00012019$ ). For brevity sake only p-values are reported. For a complete list of all rANOVAs and t-test results as well as the

corrected degrees of freedom, please refer to the appendix (Table 5.1 and 5.2). A negative  $t$ -value in the  $t$ -test-tables indicates a higher response for 10Hz than 1Hz generated BOLDs.

### **5.3.1 Global effects of color, contrast and velocity**

Without exception, the rANOVAs yielded a highly significant main effect of color in all ROIs of both subjects (all  $p < 0.00001$ ), indicating that different colors yield different responses in all visual areas, which was already reported in Experiment 2 (Figure 4.3). Similarly, a significant effect is observed for the factor contrast in all ROIs and for both subjects, which could be expected since BOLD-responses are known to increase as stimulus contrast is raised (Boynton *et al.*, 1996; Liu & Wandell, 2005).

The effect of speed for each visual area was very similar between subjects. Significant main effects of speed for both subjects were observed in the following areas: V2d (Dn45:  $p = 0.002$ , Lk13: V2d,  $p < 0.000$ ), V3d (Dn45:  $p < 0.000$ , Lk13:  $p < 0.000$ ), V3v (Dn45:  $p = 0.005$ , Lk13:  $p = 0.001$ ), hV4 (Dn45:  $p < 0.000$ , Lk13:  $p = 0.001$ ) and V3A (Dn45:  $p < 0.000$ , Lk13:  $p = 0.002$ ). A Bonferroni corrected significant effect in area MT+ was only observed in subject Dn45 ( $p = 0.002$ ). This indicates, that speed has a differential effect on the BOLD-responses in some but not all visual areas. For instance, both subjects do not show significant effects of speed in V1 ( $p > 0.05$ ). The reason becomes clear as one examines the contrast response functions for the two velocities for a given color direction in V1 (Figure 5.4), which will be reported in section 5.3.3.1.

### **5.3.2 Interactions**

Bonferroni corrected significant interactions of factors color and contrast were observed in all ROIs investigated in subject Lk13 ( $p < 0.000$ ) whereas this interaction was significant after Bonferroni correction for subject Dn45 only in hV4 ( $p < 0.000$ ) and V3A ( $p = 0.002$ ); and uncorrected significant in the following ROIs: V1,  $p = 0.019$ ; V2v,  $p = 0.037$ ; V3v,  $p = 0.034$  and MT+,  $p = 0.008$ . This interaction indicates for the visual areas where this effect was significant that BOLD-responses to different colors are differentially effected by contrast.

The interaction between velocity and contrast was significant (uncorrected) in all visual areas for both subject, but after Bonferroni-correction only the following regions showed a significant effect in both subjects: V1 (Dn45:  $p = 0.003$ , Lk13:  $p < 0.000$ ), V2d (Dn45:  $p < 0.000$ , Lk13:  $p < 0.000$ ), V2v (Dn45  $p = 0.001$ , Lk13:  $p = 0.001$ ) and V3d (Dn45:  $p < 0.000$ , Lk13:  $p = 0.002$ ). The following ROIs yielded additional Bonferroni corrected

interactions in subject Dn45: V3v,  $p < 0.000$ ; hV4,  $p < 0.000$ ; V3A,  $p < 0.000$ ; MT+,  $p < 0.000$ ; but not in subject Lk13.

Finally, the interaction between velocity and color was significant after Bonferroni correction in very few visual areas under investigation for subject Dn45: hV4,  $p < 0.000$ ; V3A,  $p < 0.008$ ; subject Lk13: V2d,  $p < 0.004$ .

The three-way interaction between velocity, color and contrast was not significant after Bonferroni correction in subject Dn45 and marginally significant in Lk13 for the following ROIs: V3d and V3v ( $p = 0.004$ ) as well as V3A ( $p = 0.003$ ). The interactions of velocity and contrast as well as between color and contrast will be explored further in the following section.

### **5.3.3 Contrast response curves**

As noted above, repeated measures ANOVAs resulted in significant interactions between velocity and contrast as well as interactions between color and contrast in a majority of visual areas. To explain this effect we now must turn to the contrast response functions within several visual areas to investigate in what way velocity and contrast or color and contrast may have a differential effect on the measured BOLD-responses. Due to limited space and to further facilitate comparisons with experiment 2, result presentation is restricted to visual area V1, hV4, V3A and MT+.

#### **5.3.3.1 Effects of stimulus contrast and velocity in V1**

For all measured visual areas the highly significant main effect of contrast can be attributed to the monotonic increase in BOLD-response as stimulus contrast increases in all visual areas (Boynton *et al.*, 1996; Liu & Wandell, 2005). Surprisingly, both subjects' rANOVAs, yielded no significant main effect of speed in area V1 but an interaction between speed and contrast. The different panels in Figure 5.4 represent contrast response curves for two speeds. The cone-contrast directions for displayed data were chosen to be the same as measured in Experiment 2 in order to facilitate comparison. Velocity differences for all other measured cone-contrast space directions can be judged in Table 5.2 of the appendix. Steeper increases for the high velocity contrast response curves for all color-conditions lead to a clear intersection between the two speed curves in every panel, indicative of an interaction between speed and contrast in V1. As stimulus contrast increases responses to high-speed stimuli exceed responses to low speed stimuli in area V1. The contrast range in which this intersection takes place differs over color directions.

Statistical comparisons between high and low speeds at the highest contrast values measured, endorse this effect. For instance, when high-speed responses exceed low speed

responses in our analysis, t-values will be negative (Table 5.2 appendix). Comparing both speed responses at the highest cone-contrast value yields negative t-values in both subjects and for all color directions. Comparing both speed responses at the lowest cone-contrast value yields positive t-values in both subjects and for all color directions. This is in concordance with the Bonferroni corrected significant interaction effect observed in V1. A response profile where high speed paired with high contrast elicits higher BOLD-responses as compared to low speeds and high contrasts in all color directions was unique to V1.

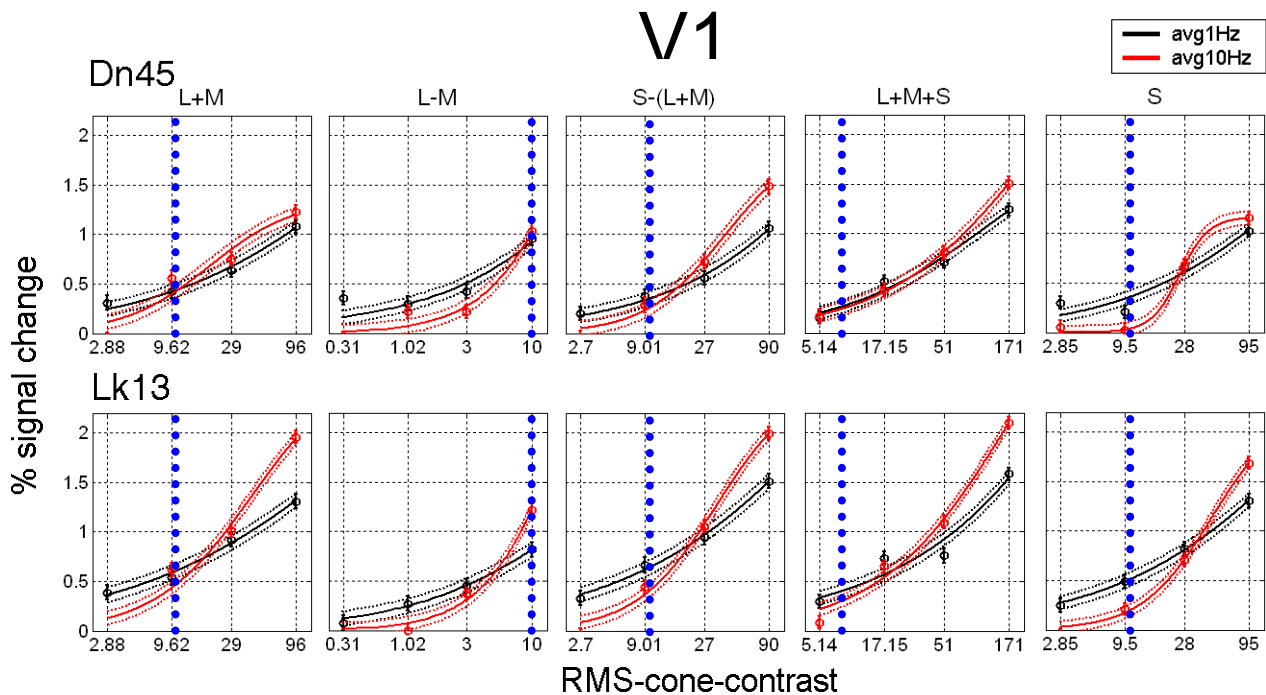


**Figure 5.4: Contrast Response Function for area V1 in Subjects Dn45 and Lk13.** Increasing cone-contrast yields increasing BOLD-responses. The X-axis uses a log scale to represent stimulus contrast. The Y-axis represents percent BOLD-signal change as measured using the WBA (see Methods). Black and red circles represent average data for 1Hz and 10Hz respectively, measured on 9 days for each color/contrast-combination and each speed separately. Black and red lines indicate 1Hz and 10Hz contrast response functions respectively. Errorbars indicate 1 standard deviation. Note that the maximally reached cone-contrast differs over color directions (x-axis). The blue dotted lines approximate 10% cone-contrast in all figure panels (the highest cone-contrast that could be reached in the L-M cone-contrast direction). This contrast value will be used as comparison value for color selectivity investigations over visual areas in section 5.3.4.

### 5.3.3.2 Effects of stimulus contrast and velocity in hV4 & V3A

Compared to V1 contrast response curves for area hV4 (Figure 5.5) and V3A (Figure 5.6) exhibit a markedly different response profile while response pattern for hV4 and V3A are remarkably similar. This provides further support for the results from experiment 2 with respect to the similarity of the response properties of area V3A and hV4. Results of experiment 2 additionally suggested a preference for slowly moving chromatic targets in these regions, while a recent report assigns a high-speed achromatic preference to V3A (Liu & Wandell, 2005). It is thus of particular interest to compare the response profiles elicited by the

two velocities for the L-M and L+M+S stimuli in V3A and hV4, because they emphasize a chromatic R/G- and achromatic B/W-mechanisms respectively.

Contrarily to the results from Liu et al. (2005) we find no support for a fast speed preference in these regions, because for subject Dn45, no Bonferroni corrected significant velocity differences at any cone-contrast stage of achromatic L+M+S stimulation was found in neither hV4 nor V3A ( $p > 0.001$ ). Furthermore, the V3A response profile to achromatic stimuli for subject Lk13 shows a Bonferroni corrected significant difference at the lowest contrast stage of 5% ( $p < 0.001$ ), but in the reverse direction as expected from Liu et al. (2005), indicating low speed preference, while no other achromatic cone-contrast stage yielded significant velocity differences in V3A. Similarly in hV4 for subject Lk13, stimuli at the lowest achromatic cone-contrast stage yielded a significant velocity difference after Bonferroni correction ( $p < 0.001$ ), while no other contrast stage showed a corrected significant differences ( $p > 0.001$ ) indicating a slow speed preference as well.

Having shown that V3A and hV4 show no preference for fast achromatic speed, we may test predictions from experiment 2, which suggested a slow speed chromatic preference in these regions. A slow speed chromatic preference for both regions becomes obvious as responses to R/G stimuli (L-M) are compared at low cone-contrast stages (Figure 5.5 and 5.6). For instance, responses to L-M stimulation in both regions clearly differed between the low and high-speed condition up until the third contrast stage of 3% for subject Lk13 after Bonferroni correction ( $p < 0.001$ ). For subject Dn45, the response difference elicited by the two velocities was Bonferroni corrected significant until the third contrast stage for V3A ( $p < 0.0001$ ) and for hV4 until the second contrast stage (1%), Bonferroni corrected ( $p < 0.0000$ ). At 10% cone-contrast, the highest L-M contrast possible, both speeds generate roughly equal responses in both areas. These response profiles clearly indicate a low speed chromatic preference for both hV4 and V3A in concordance with experiment 2. In addition, a response profile as observed in V1 where the high-speed contrast response curves exceed the low speed curves at sufficiently high contrasts was not prevalent in either hV4 or V3A.

It should be noted that both areas gave strong responses at the two lowest cone-contrast stages for the chromatic conditions L-M and pure S-cone stimuli at low velocity, indicating a very high sensitivity to low chromatic contrast in area hVA and V3A. This differs to response profiles measured in motion sensitive cortex MT+, which are presented in the next section.

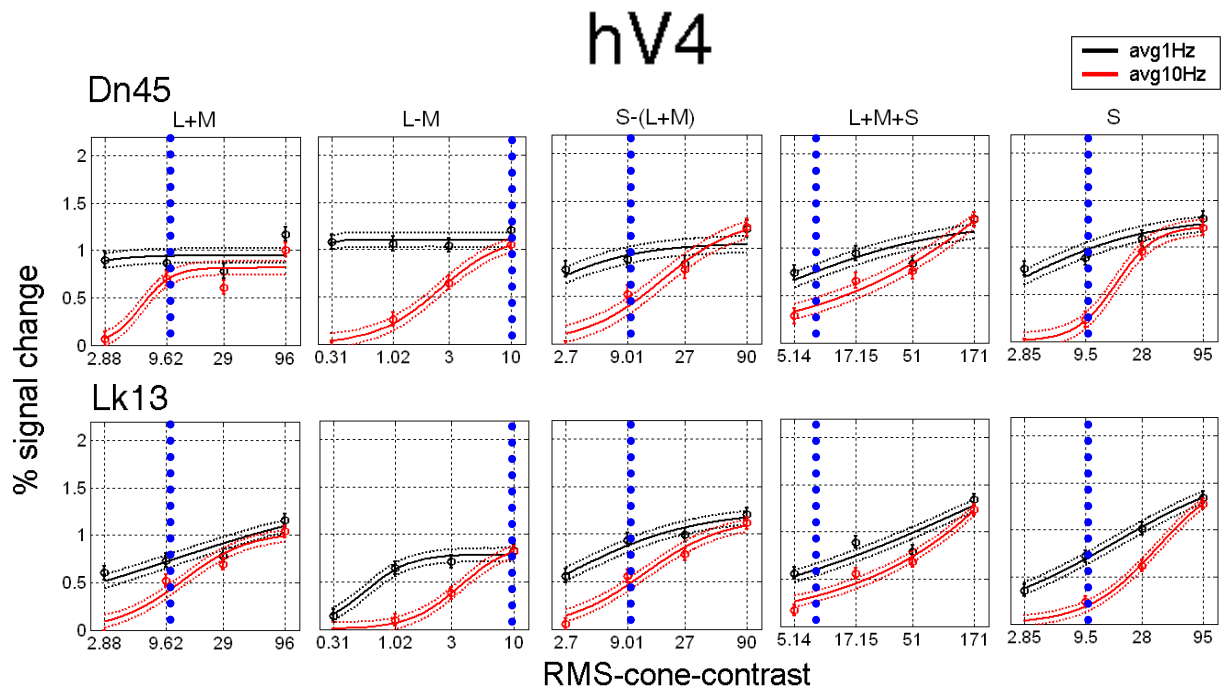


**Figure 5.5: Contrast Response Function for hV4 in Subjects Dn45 and Lk13.**  
 Plotting conventions as in Figure 5.4

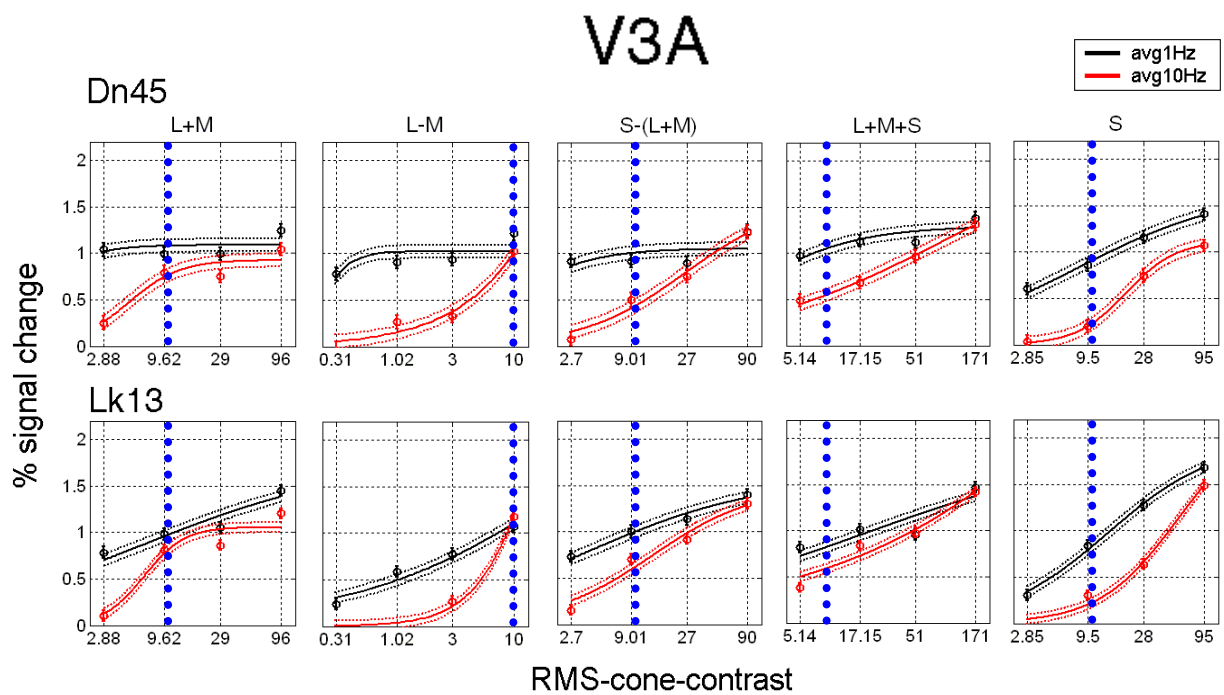


**Figure 5.6: Contrast Response Function for V3A in Subjects Dn45 and Lk13.**  
 Plotting conventions as in Figure 5.4

### 5.3.3.3 Effects of stimulus contrast and velocity in MT+

A yet different contrast response profile was observed for visual area MT+ (Figure 5.7). In both subjects, the two contrast response curves per speed and color direction were more similar (closer) to one another with respect to response magnitude as compared to the two velocity contrast response functions in area hV4 and V3A. This effect appears to be due to a general attenuation of low speed responses, observed across all color directions.

Motion sensitive region MT+ is believed to receive visual information mainly by means of the magnocellular pathway, while parvo- and konio-cellular pathway contributions have been reported, but seem not fully established (Maunsell *et al.*, 1990; Gegenfurtner *et al.*, 1994; Thiele *et al.*, 1999; Wandell *et al.*, 1999; Nassi & Callaway, 2006). It is thus of interest, to compare response differences elicited by color-directions, which are assumed to emphasize these pathways (Krauskopf, 2000a) and in addition investigate possible velocity effects.

Color-directions, which are believed to be primarily transmitted through the magnocellular pathway, are L+M and L+M+S (Gegenfurtner & Sharpe, 1999). Testing velocity differences between the two speed conditions at each cone-contrast stage for perceptually achromatic L+M+S stimuli with t-tests, reveals no significant difference after Bonferroni correction for both subjects ( $p > 0.01$ ). Indicating a speed invariant response profile to achromatic stimuli in area MT+. Testing speed differences for stimulation modulated along the L+M cone-contrast direction in both subjects revealed also no significant velocity difference after Bonferroni correction ( $p > 0.01$ ), for all but the lowest cone-contrast stage in subject Lk13 ( $p < 0.001$ ). The contrast response curves in Figure 5.7 illustrate these effects.

Chromatic stimulation, typically associated with parvo-cellularly driven transmission, is best modulated along the L-M-axis in cone-contrast space (Derrington *et al.*, 1984). Comparing responses at each cone-contrast stage over velocities, reveals no Bonferroni corrected significant differences for subject Lk13 ( $p > 0.01$ ), while at the lowest L-M-cone-contrast stage comparison (0.3%), a significant difference was observed for subject Dn45 ( $p < 0.0001$ ). It is worth noting that a strong slow-speed response produced this difference.

Stimulation emphasizing the konio-cellularly driven path, while keeping L+M stimulation constant, modulates the S-cones only, representing yet another purely chromatic cone-contrast direction. Testing velocity response differences along the S-cone axis in cone-contrast space reveals no Bonferroni corrected significant difference ( $p > 0.001$ ), for both subject at all but the lowest cone-contrast stage of 2.85% ( $p < 0.0001$ ) in subject Dn45. Again, this effect was produced by a slow-speed response.

In summary, all but a few cone-contrast directions and those inconsistent across subjects revealed no significant effects of velocity compared at the respective cone-contrast

stage in area MT+. If comparisons were significant at a Bonferroni corrected level, they tended to be for very low cone-contrast values. The relative speed invariance as reported in experiment 2 can thus be confirmed.

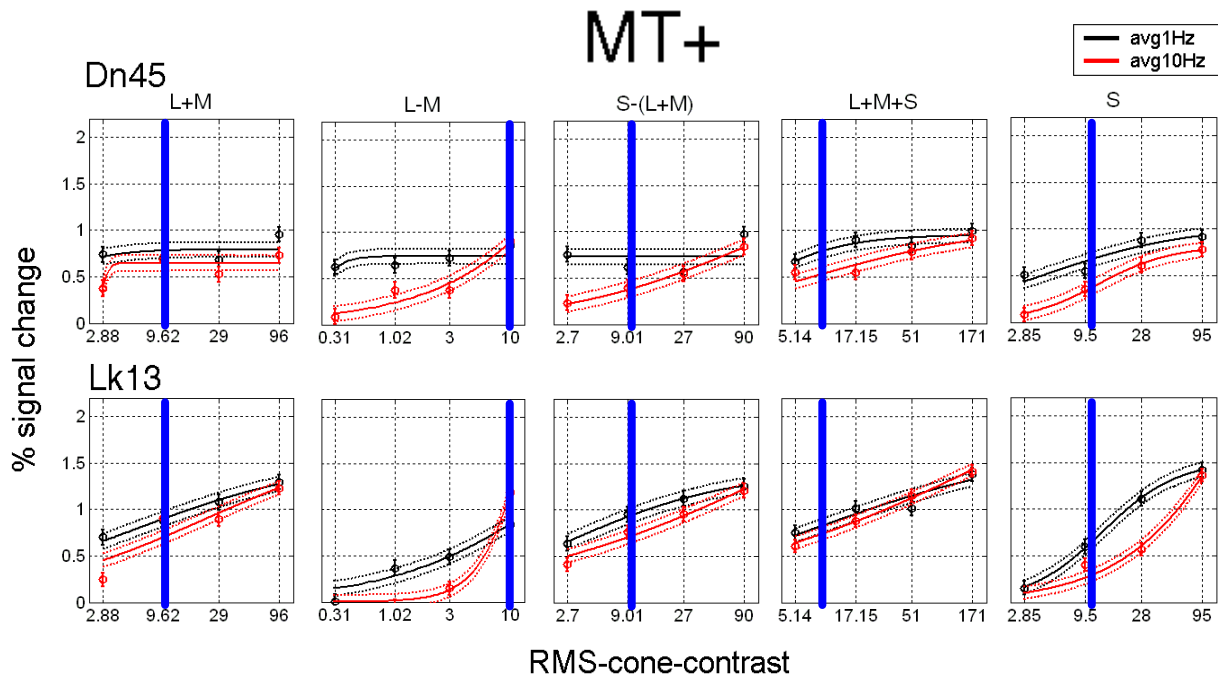


**Figure 5.7: Contrast Response Function for MT+ in Subjects Dn45 and Lk13.**  
Plotting conventions as in Figure 5.4

### 5.3.4 Comparison at equal cone-contrast

The analysis of BOLD-responses in experiment 3 has so far focused on cone-contrast directions, which emphasize the stimulation of known post-receptoral mechanisms while keeping contribution from other mechanisms constant. We chose to compare the responses at several cone-contrast levels for these color directions in experiment 3, to uncover sensitivity differences in several visual areas, expected from psychophysical studies, and to confirm predictions made in experiment 2, regarding the association of several visual areas to postulated mechanisms of motion perception. It is however of high interest to study the BOLD-responses to cone-contrast directions that do not emphasize only one single mechanism but lie in between cardinal directions, and thus, stimulate several mechanisms simultaneously<sup>3</sup>. This is of high interest because these cone-contrast combinations span planes in cone contrast space, which have previously not been investigated.

We measured thirteen cone-contrast space directions at individually scaled cone-contrast levels, the responses of which have been interpolated with a sigmoid interpolation

<sup>3</sup> For simplicity, these cone-contrast directions are referred to as ‘mixed colors’

function for each color and velocity combination separately (see section 5.2.4). We refrain from presenting cone-contrast response functions to all of these directions due to limited space, and chose to present responses to all cone-contrast direction at an equal cone contrast for visual areas V1, hV4, V3A and MT+ (see sections 1.2.3.6, 1.3 and 2.1.2). This characterizes chromatic selectivity within one visual area for equal physical contrast at the initial input stage (see section 1.2.1.1) and provides clues, how chromatic selectivity may change as we compare effects of velocity or color within and across areas.

Statistical analysis is omitted at this point, because the responses shown are interpolated values determined at the 10% cone contrast point shown as blue dotted lines in figures 5.4 to 5.7. Error bars can be regarded as a measure for reproducibility since 18 measurements went into every value (9 scanning sessions & 2 hemispheres, see Section 5.2.4). The 10% cone contrast value was chosen as the color sensitivity comparison value, because it was the highest achievable equal cone contrast in the L-M direction, which in addition lay well within the range of all other achievable colors of the equipment and assured measurable responses in all visual areas at both speeds. Comparable color conditions, actually measured at cone-contrast stages fairly close to the 10% criterion, are as follows: L+M (9.6%), S (9.5%), S-L-M (9%), L-M (10%), L-M+S (12%), L-M-S (12%), L (14%), M (14%) and L+M+S (17%).

#### **5.3.4.1 Effects of stimulus velocity and color**

This section compares BOLD-responses at equal 10% cone-contrast, similar to experiment 2, in order to assess chromatic selectivity and the effect of speed in the visual areas. We find that for all ROIs and for both subjects the effect of color is more pronounced than the effect of speed, which means that the effect of speed does not override the effect of color. This becomes clear as one examines Figures 5.8 to 5.11.

At 10% cone-contrast, one can for instance apply the following general rule: If a 1Hz response in color direction X is stronger than the response to 1Hz stimuli in color direction Y, the same response relation will be observed for 10Hz stimuli. The values for factor speed are exchangeable in this rule. In other words color leads speed with respect to magnitude of BOLD-responses.

Color selectivity profiles measured for several visual areas in both subjects are highly similar for the same areas in both subjects. The effect of stimulus color in V1 is quite striking. Figure 5.8 reveals that at a cone-contrast of 10%, V1 responses to stimuli, putting emphasis on the B/Y mechanisms (S) and achromatic mechanism (L+M+S) are smallest for both speeds, while R/G modulations (L-M) exceed them by far. The response to luminance stimuli

(L+M) exceed responses to stimuli emphasizing the achromatic mechanism (L+M+S) in both subjects, indicating a probable inhibitory property of S-cone contribution on the BOLD-response, which is also indicated by responses to stimuli containing pure S-cone contribution, opposed by the luminance channel (L+M). Responses to those colors (S-(L+M)) are also smaller than to L-M especially at high speeds (reproduced as in Experiment 2).

In addition, the expected response magnitude hierarchy (L-M > L+M > S-responses) can be confirmed at both speeds for V1 neuronal populations (Engel *et al.*, 1997b; Liu & Wandell, 2005). The higher responses to fast moving colors, reported in section 5.3.3.1, can already be observed for some color directions, while some need a higher contrast stage to show this effect (Figure 5.8).

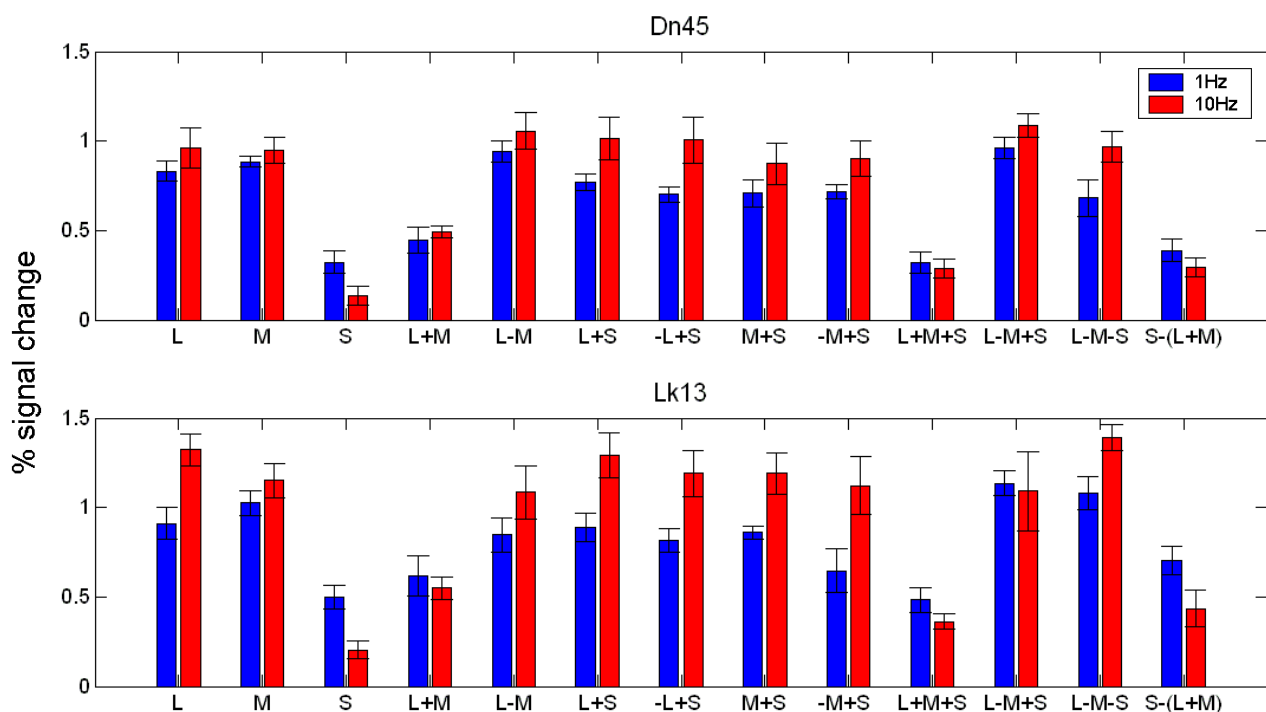


**Figure 5.8: V1- BOLD-responses at 10% equal cone-contrast**

Data are shown for all 13 cone-contrast-space directions for 1Hz (blue bars) and 10Hz (red bars) speeds. Subject Dn45 upper panel ; subject Lk13 lower panel. Error bars indicate the standard error derived from 18 values (see section 5.2.4) at 10% cone-contrast determined from the each separately fitted contrast response function. The lowest responses were obtained for stimuli that emphasize putative mechanisms except for L-M (R/G-mechanism). Responses to high velocities exceed responses to low velocities for some color directions. As contrast is raised all responses to high velocities will exceed the low speed response (see contrast response curves in section 5.3.3.1).

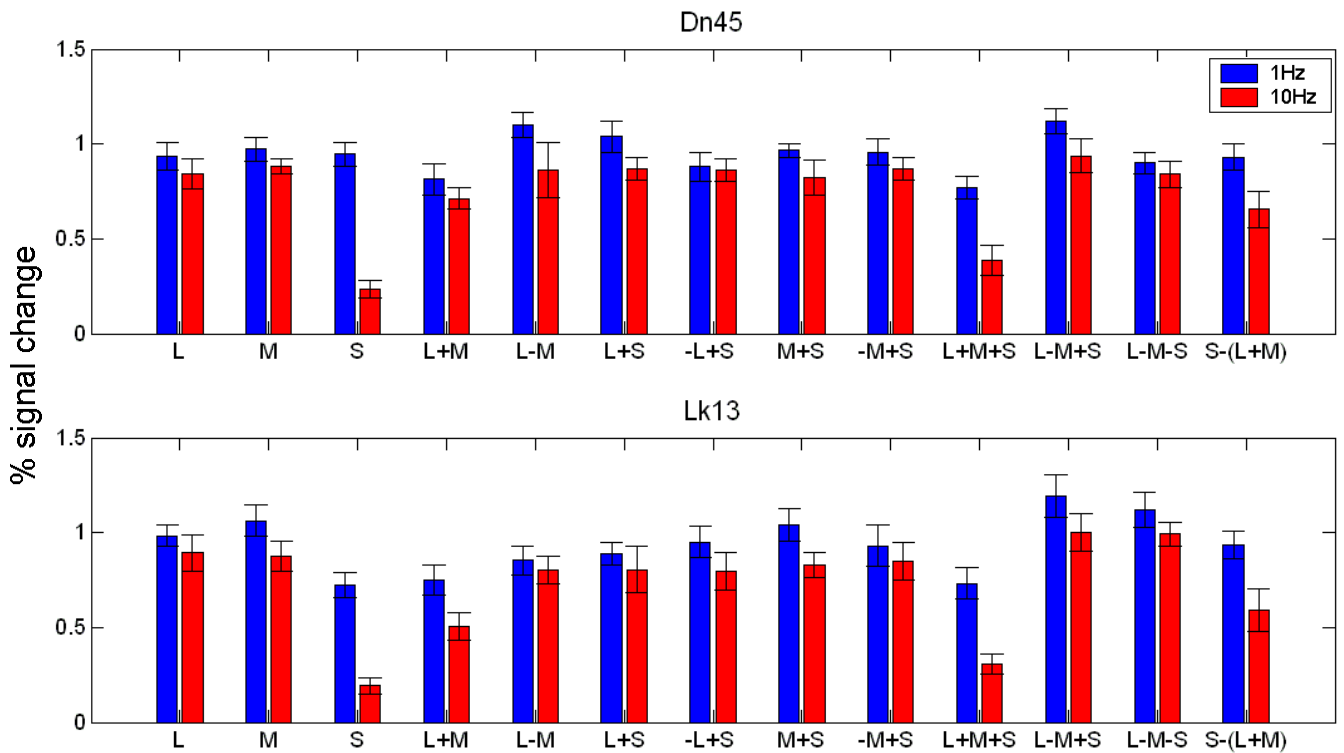


**Figure 5.9: hV4 BOLD-responses at 10% equal cone-contrast**

Conventions are the same as in Figure 5.8. Compared to 10% cone-contrast responses in V1, hV4 responses at slow speeds are substantially amplified, while high-speed responses are always lower than low speed responses.

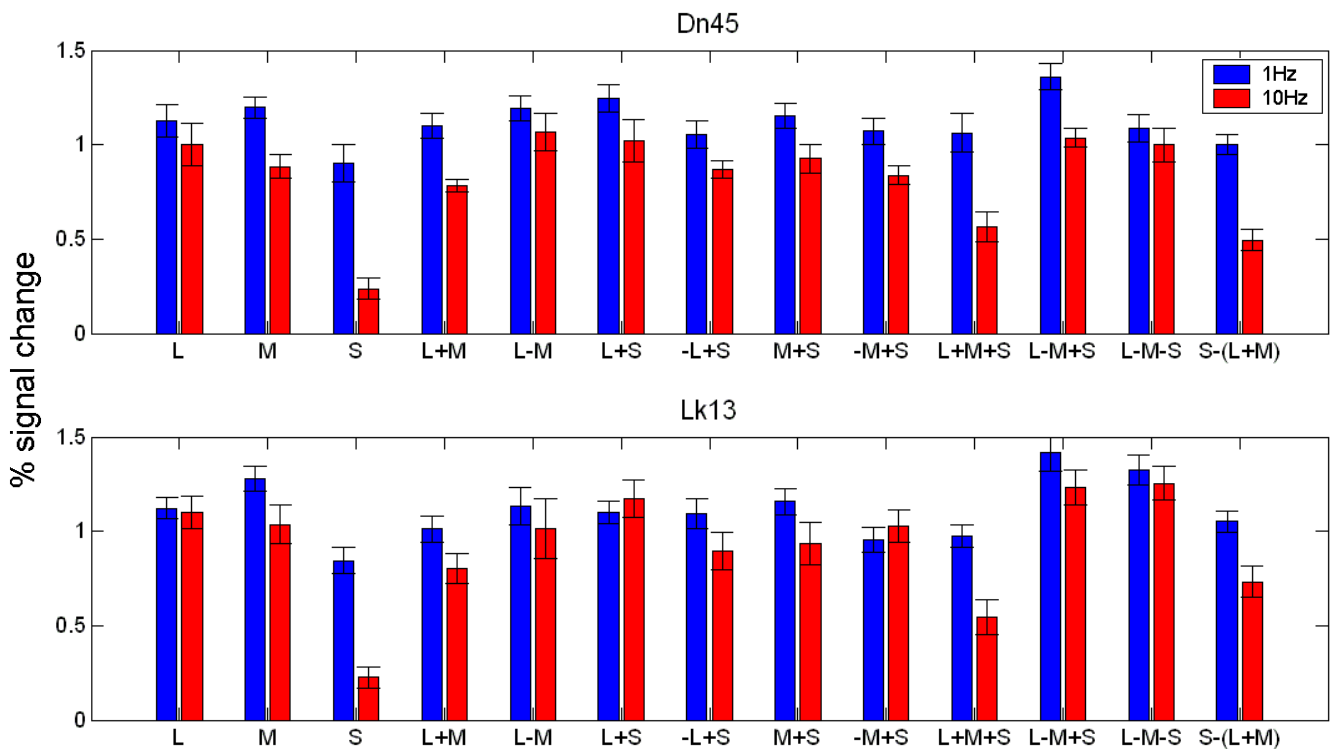


**Figure 5.10: V3A BOLD-responses at 10% equal cone-contrast**

Conventions are the same as in Figure 5.8. Compared to 10% cone-contrast responses in V1, V3A responses at slow speeds are substantially amplified, while high-speed responses are always lower than low speed responses.

Comparing equal 10% cone-contrast responses in areas hV4 and V3A in Figures 5.9 and 5.10 to V1 (Figure 5.8), the picture changes substantially, while response profiles for hV4 and V3A are highly similar. The above mentioned sensitivity hierarchy of response magnitude in the order of  $L-M > L+M > S$ , is well pronounced at 10Hz stimuli but weaker for 1Hz stimuli. Responses to 1Hz moving patterns appear more similar in both regions. This emphasizes hV4 and V3A as highly sensitive to all color combinations and clearly indicates their preference for low speeds because responses to slow moving colors are amplified compared to V1, while fast moving color responses mirror the V1 profile.

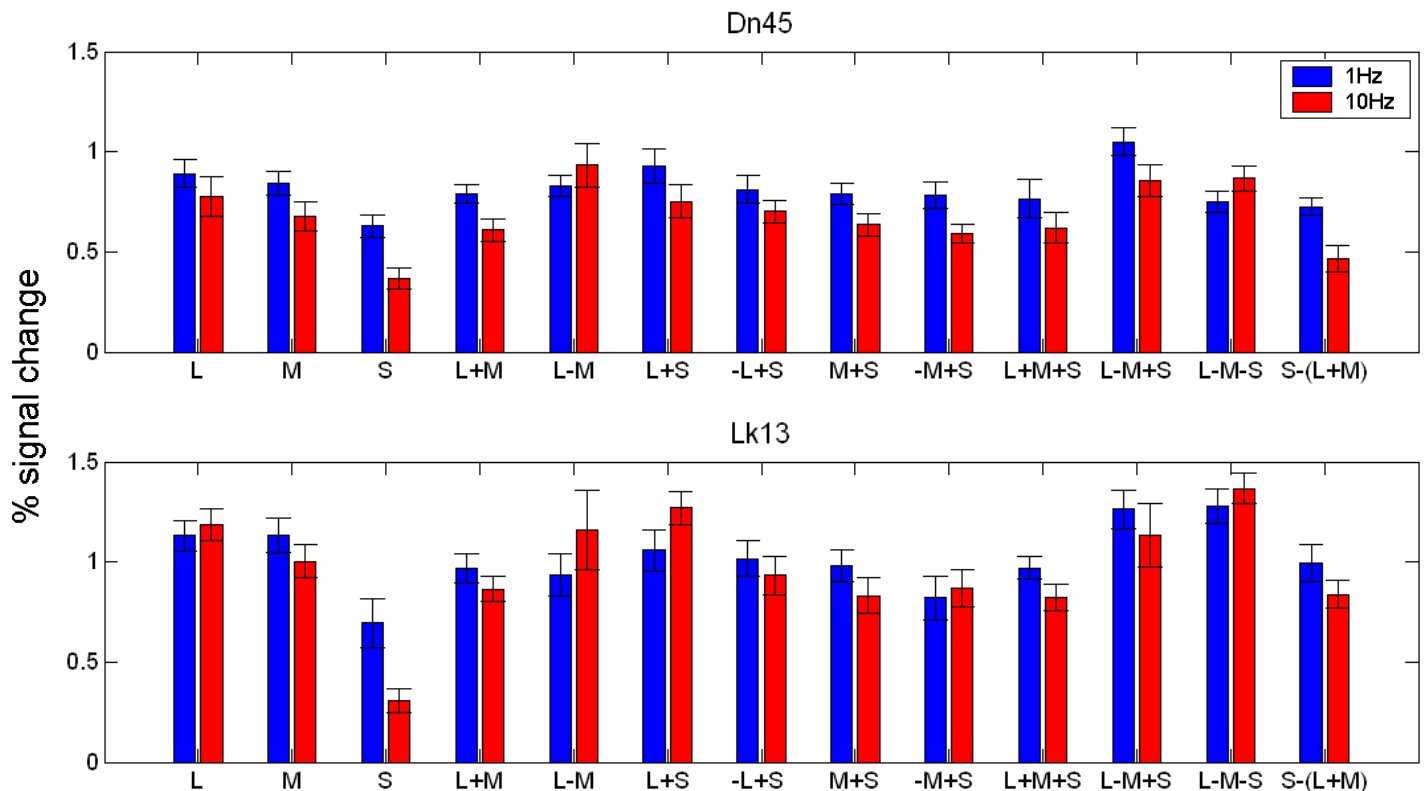


**Figure 5.11: MT+- BOLD-responses at 10% equal cone-contrast**

Conventions are the same as in Figure 5.8. Compared to 10% cone-contrast responses in hV4 and V3A, MT+ responses at slow and high speeds are roughly equal.

The color and speed response profile is different to hV4 and V3A in a way that slow speed preferences are far less prevalent especially for achromatic stimuli (Figure 5.11). While in hV4 and V3A fast achromatic responses are well below slow chromatic responses, this difference is marginal in area MT+. We thus reproduced results from experiment 2, in which we found no achromatic fast speed preference in these regions but a slow chromatic preference. In addition, a preference in MT+ for stimuli emphasizing a luminance or achromatic mechanism, as expected from a region, assumed to be primarily driven by magnocellular signals (Maunsell *et al.*, 1990) cannot be confirmed, as responses to L+M, L+M+S and L-M stimuli are compared. Responses to these colors are found to be roughly

equal to one another and to both speeds, indicating a relative indifference to cone-contrast direction. However, the well described weak response to pure S-cone stimuli in MT+, can be confirmed here as well (Seidemann *et al.*, 1999; Wandell *et al.*, 1999), especially at high temporal frequencies.

Interestingly, for both subjects and in all visual areas measured, highest responses are evoked by ‘mixed colors’, which may put emphasis on several cortico-geniculate channels simultaneously. The effect is most pronounced for color directions emphasizing the B/Y- and R/G- mechanism simultaneously (L-M+S & L-M-S). If two different color mechanisms are stimulated simultaneously, a fairly high BOLD-signal is expected, since separate cell populations tuned to those mechanisms in the respective visual areas, will respond (but see discussion).

### **5.3.5 Ellipse fits**

#### **5.3.5.1 Effects of stimulus contrast, color and velocity**

In order to derive a more complete understanding of human cortical color processing and its dependence on stimulus speed, this section aims to summarize the data for all color directions in the contrast range. Due to limited space, a presentation of cone-contrast response curves to all used color directions was omitted in section 5.3.3, and the presented bar plots in section 5.3.4 do not allow to judge the effects of increasing contrast over all color directions. To exemplify the relationship between cone-contrast and all measured color-directions, ellipse fit plots have been constructed, in which over 4 equal-cone contrast stages, the effects of stimulus contrast can be comparably judged across all color directions within one ROI in addition to the effects of velocity (Figures 5.12 to 5.15). Similar plots have been provided by Engel *et al.* (1997), who sampled responses in two cone-contrast planes (Engel *et al.*, 1997b). Responses to stimuli in the same two planes used by Engel *et al.* (1997) appear in the two left most columns, while the additional three planes from this study appear in the three right most columns. Since measurements in primary visual cortex revealed the most unique effects of velocity over contrasts for all color directions, we chose to present V1 ellipse fit plots for both subjects. To underline the uniqueness of V1 contrast and speed effects we provide the same ellipse-fit plots for the motion sensitive region MT+.

Each row in Figures 5.12 to 5.15 represents BOLD-responses at increasing equal cone-contrast of 2.5%, 5%, 7.5% and 10% respectively. The higher contrast levels are not displayed because no data could be obtained for contrasts higher than 10% in the L-M direction. All values are based on fitting equation 5.1 to the responses at every cone-contrast level for every

scanning session and for each ROI/color/contrast condition, which were intercepted at the requested contrast values (2.5%, 5%, 7.5% and 10%). The average of eighteen values obtained this way is plotted along the appropriate axis, representing measurements from two hemispheres at nine days for 1Hz and 10Hz respectively.

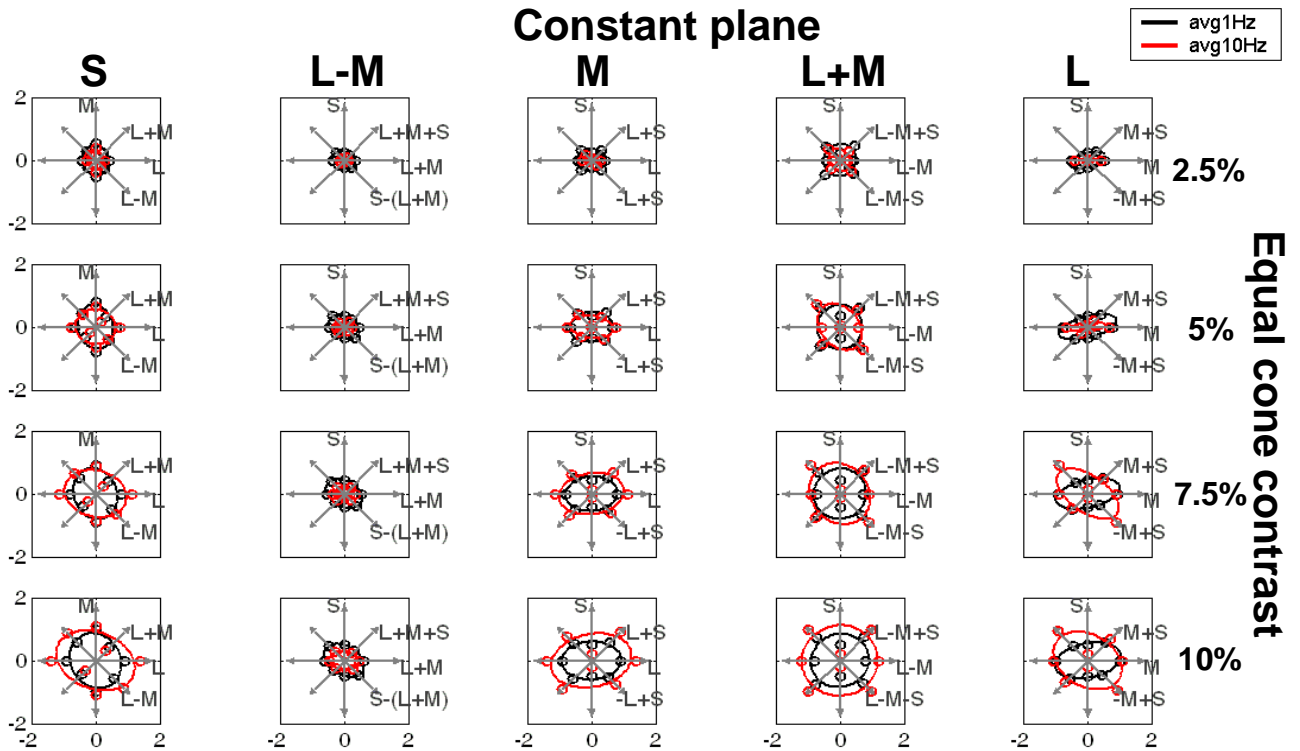


**Figure 5.12: Ellipse-fit-plots of V1 BOLD responses, subject Lk13.**

Each panel represents BOLD responses in one plane of cone-contrast space at equal cone-contrast. Each row represents equal cone-contrasts in five planes: Rows: 1<sup>st</sup>. 2.5%-; 2<sup>nd</sup>. 5%-; 3<sup>rd</sup>.7.5%-; 4<sup>th</sup>. 10% equal cone-contrast. Each column represents the same cone-contrast plane in which contributions from specific cone-classes or combinations of them are kept constant: Columns: 1<sup>st</sup>. constant S-; 2<sup>nd</sup> :constant L-M-; 3<sup>rd</sup> : constant M-; 4<sup>th</sup> : constant L+M-; 5<sup>th</sup> : constant L-plane. BOLD-responses within each plane are displayed along four cone-contrast space directions depicted by gray arrows. Distance from the coordinate systems center represents BOLD-response magnitude plotted on the appropriate color axis. The circles represent interpolation values, black and red for 1 and 10Hz respectively. BOLD-response values are fitted with an ellipse: Black lines 1 Hz; Red lines 10 Hz responses. BOLD-responses increase with increasing cone-contrast along rows. Responses to fast moving stimuli exceed responses to slow moving stimuli, but the contrast values at which this occurs differs across cone-contrast space directions. Highest responses are observed along directions opposing L-M and S-cone signals. The ellipse area in the constant L-M planes (2<sup>nd</sup> column) is substantially smaller as compared to MT+ (Figures 5.14 and 5.15). For further details see section 5.3.5.1.

Each column represents stimuli, from four color direction, that lie within one plane of cone-contrast space. In the first column, for example, x- and y-axis represent pure L-cone and pure M-cone stimuli respectively. The luminance mechanism is along the L+M diagonal because it is assumed to sum L- and M-cone signals. The R/G-mechanism is represented by the L-M diagonal, because it takes the difference between L- and M-cones, representing an opponent color mechanism. S-cone stimulation is held constant within this plane and would form the z-

axis, pointing towards the reader. The plane in the second column keeps L-M contributions constant, the third column for instance keeps M-cone contributions constant, the fourth column keeps the luminance contributions constant (L+M), while within the fifth column, L-cone influence is constant.

As contrast increases from the first to the fourth row BOLD-responses increase. These plots are well suited to judge, for example the contrast value at which high- speed stimuli exceed slow speed stimuli in the different color directions.

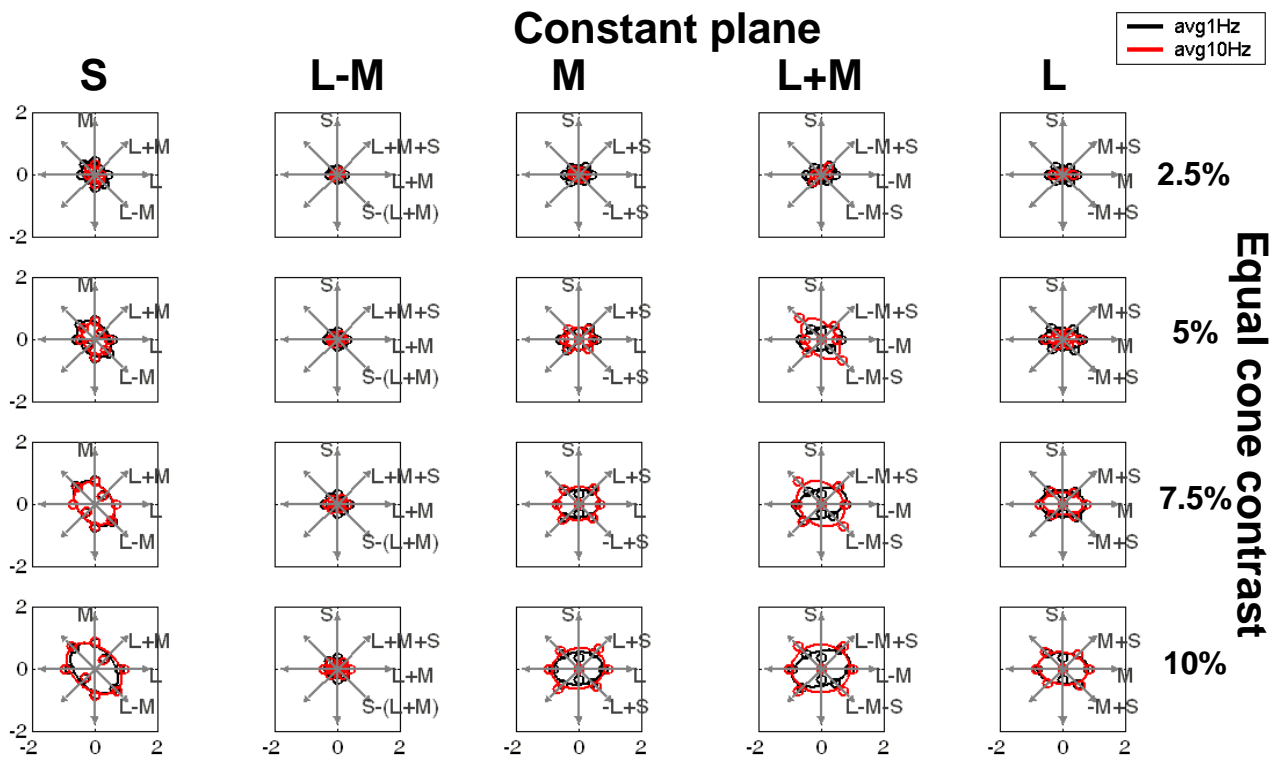


**Figure 5.13: Ellipse-fit-plots of V1 BOLD responses, subject Dn45.**

Plotting conventions as in Figure 5.12. BOLD-responses increase with increasing cone-contrast along rows. Responses to fast moving stimuli exceed responses to low moving stimuli, but the contrast values at which this occurs differs across cone-contrast space directions. Highest responses are observed along directions opposing L-M and S-cone signals at 10% equal cone-contrast. For further details see section 5.3.5.1.

For instance in Figure 5.12 (V1) it can be seen that while the BOLD-response elicited by fast L+M stimuli is below the response to the slow stimuli at 10% cone-contrast (4<sup>th</sup> row), a fast pure L-cone stimulus elicits similar responses to slowly moving L-cone patterns at 5% cone-contrast but exceeds them at 7.5% cone-contrast. The same response profile where responses to fast moving stimuli exceed responses to slow moving stimuli is observed for the L-M (R/G) mechanism. Interestingly for both subjects V1s, ellipse fits in the second column reveal that the area spanned by the fitted ellipses (i.e. BOLD-responses) is relatively small when the contrast in L-M direction is set to zero, suggesting a stronger contrast gain for the L-M mechanisms as compared to the pure S-mechanism.

The pattern of results changes substantially in MT+ for both subjects (Figure 5.14 and 5.15). In MT+, the BOLD-response to additive cone signals such as L+M and L+M+S increase more strongly with increasing contrast as compared to V1. In both subjects, L+M and L+M+S response magnitude in MT+, exceed V1 responses to these stimuli at the lowest contrast level. This can be interpreted as indicator for higher contrast sensitivity to luminance signals in MT+ as compared to V1.

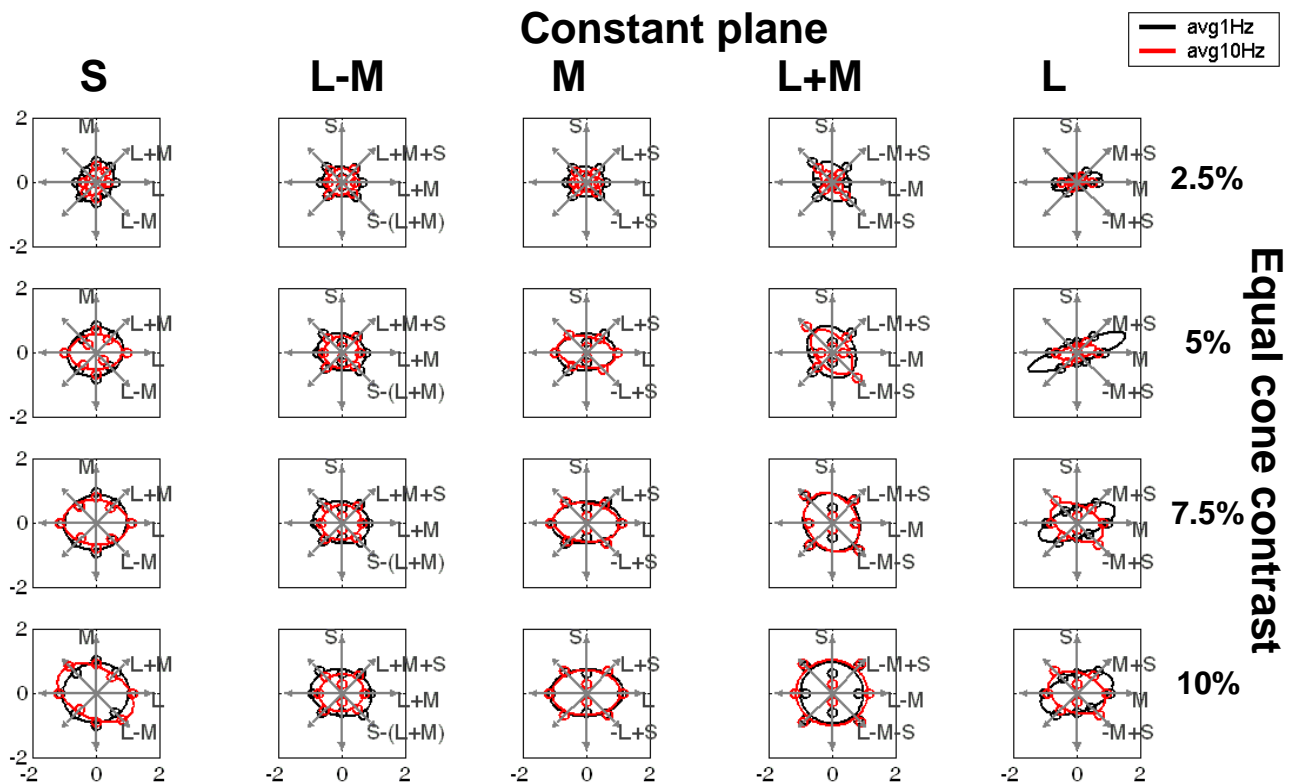


**Figure 5.14: Ellipse-fit-plots of MT+ BOLD responses, subject Lk13.**

Plotting conventions as in Figure 5.12. BOLD-responses increase with increasing cone-contrast along rows. Responses to fast moving stimuli do not exceed responses to low moving stimuli. Highest responses are observed along directions opposing L-M and S-cone signals at 10% equal cone-contrast. The ellipse area in the constant L-M planes (2<sup>nd</sup> column) is substantially larger as compared to V1 (Figures 5.12 and 5.13) For further details see section 5.3.5.1.

As we compare V1 and MT+ with respect to cone-contrast-planes not investigated in prior human imaging reports (three right columns in Figures 5.12 – 5.15), higher response magnitudes are observed in MT+ for both speeds at every cone-contrast level, indicating a motion signal amplification as it is transmitted from primary visual cortex to MT+. It appears that no response to fast moving stimuli exceeded slow moving stimuli in MT+ as was observed in V1. This holds for all cone-contrast directions tested in MT+.

The most interesting similarity between V1 and MT+ for both subjects is that considerable contrast-dependent changes occur in responses to directions with L- and M-cone contributions of opposite sign underlining the pivotal role of the L-M mechanism in early visual cortex as well as higher tier areas. Indeed the most extensive increases with contrast

were seen in the plane containing the L-M stimuli opposed by the pure S-cone stimulation (4<sup>th</sup> column), constituting essentially a stimulus emphasizing the L-M- and S-mechanisms while leaving the luminance mechanism constant. These stimuli elicit highest BOLD-responses at very low contrasts in V1 as well as in MT+ of both subjects. In addition, neural populations underlying these high BOLD-signals are highly motion-sensitive, indicated by high responses for high and low speeds starting as low as 2.5% contrast. From data reported here it can however not securely be concluded whether responses to L-M opposed by S-cone stimuli are generated by a unique cell population tuned to these kind of stimulus configurations, or if indeed the high BOLD-responses are a consequence of several cell populations responding simultaneously, such as L-M and S responsive cells.

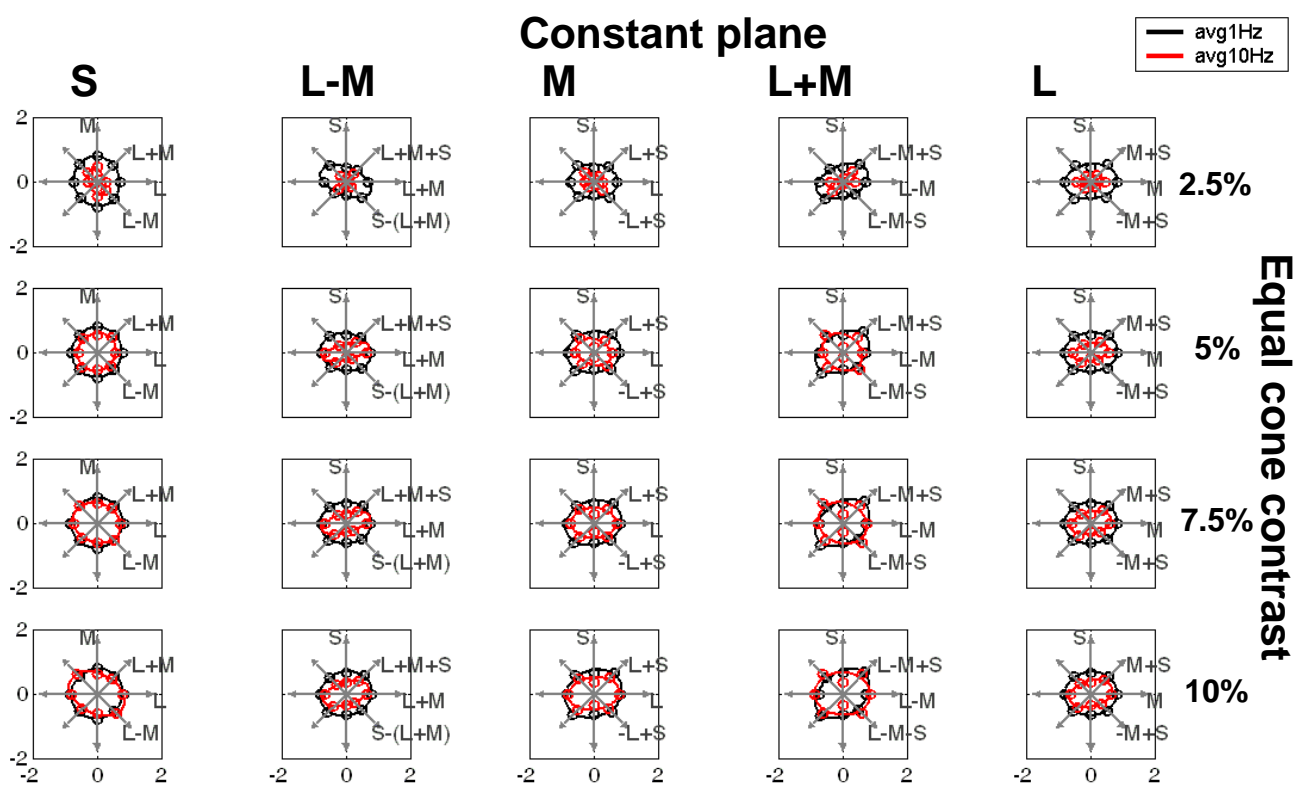


**Figure 5.15: Ellipse-fit-plots of MT+ BOLD responses, subject Dn45.**

Plotting conventions as in Figure 5.12. BOLD-responses increase with increasing cone-contrast along rows. Responses to fast moving stimuli do not exceed responses to low moving stimuli. Highest responses are observed along directions opposing L-M and S-cone signals at 10% equal cone-contrast. The ellipse area in the constant L-M planes (2<sup>nd</sup> column) is substantially larger as compared to V1 (Figures 5.12 and 5.13) For further details see section 5.3.5.1.

## **5.4 Discussion**

The third experiment investigated BOLD-response differences in several visual areas as a function of speed, cone-contrast and color. The results of which point towards preferences in separate visual areas for specific stimulus combinations of velocity, chromaticity and contrast while no visual area is solely designated for either single stimulus attribute. It was found that hV4 and V3A respond strikingly similar but clearly distinguishable to contrast response profiles observed in area MT+.

While MT+ responses were roughly equal at high and low velocities, especially for additive cone signals over a wide range of contrasts, hV4 and V3A respond substantially stronger to slowly moving low chromatic contrast patterns compared to fast moving contrast patterns at low contrasts. Furthermore, since slow speed responses at low chromatic contrasts in V3A and hV4 exceeded those of MT+ for the same conditions, an additional criterion to associate visual areas to psychophysically derived motion perception channels, stating higher chromatic sensitivity in cortical regions associated with the slow motion channel, is fulfilled, and the conclusions made in experiment 2 can be consolidated. Areas V3A and hV4 are very likely to account for the slow motion channel of motion perception, while MT+ is likely to account for the fast motion mechanism.

Primary visual cortex was found to exhibit yet another contrast response profile. Responses to fast moving stimuli exceed those of slowly moving stimulus patterns at sufficiently high cone-contrast levels, not observed in any other region. The cone-contrast value at which higher speeds exceed responses to lower speeds depends on the cone-contrast direction of the stimulus.

### **5.4.1 Neurophysiological studies and speed in V1**

As suggested in Experiment 2 for V1, stimuli comprised of certain color and contrast combinations can yield higher BOLD-responses to fast speeds as compared to slow speeds. In concordance to that view, experiment 3 suggests that the ratio of slow and high speed BOLD-responses is not constant over different contrast levels and may even reverse with increasing contrast. The contrast range, at which this reversal speed preference takes place, differs between color directions, as we compare BOLD-responses to low (1Hz) and high-speed (10Hz) stimulation in experiment 3. Note that in experiment 2, the speed response profile to L-M stimuli already suggested such an effect. In experiment 2 where three speed conditions were investigated, it was found for L-M stimuli, that responses increased as speed increased while cone-contrast was constant at 14% cone-contrast. Experiment 3 extends this finding by

showing that specifically in V1, high-speed responses can exceed slow speed responses for all color directions provided that a sufficiently high cone-contrast is applied.

For the L-M mechanism, a 14% cone-contrast employed in Experiment 2, is more than sufficient to elicit higher responses to fast speeds as compared to slow speeds, because as can be seen in Figure 5.4, interception occurs already at around 10% cone-contrast for this color direction. None of the other colors in Figure 5.4, which are the same as in experiment 2, show this kind of behavior until a cone-contrast of roughly 20% is reached while pure S-cone stimuli must reach nearly 30% cone-contrast to yield higher responses to high speeds compared to low speeds. From the results of experiment 3 we would expect no other color stimulus besides L-M in Experiment 2 to show this kind of response pattern, but since all cone-contrast space directions clearly showed an intersection of the two velocities contrast response curves at some cone-contrast value, a general property of V1 may have been uncovered. This finding underscores that it is highly important to take the contrast level into account when conclusions about speed preferences are drawn, at least for human V1. This is not only important when responses are compared over different directions in cone contrast space but even when stimuli with the same direction in cone contrast space are used. The conclusions may depend heavily on the contrast level employed. But what might be the neurophysiological underpinnings of this phenomenon?

V1 receives its bottom up input from the LGN, making it possible that the specific velocity tuning changes over contrast levels towards higher frequencies may reflect the LGN input signal. It has however been shown in cats and monkeys, that LGN neurons are able to follow much higher temporal frequencies than V1 Neurons (Movshon *et al.*, 1978; Orban *et al.*, 1985; Hawken *et al.*, 1996), and extensive low-pass temporal filtering between primary visual cortex and LGN has been proposed (Movshon *et al.*, 1978; Orban *et al.*, 1985; Hawken *et al.*, 1996). These findings suggest that it is likely that a contrast dependent speed tuning evolves within V1 neuronal connections. Further support for the existence of a contrast dependent speed tuning effect in V1 neuronal networks, comes from studies, investigating temporal frequency tuning of cortical neurons as a function of stimulus contrast in non-human primates (Holub & Morton-Gibson, 1981; Foster *et al.*, 1985; Albrecht, 1995; Hawken *et al.*, 1996; Kayser *et al.*, 2001; Alitto & Usrey, 2004). A direct comparison of the conclusions of two of these studies, investigating temporal frequency tuning in monkey V1 neurons by applying substantially different contrast values, underscores the influence stimulus contrast can have to measurements of temporal frequency tuning in monkeys. An early study investigating cortical temporal frequency selectivity in macaque V1 and V2 (Foster *et al.*, 1985), using a contrast level of around 35% found the preferred temporal frequency tuning in

V1 cells to be in the range of 5.6-8Hz. A more recent study, applying a much higher contrast level of 65%, measuring temporal frequency tuning in macaque primary visual cortex and LGN, find higher preferred peak temporal frequencies for simple-, complex- and LGN-cells to be 9.5, 11.2 and 16Hz respectively (Hawken *et al.*, 1996). The direction of the speedtuning distribution shift is rightward, indicating an increase of preferred temporal frequencies in V1 neurons with increasing stimulus contrast, which is in concordance with the data presented in experiment 3. We showed that higher stimulus contrast leads to higher responses to fast stimulus speeds as compared to slow stimulus speeds in primary visual cortex of humans (Figure 5.4).

A reported contrast gain control (CGC), as for instance originally used to describe retinal ganglion cells of cats (Shapley & Victor, 1978, 1981), could be characterized as contrast-dependent shift in temporal frequency tuning (Benardete *et al.*, 1992 ; Yeh *et al.*, 1995; Kremers *et al.*, 1997; Benardete & Kaplan, 1999; Usrey & Reid, 2000). Besides the known CGC-mechanisms in LGN and retina (Yeh *et al.*, 1995a; Kremers *et al.*, 1997), recent reports suggest additional cortical nonlinearities to be able to explain the contrast dependent increase in cortical responses to high temporal frequency stimuli (Carandini *et al.*, 1997; Kayser *et al.*, 2001; Alitto & Usrey, 2004). A simple increase in contrast of fast moving gratings causes a rightward shift in temporal frequency tuning of simple and complex cells in primary visual cortex of cats (Holub & Morton-Gibson, 1981; Albrecht, 1995; Kayser *et al.*, 2001), ferrets (Alitto & Usrey, 2004) and monkeys (Albrecht, 1995), while it has never been demonstrated in human visual cortex.

Contrast response curves presented in this thesis lead us to speculate, that human primary visual cortex is affected by a contrast gain control mechanism, in which high contrast stimuli moving with reasonably high velocity may be cortically enhanced. Data presented in Figure 5.4 shows, that the contrast values, at which the contrast response curves for high and low speeds intersect, differ between color directions. As stated above, the intersection-contrast-value ranges from ~10% (L-M) to at least ~30% cone-contrast (S). Since the applied color conditions emphasized specific geniculo-cortical channels it is possible, that this proposed CGC-mechanism may act differently on these channels, which could be demonstrated in anesthetized monkeys (Solomon & Lennie, 2005). In addition, it is also feasible, that distinct layers in primary visual cortex, containing separate cortical termination sites for the geniculo-cortical channels (Chatterjee & Callaway, 2003), exhibit differential contrast gain properties which we may have been able to measure, because our stimulation was designed to put emphasis on these channels. The argument of differential contrast gain properties depending cortical layer, is supported by the finding of Hawken and colleagues,

who report the integration time for simple cells in V1 to be highly variable at different levels of cortical processing (layers) (Hawken *et al.*, 1996). They conclude that V1 cells may not simply inherit their tuning from LGN and emphasize the existence of a cortical contrast gain control mechanisms (Solomon & Lennie, 2005), which, as the authors stress, may be polysynaptic and reflects temporal integration through a cortical network (Hawken *et al.*, 1996).

The former argument goes well in line with the neurophysiological finding, that high stimulus contrast speeds up the responses in V1 cells, causing high contrast responses to occur earlier in the stimulus generated processing cycle (Dean & Tolhurst, 1986; Albrecht, 1995). We speculated that this could consequently allow the effective cortical processing within the proposed polysynaptic cortical network (Hawken *et al.*, 1996) to occur at faster and higher rates when stimuli are presented at high contrasts and fast speeds. If an intracortical network with elaborate intrinsic connections, like V1, is highly active because stimulus properties such as high temporal frequency and high stimulus contrast demand faster processing at a given stimulus presentation time, a higher metabolism is consequently reflected in higher BOLD-signals as compared to stimulus combinations of low speed and low contrast, which is what we observe.

### **5.4.2 Neurophysiological studies and color in V1**

The most heterogeneous response profile regarding speed and color responses at equal cone-contrast was observed in area V1 (Figure 5.8). To be specific, response magnitude in V1 elicited by 10% cone-contrast stimuli that put emphasis on a single cortico-geniculate channel, such as L+M+S or S, are found to be substantially lower as cone-contrast colors that may emphasize several of these channels simultaneously (Derrington *et al.*, 1984; Lennie, 1988; Lennie *et al.*, 1990), which, for simplicity reasons, we chose to refer to as ‘mixed colors’, if not otherwise indicated. Response magnitude to stimulation emphasizing the R/G-channel (L-M), however, was found to be equally high as compared to ‘mixed colors’. It appears as if cortical representation of R/G-, B/Y- and achromatic stimuli may fundamentally differ.

If the assumption is employed that oxygen consumption and related blood volume changes, the basis for the presented functional imaging data (Ogawa *et al.*, 1990; Ogawa *et al.*, 1992), is equal across all active V1 cells, a most parsimonious explanation for varying response magnitudes in V1 may be generated. This explanation would state that primary visual cortex contains separate neuronal populations, which are tuned to the stimulus configurations of the geniculo-cortical channels but differ in total cell count. Neurophysiological investigations on non-human primates have indeed found that V1

contains separate populations of achromatic, R/G and B/Y color-opponent neurons (Livingstone & Hubel, 1984; Thorell *et al.*, 1984; Ts'o & Gilbert, 1988; Landisman & Ts'O, 2002), while the approximate number comprising separate populations was different (Landisman & Ts'O, 2002; Chatterjee & Callaway, 2003).

For instance, Chatterjee *et al.* encounter nearly double as many achromatic versus R/G cortical projection sites in macaque primary visual cortex. If the above assumption of equal metabolism across different cell populations holds, this observation leads us to expect a BOLD-response magnitude for achromatic stimuli (L+M+S) that is roughly twice as large as compared to R/G-stimuli (L-M) in human visual cortex. We and other imaging studies find the contrary, considering L+M stimuli as achromatic for now (Kleinschmidt *et al.*, 1996; Engel *et al.*, 1997b; Engel & Furmanski, 2001; Liu & Wandell, 2005). The typical BOLD-response amplitude hierarchy that is measured in human fMRI, is consistently found to be highest for L-M which is higher than L+M(+S) which in turn is higher than pure S-cone-stimuli responses at equal cone-contrast levels, which contradicts the reported cell counts.

The above inconsistency between cell count and BOLD-magnitude leads us to speculate that distinct cell populations in primary visual cortex might substantially differ with respect to their metabolism. This argument is supported by differential physiology of cells in different layers of V1 (Livingstone & Hubel, 1988), which may cause possible metabolic differences between neuronal subpopulations. Specifically the cytochrome-oxidase blobs in layers 2 and 3, are known to contain specialized vasculature (Zheng *et al.*, 1991), which could cause neurons therein to be over-represented in BOLD-responses. However, the cell-count across blobs may be informative and predict measured fMRI responses.

Landisman and Ts'O (2002) found patches in V1 that are preferentially activated by chromatic gratings compared with luminance gratings. These imaged color patches were correlated, with the cytochrome-oxidase (CO) blobs, while luminance sensitive cells were located in between blobs. Interestingly, the results indicate that individual blobs tend to contain neurons of only one color-opponent cell type: either red/green (L-M) or blue/yellow (S-(L+M)). It has been reported, that there are more R/G than B/Y color-opponent cells associated with CO-rich blobs in V1 (Livingstone & Hubel, 1984). If we additionally assume, that the applied R/G and B/Y stimulation only activates color-opponent cells in the blobs, a response comparison at equal cone-contrast should yield higher responses to L-M than to S-(L+M) stimuli, which we observed for the two subjects contrast response curves of experiment 3, also confirming results reported in experiment 2.

Nonetheless, to date it is not known in what way different cell populations in distinct laminar organization of primary visual cortex may differ regarding their energy consumption

when excited. For instance, BOLD-signals generated by small amounts of cells with a high metabolic rate could exceed signals from a larger number of cells with low metabolic rate. The finding that responses to achromatic stimuli are well below L-M color opponent responses, while their designated cell count may lead us to expect an opposite response profile, suggests that different neuronal classes in distinct cortical layers differ regarding their energy consumption. Future neurophysiological work is needed, examining metabolic properties of different classes of neurons in the laminar structure of V1. This knowledge will provide a better link between activity of cell populations and the associated BOLD-signal.

Yet another explanation for the observed response differences especially for stimuli emphasizing cortico-geniculate pathways could be, that V1 may plainly mirror the input level from LGN-projections because, BOLD-signals are believed to mainly reflect the specific inputs into a cortical area rather than its spiking output (Logothetis *et al.*, 2001; Logothetis, 2003). The cell ratio for the magno-, parvo-, and koniocellular layers in LGN can roughly be estimated to be 10%, 80% and 10% respectively, which explains the observed response profile in human primary visual cortex only poorly. In addition, cells that respond strongest to stimulation opposing the R/G information with S-cones have not been found in the LGN, while we measured highest responses to stimuli such as L-M-S and L-M+S (Figure 5.8). We must thus assume that these kinds of ‘mixed color’ responses in humans emerge in cell populations of V1.

Clues supporting this claim bear on more recent neurophysiological investigations of chromatic responses in single cortical cells of the macaque. Conway and Livingstone confirmed that L-M+S double-opponent cells exist, and Solomon and Lennie found the most common cortical organization to be L-M-S (Solomon & Lennie, 2005; Conway & Livingstone, 2006). Given that distinct cell populations can be found in V1, which respond preferentially to ‘mixed colors’ and we measure BOLD-responses to these stimuli that were among the highest of all applied colors, these cells must either be very numerous, have an extraordinary metabolism or another explanation is in order.

Assuming that purely L-M, S, and variations of L-M+S responding cells exist, it is most likely that the observed high BOLD-responses are the combined sum of all of these cell populations as all three are presumably excited by the mixed color stimuli described above. Similarly L-M stimuli could excite L-M-S or L-M+S neurons, which may have added to the large measured BOLD-responses observed for L-M.

We speculate that a merging of signals from R/G and B/Y responsive cells occurs somewhere in V1 (Fitzpatrick *et al.*, 1985; Callaway, 2004, 2005; Yoshimura & Callaway, 2005; Briggs & Callaway, 2005 ), possibly by means of the L-M+S responsive populations

and that both of these stages contribute to the measured BOLD-signal. Evidence from other studies also supports coupling of M- and S- cones opposed by L-cone input in V1 (Conway, 2001; Wachtler *et al.*, 2003), which was not part of the color stimuli we used.

One may consider using the ‘mixed color’ configurations in future retinotopic mapping experiments since at 10% contrast BOLD-activations are so much higher than conventional black and white (L+M+S) responses. This is however not suitable (as of yet), because additive L-, M- and S-cone stimuli are much easier to generate and even more so, can reach the highest overall contrast (170% RMS), which in turn will elicit highest BOLD-responses. Nonetheless, as experimental presentation techniques progress it might be possible in the future to generate L-M-S and L-M+S stimuli that exceed 12% cone-contrast (see visual stimulation Experiment 2). In order to do that, displays could be designed containing light sources that enable researchers to maximally avoid simultaneous excitation of the L- and M-cones, in order to increase the L-M cone-contrast. Once achieved, colors could be computed which will yield higher BOLD-signals as L+M+S at highest contrast levels, because the ‘mixed’ color conditions at 12% cone-contrast (not shown) are already yielding responses that approach responses from 170% L+M+S cone-contrast, at least in extra-striate regions, which will be discussed next.

### **5.4.3 Neurophysiological studies and extra-striate cortex**

Response properties of human extra-striate visual areas MT+, hV4 and V3A can be regarded relatively unexplored territory with respect to cone-contrast controlled stimuli and the effect of stimulus velocity using fMRI (Wandell *et al.*, 1999; Liu & Wandell, 2005). Neurophysiological investigations on the macaque monkey have served as a framework to compare differences in sensitivity to color and motion stimuli of visual areas such as MT (Maunsell *et al.*, 1990; Gegenfurtner *et al.*, 1994; Seidemann *et al.*, 1999) or V4 (Schein & Desimone, 1990; Heywood *et al.*, 1992; Yoshioka *et al.*, 1996). To our knowledge, no single-unit study on monkeys exist, investigating cone-contrast responses as a function of temporal frequency in dorsal area V3A, while some work has been published regarding color responsivity in macaque V3 (Felleman & Van Essen, 1987; Gegenfurtner *et al.*, 1997) and V2 (Gegenfurtner *et al.*, 1996). This study aims to close that gap and to further advance the understanding of cortical color processing in humans.

Sensitivity difference of the extra-striate visual areas regarding color or motion responses have been used to assign these regions to presumed cortical ventral and dorsal pathways (Zeki, 1974; Ungerleider & Mishkin, 1982; Mishkin *et al.*, 1983; Zeki, 1983c). While color was assumed to be the critical stimulus property of the ventral WHAT-path,

motion preference was assigned to the dorsal WHERE-path (Zeki, 1974; Ungerleider & Mishkin, 1982). This strict segregation would entail the dorsal path to be non-responsive to color and the ventral path to be non-responsive to motion. Numerous studies were subsequently conducted, the results of which were evidently not in concordance with such a strict segregation and receive support from results presented in this thesis regarding human visual extra-striate regions. The following two sections discuss extra-striate regions representing the dorsal (MT+ and V3A) and ventral path (hV4), which all show substantial contributions to their response profile from visual attributes not specifically assigned to the path each region is assumed to solely represent. In line with existing macaque data we find clear color responses in human motion selective cortex MT+ (Figure 5.7), representing the dorsal path, as well as clear luminance motion signals in ventral path region hV4 (Figure 5.5), which is not in line with a strict segregation of ventral and dorsal path (Ungerleider & Mishkin, 1982; Mishkin *et al.*, 1983).

#### **5.4.3.1 MT+**

Area MT+ is believed to receive mainly magnocellular input preferring luminance stimuli (Maunsell *et al.*, 1990). We found that responses in MT+ elicited through chromatic stimulation, such as L-M (parvocellular) or pure S-cone stimuli (koniocellular), presented with sufficiently high contrast, can equal luminance responses in that area. Given the fact that up until the first input projection sites to primary visual cortex, chromatic and luminance signals remain fairly segregated, by means of parvo- and magnocellular projection paths respectively (Chatterjee & Callaway, 2003), this finding suggests a cortical fusion of these paths and indicates that color opponent information, originating in the parvocellular stream is available to MT+ in humans as reported in monkeys (Nassi & Callaway, 2006).

Support for contributions to MT+ responses other than of magnocellular origin comes from a recent functional imaging study, emphasizing S-cone signals in MT+ (Wandell *et al.*, 1999). The authors report L-M responses to be only slightly less pronounced than L+M responses without giving exact contrast values constituting their L-M measurements (Wandell *et al.*, 1999). At a cone-contrast value of 10% we would reach the same conclusion (Figure 5.11), while comparisons at contrasts below 10% RMS-cone-contrast would clearly favor luminance responses in MT+ (Figure 5.7). This observation is in concordance with results of a single-unit investigation in macaque MT, reporting higher contrast gain for luminance as compared to chromatic stimuli, while spiking was roughly equal at contrast levels as high as 10% for both luminance and chromatic stimulation (Gegenfurtner *et al.*, 1994).

Furthermore, chromatic responses in motion sensitive region MT+ seem to interdepend more strongly on the stimulus contrast and velocity combination than luminance responses. While for all color directions measured, lower speeds elicited generally higher responses in human MT+ for all contrast levels, the response difference between high and low speeds is much more pronounced for chromatic targets at low contrast levels (Figure 5.7). This finding may indicate a speed independent processing for luminance targets in human MT+, while responses to chromatic targets may depend more on velocity at low contrast levels as compared to luminance signals.

#### **5.4.3.2 V3A & hV4**

A theoretical constraint, derived from psychophysical measurements on detection thresholds regarding the direction of stimulus motion, associated with the chromatic slow velocity mechanism of motion perception, entails a higher sensitivity to slowly moving, chromatic stimuli in visual areas other than MT+. The restriction is imposed on MT+, because its neural sensitivity, as assessed with single unit recordings, cannot explain the excellent chromatic contrast motion detection and identification thresholds observed in humans and monkeys (Gegenfurtner & Hawken, 1995, 1996). The hV4 and V3A BOLD-response profiles measured in experiment 3 suggest an association of these two regions to the mechanism of slow chromatic motion perception.

Cone-contrast response measurements in experiment 3 show, that while MT+ responses appear to be relatively speed invariant for luminance-emphasizing stimuli (Figure 5.7) dorsal area V3A (Figure 5.6) and ventral area hV4 (Figure 5.7) showed marked speed dependence across all color directions tested. Low contrasts at low speeds elicit higher BOLD-signals compared to low contrasts at high speeds as expected from observations in Experiment 2.

As stated above and in section 5.1, the critical criterion in order to associate a visual area to the slow channel of motion perception, this region must exhibit higher chromatic contrast sensitivity as MT+, because MT+ single-cell responses cannot be held responsible for chromatic detection and discrimination thresholds for slowly moving targets (Metha *et al.*, 1994; Gegenfurtner & Hawken, 1995; Stromeyer *et al.*, 1995). We must thus compare chromatic responses at low contrast levels in MT+ to candidate regions. The relative responses to low contrast L-M stimuli in both areas (V3A: Figure 5.6, hV4: Figure 5.5, 0.3% and 1% RMS-cone-contrast), exceeds responses at the same contrast levels in MT+ (Figure 5.7), especially at low velocities. The same effect becomes clear, comparing low contrast responses for an additional purely chromatic color-direction. Low contrast S-cone responses

(2.85% & 9.5% RMS-cone-contrast) for visual area V3A and hV4 exceed responses to the same stimulus combinations in MT+. Hence, extending the stimulus range into the contrast domain, further strengthens the conclusions made in Experiment 2.

MT+ is highly likely to account for the fast motion mechanism because it is responsive to high stimulus velocities at the lowest luminance contrasts while also responding to chromatic stimulation when contrast is sufficiently high. Low chromatic contrast sensitivity is clearly observed for visual areas V3A and hV4, while the responses are enhanced for slow moving targets as opposed to fast moving stimuli. These observations make it highly likely that V3A and hV4 mediate the chromatic slow velocity mechanism.

#### **5.4.4 Striate vs. extra-striate cortex**

Comparing response patterns in striate and extra-striate areas reveals differences as well as similarities. Cone-contrast stimuli theoretically stimulating the two chromatic corticogeniculate mechanisms while keeping the luminance mechanism stimulation constant, elicited highest BOLD-responses in V1 at low and high speeds. These ‘mixed colors’ continue to generate highest responses in extra-striate cortex as well. The reasons for this effect remain speculative as was discussed in section 5.4.2.

The most differential response patterns between striate and extra-striate cortex are observed as responses to stimuli emphasizing geniculo-cortical pathways are compared to ‘mixed’ colors. In V1 responses to S, L+M, L+M+S or even S-(L+M) cone-contrast stimuli elicit the weakest response strength irrespective of stimulus velocity. This observation underlines that cardinal mechanisms are still prevalent in V1. This changes in extra-striate visual areas hV4 and V3A. No particular color seems to be substantially preferred over other color combinations at low temporal frequencies, while at high temporal frequencies, cardinal color responses drop considerably. We speculate that conscious chromatic motion perception may be tight to activity in these two regions, because their motion sensitivity profile may correspond to perceptual desaturation of fast moving colors.

However, these observations suggest a strong common response characteristic between V3A and hV4 as described in Experiment 2. Strong, color indifferent BOLD-responses at low temporal frequencies support the argument that both visual areas are involved in the processing of slowly moving chromatic stimuli. Further support to this hypothesis is given by the fact that low contrast chromatically opponent stimuli elicited relatively stronger responses in V3A and hV4 as compared to MT+, while the human medial temporal area responds relatively stronger to low contrast achromatic stimuli as compared to low contrast opponent colors.

It seems thus feasible to conclude that the exquisite detection and motion discrimination sensitivity to R/G-stimuli (Lee & Stromeyer, 1989) is mediated by visual areas such as hV4 and V3A, because at very low chromatic contrasts MT+ tends to either respond sparsely as shown in experiment 3 in human subjects or not at all, shown in neurophysiological studies using monkeys (Gegenfurtner & Hawken, 1995, 1996). MT+ however exhibits properties making it highly likely to be involved in the fast motion channel because it does respond well to opponent color stimuli (Gegenfurtner & Hawken, 1995; Thiele *et al.*, 1999; Wandell *et al.*, 1999) and in addition, responses do not decline for high temporal frequency moving patterns, at which responses in hV4 and V3A drop considerably at low contrasts.

How the response profiles in MT+, V3A and hV4 may depend on activity in V1 cannot unequivocally be determined on the bases of the presented data set. It is highly likely that the V1 response profile has a strong influence on these regions (Ferrera *et al.*, 1994; Wandell, 1995; Nassi & Callaway, 2006). We speculate that stimulus combinations containing additional stimulus attributes, such as depth cues, form or moving objects, in for instance natural scenes, may yield a slightly different response profile in V1 as observed in this thesis, which could also lead to changes in the response profiles in hierarchically higher regions as well. Suggestions to investigate this hypothesis are provided in the next section.

## 6 GENERAL DISCUSSION

Three functional magnetic resonance imaging experiments investigated the precise nature of differential responses in human visual areas to varying stimulus combination of color, contrast and velocity. Experiment 1 securely defined the borders of cortical visual areas by means of the phase encoding approach and applying functional localizer measurements to define motion sensitive regions. Experiment 2 focused on differential speed dependencies in various visual areas by presenting radial gratings with equal cone-contrast, selectively emphasizing psychophysically determined chromatic and achromatic detection mechanisms and rotating at three different speeds. MT+ could be associated to a psychophysically derived fast channel for motion perception, because it responds to chromatic stimuli and responses do not decline at fast moving stimulus pattern. Experiment 3 investigated cone-contrast sensitivity of human visual areas by measuring responses to stimuli modulated along thirteen directions in cone-contrast space, parameterized in four contrast levels and presented at two different speeds. Visual regions hV4 and V3A were associated with a psychophysically derived slow channel for motion perception, because both regions prefer slow stimulus velocities especially at low contrasts and chromatic sensitivity is higher as in MT+. Speed preference in primary visual cortex was found to be strongly contrast dependent, because the preferences change from low to high temporal frequencies as cone-contrast is increased.

The results point towards a widely distributed network of cortical regions sensitive to stimuli defined by a combination of color and motion, while no stimulus property is the exclusive domain of either visual area. Hence, and in concordance with newer studies (Gegenfurtner & Hawken, 1996; Thiele *et al.*, 1999; Wandell *et al.*, 1999; Liu & Wandell, 2005) color and motion information seem to undergo a convergence rather than a strict segregation as the widely held view of a ventral- (color) and dorsal- (motion) pathways would predict (Ungerleider & Mishkin, 1982; Hubel & Livingstone, 1987). We observed a rather gradual difference between response properties across visual areas pertaining to these important visual attributes. Without a doubt, substantial chromatic information processing is found in dorsal areas while a ventral area was clearly involved in processing motion stimuli. The results are well in line with existing physiological reports in monkeys (Maunsell *et al.*, 1990; Nealey *et al.*, 1991; Ferrera *et al.*, 1994; Thiele *et al.*, 1999; Conway & Livingstone, 2006; Nassi & Callaway, 2006; Nassi *et al.*, 2006) and complement results from human imaging data regarding striate and extra-striate color and motion processing (Engel *et al.*, 1997b; Wandell *et al.*, 1999; Liu & Wandell, 2005).

It was found, that visual areas do exhibit preferred stimulus combinations which led us to assign distinct visual areas to psychophysically defined motion channels (Gegenfurtner & Hawken, 1996). The fast motion channel is believed to exhibit band-pass temporal frequency tuning and some color selectivity while the slow motion channel is extremely color sensitive and exhibits a low-pass temporal frequency tuning (Gegenfurtner *et al.*, 1994; Gegenfurtner & Hawken, 1995, 1996). Experiment 2 demonstrated temporal frequency tuning curves for area hV4 and V3A. Strong responses were found for these regions up to 4Hz, which declined at higher velocities (10Hz). This low-pass property makes it highly likely that neurons in V3A and hV4 are tuned to process slowly moving chromatic stimuli. Contrarily, responses in area MT+ on the temporal cortical surface did not decline substantially at higher speeds, preferred medium velocities and responded well to chromatic stimuli. These properties make MT+ highly likely to be responsible for fast moving stimuli defined by either color or luminance contrast. Furthermore, it has been proposed that neurons in monkeys MT are not sensitive enough to account for the exquisite chromatic contrast sensitivity for slowly moving chromatic gratings (Gegenfurtner *et al.*, 1994; Gegenfurtner & Hawken, 1996) Our finding that BOLD responses in V3A and hV4 exceed MT+ responses to low chromatic contrast patterns moving at 1Hz is in concordance with and supports the view that both areas, V3A and hV4 are more sensitive to chromatic motion than MT+ and can thus be held responsible for the slow channel of motion perception derived psychophysically (Gegenfurtner & Hawken, 1996).

Moreover, responses to stimuli comprising thirteen cone-contrast colors were measured in several regions of human visual cortex, giving insight into transformation processing from primary cortex to extra-striate areas. Responses to stimuli emphasizing detection mechanisms (cardinal directions) are substantially reduced in primary visual cortex as compared to ‘mixed colors’, with the exception of the R/G-mechanism (L-M), generating quite substantial signals in V1 as well. As the visual signal is passed on to extra-striate cortex, particularly to dorsal area V3A and ventral area hV4 these differences vanish for slow moving colors. Both areas respond to all presented slowly moving stimuli roughly equal at 10% cone-contrast and must thus apply some form of amplification pertaining to signals from cardinal directions as they are forwarded from V1. This finding suggests that cardinal mechanisms are not as prevalent in the neuronal population of higher tier visual areas as compared to V1. At high speeds however, signals are reduced in both, V3A and hV4, especially for achromatic stimuli, emphasizing their preference for slowly moving chromatic stimuli. The effect of velocity on MT+ BOLD-responses however is less pronounced. The difference between the hV4/V3A network and the MT+ complex becomes most obvious as high-speed achromatic

responses are compared. Most likely magno-cellularly driven fast achromatic signals generate substantially high responses in MT+, while V3A and hV4 must receive considerably less magnocellular signals (Nealey *et al.*, 1991; Ferrera *et al.*, 1994) as their high-speed achromatic signal is well below MT+ responses at equal cone-contrast level.

The conclusions of this thesis may also help to explain results from a recent report, demonstrating that residual chromatic motion detection and discrimination in patients with cerebral achromatopsia is indeed similar to normal observers as long as chromatic contrast is high enough (Cavanagh *et al.*, 1998). This report came as a surprise, because the ventral putative color regions in these patients have been severely damaged. The authors rejected the notion that the residual motion processing takes place in MT+ applying the argument that the contribution of color to motion detection in these patients was much stronger than the color responses of monkey area MT (Cavanagh *et al.*, 1998). At the time of the study, no chromatic motion sensitive region besides MT+ or hV4 was known, which could account for the patients excellent motion detection and discrimination at slow speeds. In light of the data presented in this thesis, it appears most likely that dorsal area V3A must be responsible for residual slow moving chromatic detection and discrimination performance in achromatopsic patients. The data presented in this thesis showed, that V3A prefers slowly moving chromatic gratings to luminance gratings and responses increase steeply as cone-contrast is raised.

The presented results may be a basis for future experiments tackling the phenomenon of conscious color perception. For instance the quantitative measurements of thirteen cone-contrast directions in V1 resulted in a heterogeneous response pattern across chromatic conditions, while cardinal direction stimuli responses were among the lowest at equal cone-contrast. We observed a substantial amplification of these cardinal directions responses in hV4 and V3A at low velocities leading to roughly equal responses at 10% cone-contrast. These responses may be biased by the heterogeneous response pattern exhibited in V1, a precursor stage of visual processing before visual information is transmitted to higher areas. Since the V1 response profile is highly similar across subjects, probably due to extensive measurements and the resultant high signal to noise ratio, it may be possible to reliably compute and present cone-contrast stimulation leading to equal responses in V1 (Engel *et al.*, 1997a; Engel, 2005) while simultaneously measuring extra-striate cortex. By doing so, cone-contrast color tuning of higher tier visual areas in humans may be measurable independent of differential V1 activity. In addition, applied stimulus contrast may be linked to responses of several visual areas in order to narrow down the regions associated with conscious color perception. It is worth noting, however, that the reported response patterns for several visual areas are doubtlessly constrained to the stimulus properties used and may very well change as

different stimulus attributes are changed, such as spatial frequency, depth, form, size, stimulus position or attention.

A possible extension of the presented results may constitute an application of differential methodology to overcome the shortcomings of functional magnetic resonance imaging to further explore and understand cortical color mechanisms and its dynamics. FMRI is limited regarding temporal resolution of brain activity. The fastest temporal sampling of brain activity was 1.5s in Experiment 2. It is known that visual scenes are processed extremely fast and that the first sweep of visual information enters V1 after roughly 70 ms and may be processed in frontal regions after 150ms (Thorpe *et al.*, 1996). It would be of interest in what way the geniculo-cortical paths play a differential role pertaining to dynamic processing. For that reason, photographs of natural scenes may be generated in such a way that they selectively stimulate either path while keeping contributions from the other two constant. Neurophysiological methods with higher temporal resolution, such as EEG or MEG should be used to gain insight into the cortical dynamics of the processing of natural scenes depending on geniculo-cortical pathways.

Color is one of the most conspicuous and penetrating features of our world. The interesting part about color however is not how it looks but rather what it represents. We as humans share, with other old world monkeys, the extraordinary gift of three receptor classes, which in a feat of evolution, have been connected in such a way, that we can actually attribute fluctuations in photon properties around us, to emotions. The ability to perceive colors develops ontogenetically earlier than human memory can trace back, making us unaware of its merits until we may tragically lose it. Color vision should not be taken for granted.

## 7 APPENDIX

### 7.1 Experiment 2 – Speedtuning

hV4																
		L+M			L-M			S-L-M			L+M+S			S		
		1Hz	4Hz	10Hz	1Hz	4Hz	10Hz	1Hz	4Hz	10Hz	1Hz	4Hz	10Hz	1Hz	4Hz	10Hz
L+M	1Hz	0	-0.07	2.96	-1.29	-1.74	-0.11	0.48	-0.47	2.42	2.42	6.81	6.10	11.74	7.13	1.80
	4Hz	1.83	0	3.95	-0.96	-2.01	-0.07	0.44	-0.34	2.08	2.21	4.63	7.33	6.24	5.58	2.07
	10Hz	0.72	-1.53	0	-3.63	-6.17	-4.12	-2.71	-3.96	0.07	-1.74	1.01	9.89	2.52	2.99	-0.39
L-M	1Hz	-0.28	-1.24	-0.82	0	-0.39	1.19	2.00	1.68	4.26	2.02	6.62	7.35	7.36	9.14	2.49
	4Hz	1.65	0.72	1.53	1.95	0	4.16	2.53	1.57	5.22	2.86	5.07	10.60	6.80	7.36	3.51
	10Hz	0.36	-1.24	-0.23	0.67	-1.80	0	0.58	-0.35	3.33	1.70	4.86	9.41	6.56	6.35	2.05
S-L-M	1Hz	-0.92	-2.61	-2.19	-0.41	-2.68	-1.41	0	-1.47	2.74	0.94	5.08	6.70	6.70	9.21	1.82
	4Hz	-0.05	-1.45	-0.69	0.28	-2.69	-0.69	0.66	0	3.34	1.63	9.38	8.52	7.91	10.19	2.35
	10Hz	-1.00	-2.31	-2.04	-1.23	-4.26	-2.16	-0.79	-1.99	0	-1.24	0.71	3.30	2.05	2.71	-0.31
L+M+S	1Hz	-0.90	-2.10	-1.46	-0.13	-2.02	-0.89	0.30	-0.32	0.71	0	3.48	5.06	6.08	4.29	0.89
	4Hz	-2.60	-3.91	-3.89	-2.26	-4.08	-3.22	-2.36	-3.27	-1.30	-2.31	0	3.07	2.11	2.64	-0.98
	10Hz	-2.84	-4.12	-5.37	-2.50	-3.46	-4.20	-3.47	-2.46	-1.65	-3.14	-0.84	0	-1.67	-0.50	-3.12
S	1Hz	-3.89	-4.68	-4.79	-3.37	-3.93	-4.31	-4.37	-3.02	-2.59	-4.31	-2.09	-2.96	0	1.44	-2.03
	4Hz	-7.68	-9.72	-9.48	-6.46	-8.46	-8.40	-13.06	-6.68	-5.81	-7.51	-4.86	-4.55	-1.39	0	-3.72
	10Hz	-2.89	-6.07	-5.72	-2.68	-7.02	-8.14	-3.44	-4.34	-2.78	-2.79	-1.70	-0.90	0.85	2.87	0

**MT+**

**Table 4.2: Paired t-test-values for all stimulus combination in hV4 and MT+**

T-values for one region were computed for the comparison of all stimulus combinations. Each entry is the t-value obtained in the comparison of BOLD response differences elicited by the stimuli along the columns versus the responses obtained in the conditions along the rows. T-values for area MT are shaded blue and green respectively. For example, in area hV4 the comparison of the BOLD responses elicited by (L-M) stimulation at 4Hz minus the BOLD-response elicited by L+M+S at 10 Hz resulted in a t-value of 10.6. Please note that minuend and subtrahend are swapped between hV4 and MT+. Consequently, the t-values from one brain area must be multiplied by -1 when compared to the other. Cone-contrast was constant at 14% for all color-directions.

		L+M			L-M			S-L-M			L+M+S			S		
		1Hz	4Hz	10Hz	1Hz	4Hz	10Hz	1Hz	4Hz	10Hz	1Hz	4Hz	10Hz	1Hz	4Hz	10Hz
L+M	1Hz	0	0	0	0	0	0	0	0	0	0	4.21	3.26	7.85	0	0
	4Hz		0	0	0	0	0	0	0	0	0	3.22	1.56	0	0	-4.00
	10Hz			0	0	-4.64	0	0	0	0	0	0	0	0	-6.49	-6.11
L-M	1Hz				0	0	0	0	0	0	0	4.37	4.85	3.99	0	0
	4Hz					0	0	0	0	0.96	0	0.98	7.14	2.87	0	-3.51
	10Hz						0	0	0	0	0	0	5.21	2.25	0	-6.08
S-L-M	1Hz						0	0	0	0	0	2.71	3.23	2.34	0	0
	4Hz							0	0	0	0	6.11	6.06	4.89	0	0
	10Hz								0	0	0	0	0	0	0	-3.10
L+M+S	1Hz										0	0	1.92	1.77	-3.22	0
	4Hz											0	0	0	0	0
	10Hz												0	0	0	0
S	1Hz													0	0	0
	4Hz														0	0
	10Hz															0

	hV4 effect (row > column)		MT+ effect (row > column)
	hV4 effect (row < column)		MT+ effect (row < column)

**Table 4.3: Stimulus combinations that modulate either MT+ or hV4**

Stimulus combinations for which a Bonferroni corrected difference was observed in either hV4 OR in MT+ have a non-zero entry. The non-zero values were obtained by subtracting the t-values for hV4 and MT+ in the respective color and speed combination. The green-shading of the numbers indicates a significant effect in hV4, and the blue shading an effect in MT+. For instance: a hV4 effect of 7.14 for the stimulus combination L+M+S 10Hz and L-M 4Hz was obtained using t-values from the same stimulus combination in both region from Table 4.2:  $10.6 - (-3.46 * -1) = 7.14$ . Note: the MT+ t-value must be multiplied with  $-1$  to mirror its value on the matrix diagonal.

		L+M			L-M			S-L-M			L+M+S			S		
		1Hz	4Hz	10Hz	1Hz	4Hz	10Hz	1Hz	4Hz	10Hz	1Hz	4Hz	10Hz	1Hz	4Hz	10Hz
L+M	1Hz	0	0	0	0	0	0	0	0	0	0	0	0	0	-0.55	0
	4Hz		0	0	0	0	0	0	0	0	0	0	0	0	-4.14	0
	10Hz			0	0	0	0	0	0	0	0	0	4.52	0	0	0
L-M	1Hz				0	0	0	0	0	0	0	0	0	0	2.68	0
	4Hz					0	0	0	0	0	0	0	0	-1.10	0	0
	10Hz						0	0	0	0	0	0	0	-2.05	0	0
S-L-M	1Hz						0	0	0	0	0	0	0	0	-3.85	0
	4Hz							0	0	0	0	0	0	3.51	0	0
	10Hz								0	0	0	0	0	0	0	0
L+M+S	1Hz										0	0	0	0	0	0
	4Hz											0	0	0	0	0
	10Hz												0	0	0	0
S	1Hz													0	0	0
	4Hz														0	0
	10Hz															0

	hV4 effect
	MT+ effect

**Table 4.4: Stimulus combinations that modulate both MT+ and hV4 significantly.**

The green shading indicates a stronger significant effect in V4 than in MT+ for the respective comparison. The blue shading indicates a stronger effect in MT+ than in hV4. The reported number is the difference of the t-values obtained in hV4 and MT+. It reflects the differences of the effect sizes between the visual areas. For instance: a hV4 effect of 4.52 for the stimulus combination L+M+S 10Hz and L+M 10Hz was obtained using t-values from the same stimulus combination in both region from Table 4.2:  $9.89 - (-5.37 * -1) = 4.52$ . Note: the MT+ t-value must be multiplied with  $-1$  to mirror its value on the matrix diagonal.

## 7.2 Experiment 3 - Colortuning

### 7.2.1 ANOVA tables

#### Dn45

Effects & Interactions	V1			V2d			V2v			V3d			V3v			hV4			V3A			MT+		
	Degrees of freedom	F - value	P - value	Degrees of freedom	F - value	P - value	Degrees of freedom	F - value	P - value	Degrees of freedom	F - value	P - value	Degrees of freedom	F - value	P - value	Degrees of freedom	F - value	P - value	Degrees of freedom	F - value	P - value	Degrees of freedom	F - value	P - value
VELOCITY (VEL)	(1.00,8.00)	0.307	0.595	(1.00,8.00)	21.943	0.002	(1.00,8.00)	10.213	0.013	(1.00,8.00)	39.092	0.000	(1.00,8.00)	15.185	0.005	(1.00,8.00)	44.982	0.000	(1.00,8.00)	34.687	0.000	(1.00,8.00)	22.200	0.002
COLOR (COL)	(4.30,34.37)	14.922	0.000	(5.04,40.33)	11.272	0.000	(4.58,36.66)	16.551	0.000	(4.62,36.98)	14.232	0.000	(5.09,40.72)	20.261	0.000	(4.15,33.16)	11.484	0.000	(4.64,37.13)	31.708	0.000	(4.24,33.95)	14.943	0.000
VEL / COL	(4.48,35.87)	3.057	0.023	(4.58,36.66)	1.197,	0.329	(4.71,37.68)	2.569	0.046	(4.77,38.18)	2.134	0.085	(5.34,42.72)	3.275	0.012	(4.43,35.40)	6.401	0.000	(4.71,37.71)	3.758	0.008	(4.04,32.28)	1.939	0.127
CONTRAST (CONT)	(1.79,14.28)	503.898	0.000	(1.45,11.57)	424.999	0.000	(1.78,14.23)	332.323	0.000	(1.66,13.31)	442.042	0.000	(2.40,19.21)	409.229	0.000	(2.29,18.33)	408.858	0.000	(1.70,13.63)	807.074	0.000	(2.11,16.88)	271.385	0.000
VEL / CONT	(1.36,10.86)	13.036	0.003	(1.85,14.78)	17.645	0.000	(1.38,11.01)	15.665	0.001	(1.42,11.37)	27.334	0.000	(2.42,19.34)	29.551	0.000	(2.34,18.72)	103.309	0.000	(1.62,12.99)	35.963	0.000	(1.88,15.04)	19.924	0.000
COL / CONT	(5.39,43.16)	2.795	0.019	(6.53,52.24)	2.141	0.059	(5.86,46.90)	2.487	0.037	(6.23,49.84)	1.955	0.088	(5.92,47.39)	2.529	0.034	(6.34,50.74)	3.413	0.000	(6.08,48.63)	4.038	0.002	(5.60,44.83)	3.475	0.008
VEL / COL / CONT	(6.03,48.27)	1.403	0.234	(5.47,43.79)	1.389	0.244	(6.41,51.28)	2.077	0.068	(5.75,46.04)	1.603	0.170	(6.54,52.34)	2.800	0.017	(6.21,49.66)	3.035	0.012	(6.07,48.58)	2.666	0.025	(6.43,51.44)	1.837	0.106

#### Lk13

Effects & Interactions	V1			V2d			V2v			V3d			V3v			hV4			V3A			MT+		
	Degrees of freedom	F - value	P - value	Degrees of freedom	F - value	P - value	Degrees of freedom	F - value	P - value	Degrees of freedom	F - value	P - value	Degrees of freedom	F - value	P - value	Degrees of freedom	F - value	P - value	Degrees of freedom	F - value	P - value	Degrees of freedom	F - value	P - value
VELOCITY (VEL)	(1.00,8.00)	0.002	0.969	(1.00,8.00)	81.942	0.000	(1.00,8.00)	4.647	0.063	(1.00,8.00)	63.867	0.000	(1.00,8.00)	28.239	0.001	(1.00,8.00)	24.242	0.001	(1.00,8.00)	21.069	0.002	(1.00,8.00)	4.251	0.073
COLOR (COL)	(4.30,34.37)	52.968	0.000	(4.60,36.78)	59.455	0.000	(3.80,30.39)	56.759	0.000	(4.67,37.32)	89.203	0.000	(3.46,27.66)	98.718	0.000	(3.38,27.06)	35.064	0.000	(4.17,33.34)	73.845	0.000	(4.65,37.23)	71.619	0.000
VEL / COL	(4.48,35.87)	1.543	0.206	(4.60,36.81)	4.352	0.004	(3.64,29.08)	1.296	0.295	(4.51,36.05)	3.320	0.017	(3.58,28.64)	1.650	0.193	(3.41,27.30)	1.340	0.281	(4.11,32.89)	3.136	0.026	(4.28,34.22)	1.370	0.264
CONTRAST (CONT)	(1.79,14.28)	724.294	0.000	(2.35,18.79)	1286.135	0.000	(1.85,14.78)	1112.761	0.000	(2.03,16.22)	1276.569	0.000	(1.57,12.56)	882.251	0.000	(1.46,11.64)	324.957	0.000	(1.15,9.23)	320.163	0.000	(1.58,12.68)	568.219	0.000
VEL / CONT	(1.36,10.86)	29.074	0.000	(1.60,12.84)	28.607	0.000	(1.46,11.68)	15.529	0.001	(1.29,10.28)	16.045	0.002	(1.44,11.54)	5.288	0.031	(1.19,9.55)	5.769	0.034	(1.13,9.05)	7.631	0.020	(1.62,12.95)	5.568	0.023
COL / CONT	(5.39,43.16)	5.419	0.000	(5.99,47.89)	9.944	0.000	(5.58,44.66)	5.949	0.000	(6.15,49.18)	16.170	0.000	(5.91,47.26)	14.262	0.000	(5.49,43.91)	6.619	0.000	(6.02,48.15)	15.103	0.000	(5.55,44.42)	9.990	0.000
VEL / COL / CONT	(6.03,48.27)	1.947	0.092	(5.37,42.98)	3.338	0.011	(5.68,45.46)	2.336	0.050	(4.75,37.97)	4.325	0.004	(6.08,48.63)	3.734	0.004	(6.08,48.62)	2.201	0.058	(4.97,39.74)	4.451	0.003	(5.96,47.65)	2.238	0.056

**Table 5.1: Eight 3-way-repeated measures ANOVAs for subjects Dn45 and Lk13 for 8 ROIs.**

Factors: speed (2 levels), color (13 levels) and contrast (4 levels). Note: Each speed/color/contrast combination contains 18 measurements from 9 different days and 2 hemispheres. Degrees of freedom are Greenhouse-Geisser corrected when appropriate. Colors code uncorrected significance values:  $p < 0.05$ ,  $p < 0.01$ ,  $p < 0.001$ . The critical p-value after Bonferroni correction for alpha level of 0.05 is 0.006.

### 7.2.2 T-test tables

**Table 5.2: Velocity differences for subjects Dn45 and Lk13.**

T-tests were computed for each ROI at every color/contrast combination to assess speed differences between 1Hz and 10Hz BOLD-responses as an exploratory measure of effect size. Each test compared 18 measurements obtained at 9 separate days for 1Hz and 10Hz respectively and 2 hemispheres. Colors code uncorrected significance levels: **p < 0.05**, **p < 0.01**, **p<0.001**. The critical p-value after Bonferroni correction for alpha level of 0.05 is 0.001 for a single ROI and 0.0001 over all ROIs. Note: a negative t-value in the t-test-tables indicates a higher response for 10Hz than 1Hz for the respective stimulus combination.

**Dn45:**

	ConeContrast	V1	V2d	V2v	V3d	V3v	hV4	V3A	MT-Post	stats
L	0.14000	-3.17535	-1.88219	-1.20126	-0.40556	-0.12622	-0.12362	0.63455	1.27060	T-value
		0.00587	0.07813	0.24713	0.69044	0.90113	0.90316	0.53469	0.22204	p-Value
	0.04200	1.39711	2.28311	2.05002	3.64458	2.94515	4.60759	3.91242	1.85648	T-value
		0.18146	0.03643	0.05712	0.00218	0.00951	0.00029	0.00124	0.08190	p-Value
	0.01400	2.39934	4.32687	2.67690	5.91836	3.38354	7.87866	6.62708	5.20296	T-value
	0.02898	0.00052	0.01684	0.00002	0.00379	0.00000	0.00001	0.00009	p-Value	
	0.00420	3.48826	4.12128	3.07526	4.53538	3.24595	8.68555	5.50148	4.94139	T-value
		0.00304	0.00080	0.00725	0.00034	0.00506	0.00000	0.00005	0.00015	p-Value
	0.14600	-1.18658	0.63706	-1.53554	1.76738	0.76792	0.62116	2.70665	0.73691	T-value
M		0.25271	0.53310	0.14419	0.09623	0.45372	0.54324	0.01556	0.47184	p-Value
	0.04380	0.96743	4.13559	2.42944	5.46991	3.82147	2.92378	4.26247	3.35822	T-value
		0.34773	0.00078	0.02727	0.00005	0.00150	0.00994	0.00060	0.00400	p-Value
	0.01460	0.38953	1.74966	2.79646	3.64747	2.36203	3.57553	5.41429	3.13094	T-value
		0.70202	0.09933	0.01294	0.00217	0.03118	0.00253	0.00006	0.00645	p-Value
	0.00440	1.58254	2.31134	3.48861	4.99418	3.16093	5.62396	6.66876	2.81480	T-value
		0.13309	0.03447	0.00304	0.00013	0.00605	0.00004	0.00001	0.01246	p-Value
S	0.95000	-1.42046	0.86591	-1.79808	1.91939	-0.18311	-0.18052	1.96100	0.99174	T-value
		0.17467	0.39934	0.09106	0.07295	0.85701	0.85901	0.06752	0.33609	p-Value
	0.28500	-0.93178	1.83284	1.93972	2.08730	1.70097	1.18444	3.99575	1.91012	T-value
		0.36530	0.08550	0.07025	0.05321	0.10830	0.25354	0.00104	0.07421	p-Value
	0.09500	1.38888	3.24417	2.54513	5.46934	2.51018	7.47127	5.17153	1.83082	T-value
	0.18390	0.00508	0.02161	0.00005	0.02319	0.00000	0.00009	0.08582	p-Value	
	0.02850	2.35904	4.63173	4.69291	5.63434	4.04425	7.42280	4.90676	5.32162	T-value
		0.03137	0.00028	0.00024	0.00004	0.00094	0.00000	0.00016	0.00007	p-Value
L+M	0.96167	-1.23517	0.81287	-0.35219	0.78129	0.80810	0.44244	1.62777	2.26271	T-value
		0.23460	0.42823	0.72929	0.44604	0.43088	0.66409	0.12310	0.03792	p-Value
	0.28850	-1.47732	0.09774	-2.63799	0.90438	-0.89831	0.51083	1.96864	1.52440	T-value
		0.15900	0.92335	0.01790	0.37921	0.38234	0.61645	0.06657	0.14693	p-Value
	0.09617	-1.86496	0.97896	0.36807	2.41184	1.24225	0.40629	2.39740	0.01192	T-value
	0.08063	0.34217	0.71764	0.02825	0.23204	0.68992	0.02907	0.99064	p-Value	
	0.02885	2.74787	3.45577	4.24593	4.70657	5.81014	7.86133	5.67429	2.71221	T-value
		0.01430	0.00325	0.00062	0.00024	0.00003	0.00000	0.00003	0.01538	p-Value
L-M	0.10182	-0.79226	0.60339	-0.34656	1.76972	1.10729	0.50031	1.20967	-0.92935	T-value
		0.43980	0.55471	0.73344	0.09583	0.28454	0.62367	0.24398	0.36652	p-Value
	0.03055	2.82574	3.07611	2.16608	4.33452	3.40734	3.31803	6.90993	3.27360	T-value
		0.01218	0.00723	0.04575	0.00051	0.00360	0.00435	0.00000	0.00478	p-Value
	0.01018	1.50576	1.92242	2.56913	4.30741	3.75634	8.93246	6.09472	2.26750	T-value
	0.15161	0.07254	0.02059	0.00054	0.00172	0.00000	0.00002	0.03757	p-Value	
	0.00311	4.31779	4.70619	6.30127	5.49458	5.04555	9.56723	7.11679	6.21389	T-value
		0.00053	0.00024	0.00001	0.00005	0.00012	0.00000	0.00000	0.00001	p-Value
L+S	0.17678	-1.84019	-0.09187	-0.57926	0.76565	0.59047	0.26648	0.97942	1.01561	T-value
		0.08437	0.92794	0.57048	0.45503	0.56313	0.79327	0.34195	0.32493	p-Value
	0.05303	0.65989	3.58831	3.02965	4.57319	6.49834	5.52145	6.14885	3.06057	T-value
		0.51871	0.00262	0.00797	0.00031	0.00001	0.00005	0.00001	0.00747	p-Value
	0.01768	2.96393	3.29992	3.35661	4.99789	4.55935	6.85255	6.15314	4.22335	T-value
	0.00914	0.00452	0.00401	0.00013	0.00032	0.00000	0.00001	0.00065	p-Value	
	0.00523	2.61254	3.34402	2.38475	5.99042	3.67306	7.16108	5.88948	4.63579	T-value
		0.01885	0.00412	0.02951	0.00002	0.00206	0.00000	0.00002	0.00027	p-Value
-L+S	0.21920	-2.89983	-1.08966	-1.88504	-0.24844	-1.47597	-0.26882	0.86713	0.34076	T-value
		0.01044	0.29200	0.07772	0.80695	0.15936	0.79150	0.39869	0.73772	p-Value
	0.06576	-0.38585	1.02788	0.80139	1.90982	0.93983	0.28964	2.54517	1.62770	T-value
		0.70469	0.31929	0.43465	0.07425	0.36128	0.77581	0.02161	0.12312	p-Value
	0.02192	0.62568	1.57847	2.00933	3.29170	3.26054	5.24070	5.73864	2.54471	T-value
	0.54035	0.13402	0.06168	0.00460	0.00491	0.00008	0.00003	0.02183	p-Value	
	0.00651	3.26939	7.72468	4.15714	8.19264	5.05690	11.43742	9.51817	9.56245	T-value
		0.00482	0.00000	0.00074	0.00000	0.00012	0.00000	0.00000	0.00000	p-Value
M+S	0.23052	-1.78143	-0.37574	-1.19072	-0.01803	-0.41226	-0.21619	0.70448	-0.32447	T-value
		0.09383	0.71205	0.25113	0.98584	0.68562	0.83157	0.49126	0.74978	p-Value
	0.06916	1.51307	4.57207	2.93779	4.41124	4.20482	5.22633	4.08158	2.68264	T-value
		0.14976	0.00031	0.00965	0.00044	0.00067	0.00008	0.00007	0.01634	p-Value
	0.02305	2.11873	3.82025	3.78992	6.21886	4.44794	7.61660	6.17770	3.87276	T-value
	0.05011	0.00151	0.00161	0.00001	0.00040	0.00000	0.00001	0.00135	p-Value	
	0.00693	1.39087	2.41302	2.53573	5.88882	3.27561	5.77464	5.52763	2.23965	T-value
		0.18331	0.02816	0.02203	0.00002	0.00476	0.00003	0.00005	0.03967	p-Value
-M+S	0.18950	-2.04068	-0.96674	-2.30863	0.28530	-0.17929	0.96981	1.23303	1.34048	T-value
		0.05814	0.34806	0.03465	0.77907	0.85996	0.34657	0.23538	0.19882	p-Value
	0.05685	3.31972	4.18821	2.07840	7.00813	2.99400	5.75376	8.26903	4.82155	T-value
		0.00434	0.00070	0.05412	0.00000	0.00859	0.00003	0.00000	0.00019	p-Value
	0.01895	2.15718	2.04855	3.16680	3.44540	3.16558	6.53844	5.29144	2.71856	T-value
	0.04654	0.05728	0.00598	0.00333	0.00600	0.00001	0.00007	0.01518	p-Value	
	0.00566	2.05980	2.41248	2.71053	6.94790	4.96755	10.43003	10.16379	5.36117	T-value
		0.05607	0.02821	0.01544	0.00000	0.00014	0.00000	0.00000	0.00006	p-Value

	1.71473	-2.13481	-0.59385	-1.67277	-0.49453	-0.75823	-0.59996	-0.26448	-0.28159	T-value
L+M+S	0.04859	0.56091	0.11381	0.62765	0.45934	0.56693	0.79479	0.78187	0.78187	p-Value
	0.51442	-0.73946	0.96312	-0.99172	0.99733	0.73674	0.75459	1.25789	0.63052	T-value
	0.17147	0.47034	0.34982	0.33610	0.33345	0.47195	0.46146	0.22648	0.53726	p-Value
	0.37596	2.54894	2.13155	3.47462	1.79830	2.99781	3.46681	2.67424	2.67424	T-value
	0.71188	0.02145	0.04890	0.00313	0.09102	0.00852	0.00318	0.01663	0.01663	p-Value
L-M+S	0.05144	0.12565	1.27394	1.45433	3.10733	1.92178	3.13069	3.63153	1.53833	T-value
	0.90157	0.22088	0.16519	0.00678	0.07263	0.00645	0.00224	0.14351	0.14351	p-Value
	0.11951	-1.38812	1.42492	0.14548	1.88335	2.19493	1.74633	2.95818	1.50528	T-value
	0.18413	0.17340	0.88615	0.07796	0.04327	0.09992	0.00925	0.15174	0.15174	p-Value
	0.03585	0.50512	1.93790	1.33763	4.05747	2.63254	3.35540	5.89920	2.74559	T-value
L-M-S	0.01195	0.62036	0.07049	0.19972	0.00091	0.01310	0.00402	0.00002	0.01195	p-Value
	1.59165	2.21957	4.33883	5.18848	4.49964	8.33213	7.55887	4.46850	4.46850	T-value
	0.13102	0.04125	0.00051	0.00009	0.00036	0.00000	0.00000	0.00039	0.00039	p-Value
	0.43166	0.89398	0.50585	1.80794	0.28980	2.93285	2.46941	0.78140	0.78140	T-value
	0.67175	0.38458	0.61986	0.08945	0.77669	0.00975	0.02517	0.44597	0.44597	p-Value
S-(L+M)	0.12124	-2.17099	-0.77837	-1.29545	-0.38630	0.41896	0.13350	0.52697	-1.26844	T-value
	0.04532	0.44771	0.21354	0.70436	0.68082	0.89546	0.60544	0.22279	0.22279	p-Value
	0.03637	-0.47372	1.92811	1.21657	4.19246	3.25723	4.63929	4.50618	2.54318	T-value
	0.64210	0.07178	0.24141	0.00069	0.00495	0.00027	0.00036	0.02170	0.02170	p-Value
	0.01212	2.61163	3.72222	6.18759	5.70064	6.59679	8.36058	5.96538	5.66973	T-value
ConeContrast	0.18889	0.00185	0.00001	0.00003	0.00001	0.00000	0.00002	0.00003	0.00003	p-Value
	0.48688	2.05601	1.77514	3.75334	2.32990	5.85330	5.42291	3.05969	3.05969	T-value
	0.63295	0.05648	0.09490	0.00174	0.03323	0.00002	0.00006	0.00749	0.00749	p-Value
	0.90067	-3.26185	-0.78439	-1.69208	-0.42446	-1.23981	-0.95683	-0.56118	0.50302	T-value
	0.00490	0.44427	0.11001	0.67688	0.23292	0.35289	0.58245	0.62180	0.62180	p-Value
ConeContrast	0.27020	-0.73305	0.45207	-1.47129	0.78155	-0.68786	0.70222	1.19080	0.83050	T-value
	0.47413	0.65729	0.16061	0.44589	0.50139	0.49263	0.25110	0.41848	0.41848	p-Value
	0.09007	0.12959	2.30612	2.11892	3.43448	2.22485	2.99850	3.17294	1.81953	T-value
	0.89851	0.03462	0.05009	0.00340	0.04083	0.00851	0.00590	0.08759	0.08759	p-Value
	0.02702	3.29761	4.09147	5.45477	6.90693	7.65344	6.54154	10.71512	5.87609	T-value
0.00454	0.00085	0.00005	0.00000	0.00000	0.00001	0.00000	0.00002	0.00002	p-Value	
	V1	V2d	V2v	V3d	V3v	hV4	V3A	MT-Post	stats	

Lk13:

	ConeContrast	V1	V2d	V2v	V3d	V3v	hV4	V3A	MT-Post	stats
L	0.14000	-4.34885	-1.60692	-2.35918	-0.03022	0.49519	0.37221	-0.23796	-0.35428	T-value
	0.00050	0.12763	0.08136	0.97627	0.62720	0.71462	0.81493	0.72775	0.72775	p-Value
	0.04200	-0.68084	2.05125	0.80631	2.38154	2.05126	3.38760	1.70334	-0.21563	T-value
	0.50570	0.05699	0.43189	0.03000	0.05699	0.00376	0.10785	0.83200	0.83200	p-Value
	0.01400	2.90115	9.03125	3.50375	10.22987	6.21170	5.66874	9.01321	4.31926	T-value
M	0.00420	0.01042	0.00000	0.00294	0.00000	0.00000	0.00003	0.00000	0.00053	p-Value
	1.77768	3.18173	0.62667	3.06554	1.82688	2.06947	2.44086	0.62592	0.62592	T-value
	0.09447	0.00580	0.53971	0.00739	0.08643	0.05505	0.02666	0.54019	0.54019	p-Value
	0.14600	-2.73421	1.92631	-0.06954	2.85571	3.50279	1.43833	1.36596	0.25767	T-value
	0.01470	0.07202	0.94542	0.01144	0.00295	0.16961	0.19085	0.79995	0.79995	p-Value
S	0.04380	1.42300	4.61366	1.86735	6.04322	4.19689	2.94894	5.66307	2.62090	T-value
	0.17394	0.00029	0.08028	0.00002	0.00068	0.00943	0.00004	0.01854	0.01854	p-Value
	0.01460	1.62486	6.30917	2.27390	6.80459	4.27072	3.59563	5.24183	1.38957	T-value
	0.12373	0.00001	0.03710	0.00000	0.00059	0.00242	0.00008	0.18369	0.18369	p-Value
	0.00440	0.35001	4.87692	1.15454	5.61491	4.81193	3.98936	5.07667	1.48736	T-value
L+M	0.73090	0.00017	0.26523	0.00004	0.00019	0.00106	0.00011	0.15636	0.15636	p-Value
	0.95000	-2.10103	1.02928	-1.29624	2.18016	1.99626	1.05478	1.40540	0.69494	T-value
	0.05184	0.31866	0.21328	0.04452	0.06321	0.30719	0.17902	0.49706	0.49706	p-Value
	0.28500	0.54559	3.85349	1.79668	7.65096	3.64303	3.92673	5.63060	4.01140	T-value
	0.59287	0.00140	0.09129	0.00000	0.00219	0.00120	0.00004	0.00101	0.00101	p-Value
L-M	0.09500	2.82419	6.75344	2.90398	7.68485	4.69871	4.35614	5.11773	1.75494	T-value
	0.01222	0.00000	0.01036	0.00000	0.00000	0.00049	0.00010	0.00940	0.00940	p-Value
	0.02850	3.54872	6.16024	3.44851	6.40930	5.68526	5.98924	4.63409	1.90068	T-value
	0.00267	0.00001	0.00330	0.00001	0.00003	0.00002	0.00002	0.00028	0.00028	p-Value
	0.96167	-4.03389	-0.56573	-2.51709	1.74802	0.81746	1.25898	1.93579	0.73688	T-value
L+S	0.00096	0.57942	0.02287	0.09962	0.42567	0.22610	0.07077	0.47186	0.47186	p-Value
	0.28850	-0.35302	1.63024	0.13997	2.08717	1.65501	1.16144	1.97127	1.64967	T-value
	0.72868	0.12258	0.89043	0.05323	0.11740	0.26250	0.06624	0.11850	0.11850	p-Value
	0.09617	-0.97358	1.02410	0.36489	2.09045	2.86768	1.90527	1.07109	-0.45584	T-value
	0.34476	0.32102	0.71997	0.05290	0.01116	0.07488	0.30002	0.65463	0.65463	p-Value
L-M	0.02885	4.43470	6.17671	6.26244	7.57094	9.20537	8.09973	7.08669	4.44745	T-value
	0.00042	0.00001	0.00001	0.00000	0.00000	0.00000	0.00000	0.00041	0.00041	p-Value
	0.10182	-3.33425	0.50178	-1.25530	0.15924	1.35205	0.44993	-0.57468	-2.08240	T-value
	0.00420	0.62266	0.22740	0.87548	0.19516	0.65879	0.57350	0.05371	0.05371	p-Value
	0.03055	0.49608	6.28808	2.41069	6.60290	4.83221	4.02811	4.72457	3.08472	T-value
L+S	0.62658	0.00001	0.02831	0.00001	0.00018	0.00097	0.00023	0.00710	0.00710	p-Value
	0.01018	3.95275	8.86520	3.16259	9.95568	5.73645	5.99219	8.05334	3.47789	T-value
	0.00114	0.00000	0.00603	0.00000	0.00003	0.00002	0.00000	0.00311	0.00311	p-Value
	0.00311	4.13674	7.94521	2.08601	7.42442	5.19463	4.20254	5.04928	1.06326	T-value
	0.00077	0.00000	0.05335	0.00000	0.00009	0.00067	0.00012	0.30345	0.30345	p-Value
L+S	0.17678	-4.70341	-1.11840	-3.18157	-0.35418	-0.12259	-0.42743	-0.74071	-2.02804	T-value
	0.00024	0.27991	0.00580	0.72783	0.90396	0.67477	0.46960	0.05954	0.05954	p-Value
	0.05303	1.77233	4.70164	3.73525	7.47637	5.79882	4.23047	5.11407	1.92107	T-value
	0.09538	0.00024	0.00180	0.00000	0.00004	0.00064	0.00010	0.07272	0.07272	p-Value
	0.01768	3.24157	5.12292	3.61850	5.49177	4.88656	5.33753	5.19937	1.77999	T-value
L+S	0.00511	0.00010	0.00231	0.00005	0.00016	0.00007	0.00009	0.09407	0.09407	p-Value
	0.00523	1.44340	3.33963	1.39650	3.91083	1.60075	2.24128	2.87948	1.99401	T-value
	0.16820	0.00416	0.18164	0.00125	0.12899	0.03954	0.01090	0.06348	0.06348	p-Value
	0.21920	-3.79787	-0.65213	-2.56666	1.04643	1.18424	1.16939	1.19057	0.73219	T-value
	0.00158	0.52358	0.02069	0.31091	0.25361	0.25937	0.25119	0.47464	0.47464	p-Value
L+S	0.06576	-0.50381	1.66374	0.51975	2.29274	1.54492	1.06289	1.67283	-0.14767	T-value
	0.62126	0.11562	0.61035	0.03575	0.14191	0.30361	0.11380	0.88445	0.88445	p-Value
	0.02192	1.75091	8.19861	2.66610	10.92019	6.39994	6.51947	6.96299	3.23863	T-value
	0.09911	0.00000	0.01690	0.00000	0.00001	0.00001	0.00000	0.00000	0.00514	p-Value
	0.00651	2.42251	5.89075	3.57518	6.08234	5.45614	5.51411	7.97172	4.44801	T-value
0.02765	0.00002	0.00253	0.00002	0.00005	0.00005	0.00000	0.00040	0.00040	p-Value	

M+S	0.23052	-2.56021	1.67987	0.38245	3.16271	2.26411	1.50768	1.12005	-0.04184	T-value
		0.02097	0.11240	0.70716	0.00603	0.03782	0.15113	0.27922	0.96714	p-Value
	0.06916	2.50266	4.50890	3.42493	5.59896	4.43019	4.11805	4.83666	2.29421	T-value
		0.02395	0.00036	0.00347	0.00004	0.00042	0.00081	0.00018	0.03965	p-Value
	0.02305	4.71453	10.45838	6.45903	13.47046	8.75611	8.91712	8.99270	3.57684	T-value
		0.00023	0.00000	0.00001	0.00000	0.00000	0.00000	0.00000	0.00252	p-Value
0.00693	1.25158	3.78047	1.32892	3.25400	3.25574	3.86914	2.43413	-0.27713	T-value	
	0.22871	0.00164	0.20251	0.00498	0.00496	0.00136	0.02702	0.78523	p-Value	
-M+S	0.18950	-1.13080	0.97923	-0.03800	2.33994	1.99076	1.20637	1.66380	0.53946	T-value
		0.27481	0.34204	0.97016	0.03258	0.06387	0.24521	0.11561	0.59700	p-Value
	0.05685	-0.86062	3.79025	0.73305	7.31365	3.31344	3.46306	4.28962	0.90617	T-value
		0.40216	0.00161	0.47413	0.00000	0.00439	0.00320	0.00056	0.37829	p-Value
	0.01895	4.02127	5.90575	4.57046	7.69018	4.79879	5.53996	7.97840	2.15657	T-value
		0.00099	0.00002	0.00031	0.00000	0.00020	0.00004	0.00000	0.04660	p-Value
0.00566	2.63212	6.97292	2.03966	6.34601	4.95469	5.11214	6.11496	1.47881	T-value	
	0.01812	0.00000	0.05825	0.00001	0.00014	0.00010	0.00001	0.15861	p-Value	
L+M+S	1.71473	-2.80758	-1.29566	-1.92212	0.41029	0.72356	0.97060	0.58885	0.20916	T-value
		0.01264	0.21347	0.07258	0.68703	0.47978	0.34619	0.56418	0.83696	p-Value
	0.51442	-3.04388	-0.51661	-0.12291	0.57311	1.58964	1.05790	1.14508	-0.73371	T-value
		0.00774	0.61250	0.90371	0.57454	0.13148	0.30581	0.88646	0.47374	p-Value
	0.17147	0.62187	3.10776	2.54563	4.22291	3.74141	3.23090	1.53307	1.03307	T-value
		0.54279	0.00677	0.02159	0.00065	0.00178	0.00523	0.14479	0.31693	p-Value
0.05144	1.75865	5.08981	2.50745	6.00999	4.67393	4.08930	4.08601	1.64753	T-value	
	0.09774	0.00011	0.02332	0.00002	0.00025	0.00086	0.00086	0.11895	p-Value	
L-M+S	0.11951	-3.40870	-0.67515	-1.35282	0.69215	1.51953	0.77115	0.44459	-1.83656	T-value
		0.00359	0.50922	0.19492	0.49876	0.14814	0.45186	0.66257	0.08492	p-Value
	0.03585	2.58042	4.78561	3.05562	5.30551	5.63440	3.27934	4.68379	2.69261	T-value
		0.02012	0.00020	0.00755	0.00007	0.00004	0.00472	0.00025	0.01601	p-Value
	0.01195	1.23748	4.80494	1.53074	6.80484	4.28794	5.73768	7.50762	1.58781	T-value
		0.23376	0.00019	0.14536	0.00000	0.00056	0.00003	0.00000	0.13189	p-Value
0.00364	1.13282	2.97926	2.29712	4.04247	3.34763	3.36959	3.31466	1.74098	T-value	
	0.27398	0.00885	0.03545	0.00094	0.00409	0.00390	0.00438	0.10088	p-Value	
L-M-S	0.12124	-2.90512	0.13081	-0.77491	1.06489	1.52856	0.94727	0.24105	-0.96685	T-value
		0.01033	0.89755	0.44969	0.30273	0.14590	0.35759	0.81258	0.34801	p-Value
	0.03637	0.07476	4.03637	0.66324	4.82578	3.01510	2.34086	3.88137	1.04451	T-value
		0.94133	0.00096	0.51662	0.00019	0.00822	0.03252	0.00132	0.31178	p-Value
	0.01212	2.61814	7.57967	2.50079	7.72712	5.53930	6.40921	6.06094	3.94496	T-value
		0.01884	0.00000	0.02364	0.00000	0.00004	0.00001	0.00002	0.00116	p-Value
0.00364	1.04223	2.13878	-0.31252	3.38270	0.95537	1.39332	2.73277	0.21326	T-value	
	0.31280	0.04822	0.75868	0.00380	0.35360	0.18258	0.01475	0.83382	p-Value	
S-(L+M)	0.90067	-4.17653	-0.71704	-2.73692	0.50097	0.97464	0.86535	0.51634	0.36530	T-value
		0.00071	0.48368	0.01462	0.62322	0.34424	0.39964	0.61268	0.71967	p-Value
	0.27020	-1.34582	2.07911	-0.86743	3.26938	2.05125	1.64948	1.85534	1.19489	T-value
		0.19712	0.05405	0.39853	0.00482	0.05699	0.11854	0.08207	0.24954	p-Value
	0.09007	1.41369	2.86134	2.36645	2.99919	3.58409	2.86138	2.37090	0.94097	T-value
		0.17662	0.01131	0.03091	0.00849	0.00248	0.01131	0.03094	0.36071	p-Value
0.02702	3.33112	8.12432	4.27605	9.72698	6.31764	5.83097	6.52420	1.96049	T-value	
	0.00423	0.00000	0.00058	0.00000	0.00001	0.00003	0.00001	0.06759	p-Value	
ConeContrast	V1	V2d	V2v	V3d	V3v	hV4	V3A	MT-Post	stats	

## 8 CITATIONS

ALBRECHT, D. G. (1995). Visual cortex neurons in monkey and cat: effect of contrast on the spatial and temporal phase transfer functions. *Vis Neurosci* **12**, 1191-1210.

ALBRECHT, D. G. & HAMILTON, D. B. (1982). Striate cortex of monkey and cat: contrast response function. *J Neurophysiol* **48**, 217-237.

ALITTO, H. J. & USREY, W. M. (2004). Influence of contrast on orientation and temporal frequency tuning in ferret primary visual cortex. *J Neurophysiol* **91**, 2797-2808.

BANDETTINI, P. A., JESMANOWICZ, A., WONG, E. C. & HYDE, J. S. (1993). Processing strategies for time-course data sets in functional MRI of the human brain. *Magn Reson Med* **30**, 161-173.

BARTELS, A. & ZEKI, S. (2000). The architecture of the colour centre in the human visual brain: new results and a review. *Eur J Neurosci* **12**, 172-193.

BEAUCHAMP, M. S., HAXBY, J. V., JENNINGS, J. E. & DEYOE, E. A. (1999). An fMRI version of the Farnsworth-Munsell 100-Hue test reveals multiple color-selective areas in human ventral occipitotemporal cortex. *Cereb Cortex* **9**, 257-263.

BECK, D. M. & KASTNER, S. (2005). Stimulus context modulates competition in human extrastriate cortex. *Nat Neurosci* **8**, 1110-1116. .

BENARDETE, E. A. & KAPLAN, E. (1999). The dynamics of primate M retinal ganglion cells. *Vis Neurosci* **16**, 355-368.

BENARDETE, E. A., KAPLAN, E. & KNIGHT, B. W. (1992 ). Contrast gain control in the primate retina: P cells are not X-like, some M cells are. *Vis Neurosci* **8**, 483-486.

BETZOLD , W. v. (1873). Über das Gesetz der Farbenmischung und die physiologischen Grundfarben. *Annalen der Physiologischen Chemie* **226**, 221 - 247.

BETZOLD , W. v. (1874). *Die Farbenlehre in Hinblick auf Kunst und Kunstgewerbe*, Braunschweig.

BOYNTON, G. M., ENGEL, S. A., GLOVER, G. H. & HEEGER, D. J. (1996). Linear systems analysis of functional magnetic resonance imaging in human V1. *J Neurosci* **16**, 4207-4221.

BRAINARD, D. H., ROORDA, A., YAMAUCHI, Y., CALDERONE, J. B., METHA, A., NEITZ, M., NEITZ, J., WILLIAMS, D. R. & GH., J. (2000). Functional consequences of the relative numbers of L and M cones. *J Opt Soc Am A* **17**, 607-614.

- BREWER, A. A., LIU, J., WADE, A. R. & WANDELL, B. A. (2005). Visual field maps and stimulus selectivity in human ventral occipital cortex. *Nat Neurosci* **8**, 1102-1109. Epub 2005 Jul 1117.
- BRIGGS, F. & CALLAWAY, E. M. (2005 ). Laminar patterns of local excitatory input to layer 5 neurons in macaque primary visual cortex. *Cereb Cortex* **15**, 479-488.
- BROWN, P. K. & WALD, G. (1964). Visual pigments in single rods and cones of human retina. *Science* **144**, 45-52.
- BUCKNER, R. L., BANDETTINI, P. A., O' CRAVEN, K. M., SAVOY, R. L., PETERSEN, S. E., RAICHEL, M. E. & ROSEN, B. R. (1996). Detection of cortical activation during averaged single trials of a cognitive task using functional magnetic resonance imaging. *Proc Natl Acad Sci* **93**, 14878-14883.
- CALKINS, D. J., TSUKAMOTO, Y., STERLING, P.,. (1996). Foveal cones form basal as well as invaginating junctions with diffuse ON bipolar cells. *Vision Res* **36**, 3373-3381.
- CALLAWAY, E. M. (2004). Feedforward, feedback and inhibitory connections in primate visual cortex. *Neural Netw* **17**, 625-632.
- CALLAWAY, E. M. (2005). Neural substrates within primary visual cortex for interactions between parallel visual pathways. *Prog Brain Res* **149**, 59-64.
- CARANDINI, M., HEEGER, D. J. & MOVSHON, J. A. (1997). Linearity and normalization in simple cells of the macaque primary visual cortex. *J Neurosci* **17**, 2161-2172.
- CASAGRANDE, V. A. (1994). A third parallel visual pathway to primate area V1. *Trends Neurosci* **17**, 305-310.
- CAVANAGH, P. & ANSTIS, S. (1991). The contribution of color to motion in normal and color-deficient observers. *Vision Res* **31**, 2109-2148.
- CAVANAGH, P., HENAFF, M. A., MICHEL, F., LANDIS, T., TROSCIANKO, T. & INTRILIGATOR, J. (1998). Complete sparing of high-contrast color input to motion perception in cortical color blindness. *Nat Neurosci* **1**, 242-247.
- CAVANAGH, P., MACLEOD, D. I. & ANSTIS, S. M. (1987 ). Equiluminance: spatial and temporal factors and the contribution of blue-sensitive cones. *J Opt Soc Am A* **4**, 1428-1438.
- CAVANAGH, P., TYLER, C. W. & FAVREAU, O. E. (1984). Perceived velocity of moving chromatic gratings. *J Opt Soc Am A* **1**, 893-899.
- CHARLES, E. R. & LOGOTHETIS, N. K. (1989). The responses of middle temporal (MT) neurons to isoluminant stimuli. *Invest Ophthalmol Vis Sci* **30**, 155-164.

- CHATTERJEE, S. & CALLAWAY, E. M. (2003). Parallel colour-opponent pathways to primary visual cortex. *Nature* **426**, 668-671.
- CHATTERJEE, S., CALLAWAY, E.M., (2002). S cone contributions to the magnocellular visual pathway in macaque monkey. *Neuron* **35**, 1135-1146.
- CIE. (1926). Commission Internationale de l'eclairage Proceedings, 1924. Cambridge University Press, Cambridge UK, 1926.
- COLE, G. R., HINE, T. & MCLHAGGA, W. (1993). Detection mechanisms in L-, M-, and S-cone contrast space. *J Opt Soc Am A*. **10**, 38-51.
- CONWAY, B. R. (2001). Spatial structure of cone inputs to color cells in alert macaque primary visual cortex (V1). *J Neurosci*. **21**, 2768-2783.
- CONWAY, B. R., HUBEL, D. H. & LIVINGSTONE, M. S. (2002). Color contrast in macaque V1. *Cereb Cortex* **12**, 915-925.
- CONWAY, B. R. & LIVINGSTONE, M. S. (2003). The neural basis for color vision. In *Encyclopedia of Cognitive Science*. ed. NADEL, L., pp. 568-576. Nature Publishing Group, London.
- CONWAY, B. R. & LIVINGSTONE, M. S. (2006). Spatial and temporal properties of cone signals in alert macaque primary visual cortex. *J Neurosci* **26**, 10826-10846.
- CORBETTA, M., MIEZIN, F. M., DOBMEYER, S., SHULMAN, G. L. & PETERSEN, S. E. (1991). Selective and divided attention during visual discriminations of shape, color, and speed: functional anatomy by positron emission tomography. *J Neurosci* **11**, 2383-2402.
- CRONER, L. J. & ALBRIGHT, T. D. (1999). Segmentation by color influences responses of motion-sensitive neurons in the cortical middle temporal visual area. *Journal of Neuroscience* **19**, 3935-3951.
- DACEY, D. M. (1993). Morphology of a small-field bistratified ganglion cell type in the macaque and human retina. *Vis Neurosci* **10**, 1081-1098.
- DACEY, D. M. (2000). Parallel pathways for spectral coding in primate retina. *Annu. Rev. Neurosci.* **23**.
- DACEY, D. M. & LEE, B. B. (1994). The 'blue-on' opponent pathway in primate retina originates from a distinct bistratified ganglion cell type. *Nature* **367**, 731-735.
- DACEY, D. M., PETERSON, B. B., ROBINSON, F. R., GAMLIN, P. D., (2003). Fireworks in the primate retina. In vitro photodynamics reveals diverse LGN-projecting ganglion cell types. *Neuron* **37** 15-27.
- DALE, A. M. (1999). Optimal experimental design for event-related fMRI. *Human Brain Mapping* **8**, 109-114.

DALE, A. M. & BUCKNER, R. L. (1997). Selective averaging of rapidly presented individual trials using fMRI. *Human Brain Mapping* **5**, 329-340.

DANIEL, P. M. & WHITTERIDGE, D. (1961). The representation of the visual field on the cerebral cortex in monkeys. *J Physiol (Paris)* **159**, 203-221.

DAW, N. W. (1968). Colour-coded ganglion cells in the goldfish retina: extension of their receptive fields by means of new stimuli. *J Physiol* **197**, 567-592.

DE MONASTERIO, F. M., SCHEIN, S. J. (1982). Spectral bandwidths of color-opponent cells of geniculocortical pathway of macaque monkeys. *J Neurophysiol* **47**, 214-224.

DE VALOIS, R. L., ABRAMOV, I. & JACOBS, G. H. (1966). Analysis of response patterns of LGN cells. *J Opt Soc Am* **56**, 966-977.

DE WEERD, P., PERALTA, M. R., 3RD, DESIMONE, R. & UNGERLEIDER, L. G. (1999). Loss of attentional stimulus selection after extrastriate cortical lesions in macaques. *Nat Neurosci* **2**, 753-758.

DEAN, A. F. & TOLHURST, D. J. (1986). Factors influencing the temporal phase of response to bar and grating stimuli for simple cells in the cat striate cortex. *Exp Brain Res* **62**, 143-151.

DERRINGTON, A. M. & HENNING, G. B. (1993). Detecting and discriminating the direction of motion of luminance and colour gratings. *Vision Res.* **33**, 799-811.

DERRINGTON, A. M., KRAUSKOPF, J. & LENNIE, P. (1984). Chromatic mechanisms in lateral geniculate nucleus of macaque. *J Physiol* **357**, 241-265.

DESIMONE, R. & SCHEIN, S. J. (1987). Visual properties of neurons in area V4 of the macaque: sensitivity to stimulus form. *J Neurophysiol.* **57**, 835-868.

DEYOE, E. A., BANDETTINI, P., NEITZ, J., MILLER, D. & WINANS, P. (1994). Functional magnetic resonance imaging (fMRI) of the human brain. *J Neurosci Methods* **54**, 171-187.

DEYOE, E. A. & VAN ESSEN, D. C. (1985). Segregation of efferent connections and receptive field properties in visual area V2 of the macaque. *Nature* **317**, 58-61.

DEYOE, E. A. & VAN ESSEN, D. C. (1988). Concurrent processing streams in monkey visual cortex. *Trends Neurosci* **11**, 219-226.

DOBKINS, K. R. & ALBRIGHT, T. D. (1994). What happens if it changes color when it moves?: the nature of chromatic input to macaque visual area MT. *J Neurosci.* **14**, 4854-4870.

- DOBKINS, K. R., GUNTHER, K. L. & PETERZELL, D. H. (2000). What covariance mechanisms underlie green/red equiluminance, luminance contrast sensitivity and chromatic (green/red) contrast sensitivity? *Vision Res* **40**, 613-628.
- DOBKINS, K. R., THIELE, A. & ALBRIGHT, T. D. (2000a). Comparison of red-green equiluminance points in humans and macaques: evidence for different L:M cone ratios between species. *J Opt Soc Am A Opt Image Sci Vis.* **17**, 545-556.
- DOUGHERTY, R. F., KOCH, V. M., BREWER, A. A., FISCHER, B., MODERSITZKI, J. & WANDELL, B. A. (2003). Visual field representations and locations of visual areas V1/2/3 in human visual cortex. *Journal of Vision* **3**, 586-598.
- DOUGHERTY, R. F., PRESS, W. A. & WANDELL, B. A. (1999). Perceived speed of colored stimuli. *Neuron.* **24**, 893-899.
- DOW, B. M. & GOURAS, P. (1973). Color and spatial specificity of single units in Rhesus monkey foveal striate cortex. *J Neurophysiol* **36**, 79-100.
- DUMOULIN, S. O., BITTAR, R. G., KABANI, N. J., BAKER, C. L., JR., LE GOUALHER, G., BRUCE PIKE, G. & EVANS, A. C. (2000). A new anatomical landmark for reliable identification of human area V5/MT: a quantitative analysis of sulcal patterning. *Cereb Cortex.* **10**, 454-463.
- EJIMA, Y., TAKAHASHI, S. (1984). Bezold-Brucke hue shift and nonlinearity in opponent-color process. *Vision Research* **24**, 1897-1904.
- ENGEL, S. A. (2005). Adaptation of oriented and unoriented color-selective neurons in human visual areas. *Neuron* **45**, 613-623.
- ENGEL, S. A. & FURMANSKI, C. S. (2001). Selective adaptation to color contrast in human primary visual cortex. *J Neurosci* **21**, 3949-3954.
- ENGEL, S. A., GLOVER, G. H. & WANDELL, B. A. (1997a). Retinotopic organization in human visual cortex and the spatial precision of functional MRI. *Cereb Cortex* **7**, 181-192.
- ENGEL, S. A., RUMELHART, D. E., WANDELL, B. A., LEE, A. T., GLOVER, G. H., CHICHILNISKY, E. J. & SHADLEN, M. N. (1994). fMRI of human visual cortex. *Nature* **369**, 525.
- ENGEL, S. A., ZHANG, X. & WANDELL, B. (1997b). Colour tuning in human visual cortex measured with functional magnetic resonance imaging. *Nature.* **388**, 68-71.
- ESKEW, R. T., MCLELLAN, J. S. & GIULIANINI, F. (1999). Chromatic detection and discrimination. In *Color Vision*. ed. GEGENFURTNER, K. R. & SHARPE, L. T., pp. 345-368. Cambridge University Press, Cambridge.

FELLEMAN, D. J. & VAN ESSEN, D. C. (1987). Receptive field properties of neurons in area V3 of macaque monkey extrastriate cortex. *J Neurophysiol* **57**, 889-920.

FELLEMAN, D. J. & VAN ESSEN, D. C. (1991). Distributed hierarchical processing in the primate cerebral cortex. *Cereb Cortex* **1**, 1-47.

FELLEMAN, D. J., XIAO, Y. & MCCLENDON, E. (1997a). Modular organization of occipito-temporal pathways: cortical connections between visual area 4 and visual area 2 and posterior inferotemporal ventral area in macaque monkeys. *J Neurosci* **17**, 3185-3200.

FERRERA, V. P., NEALEY, T. A. & MAUNSELL, J. H. (1994). Responses in macaque visual area V4 following inactivation of the parvocellular and magnocellular LGN pathways. *J Neurosci*, **4**.

FITZPATRICK, D. (1996). The functional organization of local circuits in visual cortex: insights from the study of tree shrew striate cortex. *Cereb Cortex* **6**, 329-341.

FITZPATRICK, D., LUND, J. S. & BLASDEL, G. G. (1985). Intrinsic connections of macaque striate cortex: afferent and efferent connections of lamina 4C. *J Neurosci* **5**, 3329-3349.

FIZE, D., VANDUFFEL, W., NELISSEN, K., DENYS, K., CHEF D'HOTEL C., FAUGERAS, O. & ORBAN, G. A. (2003). The retinotopic organization of primate dorsal V4 and surrounding areas: A functional magnetic resonance imaging study in awake monkeys. *J Neurosci* **23**, 7395-7406.

FOSTER, K. H., GASKA, J. P., NAGLER, M. & POLLEN, D. A. (1985). Spatial and temporal frequency selectivity of neurones in visual cortical areas V1 and V2 of the macaque monkey. *J Physiol* **365**, 331-363.

GEGENFURTNER, K. R. & HAWKEN, M. J. (1995). Temporal and chromatic properties of motion mechanisms. *Vision Res.* **35**, 1547-1563.

GEGENFURTNER, K. R. & HAWKEN, M. J. (1996). Interaction of motion and color in the visual pathways. *Trends Neurosci* **19**, 394-401.

GEGENFURTNER, K. R. & KIPER, D., C., (2003). Color vision. *Annu Rev Neurosci* **26**, 181-206.

GEGENFURTNER, K. R., KIPER, D. C., BEUSMANS, J. M., CARANDINI, M., ZAIDI, Q. & MOVSHON, J. A. (1994). Chromatic properties of neurons in macaque MT. *Vis Neurosci.* **11**, 455-466.

GEGENFURTNER, K. R., KIPER, D. C. & FENSTEMAKER, S. B. (1996). Processing of color, form, and motion in macaque area V2. *Vis Neurosci* **13**, 161-172.

GEGENFURTNER, K. R., KIPER, D. C. & LEVITT, J. B. (1997). Functional properties of neurons in macaque area V3. *J Neurophysiol.* **77**, 1906-1923.

- GEGENFURTNER, K. R. & SHARPE, L. T. (1999). *Color vision: from genes to perception*. Cambridge UP, Cambridge, UK.
- GEGENFURTNER, K. R., SHARPE, L.T.,. (1999). *Color Vision: from genes to perception*. Cambridge University Press., Cambridge.
- GHOSE, G. M. & TS'O, D. Y. (1997). Form processing modules in primate area V4. *J Neurophysiol.* **77**, 2191-2196.
- GOODALE, M. A. & MILNER, A. D. (1992). Separate visual pathways for perception and action. *Trends Neurosci* **15**, 20-25.
- GOURAS, P. (1974). Opponent-colour cells in different layers of foveal striate cortex. *J Physiol* **238**, 583-602.
- GRILL-SPECTOR, K. & MALACH, R. (2001). fMR-adaptation: a tool for studying the functional properties of human cortical neurons. *Acta Psychol (Amst)* **41**, 1409-1422.
- GRILL-SPECTOR, K., SAYRES, R. & RESS, D. (2006). High-resolution imaging reveals highly selective nonface clusters in the fusiform face area. *Nat Neurosci* **9**, 1177-1185.
- GRUNERT, U., GREFERATH, U., BOYCOTT, B. B., WASSLE, H. (1993). Parasol (P alpha) ganglion-cells of the primate fovea: immunocytochemical staining with antibodies against GABAA-receptors. *Vision Res* **33**, 1-14.
- GULYAS, B., HEYWOOD, C. A., POPPLEWELL, D. A., ROLAND, P. E. & COWEY, A. (1994). Visual form discrimination from color or motion cues: functional anatomy by positron emission tomography. *Proc Natl Acad Sci U S A* **91**, 9965-9969.
- GUR, M. & SNODDERLY, D. M. (1997). A dissociation between brain activity and perception: chromatically opponent cortical neurons signal chromatic flicker that is not perceived. *Vision Res.* **37**, 377-382.
- HADJIKHANI, N., LIU, A. K., DALE, A. M., CAVANAGH, P. & TOOTELL, R. B. (1998). Retinotopy and color sensitivity in human visual cortical area V8. *Nat Neurosci* **1**, 235-241.
- HAGSTROM, S. A., NEITZ, J. & NEITZ, M. (1998). Variations in cone populations for red-green color vision examined by analysis of mRNA,. *NeuroReport* **9**, 1963-1967.
- HASSON, U., HAREL, M., LEVY, I. & MALACH, R. (2003). Large-scale mirror-symmetry organization of human occipito-temporal object areas. *Neuron* **37**, 1027-1041.

- HASSON, U., LEVY, I., BEHRMANN, M., HENDLER, T. & MALACH, R. (2002). Eccentricity bias as an organizing principle for human high-order object areas. *Neuron* **34**, 479-490.
- HAWKEN, M. J., GEGENFURTNER, K. R. & TANG, C. (1994). Contrast dependence of colour and luminance motion mechanisms in human vision. *Nature* **367**, 268-270.
- HAWKEN, M. J., SHAPLEY, R. M. & GROSOFF, D. H. (1996). Temporal-frequency selectivity in monkey visual cortex. *Vis Neurosci.* **13**, 477-492.
- HEEGER, D. J. (1999). Linking visual perception with human brain activity. *Curr Opin Neurobiol* **9**, 474-479.
- HELMHOLTZ, H. V. (1867/1925). *Handbuch der Physiologischen Optik*, vol. 1st ed. Voss, Leipzig.
- HENDRY, S. H. & YOSHIOKA, T. (1994). A neurochemically distinct third channel in the macaque dorsal lateral geniculate nucleus. *Science* **264**, 575-577.
- HERING, E. (1878/1964). *Handbuch der gesamten Augenheilkunde. Grundzüge der Lehre vom Lichtsinn.*, Berlin, 1905.
- HERING, E. (1964). *Outlines of a theory of the light sense*. Harvard University Press, Cambridge.
- HESS, R. H., BAKER, C. L., JR. & ZIHL, J. (1989). The "motion-blind" patient: low-level spatial and temporal filters. *J Neurosci.* **9**, 1628-1640.
- HEYWOOD, C. A. & COWEY, A. (1987). On the role of cortical area V4 in the discrimination of hue and pattern in macaque monkeys. *J Neurosci* **7**, 2601-2617.
- HEYWOOD, C. A., GADOTTI, A. & COWEY, A. (1992). Cortical area V4 and its role in the perception of color. *J Neurosci* **12**, 4056-4065.
- HICKS, T. P., LEE, B. B. & VIDYASAGAR, T. R. (1983). The responses of cells in macaque lateral geniculate nucleus to sinusoidal gratings. *J Physiol* **337**, 183-200.
- HINRICHS, H., SCHOLZ, M., TEMPELMANN, C., WOLDORFF, M. G., DALE, A. M. & HEINZE, H. J. (2000). Deconvolution of event-related fMRI responses in fast-rate experimental designs: tracking amplitude variations. *J Cogn Neurosci* **12**, 76-89.
- HOLUB, R. A. & MORTON-GIBSON, M. (1981). Response of Visual Cortical Neurons of the cat to moving sinusoidal gratings: response-contrast functions and spatiotemporal interactions. *J Neurophysiol* **46**, 1244-1259.

- HORN, B. K. P. (1974). Determining lightness from an image. *Computer Graphics Image Processing* **3**, 111–299.
- HORTON, J. C. & HOYT, W. F. (1991a). The representation of the visual field in human striate cortex. A revision of the classic Holmes map. *Arch Ophthalmol* **109**, 816-824.
- HUBEL, D. H. & LIVINGSTONE, M. S. (1987). Segregation of form, color, and stereopsis in primate area 18. *J Neurosci* **7**, 3378-3415.
- HUBEL, D. H. & WIESEL, T. N. (1968). Receptive fields and functional architecture of monkey striate cortex. *J Physiol* **195**, 215-243.
- HUBEL, D. H. W. T. N. (1959). Receptive fields of single neurons in the cat's striate Cortex. *J. Physiol. (Lond.)* **148**, 574-591.
- HUBEL, D. H. W. T. N. (1962). Receptive fields, binocular interaction, and functional architecture of the cat's visual cortex. *Journal of Physiology (London)* **160**, 106-154.
- HUK, A. C., DOUGHERTY, R. F. & HEEGER, D. J. (2002). Retinotopy and functional subdivision of human areas MT and MST. *J Neurosci* **22**, 7195-7205.
- HUK, A. C. & HEEGER, D. J. (2000). Task-related modulation of visual cortex. *J Neurophysiol* **83**, 3525-3536.
- HURVICH, L. M. & JAMESON, D. (1955). Some quantitative aspects of an opponent-colors theory. II. Brightness, saturation, and hue in normal and dichromatic vision. *J Opt Soc Am* **45**, 602-616.
- HURVICH, L. M. & JAMESON, D. (1957). An opponent process theory of color vision. *Psychological Review* **64**, 384-404.
- HURVICH, L. M., JAMESON, D. (1956). Some quantitative aspects of an opponent-colors theory. IV. A psychological color specification system. *J Opt Soc Am* **46**, 416-421.
- INOUE, T. (1909). *Die Sehstörungen bei Schussverletzungen der kortikalen Sehsphäre nach Beobachtungen an Verwundeten der letzten japanischen Kriege*. Engelmann, Leipzig.
- JACOBY, R. A., WIECHMANN, A.F., AMARA, S.G., LEIGHTON, B.H., MARSHAK, D.W., (2000). Diffuse bipolar cells provide input to OFF parasol ganglion cells in the macaque retina. *J Comp Neurol* **416**, 6-18.
- JAMESON, D., HURVICH, L.M. (1956 ). Some quantitative aspects of an opponent-colors theory. III. Changes in brightness, saturation, and hue with chromatic adaptation. *J Opt Soc Am* **46**, 405-415.

- JOHNSON, E. N., HAWKEN, M. J. & SHAPLEY, R. (2001). The spatial transformation of color in the primary visual cortex of the macaque monkey. *Nat Neurosci* **4**, 409-416.
- JOHNSON, E. N., HAWKEN, M. J. & SHAPLEY, R. (2004). Cone inputs in macaque primary visual cortex. *J Neurophysiol.* **91**, 2501-2514. Epub 2004 Jan 2528.
- JOSEPHS, O., TURNER, R. & FRISTON, K. J. (1997). Event-Related fMRI. *Human Brain Mapping* **5**, 243-248.
- KAISER, P. K. & BOYNTON, R. M. (1996). *Human Color Vision*. Opt. Soc. Am., Washington, DC.
- KAUFMAN, L. (1974). *Sight and Mind: An introduction to visual perception*. Oxford University Press, Oxford.
- KAYSER, A., PRIEBE, N. J. & MILLER, K. D. (2001). Contrast-dependent nonlinearities arise locally in a model of contrast-invariant orientation tuning. *J Neurophysiol* **85**, 2130-2149.
- KIPER, D. C., FENSTEMAKER, S. B. & GEGENFURTNER, K. R. (1997). Chromatic properties of neurons in macaque area V2. *Vis Neurosci.* **14**, 1061-1072.
- KLEINSCHMIDT, A., LEE, B. B., REQUARDT, M. & FRAHM, J. (1996). Functional mapping of color processing by magnetic resonance imaging of responses to selective P- and M-pathway stimulation. *Exp Brain Res* **110**, 279-288.
- KLUG, K., TUSKAMOTO, Y., STERLING, P., SCHEIN, S.J.,. (1993). Blue cone off-midget ganglion cells in macaque. *Investigative Ophthalmology and Visual Science* **34**, 1993.
- KRAUSKOPF, J. (2000a). A journey in color space. In *Color Research & Application. Special Issue: The Proceedings of the International Colour Vision Society . Issue Edited by C. R. Cavonius, Kenneth Knoblauch, Barry B. Lee, Joel Pokorny.*, vol. 26S2 - S11, pp. S2 - S11.
- KRAUSKOPF, J. (2000b). Relative number of long- and middle-wavelength-sensitive cones in the human fovea. *Journal of the Optical Society of America A* **17** 510-516.
- KRAUSKOPF, J. & FARELL, B. (1990). Influence of colour on the perception of coherent motion. *Nature.* **348**, 328-331.
- KRAUSKOPF, J., WILLIAMS, D. R. & HEELEY, D. W. (1982). Cardinal directions of color space. *Vision Res* **22**, 1123-1131.
- KREMERS, J., WEISS, S. & ZRENNER, E. (1997). Temporal properties of marmoset lateral geniculate cells. *Vision Res* **37**, 2649-2660

- KRIES VON, J. (1905). *Die Gesichtsempfindungen*. In W. Nagel (Ed.), *Handbuch der Physiologie der Menschen*. Vieweg, Brunswick.
- LACHICA, E. A., BECK, P. D. & CASAGRANDE, V. A. (1992). Parallel pathways in macaque monkey striate cortex: anatomically defined columns in layer III. *Proc Natl Acad Sci U S A* **89**, 3566-3570.
- LAND, E. H. (1959). Experiments in color vision. *Sci Am* **200**, 84-94.
- LAND, E. H. (1977). The retinex theory of color vision. *Sci Am* **237**, 108-128.
- LAND, E. H. & McCANN, J. J. (1971 ). Lightness and retinex theory. *J Opt Soc Am*. **61**, 1-11
- LANDISMAN, C. E. & Ts'O, D. Y. (2002). Color Processing in Macaque Striate Cortex: Electrophysiological Properties. *The Journal of Neurophysiology* **87**, 3138-3151.
- LEE, B. B. (1996). Receptive field structure in the primate retina. *Vision Res* **36**, 631-644.
- LEE, B. B., MARTIN, P. R. & VALBERG, A. (1988). The physiological basis of heterochromatic flicker photometry demonstrated in the ganglion cells of the macaque retina. *J Physiol* **404**, 323-347.
- LEE, B. B., POKORNY, J., SMITH, V. C., MARTIN, P. R., VALBERG, A. (1990). Luminance and chromatic modulation sensitivity of macaque ganglion cells and human observers. *J Opt Soc Am A*. **7**, 2223-2236.
- LEE, B. B., SILVEIRA, L.C., YAMADA, E., KREMERS, J.,. (1996a). Parallel pathways in the retina of Old and New World primates. *Rev Bras Biol* **56** :, 323-338.
- LEE, J. & STROMEYER, C. F., 3RD. (1989). Contribution of human short-wave cones to luminance and motion detection. *J Physiol* **413**, 563-593.
- LENNIE, P., D'ZMURA, M. . (1988). Mechanisms of color vision. *Crit. Rev. Neurobiol.* **3**, 333-400
- LENNIE, P., KRAUSKOPF, J. & SCLAR, G. (1990). Chromatic mechanisms in striate cortex of macaque. *J Neurosci* **10**, 649-669.
- LENNIE, P., POKORNY, J. & SMITH, V. C. (1993). Luminance. *J Opt Soc Am A* **10**, 1283-1293.
- LEVINSON, E. & SEKULAR, R. (1975). The independence of channels in human vision selective for direction of movement. *J Physiol.* **250(2)**, 347-366.
- LEVITT, J. B., KIPER, D. C. & MOVSHON, J. A. (1994). Receptive fields and functional architecture of macaque V2. *J Neurophysiol* **71**, 2517-2542.

- LEVY, I., HASSON, U., AVIDAN, G., HENDLER, T. & MALACH, R. (2001). Center-periphery organization of human object areas. *Nat Neurosci* **4**, 533-539.
- LINDSEY, D. T. & TELLER, D. Y. (1990). Motion at isoluminance: discrimination/detection ratios for moving isoluminant gratings. *Vision Res* **30**, 1751-1761.
- LIU, J. & WANDELL, B. A. (2005). Specializations for chromatic and temporal signals in human visual cortex. *J Neurosci*. **25**, 3459-3468.
- LIU, T., SLOTNICK, S. D. & YANTIS, S. (2004). Human MT+ mediates perceptual filling-in during apparent motion. *Neuroimage*. **21**, 1772-1780.
- LIVINGSTONE, M. & HUBEL, D. (1988). Segregation of form, color, movement, and depth: anatomy, physiology, and perception. *Science* **240**, 740-749.
- LIVINGSTONE, M. S. & HUBEL, D. H. (1984). Anatomy and physiology of a color system in the primate visual cortex. *J Neurosci* **4**, 309-356.
- LIVINGSTONE, M. S. & HUBEL, D. H. (1987). Connections between layer 4B of area 17 and the thick cytochrome oxidase stripes of area 18 in the squirrel monkey. *J Neurosci* **7**, 3371-3377.
- LOGOTHETIS, N. K. (2003). The underpinnings of the BOLD functional magnetic resonance imaging signal. *J Neurosci* **23**, 3963-3971.
- LOGOTHETIS, N. K., PAULS, J., AUGATH, M., TRINATH, T. & OELTERMANN, A. (2001). Neurophysiological investigation of the basis of the fMRI signal. *Nature* **412**, 150-157.
- LOGOTHETIS, N. K. & WANDELL, B. A. (2004). Interpreting the BOLD signal. *Annu Rev Physiol* **66**, 735-769.
- LUECK, C. J., ZEKI, S., FRISTON, K. J., DEIBER, M. P., COPE, P., CUNNINGHAM, V. J., LAMMERTSMA, A. A., KENNARD, C. & FRACKOWIAK, R. S. (1989). The colour centre in the cerebral cortex of man. *Nature* **340**, 386-389.
- LUND, J. S., WU, Q., HADINGHAM, P. T. & LEVITT, J. B. (1995). Cells and circuits contributing to functional properties in area V1 of macaque monkey cerebral cortex: bases for neuroanatomically realistic models. *J Anat* **187**, 563-581.
- MACLEOD, D. I. & BOYNTON, R. M. (1979). Chromaticity diagram showing cone excitation by stimuli of equal luminance. *J Opt Soc Am* **69**, 1183-1186.
- MARKS, W. B., DOBELLE, W. H. & MACNICHOL, M. F. J. (1964). Visual pigment of single primate cones. *Science* **143**, 1181-1183.
- MARROCCO, R. T., MCCLURKIN, J. W. & YOUNG, R. A. (1982). Spatial summation and conduction latency classification of cells of the lateral geniculate nucleus of macaques. *J Neurosci* **2**, 1275-1291.

- MAUNSELL, J. H., NEALEY, T. A. & DEPRIEST, D. D. (1990). Magnocellular and parvocellular contributions to responses in the middle temporal visual area (MT) of the macaque monkey. *J Neurosci* **10**, 3323-3334.
- MAXWELL, J. C. (1855). Experiments on colour, as perceived by the eye, with remarks on colour-blindness. *Transactions of the Royal Society, Edinburgh* **21**, 275-298.
- MCKEEFRY, D. J. & ZEKI, S. (1997). The position and topography of the human colour centre as revealed by functional magnetic resonance imaging. *Brain* **120 ( Pt 12)**, 2229-2242.
- MEADOWS, J. C. (1974). Disturbed perception of colours associated with localized cerebral lesions. *Brain* **97**, 615-632.
- MERIGAN, W. H. (1996). Basic visual capacities and shape discrimination after lesions of extrastriate area V4 in macaques. *Vis Neurosci* **13**, 51-60.
- MERIGAN, W. H. (2000). Cortical area V4 is critical for certain texture discriminations, but this effect is not dependent on attention. *Vis Neurosci* **17**, 949-958.
- MERIGAN, W. H. & MAUNSELL, J. H. (1993). How parallel are the primate visual pathways? *Annu Rev Neurosci* **16**, 369-402.
- MERIGAN, W. H., MAUNSELL, J.H. (1993). How parallel are the primate visual pathways? *Annu Rev Neurosci* **16**, 369-402.
- MERIGAN, W. H. & PHAM, H. A. (1998). V4 lesions in macaques affect both single- and multiple-viewpoint shape discriminations. *Vis Neurosci* **15**, 359-367.
- METHA, A. B., VINGRYS, A. J. & BADCOCK, D. R. (1994). Detection and discrimination of moving stimuli: the effects of color, luminance, and eccentricity. *J Opt Soc Am A Opt Image Sci Vis.* **11**, 1697-1709.
- MISHKIN, M., UNGERLEIDER, L. G. & MACKO, K. A. (1983). Object Vision and Spatial Vision: Two cortical pathways. *Visual Perception*.
- MORAN, J. & DESIMONE, R. (1985). Selective attention gates visual processing in the extrastriate cortex. *Science* **229**, 782-784.
- MORRONE, M. C., DENTI, V. & SPINELLI, D. (2002). Color and luminance contrasts attract independent attention. *Curr Biol* **12**, 1134-1137.
- MOVSHON, J. A., ADELSON, E. H., GIZZI, M. S. & NEWSOME, W. T. (1985). The analysis of moving visual patterns. In *Study Week on Pattern Recognition Mechanisms*. ed. CHAGAS, C., GATTASS, R. & GROSS, C., pp. 117-151. Vatican Press, Rome.

- MOVSHON, J. A., THOMPSON, I. D. & TOLHURST, D. J. (1978). Spatial and temporal contrast sensitivity of neurones in areas 17 and 18 of the cat's visual cortex. *J Physiol* **283**, 101-120.
- MUCKLI, L., KOHLER, A., KRIEGESKORTE, N. & SINGER, W. (2005). Primary visual cortex activity along the apparent-motion trace reflects illusory perception. *PLoS Biol* **3**, e265. Epub 2005 Jul 2019.
- MULLEN, K. T. (1985). The contrast sensitivity of human colour vision to red-green and blue-yellow chromatic gratings. *J Physiol* **359**, 381-400.
- MULLEN, K. T. & BOULTON, J. C. (1992). Absence of smooth motion perception in color vision. *Vision Res* **32**, 483-488.
- MULLEN, K. T., DUMOULIN, S. O., MCMAHON, K. L., BRYANT, M., DE ZUBICARAY, G. I. & HESS, R. F. (2005). A comparison of the BOLD fMRI response to achromatic, L/M opponent and S-cone opponent cardinal stimuli in human visual cortex: I. perceptually matched vs contrast matched stimuli [Abstract]. *Journal of Vision* **5**, 95a.
- MÜLLER, G. E. (1924). *Darstellung und Erklärung der verschiedenen Typen der Farbenblindheit*. Vandenhoe & Ruprecht, Göttingen.
- NASSI, J. J. & CALLAWAY, E. M. (2006). Multiple circuits relaying primate parallel visual pathways to the middle temporal area. *J Neurosci* **26**, 12789-12798.
- NASSI, J. J., LYON, D. C. & CALLAWAY, E. M. (2006). The parvocellular LGN provides a robust disynaptic input to the visual motion area MT. *Neuron* **50**, 319-327.
- NEALEY, T. A., FERRERA, V. P. & MAUNSELL, J. H. R. (1991). Magnocellular and parvocellular contributions to the ventral extrastriate cortical processing stream. *Soc. neurosci. Abstr.* **17**, 525.
- NERGER, J. L. & CICERONE, C. M. (1992). The ratio of L cones to M cones in the human parafoveal retina. *Vision Res* **32**, 879-888.
- NEWSOME, W. T., BRITTEN, K. H., SALZMAN, C. D. & MOVSHON, J. A. (1991). Neuronal mechanisms of motion perception. *Cold Spring Harb Symp Quant Biol* **55**, 697-705.
- NEWSOME, W. T., WURTZ, R. H., DURSTELER, M. R. & MIKAMI, A. (1985). Deficits in visual motion processing following ibotenic acid lesions of the middle temporal visual area of the macaque monkey. *J Neurosci* **5**, 825-840.
- NEWTON, I. (1704). *Optiks*. Smith and Walford, London.
- NEWTON, J. R. & ESKEW, R. T. (2003). Chromatic detection and discrimination in the periphery: a postreceptoral loss of color sensitivity. *Vis Neurosci* **20**, 511-521.

- OGAWA, S., LEE, T. M., KAY, A. R. & TANK, D. W. (1990). Brain magnetic resonance imaging with contrast dependent on blood oxygenation. *Proc Natl Acad Sci U S A* **87**, 9868-9872.
- OGAWA, S., TANK, D. W., MENON, R., ELLERMANN, J. M., KIM, S. G., MERKLE, H. & UGURBIL, K. (1992). Intrinsic signal changes accompanying sensory stimulation: functional brain mapping with magnetic resonance imaging. *Proc Natl Acad Sci U S A* **89**, 5951-5955.
- ORBAN, G. A., HOFFMANN, K. P. & DUYSSENS, J. (1985). Velocity selectivity in the cat visual system. I. Responses of LGN cells to moving bar stimuli: a comparison with cortical areas 17 and 18. *J Neurophysiol* **54**, 1026-1049.
- PALMER, G. (1777). *Theory of light*, London:Leacroft.
- PANIGRAHI, G. (1973). *Penetrod Land Color Display System (PENTECOST) and some observations concerning color perception*, UIUCDCS-R-73-583, Department of Computer Science, University of Illinois at Urbana-Champaign, Urbana, Illinois, Oct. 1973.
- PASUPATHY, A. & CONNOR, C. E. (2001). Shape representation in area V4: position-specific tuning for boundary conformation. *J Neurophysiol.* **86**, 2505-2519.
- PAZO-ALVAREZ, P., AMENEDO, E. & CADAVEIRA, F. (2004). Automatic detection of motion direction changes in the human brain. *Eur J Neurosci* **19**, 1978-1986.
- PERRY, V. H. & COWEY, A. (1985). The ganglion cell and cone distributions in the monkey's retina: implications for central magnification factors. *Vision Res* **25**, 1795-1810.
- PERRY, V. H., OEHLER, R., COWEY, A. (1984). Retinal ganglion cells that project to the dorsal lateral geniculate nucleus in the macaque monkey. *Neuroscience* **12**, 1101-1123.
- PETERHANS, E. & VON DER HEYDT, R. (1993). Functional organization of area V2 in the alert macaque. *Eur J Neurosci* **5**, 509-524.
- POGGIO, G. F., BAKER, F. H., MANSFIELD, R. J., SILLITO, A. & GRIGG, P. (1975). Spatial and chromatic properties of neurons subserving foveal and parafoveal vision in rhesus monkey. *Brain Res* **100**, 25-59.
- PRESS, W. A., BREWER, A. A., DOUGHERTY, R. F., WADE, A. R. & WANDELL, B. A. (2001). Visual areas and spatial summation in human visual cortex. *Vision Res* **41**, 1321-1332.
- RAMACHANDRAN, V. S. & GREGORY, R. L. (1978). Does colour provide an input to human motion perception? *Nature* **275**, 55-56.

- RODIECK, R. W. (1998). *The first steps in seeing*. Sinauer.
- ROE, A. W. & TS'O, D. Y. (1999). Specificity of color connectivity between primate V1 and V2. *J Neurophysiol* **82**, 2719-2730.
- ROORDA, A., WILLIAMS, D. R. (1999). The arrangement of the three cone classes in the living human eye. *Nature* **397**, 520-522.
- ROSEN, B. R., BUCKNER, R. L. & DALE, A. M. (1998). Event-related functional MRI: past, present, and future. *Proc Natl Acad Sci* **95**, 773-780.
- SAITO, H., YUKIE, M., TANAKA, K., HIKOSAKA, K., FUKADA, Y. & IWAI, E. (1986). Integration of direction signals of image motion in the superior temporal sulcus of the macaque monkey. *J Neurosci.* **6**, 145-157.
- SALIN, P. A. & BULLIER, J. (1995). Corticocortical connections in the visual system: structure and function. *Physiol Rev* **75**, 107-154.
- SALZMAN, C. D., BRITTEN, K. H. & NEWSOME, W. T. (1990). Cortical microstimulation influences perceptual judgements of motion direction. *Nature* **346**, 174-177.
- SANKERALLI, M. J. & MULLEN, K. T. (1996). Estimation of the L-, M- and S-cone weights of the post-receptoral detection mechanisms. *Journal of the Optical Society of America A* **13**, 906-915.
- SCHEIN, S. J. & DESIMONE, R. (1990). Spectral properties of V4 neurons in the macaque. *J Neurosci* **10**, 3369-3389.
- SCHEIN, S. J., MARROCCO, R. T. & DE MONASTERIO, F. M. (1982). Is there a high concentration of color-selective cells in area V4 of monkey visual cortex? *J Neurophysiol* **47**, 193-213.
- SCHILLER, P. H. (1993). The effects of V4 and middle temporal (MT) area lesions on visual performance in the rhesus monkey. *Vis Neurosci* **10**, 717-746.
- SCHILLER, P. H. (1995). Effect of lesions in visual cortical area V4 on the recognition of transformed objects. *Nature* **376**, 342-344.
- SCHLUPPECK, D. & ENGEL, S. A. (2002). Color opponent neurons in V1: a review and model reconciling results from imaging and single-unit recording. *J Vis* **2**, 480-492.
- SCHNAPF, J. L., KRAFT, T. W. & BAYLOR, D. A. (1987). Spectral sensitivity of human cone photoreceptors. *Nature*. **325**, 439-441.
- SEIDEMANN, E., POIRSON, A. B., WANDELL, B. A. & NEWSOME, W. T. (1999). Color signals in area MT of the macaque monkey. *Neuron*. **24**, 911-917.

- SERENO, M. I., DALE, A. M., REPPAS, J. B., KWONG, K. K., BELLIVEAU, J. W., BRADY, T. J., ROSEN, B. R. & TOOTELL, R. B. (1995). Borders of multiple visual areas in humans revealed by functional magnetic resonance imaging. *Science*. **268**, 889-893.
- SHADLEN, M. N., BRITTEN, K. H., NEWSOME, W. T. & MOVSHON, J. A. (1996). A computational analysis of the relationship between neuronal and behavioral responses to visual motion. *J Neurosci* **16**, 1486-1510.
- SHAPLEY, R. M. & VICTOR, J. D. (1978). The effect of contrast on the transfer properties of cat retinal ganglion cells. *285*.
- SHAPLEY, R. M. & VICTOR, J. D. (1981). How the contrast gain control modifies the frequency responses of cat retinal ganglion cells. *J Physiol* **318**, 161-179.
- SHARPE, L. T. & NORDBY, K. (1990). The photoreceptors in the achromat. In: *In Night Vision: Basic, Clinical and Applied Aspects*. ed. HESS RF, S., L.T., NORDBY, K., ED, pp. 335-389. Cambridge University Press, Cambridge.
- SHIPP, S., DE JONG, B. M., ZIHL, J., FRACKOWIAK, R. S. & ZEKI, S. (1994). The brain activity related to residual motion vision in a patient with bilateral lesions of V5. *Brain*. **117**, 1023-1038.
- SINCICH, L. C. & HORTON, J. C. (2005). The circuitry of V1 and V2: integration of color, form, and motion. *Annu Rev Neurosci* **28**, 303-326.
- SLOAN, K. R. J. & BAJCSY, R. (1975). A computational structure for color perception. *Proceedings of the 1975 annual conference*, 42 - 45.
- SMITH, A. T., GREENLEE, M. W., SINGH, K. D., KRAEMER, F. M. & HENNIG, J. (1998). The processing of first- and second-order motion in human visual cortex assessed by functional magnetic resonance imaging (fMRI). *J Neurosci*. **18**, 3816-3830.
- SMITH, A. T., SINGH, K. D., WILLIAMS, A. L. & GREENLEE, M. W. (2001). Estimating receptive field size from fMRI data in human striate and extrastriate visual cortex. *Cereb Cortex* **11**, 1182-1190.
- SMITH, V. C., POKORNY, J., DAVIS, M. & YEH, T. (1994). Mechanisms subserving temporal modulation sensitivity in silent-cone substitution. *J Opt Soc Am A Opt Image Sci Vis* **12**, 241-249.
- SOLOMON, S. G. & LENNIE, P. (2005). Chromatic gain controls in visual cortical neurons. *J Neurosci* **25**, 4779-4792.
- SPELLMANN, L. & WERNER, J., EDITORS. (1990). *Visual Perception: The neurophysiological foundations*. Academic Press.
- STOCKMAN, A. & SHARPE, L. T. (1998). Human cone spectral sensitivities: a progress report. *Vision Res*. **38**, 3193-3206.

STOCKMAN, A. & SHARPE, L. T. (2000). The spectral sensitivities of the middle- and long-wavelength-sensitive cones derived from measurements in observers of known genotype. *Vision Res* **40**, 1711-1737.

STOCKMAN, A., SHARPE, L. T. & FACH, C. (1999). The spectral sensitivity of the human short-wavelength sensitive cones derived from thresholds and color matches. *Vision Res* **39**, 2901-2927.

STROMEYER, C. F., 3RD, KRONAUER, R. E., RYU, A., CHAPARRO, A. & ESKEW, R. T., JR. (1995). Contributions of human long-wave and middle-wave cones to motion detection. *J Physiol.* **485**, 221-243.

TALBOT, S. & MARSHALL, W. (1941). Physiological studies on neural mechanisms of visual localization and discrimination. *Am J Ophthalmol* **24**, 1255-1263.

TEO, P. C., SAPIRO, G. & WANDELL, B. A. (1997). Creating connected representations of cortical gray matter for functional MRI visualization. *IEEE Trans Med Imaging.* **16**, 852-863.

THIELE, A., DOBKINS, K. R. & ALBRIGHT, T. D. (1999). The contribution of color to motion processing in Macaque middle temporal area. *J Neurosci.* **19**, 6571-6587.

THORELL, L. G., DE VALOIS, R. L. & ALBRECHT, D. G. (1984). Spatial mapping of monkey V1 cells with pure color and luminance stimuli. *Vision Res* **24**, 751-769.

THORPE, S., FIZE, D. & MARLOT, C. (1996). Speed of processing in the human visual system. *Nature* **381**, 520 - 522.

THULBORN, K. R., WATERTON, J. C., MATTHEWS, P. M. & RADDA, G. K. (1982). Oxygenation dependence of the transverse relaxation time of water protons in whole blood at high field. *Biochim Biophys Acta* **714**, 265-270.

TOLIAS, A. S., KELIRIS, G. A., SMIRNAKIS, S. M. & LOGOTHETIS, N. K. (2005a). Neurons in macaque area V4 acquire directional tuning after adaptation to motion stimuli. *Nat Neurosci* **8**, 591-593.

TOLIAS, A. S., KELIRIS, G. A., SMIRNAKIS, S. M. & LOGOTHETIS, N. K. (2005b). Neurons in macaque area V4 acquire directional tuning after adaptation to motion stimuli. *Nat Neurosci.* **8**, 591-593. Epub 2005 Apr 2017.

TOLIAS, A. S., MOORE, T., SMIRNAKIS, S. M., TEHOVNIK, E. J., SIAPAS, A. G. & SCHILLER, P. H. (2001a). Eye movements modulate visual receptive fields of V4 neurons. *Neuron.* **29**, 757-767.

TOLIAS, A. S., SMIRNAKIS, S. M., AUGATH, M. A., TRINATH, T. & LOGOTHETIS, N. K. (2001b). Motion processing in the macaque: revisited with functional magnetic resonance imaging. *J Neurosci.* **21**, 8594-8601.

TOOTELL, R. B., HADJIKHANI, N., HALL, E. K., MARRETT, S., VANDUFFEL, W., VAUGHAN, J. T. & DALE, A. M. (1998). The retinotopy of visual spatial attention. *Neuron* **21**, 1409-1422.

TOOTELL, R. B., HADJIKHANI N.,. (2001). Where is 'dorsal V4' in human visual cortex? Retinotopic, topographic and functional evidence. *Cereb Cortex* **11**, 298-311.

TOOTELL, R. B., MENDOLA, J. D., HADJIKHANI, N. K., LEDDEN, P. J., LIU, A. K., REPPAS, J. B., SERENO, M. I. & DALE, A. M. (1997). Functional analysis of V3A and related areas in human visual cortex. *J Neurosci* **17**, 7060-7078.

TOOTELL, R. B., REPPAS, J. B., DALE, A. M., LOOK, R. B., SERENO, M. I., MALACH, R., BRADY, T. J. & ROSEN, B. R. (1995a). Visual motion aftereffect in human cortical area MT revealed by functional magnetic resonance imaging. *Nature*. **375**, 139-141.

TOOTELL, R. B., REPPAS, J. B., KWONG, K. K., MALACH, R., BORN, R. T., BRADY, T. J., ROSEN, B. R. & BELLIVEAU, J. W. (1995b). Functional analysis of human MT and related visual cortical areas using magnetic resonance imaging. *J Neurosci*. **15**, 3215-3230.

TS'O, D. Y. & GILBERT, C. D. (1988). The organization of chromatic and spatial interactions in the primate striate cortex. *J Neurosci*. **8**, 1712-1727.

TURNER, R., LE BIHAN, D., MOONEN, C. T., DESPRES, D. & FRANK, J. (1991). Echo-planar time course MRI of cat brain oxygenation changes. *Magn Reson Med* **22**, 159-166.

TYLER, C. W., LIKOVA, L. T., CHEN, C. C., KONTSEVICH, L. L., SCHIRA, M. M. & WADE, A. R. (2005). Extended Concepts of Occipital Retinotopy. *Current Medical Imaging Reviews* **1**, 319-329(311).

UNGERLEIDER, L. D. & MISHKIN, M. (1982). *Two cortical visual systems*. In: *Analysis of visual behavior*. MIT Press, Ingle, D.J., Goodale. M.D. & Mansfield, R.J. (Ed.), Cambridge.

USREY, W. M. & REID, R. C. (2000). Visual physiology of the lateral geniculate nucleus in two species of new world monkey: *Saimiri sciureus* and *Aotus trivirgatus*. *J Physiol* **523** 755-769.

VAN ESSEN, D. C., ANDERSON C.H. (1990). Information processing strategies and pathways in the primate retina and visual cortex. In *Introduction to Neural and Electronic Networks*. ed. S.F. ZORNETZER, J. L. D., C. LAU, pp. 43-72. Academic Press, Orlando.

VAN ESSEN, D. C., ANDERSON, C. H. & FELLEMAN, D. J. (1992). Information processing in the primate visual system: an integrated systems perspective. *Science* **255**, 419-423.

- VAN ESSEN, D. C. & DEYOE, E. A. (1995). Concurrent processing in the primate visual cortex. In *The cognitive neuroscience*. ed. GAZZANIGA, M. S., pp. 383-400. MIT Press, Cambridge, MA.
- VAN ESSEN, D. C. & GALLANT, J. L. (1994). Neural mechanisms of form and motion processing in the primate visual system. *Neuron* **13**, 1-10.
- WACHTLER, T., SEJNOWSKI, T. J. & ALBRIGHT, T. D. (2003). Representation of color stimuli in awake macaque primary visual cortex. *Neuron* **37**, 681-691.
- WADE, A. R., BREWER, A. A., RIEGER, J. W. & WANDELL, B. A. (2002). Functional measurements of human ventral occipital cortex: retinotopy and colour. *Philos Trans R Soc Lond B Biol Sci* **357**, 963-973.
- WALSH, V., BUTLER, S. R., CARDEN, D. & KULIKOWSKI, J. J. (1992). The effects of V4 lesions on the visual abilities of macaques: shape discrimination. *Behav Brain Res* **50**, 115-126.
- WALSH, V., LE MARE, C., BLAIRE, A. & COWEY, A. (2000). Normal discrimination performance accompanied by priming deficits in monkeys with V4 or TEO lesions. *NeuroReport* **11**, 1459-1462.
- WANDELL, B. (1995). *Foundations of vision*. Sinauer, Sunderland, Massachusetts.
- WANDELL, B. A. (1999). Computational neuroimaging of human visual cortex. *Annu Rev Neurosci* **22**, 145-173.
- WANDELL, B. A. (2004). Computational neuroimaging: Cortical color signals. *Biophysical Journal* **86**, 515a-515a.
- WANDELL, B. A., BREWER, A. A. & DOUGHERTY, R. F. (2005). Visual field map clusters in human cortex. *Philos Trans R Soc Lond B Biol Sci* **360**, 693-707. Review.
- WANDELL, B. A., POIRSON, A. B., NEWSOME, W. T., BASELER, H. A., BOYNTON, G. M., HUK, A., GANDHI, S. & SHARPE, L. T. (1999). Color signals in human motion-selective cortex. *Neuron* **24**, 901-909.
- WÄSSLE, H., GRUNERT, U., ROHRENBECK, J. & BOYCOTT, B. B. (1990). Retinal ganglion cell density and cortical magnification factor in the primate. *Vision Res* **30**, 1897-1911.
- WATSON, A. B. & ROBSON, J. G. (1981). Discrimination at threshold: labelled detectors in human vision. *Vision Res* **21**, 1115-1122.
- WATSON, A. B., THOMPSON, P. G., MURPHY, B. J. & NACHMIAS, J. (1980). Summation and discrimination of gratings moving in opposite directions. *Vision Res* **20**, 341-347.

- WATSON, J. D., MYERS, R., FRACKOWIAK, R. S., HAJNAL, J. V., WOODS, R. P., MAZZIOTTA, J. C., SHIPP, S. & ZEKI, S. (1993). Area V5 of the human brain: evidence from a combined study using positron emission tomography and magnetic resonance imaging. *Cereb Cortex*. **3**, 79-94.
- WEBSTER, M. A. & MOLLON, J. D. (1993). Contrast adaptation dissociates different measures of luminous efficiency. *J Opt Soc Am A* **10**, 1332-1340.
- WEBSTER, M. A. & MOLLON, J. D. (1997). Motion minima for different directions in color space. *Vision Res* **37**, 1479-1498.
- WIESEL, T. N. & HUBEL, D. H. (1966). Spatial and chromatic interactions in the lateral geniculate body of the rhesus monkey. *J Neurophysiol.* **29**, 1115-1156.
- WIKLER, K. C., WILLIAMS, R. W. & RAKIC, P. (2004). Photoreceptor mosaic: Number and distribution of rods and cones in the rhesus monkey retina. *The Journal of Comparative Neurology* **297**, 499 - 508.
- WYSZECKI, G. & STILES, W. S. (1982). *Color Science Concepts and Methods, Quantitative Data and Formulae, second edition*. John Wiley, New York.
- YANTIS, S. (2005). How visual salience wins the battle for awareness. *Nat Neurosci.* **8**, 975-977.
- YEH, T., LEE, B. B. & KREMERS, J. (1995a). Temporal response of ganglion cells of the macaque retina to cone-specific modulation. *J Opt Soc Am A Opt Image Sci Vis* **12**, 456-464.
- YEH, T., LEE, B. B., KREMERS, J., COWING, J. A., HUNT, D. M., MARTIN, P. R. & TROY, J. B. (1995). Visual responses in the lateral geniculate nucleus of dichromatic and trichromatic marmosets (*Callithrix jacchus*). *J Neurosci* **15**, 7892-7904.
- YOSHIMURA, Y. & CALLAWAY, E. M. (2005). Fine-scale specificity of cortical networks depends on inhibitory cell type and connectivity. *Nat Neurosci* **8**, 1552-1559.
- YOSHIOKA, T., DOW, B. M. & VAUTIN, R. G. (1996). Neuronal mechanisms of color categorization in areas V1, V2 and V4 of macaque monkey visual cortex. *Behav Brain Res* **76**, 51-70.
- YOSHIOKA, T., LEVITT, J. B. & LUND, J. S. (1992). Intrinsic lattice connections of macaque monkey visual cortical area V4. *J Neurosci* **12**, 2785-2802.
- YOSHIOKA, T., LEVITT, J. B. & LUND, J. S. (1993). Anatomical basis for channel interactions in macaque cortical visual area V1. *Invest. Opth. and Vis. Sci.* **34**.
- YOUNG, T. (1802). *On the theory of light and colors*, London: The Society.
- ZEKI, S. (1983a). Colour coding in the cerebral cortex: the reaction of cells in monkey visual cortex to wavelengths and colours. *Neuroscience.* **9**, 741-765.

- ZEKI, S. (1983b). Colour coding in the cerebral cortex: the responses of wavelength-selective and colour-coded cells in monkey visual cortex to changes in wavelength composition. *Neuroscience*. **9**, 767-781.
- ZEKI, S. (1983c). The distribution of wavelength and orientation selective cells in different areas of monkey visual cortex. *Proc R Soc Lond B Biol Sci*. **217**, 449-470.
- ZEKI, S. (1983d). The relationship between wavelength and color studied in single cells of monkey striate cortex. *Prog Brain Res* **58**, 219-227.
- ZEKI, S. (1990). A century of cerebral achromatopsia. *Brain* **113**, 1721-1777.
- ZEKI, S. (1991). Cerebral akinetopsia (visual motion blindness). A review. *Brain*. **114**, 811-824.
- ZEKI, S. & MARINI, L. (1998). Three cortical stages of colour processing in the human brain. *Brain*. **121**, 1669-1685.
- ZEKI, S., WATSON, J. D., LUECK, C. J., FRISTON, K. J., KENNARD, C. & FRACKOWIAK, R. S. (1991). A direct demonstration of functional specialization in human visual cortex. *J Neurosci*. **11**, 641-649.
- ZEKI, S. M. (1973). Colour coding in rhesus monkey prestriate cortex. *Brain Res* **53**, 422-427.
- ZEKI, S. M. (1974). Functional organization of a visual area in the posterior bank of the superior temporal sulcus of the rhesus monkey. *J Physiol*. **236**, 549-573.
- ZEKI, S. M. (1978a). The cortical projections of foveal striate cortex in the rhesus monkey. *J Physiol* **277**, 227-244.
- ZHENG, D., LAMANTIA, A. S. & PURVES, D. (1991). Specialized vascularization of the primate visual cortex. *Journal of Neuroscience* **11**, 2622-2629.
- ZIHL, J., VON CRAMON, D. & MAI, N. (1983). Selective disturbance of movement vision after bilateral brain damage. *Brain* **106 (Pt 2)**, 313-340.

## ***Curriculum Vitae***

### ***Personal Information:***

Name	Marcus Grüschow
Birthday	08.09.1976
Birthplace	Magdeburg
Address	Halberstädterstrasse 52, Magdeburg, 39112
Family status	Unwed
Nationality	german

### ***School Education:***

1983-90	Hubert-Materlik Oberschule, Magdeburg, Germany
1990-93	Geschwister Scholl Gymnasium, Magdeburg, Germany
1993-94	Tolland Highschool, Connecticut, USA, Honorary Diploma
1994-96	Geschwister Scholl Gymnasium, Magdeburg, Germany (Abitur)

### ***University Education:***

Sept 1997- Sept 1998	Otto-von-Guericke University, Magdeburg, Germany (Major: Education, Minors: Psychology and English)
Oct 1998- Oct 1999	State University of New York at Oswego, USA (2 Semesters, Major: Psychology, Minors: Communications, Percussions)
Oct 1999- Sept 2003	Otto-von-Guericke University, Magdeburg, Germany (Major: Psychology); Dipl. Psych. Sept 2003
Since Oct 2003	Ph.D. Thesis at the Faculty of Natural Sciences at the Otto-von-Guericke-University Magdeburg and the Center for Advanced Imaging

Magdeburg, February 2007